University of Alberta

An NMR-based approach to the structural and functional investigation of the Na^+/H^+ exchanger NHE1

by

Brian Lornkay Lee

A thesis submitted to the Faculty of Graduate Studies and Research
in partial fulfillment of the requirements for the degree of

Doctor of Philosophy

Department of Biochemistry

Fall 2013
Edmonton, Alberta

Abstract

The Na^+/H^+ exchanger isoform 1 (NHE1) is the predominant isoform in mammalian cells, and regulates intracellular pH and ion concentrations. NHE1 also interacts with numerous proteins and signalling pathways. Consequently, it has been found to influence cell volume, growth, differentiation, and motility, and has roles in heart disease and cancer. While a wealth of biochemical and physiological data is available on NHE1, little is known about its structure or mechanism of function. In this thesis, a "divide and conquer" approach was used to study the structure and function of NHE1. The structures of individual transmembrane (TM) segments were determined using nuclear magnetic resonance (NMR) spectroscopy, and the function of the TM segments in the full protein were investigated using site-directed mutagenesis in cultured cells. We first examined the structures and functions of the second (EL 2) and fourth (EL 4) extracellular loops of NHE1. Both loops contained functionally important residues, however, EL 2 was found to be structured by NMR while EL 4 was unstructured. Next, we investigated two critical TM segments in NHE1, TM VI and TM XI, as well as TM IV of sod2, a yeast Na^+/H^+ exchanger. These TM segments were found to have unusual structures consisting of a N- and C- terminal alpha-helix, with an extended segment in between, and the structures correlated well with the functional data. We also looked at larger regions of NHE1 using NMR to examine the TM–TM interactions in the protein, starting with a structure of a two-TM segment of NHE1, TM VI–VII. We also present preliminary NMR experiments on two three-TM segments, TM V–VII and TM X–XII, as well

as full-length *Escherichia coli* NhaA. Overall, the "divide and conquer" approach has allowed us to successfully examine the structures and functions of single-TM segments of NHE1. Furthermore, studies on multi-TM segments and NhaA suggest that we may be able to assemble the structure of NHE1 from its segments or even study the complete protein by NMR spectroscopy.

Acknowledgements

This thesis developed as a collaboration between the labs of Dr. Brian Sykes and Dr. Larry Fliegel, and, as with any collaboration, would not have been possible without the help of many others.

I would first like to thank my supervisor, Dr. Brian Sykes, for his patient instruction, encouragement, and advice throughout my time in his lab. I would also like to thank my co-supervisor, Dr. Larry Fliegel, who first introduced me to this collaboration, for his knowledge and guidance during this project.

The work presented in this thesis includes the contributions from many of the people in the Fliegel lab. In particular, Xiuju Li, Yongsheng Liu, and Jennifer Tzeng, who performed the mutagenesis work in the earlier parts of this thesis, Asad Ullah, for the sod2 studies, and Claudia Alves, Grant Kemp, and Arghya Basu, who performed the protein/peptide expression in the latter part of this thesis.

I would like to thank those involved in the other collaborative projects in the appendices of this thesis: Dr. Robert Ryan, Dr. Luc Berthiaume, Dr. Joanne Lemieux, Kasuen Mauldin, Marta Oleszczuk, Dale Martin, and Melissa Morrison, and of course, Dr. Brian Sykes, who helped start these collaborations.

I would like to thank Dr. Joel Weiner as part of my supervisory committee, for his time and suggestions over the project, and Dr. James Young and Dr. Natalie Goto, for taking time out of their busy schedules to attend my Ph.D. defence.

Thank you to all the other people in the Sykes and Fliegel labs for insightful discussions and critique, help around the lab(s), and various activities, including golf,

curling, barbecues, and cake: Olga Baryshnikova, Ryan Hoffman, Stacy Reinke, Sam Szeto, Olivier Julien, Ian Robertson, Sandra Pineda, Gump Zhao, Subhrangsu Chatterjee, John-Paul Glaves, Peter Hwang, Jonathan Pan, Peter Holmes, Nick Shaw, David Corson, Melissa Crane, Angela Thiessen, Robert Boyko, Pascal Mercier, Ersilia Coccaro, Pratap Karki, Maxime Ndayizeye, Fatima Mraiche, Aruna Augustine, Ayodeji Aderibigbe, Ray Amith, and Jodi Wilkinson.

Thank you to the staff in the Department of Biochemistry: Jack Moore and Paul Semchuck for purifying many of the peptides used in this thesis, Ryan McKay and Derek Webb at NANUC for assistance and maintenance of the 800 MHz spectrometer, Dean Schieve for technical support, and Sue Smith, Kim Arndt, Barb Thom, and Colleen Iwanicka for help with various student matters.

I would like to extend a special thanks to my family, for their patience, love, and support over the past six years.

Finally, I would like to thank the Heart and Stroke Foundation of Canada, Alberta Innovates – Health Solutions, and the University of Alberta for the financial support.

Table of Contents

List of Figures

List of Tables

List of Abbreviations

1D, 2D, 3D	One-, two-, three-dimensional
$^{3}J_{\mathrm{HNH}\alpha}$	Three-bond scalar coupling constant between ^{1}HN and $^{1}\mathrm{H}\alpha$
ApoA-V	Apolipoprotein A-V
BCECF-AM	2′,7′-bis-(2-carboxyethyl)-5(6)-carboxyfluorescein acetoxymethyl ester
CD	Circular dichromism
CSI	Chemical shift index
CTnC	C-terminal domain of troponin C
DDM	Dodecylmaltoside
DFBP-O	2′,4′-difluoro-(1,1′-biphenyl)-4-yloxy acetic acid
DMPC	Dimyristoyl phosphatidylcholine
DMSO	Dimethyl sulfoxide
DPC	Dodecylphosphocholine
DQF-COSY	Double-quantum filtered correlation spectroscopy
DSS	2,2-Dimethyl-2-silapentane-5-sulfonic acid
EL	Extracellular loop
EM	Electron microscopy
EMD87580	NHE1 inhibitory compound
GB1	Streptococcal protein G immunoglobulin-binding domain B1
GFP	Green fluorescent protein
HA	Hemagglutinin
HPLC	High-performance liquid chromatography
HSQC	Heteronuclear single-quantum correlation
HTT	Huntingtin
IL	Intracellular loop
IPA	Isopropanol

IPTG	Isopropyl β-D-1-thiogalactopyranoside
LDL	Low-density lipoprotein
MAS	Magic-angle spinning
MBP	Maltose-binding protein
MTSES	2-Sulfonatoethyl methanethiosulfonate
MTSET	(2-(Trimethylammonium)ethyl) methanethiosulfonate
NhaA	*E. coli* Na^+/H^+ antiporter A
NHE1	Human Na^+/H^+ exchanger isoform 1
NMR	Nuclear magnetic resonance
NOE(SY)	Nulcear Overhauser effect (spectroscopy)
NTnC	N-terminal domain of troponin C
OR1896-CF_3	Fluorinated levosimendan metabolite derivative
PINK1	PTEN-induced putative kinase 1
PL-C	Phospholipase C
ppm	Parts per million
PRE	Paramagnetic relaxation enhancement
rHDL	Reconstituted high-density lipoprotein
RMS(D)	Root-mean-square (deviation)
ROESY	Rotational Overhauser effect spectroscopy
SDS	Sodium dodecylsulfate
S.D.	Standard deviation
S.E.	Standard error
T_1	Longitudinal relaxation time
T_2	Transverse relaxation time
TEV	Tobacco etch virus
TFA	Trifluoroacetate
TFE	Trifluoroethanol
TFP	Trifluoperazine
TG	Triglyceride
TM	Transmembrane (helix)
TnC	Troponin C
TnI	Troponin I
TOCSY	Total correlation spectroscopy

Chapter 1

Introduction

Portions of this chapter have been published elsewhere in modified form:

- Lee, B. L., Sykes, B. D., and Fliegel, L. (2011) Structural analysis of the Na^+/H^+ exchanger isoform 1 (NHE1) using the divide and conquer approach. *Biochem. Cell. Biol. 89*, 189–199.
- Lee, B. L., Sykes, B. D., and Fliegel, L. (2013) Structural and functional insights into the cardiac Na^+/H^+ exchanger. *J. Mol. Cell. Cardiol. 61*, 60–67.

Membrane proteins

Integral membrane proteins function by allowing the cell to interact with its environment by transversing the membrane bilayer to provide a connection between the outside and inside of the cell, that otherwise acts as a barrier. The various functions of membrane proteins include transporters that allow molecules to cross the membrane, receptors that convey signals to the cell in response to external stimuli, cell adhesion molecules to allow the cell to interact with its neighbours, as well as enzymes that catalyze important reactions within the cell. The importance of membrane proteins can be emphasized by the fact that they make up 20–30% of the genome of an organism (*1*). The function of membrane proteins also make them important in the pharmaceutical industry, where they represent 40–60% of the proteins that are currently targeted by drugs (*2*).

Because of their importance in cellular function and in the pharmaceutical industry, the structures of membrane proteins are of great interest. The three-dimensional structure of membrane proteins can provide insight into the details of the molecular mechanisms of the protein, as well as provide a starting point for the rational design of drugs that could specifically target that protein and its

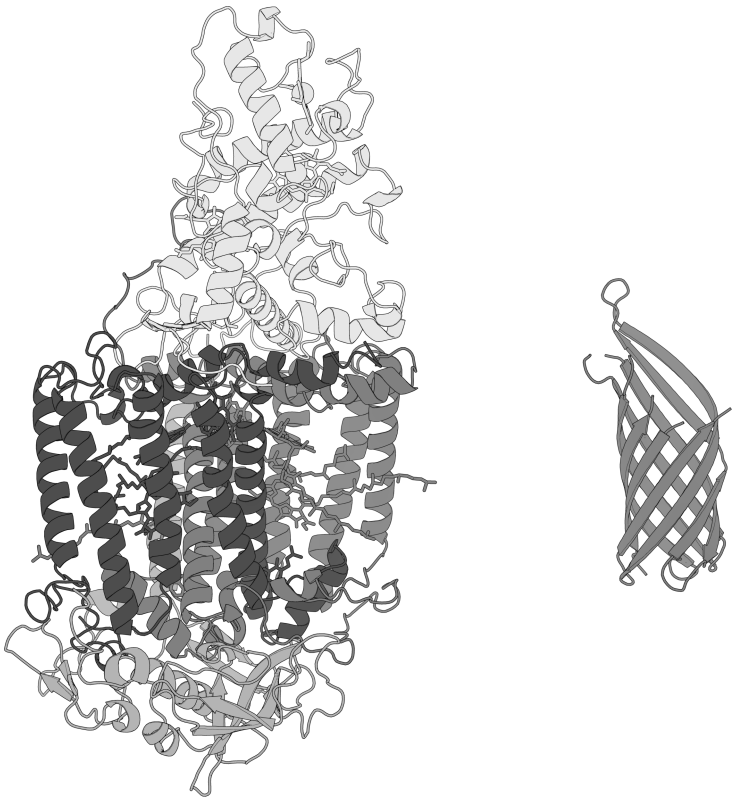

Figure 1-1. Structures of integral membrane proteins. (Left) The first high resolution membrane protein structure: the photosynthetic reaction center of *Rhodopseudomonas viridis*, an alpha-helical membrane protein. The four subunits are coloured in different shades of grey, with the polypeptide backbone shown in a cartoon representation, co-factors shown as sticks, and bound ferrous ion shown as a sphere. (Right) The beta-barrel membrane protein OmpA from *Escherichia coli*, in a cartoon representation.

function. The first high resolution protein structure was determined in the 1950's (*3*), and since then, the number of protein structures has grown almost exponentially. There are currently around 87000 protein structures representing around 21000 unique sequences (structures with less than 30% sequence similarity) deposited in the Protein Data Bank (*4*). The determination of membrane protein structures, however, has lagged behind. The first membrane protein structure was published in 1985, and there are currently about 1200 high resolution structures representing about 400 different proteins (*5*).

The first membrane protein structures, a low resolution electron diffraction structure of bacteriorhodopsin and a high resolution x-ray structure of a photosynthetic reaction center (Figure 1-1), were published in 1975 and 1985, respectively (*6*, *7*). These structures exemplified many of the characteristics of membrane proteins

recognized today. They contain long stretches of hydrophobic amino acids that fold into alpha-helices and insert into the hydrophobic environment of the membrane bilayer. Membrane proteins often contain more positively charged residues compared to negatively charge residues in the helix-connecting intracellular loops: the "positive inside rule" (*8*), as well as a higher proportion of aromatic residues at the membrane-solvent interface, an "aromatic belt" (*9*). More recent structures have found that membrane proteins do not just consist of bundles of alpha-helices, but include many less regular structural features, such as proline induced kinks, re-entrant loops, and discontinuous helices which were found to be important for the function of the proteins (*10*, *11*). The properties of the membrane are also important to membrane proteins (*12*, *13*). The structures and functions of membrane proteins can be affected by membrane thickness, surface charge, curvature, and some proteins require specific lipids for their function.

While the majority of membrane proteins are primarily alpha-helical in structure, a small percentage of membrane proteins contain a beta-barrel structure (Figure 1-1). In bacteria, beta-barrel membrane proteins make up around 2–3% of the genome. They are found primarily on the outer membranes of bacteria, mitochondria, and chloroplasts. This thesis focuses on the structural and functional aspects of the larger class of alpha-helical membrane proteins, and specifically on the ubiquitous human Na^+/H^+ exchanger isoform 1 (NHE1).

Membrane protein structure determination

Because of the disparity between the number of structures of soluble proteins and the structures of membrane proteins compared to their importance in cell function and disease, there is a need for more structural information about membrane proteins. However, membrane protein structures have been difficult to obtain. While many soluble proteins that have been crystallized have been expressed in prokaryotic systems such as *Escherichia coli*, membrane proteins, particularly eukaryotic membrane proteins, may have more specialized requirements for their expression (*14*), such as post-translational modifications, or specialized insertion or folding systems not found in bacteria. The yield of membrane proteins from overexpression is often lower than soluble proteins, as their expression can become toxic to the cell. Furthermore, their hydrophobic nature can make them difficult to purify and handle compared to soluble proteins, requiring the use of detergents, which can affect their stability and structure.

Initial predictions of the structure or topology of membrane proteins usually involves an examination of the sequence of the protein. Important residues can be found through comparison with closely related sequences, where functionally important residues are usually conserved. The sequences also reveal long stretches of primarily hydrophobic residues which suggest the location of the hydrophobic transmembrane (TM) helices (*15*, *16*). More modern prediction methods are relatively accurate and can usually predict the general topology of the protein (*17*). If structures of homologous proteins are available, one could attempt to model the sequence onto the three-dimensional structure of the homologous protein. These methods only provide a prediction of the general topology of the protein and requires experimental validation. More difficult to predict are the more unusual but functionally important features that have been found in many recent membrane protein structures, such as discontinuous helices, extended segments in the center of a TM helices, and re-entrant loops, structured intra- or extracellular loops that enter and exit the membrane, as well as helix distorting kinks (*10*, *11*, *18*).

These predictions can be experimentally tested using biochemical methods. The topology of the protein can be investigated using protein or chemical tags, or enzymatic cleavage (*19*). Chemical cross linking, fluorescence and electron paramagnetic resonance spectroscopy can provide site-specific information about the three dimensional structure (*20*). However, these techniques only give a low resolution picture of the structure of the protein.

Diffraction techniques such as x-ray crystallography and electron crystallography have been the main methods for obtaining high resolution structural data for entire membrane proteins. These techniques can provide atomic resolution detail of very large and complex proteins. As with studying membrane proteins in general, the amount of protein that can be produced is a limiting factor. For crystallography specifically, obtaining well diffracting crystals is the primary challenge. Some strategies that have been developed to attempt to form crystals have included using chimeric proteins (*21*), or unusual lipid phases (*22*). Despite these difficulties, the majority of membrane protein structures have been determined by these methods, and many more structures will follow in the future.

Another method for obtaining high resolution structural information is nuclear magnetic resonance spectroscopy (NMR). NMR is an attractive method for studying the structure and function of membrane proteins and proteins in general, in that proteins can be studied in physiologically relevant conditions and without the demanding need for the formation of crystals. NMR is also useful for determining

the structures of dynamic and flexible proteins, which do not crystallize well. As with crystallography, the expression of sufficient amounts of protein can be a limiting factor. High concentrations of protein are needed for NMR, and protein yields may be reduced due to the need for potentially expensive isotopic labelling necessary for NMR structure determination experiments. The quality of the NMR spectra of membrane proteins can also make structure determination difficult. The repetitive helical structure and often large size of many membrane proteins can result in extensive crowding and overlap between the peaks in the NMR spectra. For these reasons, NMR studies have traditionally been limited to smaller proteins and peptides. The first NMR protein structures were of small proteins around 50 residues in size (*23*). For membrane proteins, the first structures were of simple single TM proteins (*24*, *25*). Recently developed methods such as transverse relaxation optimized correlation spectroscopy (TROSY), perdeuteration, selective labelling schemes (*26*) as well as solid-state magic angle spinning NMR (*27*) have been used to study larger and more complex systems with NMR spectroscopy. This has allowed for the determination of large proteins such as the 82 kDa malate synthase (*28*) and the 27 kDa membrane protein sensory rhodopsin (*29*) using solution state NMR. Solid-state NMR techniques allowed for the structure determination of the 34 kDa G-protein coupled receptor, CXCR1 (*30*). Site specific studies of even larger proteins such as the 670 kDa 20S proteosome core particle have also been shown to be possible (*31*).

Na^+/H^+ exchangers

The focus of this thesis is the structure and function of the first characterized human Na^+/H^+ exchanger (NHE) isoform, NHE1. Na^+/H^+ exchangers are a family of membrane proteins that catalyze the transmembrane exchange of sodium ions for protons. NHEs are widely distributed across phyla and kingdoms. In lower organisms, they are mainly involved in exporting sodium ions for salt tolerance, while in eukaryotes, they play a large role in regulating intracellular and intercompartmental pH. Three cation/proton antiporter families have been described: CPA1, CPA2, and a Na^+-transporting carboxylic acid decarboxylase family (*32*). The CPA1 family includes many well-studied examples of NHEs from fungi, plants, and mammals. It includes the eukaryotic NHE clade with several subgroups. Nine isoforms of mammalian NHEs (NHE1–NHE9) have been identified in this family and are thought to be electroneutral transporters (*32*, *33*). The CPA2 family consists of several clades, some members of which are electrogenic. Its members include the

well studied *E. coli* NhaA, as well as the yeast sod2, and the human Nha1 and Nha2 (*32*, *34*). The mammalian sperm-specific NHEs are found in the remaining family (*32*).

NHE1

Cation/proton exchange was proposed as part of Peter Mitchell's chemiosmotic hypothesis (*35*), and was first demonstrated in rat liver mitochondria (*36*). Mammalian Na^+/H^+ exchange was first demonstrated in rat intestinal and renal microvilli by Murer et al. in 1976 (*37*), and the first isoform, NHE1, was cloned and sequenced by Sardet et al. in 1989 (*38*). In humans, nine isoforms, numbered NHE1 through NHE9, have since been identified, along with three more distantly related isoforms, NHA1, NHA2 and a sperm-specific NHE (*32*). NHE 1–5 are located primarily on the plasma membrane. NHE1 is ubiquitous, and is considered the "housekeeping" isoform. NHE 2–4 are found primarily in the kidney and gastrointestinal tract. NHE5 is found in the brain. NHE 6–9 are found in intracellular membranes and regulate organellar pH.

Human NHE1 contains 815 amino acids, with a 500 amino acid N-terminal membrane domain responsible for ion transport and pH sensing, and a 315 amino acid C-terminal regulatory domain. The membrane domain functions by removing intracellular protons in exchange for extracellular sodium in a 1:1 ratio to regulate the intracellular pH. The energy for transport comes from the sodium electrochemical gradient normally maintained by the Na^+/K^+ ATPase. NHE1 shows little activity under physiological resting conditions. However, it is activated through a "pH sensor" on the intracellular side of the membrane domain by a decrease in intracellular pH. Its activation is also modulated by its regulatory domain through its phosphorylation and its interactions with numerous regulatory proteins (*33*). NHE1 has also been shown to be involved in cell volume regulation (*39*), cell motility (*40*), and is involved in cell growth and differentiation (*41*).

NHE1 has several pathological roles (*42*). NHE1 has been implicated in ischemic heart disease. The build-up of intracellular acid under hypoxic conditions in ischemia leads to activation of NHE1 and an influx of sodium. The function of the Na^+/K^+ ATPase that would normally remove sodium is inhibited, due to the decreased levels of ATP under anaerobic conditions. The influx of sodium ions from NHE1 must then be handled by other proteins such as the Na^+/Ca^{2+} exchanger acting in reverse. This results in a detrimental influx of calcium that affects various

cell signalling pathways, and promotes cell death. The activation of NHE1 has also been shown to be involved in cardiac hypertrophy (*42*). NHE1 has been shown to be involved in cancer metastasis and invasiveness, by promoting the abnormal pH microenvironments and cell migration characteristics of cancers (*43*). An unusual splice variant of NHE1, missing TMs II–IV of the Wakabayashi model (see below), may be involved in Na^+/Li^+ countertransport in erythrocytes, and may be associated with hypertension and diabetic nephropathy (*44*, *45*). The increased activity of NHE1 in these various diseases suggests that NHE1 could present a target for drugs aimed at treating these diseases. However, clinical trials in humans have proven inconclusive or disappointing (*46*), possibly due to the specificity of the inhibitors and the route or timing of administering the drugs.

While there is a large body of research into the roles of NHE1 in cellular function and its role in a variety of diseases, there is little known about the structure of NHE1. A better understanding of the detailed structure of NHE1 could help in understanding how it carries out its functions, as well as allow for the design of better drugs and treatment strategies targeting NHE1. The complete high resolution structure of NHE1 is currently not known. However, progress had been made into elucidating the topology of NHE1, the structures of homologous Na^+/H^+ exchanger proteins, and the structures of smaller regions of NHE1 including a few isolated TM helices and regions of the C-terminus.

NHE1 topology

The sequence of human NHE1 was first determined by Sardet et al. (*38*), who predicted that the membrane domain consisted of 500 amino acids with 10 TM helices using hydropathy analysis (*16*). They predicted two potential N-linked glycosylation sites; it was later shown that only N75 between the first two TM helices acts as a N-linked glycosylation site (*47*). The hydrophilic C-terminal tail of about 300 amino acids contained a net positive charge and several putative phosphorylation sites, and thus was placed in an intracellular orientation. Phosphorylation of the C-terminal tail (*48*), and detection of a C-terminal domain epitope only in permeabilized cells (*49*) later confirmed the intracellular placement. Orlowski et al. (*50*) cloned and sequenced rat NHE 1–4, and using hydropathy analysis (*15*) and sequence alignment between the isoforms also suggested that NHE1 contained 10 TM helices. In comparison to the topology proposed by Sardet et al. (*38*), the first two helices were discarded and two additional helices were added, which while not as hydrophobic as

the surrounding helices, contained highly conserved polar or charged residues that were likely to be important for function. Differences in predictions seem to result from differences in the hydrophobicity scales used and from window sizes used to predict the TM regions.

Detailed analysis of the topology of NHE1 was performed by Wakabayashi et al. (*51*), using the cysteine scanning accessibility method (*52*). This method involves introducing an individual cysteine mutation into a cysteineless mutant of the protein and testing the accessibility of that cysteine to the sulfhydryl reactive reagents. The use of whole vs. permeabilized cells allowed them to test for extracellularly vs. intracellularly accessible cysteines in NHE1. They confirmed the intracellular localization of the N-terminus. They proposed a 12 TM model (referred to here as TMs I–XII) based on the accessibility of the residues tested (Figure 1-2, top) with the N- and C-terminus in the cytoplasm and the glycosylation site at N75 between TM I and II. The tenth TM in the hydrophobicity model contained residues on either end accessible extracellularly and was proposed to be a re-entrant loop rather than a TM segment, entering and exiting on the same side of the membrane. Two intracellular loops, between TMs IV–V and VIII–XI, were also suggested to be re-entrant loops, as these two loops contained both extracellularly and intracellularly accessible residues. They suggested that these re-entrant loops might line the pore and play a role in ion translocation. Experiments by Sato et al. (*53*, *54*) using a cell-free protein expression and membrane insertion system support the cytosolic localization of the N-terminus and the unusual topology of the re-entrant segment. They also showed that a plant NHE, Nhx1, has a similar topology. Finally, Wakabayashi et al. found that the predicted extracellular loop between the last two TM helices was found to be inaccessible and was reassigned as TM XI (*51*, *55*).

Brett et al. (*32*) analyzed the evolutionary relationship between a large sample of proteins in the cation/proton antiporter superfamily, which includes NHE1. The family of proteins appear to have a common fold in the transmembrane domain corresponding to TM III–XII of the topology model of Wakabayashi (*51*) as suggested by the similar hydropathy profiles of the exchangers. TM I–II appeared to be poorly conserved, and in the mammalian NHEs, TM I often appeared to be missing in sequence alignments. The C-terminal regulatory region varied in size and has low sequence similarity, which could reflect differences in regulation, localization, and function of the different isoforms.

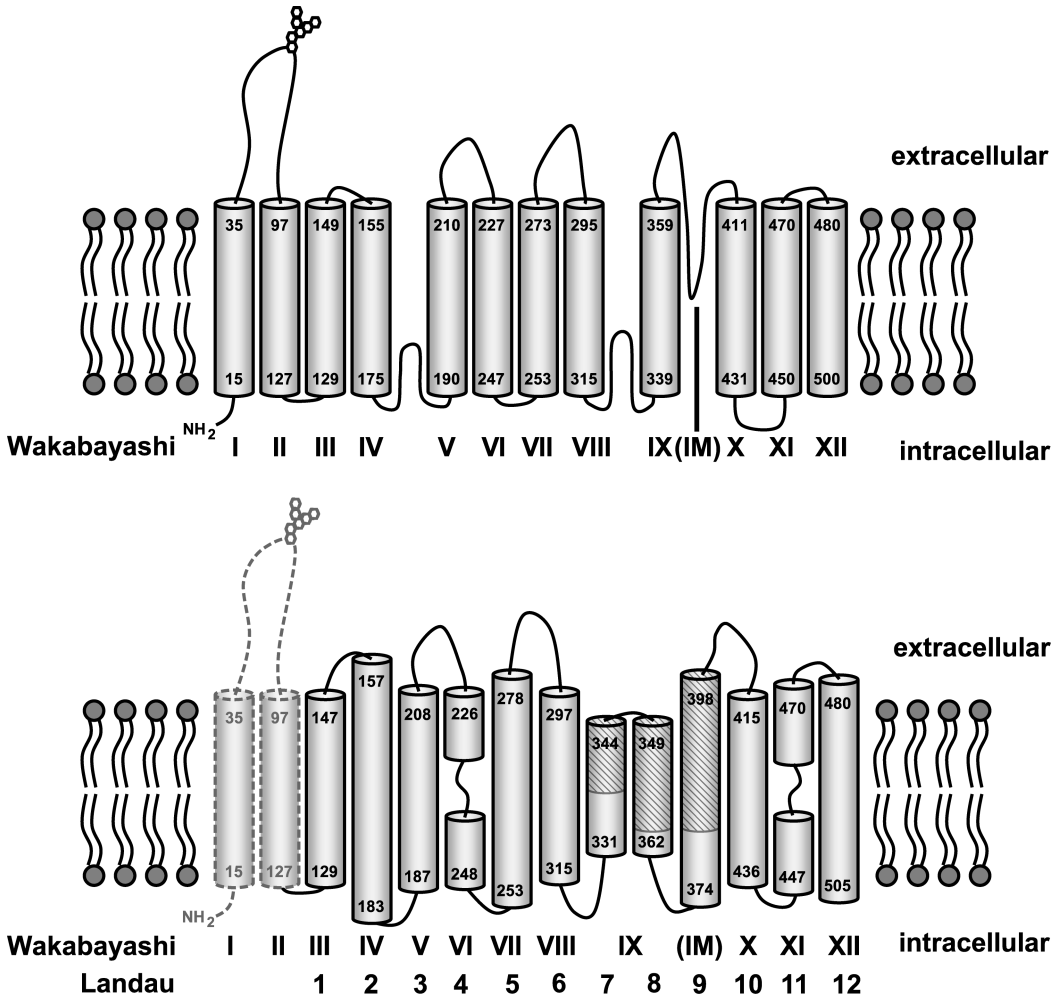

Figure 1-2. Topology models of NHE1. (Top) Wakabayashi topology model. (Bottom) Landau topology model. The residues forming the ends of the transmembrane helices are labelled. The numbering of the helices is shown below each model in roman numerals for the Wakabayashi model and Arabic numerals for the Landau model. NH_2, N-terminus. The C-terminal cytoplasmic domain is not shown. IM, putative re-entrant (intra-membrane) loop in the Wakabayashi model. Hatched regions in the Landau model indicate TM XI and the IM of the Wakabayashi model.

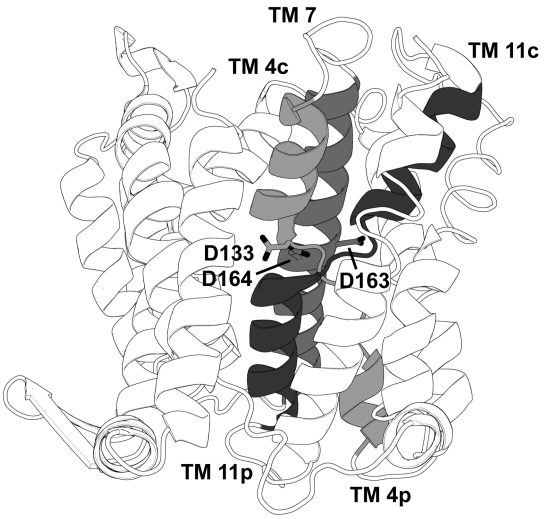

Figure 1-3. Crystal structure of NhaA. TM 4, 5 and 11 are shaded grey and labelled. c, cytoplasmic halves of TM 4 and 11. p, periplasmic halves of TM 4 and 11. Key aspartate residues implied in ion binding are shown as sticks and labelled.

NhaA

NhaA is a distant bacterial homologue of NHE1 which functions in salt tolerance. Unlike NHE1, it removes sodium using the proton gradient in a 1:2 sodium:proton ratio, and it is active at basic pH. The membrane domain is smaller, with 388 amino acids, and NhaA does not contain a C-terminal regulatory domain. NhaA is also insensitive to most eukaryotic NHE inhibitors (*56*). The ability to overexpress and purify active NhaA in milligram quantities was crucial to the determination of the complete structure as well as in functional studies of the protein (*57*). The high-resolution structure of NhaA has provided a starting point to interpreting the functional data on NhaA and providing insights in to the mechanism of Na^+/H^+ exchange.

The structure of *E. coli* NhaA was solved at a high resolution by X-ray crystallography (*58*). NhaA consists of 12 TM helices and has a novel fold. The structure showed a long loop between TMs 1 and 2 and contained a surface associated helix and a 2 strand beta sheet that was important for dimerization (*56*). When the beta-sheet was removed, monomers of NhaA were functional though with altered kinetics, suggesting that monomers were the principal functional unit. NhaA also contains a group of 6 TMs which contains two bundles of TM helices containing three TMs each, TM 3–5 and TM 10–12, which are related by a pseudo two fold symmetry. Two of the helices, TM 4 and TM 11, were “discontinuous helices” that contained extended regions in the center of each helix and which crossed each

other. These are a critical part of the novel fold of NhaA. Many membrane protein structures contain similar internal structural repeats (*59*) or discontinuous helices (*11*) in their structures, which may be important in substrate binding and transport. The TM 4/11 region of NhaA contains a negatively charged D133 on TM 4 and positively charged K300 on the nearby TM 10, both of which could compensate for the introduction of helix dipole partial charges introduced by the breaks in TM 4 and 11 in the center of the membrane. Two highly conserved aspartate residues, D163 and D164 on TM 5, are believed to be important in cation binding. Figure 1-3 shows the structure of NhaA, highlighting the critically important TMs 4, 5, and 11.

The structure of NhaA was solved at pH 4, where it is in an inactive, "acid-locked" state. In this state, the important D163–D164 site is only partly accessible from the cytoplasmic side and completely inaccessible from the periplasmic side. Studies using electron microscopy (*60*), computational simulations (*61*, *62*), and various biochemical analyses suggest a mechanism for the activation and transport mechanism of NhaA. Charged residues located around the cytoplasmic end of TM 9 and the N-terminus act as a pH sensor, which undergoes a conformational change (*60*, *63*) at basic pH. This in turn triggers a change in conformation of TMs 4, 11, and 10 to fully expose the cytoplasmic ion binding site and readies the protein for transport (*60*, *64*). Ion transport can then proceed by an "alternating access" mechanism. Na^+ binds in the pore near D163 and D164 (*62*, *65*). Binding causes a disruption of the delicate electrostatic balance between the charged residues and helix dipoles, which triggers conformational changes in the transporter that releases the Na^+ ion to the periplasm. Two H^+ can then bind in the pore and are transported into the cytoplasm, resetting the transporter for Na^+ binding once again.

A 2D topology and a 3D model of NHE1 was proposed based on the bacterial crystal structure of NhaA as a template (*66*). They used modern TM helix prediction and protein alignment algorithms to model the NHE1 sequence onto the NhaA structure. The 2D topology of this model is shown in Figure 1-2. While the 12 TM helices of NhaA and the 12 TM helices of the Wakabayashi model suggest that there could be a 1-to-1 correlation between the NhaA and Wakabayashi topologies, the topology developed by Landau et al. assigns some helices differently. This topology model also contains 12 TM helices (labelled as TMs 1–12); however, it does not include the first two helices of the model of Wakabayashi (*51*). Landau et al. argued that these helices do not appear to be important for the function of the protein and are poorly conserved. Furthermore, enzymatic cleavage of NHE1 between TM II and III did not affect NHE1 function (*67*). However, both fully and

partially glycosylated NHE1 are visible in western blots of NHE1, and Wakabayashi et al. locate the N-terminus in the cytoplasm (*51*), which suggests that these two helices and the intervening loop are present. This could suggest that there are 14 TMs in NHE1: the twelve predicted by Landau plus two additional N-terminal TM helices. The assignment of the next 6 TMs (TM III–VIII, now numbered TM 1–6) is the same. TM IX is split into two short helices (TM 7–8) and the re-entrant segment between TM IX–X is reassigned as TM 9. This rearrangement of the re-entrant loop, however, places the fifth extracellular loop, with numerous extracellularly accessible residues (*51*), on the inside of the membrane. They suggest that this loop could be near the pore of the protein, similar to the re-entrant loops suggested in the model of Wakabayashi. The remaining three TMs (TM 10–12) are the same in both models. They also predict that TM 4 (TM VI) and 11 (TM XI) contain unwound central regions, like the TM 4/11 assembly observed in NhaA. Charged residues that are evolutionarily conserved among NHE family members are placed in the core of the protein and are proposed to play a role similar to the corresponding residues in NhaA. D238 is thought to be similar to D133 in NhaA, compensating for the helix dipole charges. D163–D164 in NhaA is replaced with N266–D267 in eukaryotic exchangers, which may play a role in ion binding. Evidence which supports this model includes the conservation of residues closer to the core and lack of conservation at the periphery of the model, and the clustering of residues important in pH regulation and in inhibition of NHE1 activity to one region of the extracellular face of the exchanger.

Homologous Na^+/H^+ exchangers

NHA2

A model of a related protein, human NHA2 (*68*), was also published using the same methodology as the study by Landau et al. (*66*). The results suggested a structure similar to that of NhaA but with unique features. The study also included model-based mutagenesis experiments to support their results. Guided by their model of NHA2, mutagenesis of conserved charged residues and residues in the protein core suggested that NHA2 may have a TM segment assembly similar to that of NhaA. The dipoles of this assembly appear to be compensated for by polar, uncharged residues rather than the negatively charged aspartates in NhaA. They also suggest that an additional positively charged arginine residue not present in NhaA or

NHE1 may play a role in the transport mechanism of NHA2.

NhaP1

A three-dimensional EM structure of the *Methanococcus janasschii* NhaP1 exchanger has been solved (*69*). The organization of the helices of NhaP1 is similar to NhaA, with a linear arrangement of helices forming a dimer interface, and a 6 TM bundle. NhaP1 shows 13 TM helices in contrast to the 12 in NhaA. The additional helix is likely at the N-terminus and interacts with the second monomer. They found that this helix is important for activity, however it did not appear to be necessary for dimerization. The Landau model (*66*) of NHE1 does not model the first two predicted TM helices TM I–II, however multiple sequence alignments by Goswami et al. (*69*) suggest that NHE1 may have 14 TM regions, including TM I–II, with 13 TMs equivalent to NhaP1 and an additional helix corresponding to TM V. This would suggest the Landau model is accurate for the region containing the TM VI–XII region, while the helices in the first half of the model may be assigned differently. Their alignment also suggests also that human NHE6 has 15 TMs, with the first TM functioning as a cleaved signal sequence (*70*).

ASBT

Recently, a crystal structure of a sodium/bile salt symporter ASBT was found to have an almost identical fold to NhaA (*71*). It contains 10 TMs, with the 6 TM bundle and 4 TM "panel" superimposable onto the NhaA structure. The emergence of a 10 TM rather than a 12 TM protein with a near identical fold to NhaA and with a completely different function, suggests that this fold could be present in many other transporter proteins as well.

Structural studies of NHE1

Electron microscopy

A low resolution envelope of full length NHE1 has been obtained using single particle electron microscopy (*72*). In this study, NHE1 was successfully overexpressed and purified in *Saccharomyces cerevisiae*. The envelope of the protein was determined by single particle reconstruction of negatively stained, purified NHE1 protein. The size of the envelope corresponded to a dimer of NHE1. NHE1 has been shown to exist as dimers, although the functional unit is a monomer (*73*).

The envelope of the NHE1 dimer contains two compact, higher density regions which are likely the two NHE1 monomers. These two regions agree with the size and shape of a dimer of NhaA. The NHE1 structure observed also contains a "ridge" which was interpreted to be the density from the combined cytoplasmic domains of the two NHE1 molecules. Recently, a low resolution envelope of a plant NHE, SOS1, has also been solved (*74*). This structure also appeared to be a dimer, and two conformations of the C-terminal domain could be observed.

Intrahelical loops

There is little structural and biochemical information on the intracellular and extracellular loops of NHE1. The extracellular loops of NhaA contain residues important for pH induced activation (*75*), and contain a beta-sheet essential for dimerization (*56*). The loop regions of NHE1 could similarly be important for pH induced activation, inhibitor binding and interacting with the C-terminal tail and associated regulatory proteins. Many charged residues on the intracellular loops were found to be important for the pH sensitivity of NHE1, and mutation of these residues shifted the intracellular pH dependence of the exchanger (*55*, *76*, *77*). Murtazina et al. (*78*) found that E391 was important for activity. This residue is located within the proposed extracellular re-entrant loop between TM IX and X, however in the Landau model (*66*), this is near the center of TM9. Extracellular loop (EL) 2 contains residues which may be important in inhibitor binding (*79*). This could be related to its proximity to TM IV, which also has many inhibitor sensitive residues. Wang et al. (*80*) identified functionally important cysteine (C477) in EL 6.

C-terminus

The C-terminus of NHE1 spans residues 500–815 and is found on the intracellular side of the membrane. Circular dichromism analysis suggests the domain contains 35% α-helix, 16% β-turn, and 49% random coil (*81*). Circular dichromism analysis of the last 180 amino acids suggests mostly sheet, turn, and coil structure, with very little helical content (*81*). The membrane-proximal region ($\sim$500–600) appears to be involved in the dimerization of NHE1 (*82*). The distal region ($\sim$600–815) may be intrinsically disordered based on NMR studies (*83*). Structures of the CHP1, CHP2 and calmodulin regulatory proteins bound to the C-terminal tail of NHE1 have been solved. Residues 503–545 of the C-terminal tail form an amphipathic helix on binding to CHP1 (*84*) or CHP2 (*85*). Calmodulin binding (*86*) to residues

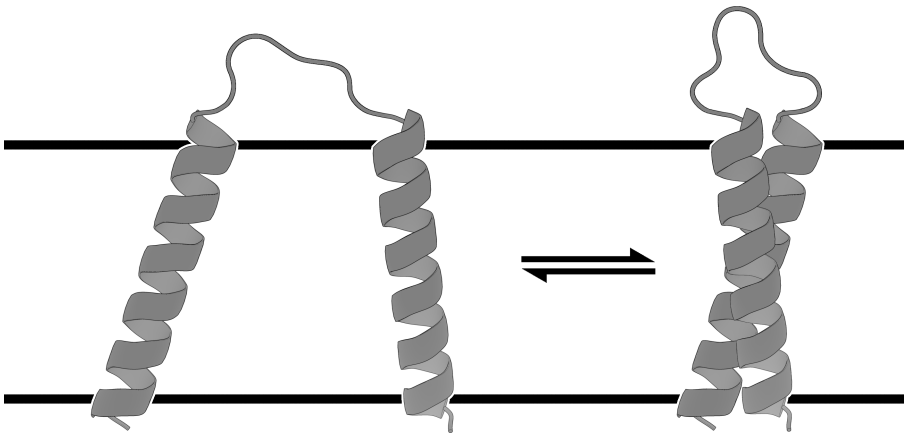

Figure 1-4. The two-stage model of membrane protein folding. (Left) Individual TM segments can fold independently into helical structures on insertion into the membrane bilayer. (Right) Folded TM alpha-helices interact and form the final three-dimensional protein structure.

622–690 of the C-terminus have also been determined. The C-terminal has been suggested to undergo Ca^{2+} dependent conformational changes. This may be an effect of calmodulin binding, through disruption of the interaction of the calmodulin binding region to an acidic D/E rich patch (residues 753–759) (*87*). The C-terminal tail also displays phosphorylation and pH-dependent conformational changes (*88*). These conformational changes may be important in the regulation of the exchanger. The complete structure of the C-terminal tail, its interactions with other proteins, and how it regulates the membrane domain activity remain to be elucidated.

The "divide and conquer" approach

While there has been a lot of progress on the development of NMR techniques for studing large proteins, there are still very few structures of large membrane proteins determined using NMR. An alternative approach to membrane protein structure is the "divide and conquer" approach, which can avoid the problems associated with expressing and studying the full-length membrane protein (*89*). This approach studies the structures and interactions of smaller peptides that represent the TM segments of the larger multi-TM protein. Such smaller peptides tend to be easier to produce, both chemically and biosynthetically, than full membrane proteins. Their smaller size is also more favourable for NMR spectroscopy, providing simpler and better resolved NMR spectra than the larger, full-length proteins.

The divide and conquer approach is based on the concept of the two-stage folding model of alpha-helical membrane proteins proposed by Popot and Engelman

(Figure 1-4) (*90*). The model reasons that TM helices are able to form energetically stable, independently folding domains in membrane environments. Alpha-helices form because it is energetically unfavourable to place exposed polar backbone C=O and N−H groups within a hydrophobic environment. This can be alleviated through the formation of hydrogen bonds between these groups (*91*) to form either alpha-helical or beta-barrel structures. Hydrophobic side chains on the outside of the structures allow the helix or barrel to insert into the hydrophobic membrane environment. Alpha-helices are thought to fold at the membrane interface, where the environment is intermediate between the solvent and membrane (*92*). Van der Waals forces and conserved motifs such as the GXXXG motif can then allow the helices in a multi-span TM protein to interact and form the final three-dimensional structure. In eukaryotes, the insertion of the TM helices is mediated by the Sec translocation machinery, which identifies and folds individual TM helices as they are translated, then allows them to exit to the bilayer where they can interact with other TMs.

The two-stage model implies that individual TM helices act as independently folding domains that, when placed in an appropriate membrane-like environment, might be expected to have similar structures both isolated and in the complete protein. NMR studies of individual TM helices and loops have shown that the structures are often very similar to the structures of helices found in crystal structures (*93–95*), and kinks or unstructured regions found in these isolated helices have functional relevance (*11*), supporting this approach. Naider et al. have used this method to examine single- and multi-TM regions of the GPCR Ste2p (*96–98*).

Due to the difficulty of studying the structure of the complete NHE1 protein, we decided to use the "divide and conquer method" (*89*) to study the structure of NHE1. Rainey et al. and Reddy et al. have previously determined the structures of some isolated TM helices of NHE1 using NMR. These were TM IV (residues 155–180) (*99*), TM VII (250–275) (*100*), and TM IX (338–365) (*101*). These helices were chosen based on the Wakabayashi et al. (*51*) model and their functional importance due to the presence of charged or helix-breaking residues and previous mutagenesis studies. Each putative TM helix did not form simple canonical alpha-helices, but rather displayed kinks and extended structures within what would be the center of the TM helices. Furthermore, these unusual features tended to correspond to regions in the TM helix that were functionally significant in the full protein based on thorough mutagenesis experiments on those TMs. Non-helical regions in TM helices have been found in the structures of many transporter proteins and are suggested to play key roles in their function (*11*).

Milligram amounts of peptide are needed for NMR structural analysis. A peptide representing TM IV was expressed in *E. coli* as a fusion protein with an N-terminal streptococcal immunoglobulin binding domain (GB1 domain) for solubility and a C-terminal poly-histidine tag for purification (*102*). Methionine residues separated the three regions of the fusion protein, allowing for purification of the TM IV peptide by cyanogen bromide cleavage and subsequent purification by high performance liquid chromatography (HPLC). This expression system allowed for stable isotopic labelling of TM IV for detailed NMR study. Attempts at expression or purification of TM VII using the GB1 system resulted in poor yield of purified peptide, so TM VII, along with TM IX, were made synthetically (*100*, *101*), without isotopic labelling. Multiple naturally occurring charged residues and/or additional non-natural lysine residues were placed at the termini of the synthetic peptides. Lysine tags have been shown to increase peptide solubility during purification (*103*). These peptides can then be studied solubilized in membrane-mimicking conditions. The structure of TM IV was determined in a mixture of chloroform, methanol and water. The mixture is similar of the membrane environment: with components representing a hydrophobic lipid core and polar solvent environment. Later peptide structures were determined in detergent micelles, which may better represent the lipid bilayer (*104*) by forming particles containing a core of hydrophobic tails, surrounded by polar head groups.

The NMR structural studies were performed simultaneously with complementary functional assays involving comprehensive mutagenesis of the residues of the TM helix being studied. Such functional assays are important to the interpretation and validation of the NMR structural data. The effects of the mutations on protein expression, trafficking, and activity were measured in cultured cells, providing insights into the role of each of the residues in the TM segment. Cysteine substituted mutants could also be reacted with sulfhydryl reactive reagents, such as negatively charged MTSES and positively charged MTSET. The treatment of specific mutants with MTSES or MTSET resulting in the inhibition of transport activity would suggest that those residues are not only extracellularly accessible, but are within the pore of the protein, as the size and/or charge of MTSES/MTSET could likely block the entry of Na^+ into the pore.

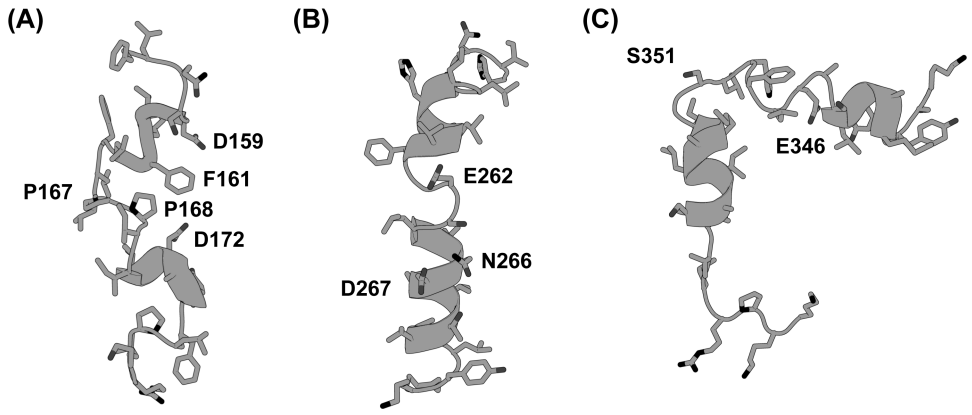

Figure 1-5. NMR structures of NHE1 TM segments. (A) TM IV. (B) TM VII. (C) TM IX. The lowest energy structures from the NMR structural ensembles are shown. The peptide backbone in shown in a cartoon representation; the thicker cartoon in (A) represents a region of beta-turns. Side chains are shown as sticks. Some of the functionally important side chains are labelled. The structures were determined in organic solvents (TM IV) or detergent micelles (TM VII and IX).

Structural and functional studies of NHE1 transmembrane helices

TM IV

The NMR structure of a peptide representing TM IV (residues 155–177) of NHE1 was determined in an organic solvent mixture of 4:4:1 chloroform/methanol/water (Figure 1-5, A) (*99*). Counter to expectations, TM IV did not adopt a canonical transmembrane alpha-helical structure. TM IV has an irregular structure, containing three structurally distinct regions. The N-terminal region (residues 159–163) contains overlapping beta turns. The central region (residues 165–168) contains two prolines and is extended. The C-terminal region (residues 169–176) contains a short helical segment at residues 170–174. While the individual regions can be superimposed in the NMR structural ensemble, the three regions rotate freely with respect to each other, so the entire structure cannot be superimposed. This could represent flexibility in the TM segment that could be important for function or could be a result of a lack of interactions between the isolated TM helix and the balance of the protein.

TM IV has been found to be important in modulating inhibitor efficacy towards NHE1. Mutations to F162, L163, F167, F165, and G174 (*105–108*) were all found to confer inhibitor resistance upon NHE1. The residues important for inhibitor sensitivity are primarily on the N-terminal beta-turn region and the extended segment in the NMR structure, which corresponds to the extracellular half of TM IV (residues

159–168). Slepkov et al. (*99*, *109*, *110*) tested many mutants of TM IV for transport activity and found it very sensitive to mutation. Of 23 cysteine mutants of TM IV, 11 resulted in an exchanger with less than 20% of wild-type activity. P167/P168 was particularly important for the folding and activity of NHE1. Labelling of a F161C mutant NHE1 protein with either extracellularly applied, positively charged MTSET or negatively charged MTSES, resulted in inhibition of transport activity. This suggested that this residue is near the ion translocation pore, where MTSES/MTSET could sterically block the pore. The pore-lining location would also be consistent with changes in inhibitor sensitivity with mutations in this region.

The NMR structure of TM IV was found to roughly resemble the crystal structure of TM 4 of NhaA (*111*), initially suggesting that there could be a one-to-one direct correlation between the 12 helices predicted by Wakabayashi et al. (*51*) and the 12 helices in NhaA. Despite the primarily non-helical nature of the TM IV NMR structure, the comparison showed there was a significant degree of similarity between the two structures. The N-terminal beta turns in the NMR structure could be superimposed onto the N-terminal helix of the crystal structure, while the central extended and C-terminal helical regions of TM IV could be superimposed on the same regions of TM 4. Owing to the presence of pivot points in the NMR structure, only the structured regions and not the entire peptide could be superimposed. The NhaA structure also contains a critical residue, D133, which corresponds to P168 in the alignment. Both proline and aspartate residues can be found to cap the N-terminus of helices (*112*), lending support for this alignment. However, D133 is also thought to play a role in electrostatic balance and conformational changes resulting from ion binding (*113*). In TM IV, no such residue is present in or close to the extended region, although it is also possible other nearby residues, D159 or D172 could play a similar role.

The Landau et al. (*66*) topology model of NHE1 suggests TM IV is equivalent to TM 2 of NhaA. TM 2 of NhaA is kinked at its center rather than extended as TM IV is in the NMR structure. P167 and P168 in NHE1 TM IV maintain the extended structure of TM IV in the NMR model, and interactions with other TMs might be required for it to more resemble TM 2 of NhaA. Prolines have been shown to be able to incorporate into helices and induce kinks (*114*). NhaA TM 2, however, does not contain prolines, although they may have been lost over the evolution of protein structures (*115*). TM 2 in NhaA also lines both the cytoplasmic and periplasmic channels which would be in agreement with the pore-lining accessibility of F161 in NHE1 TM IV. Aspartates 159 and 172 in TM IV are on the structured helical or

beta turn regions in the NMR structure, not near the center of the TM, making them unlikely to be directly involved in ion translocation like D133 in NhaA. Studies on NhaA suggest that aspartates of TM 2 could play a role in pH induced activation of the exchanger (*75*), which could suggest a similar role for the TM IV aspartates of NHE1. Mutation of these two aspartates did affect the activity of the exchanger. However, there was no clear correlation between the changes in activity and the properties of the amino acid mutations (*78*). This could also suggest a regulatory, rather than direct role, for TM IV in the transport mechanism.

TM VII

The structure of TM VII (residues 250–275) was solved in DPC micelles (Figure 1-5, B) (*100*). It is primarily helical, with a kink at residues G261–S263 in the center of the helix. The peptide appears to show two conformations in solution: one where the TM helix is relatively straight, and one where the two halves are folded together around the kink. Further NMR based dynamic studies on this system suggest slow interconversion between these two states (*116*) that may be important for conformational changes necessary in ion transport. Mutations in the kink to residues with stronger helical propensity such as alanine or isoleucine inhibited activity, possibly by limiting this flexibility.

Mutagenesis of the amino acid residues in TM VII affected the activity of NHE1, with mutation of several residues influencing inhibitor efficacy (*78*, *100*, *117*). TM VII was less sensitive to mutation than TM IV, with only a few key residues showing significant effects on NHE1 activity when mutated. N266, and D267 were critical to NHE1 function, as with their mutation to cysteine or alanine, NHE1 was nearly inactive. In contrast, retention of the charge with a D267E mutation maintains activity. In addition, inserting an additional amino acid into TM VII inhibited activity of NHE1, showing that the positioning of D267 is also important. These results together suggested a putative role in ion binding. When E262 was mutated and NHE1 was expressed in mammalian cells, there was generally increased intracellular protein and a moderate decrease in activity, suggesting that E262 may be important in proper protein folding or in attracting cations. Cysteine accessibility studies also suggest that L255 and L258 are pore lining (*117*). Mutations of various hydrophobic residues in TM VII to alanine show altered sensitivity to the inhibitor EMD87580, which further supports the critical and pore lining role of this segment.

It seems unlikely that TM VII of NHE1 could be equivalent to TM 7 of NhaA. TM 7 is a short helix containing only about 15 residues instead of the approximately

20 residues predicted for TM VII. Alignment of the sequences of TM VII and TM 7 suggested that the N-terminal half of TM VII would align with TM 7, while the C-terminal half would form part of TM 8. This would suggest that the break at residues 261–263 in the NMR structure could consist of an extracellular loop, with the critical E262 and D267 at either end of the loop. However, the peripheral location of TM 7/8 in NhaA contradicts the critical role and positioning of the residues in TM VII in NHE1 activity.

Landau et al. (*66*) suggest that TM VII is equivalent to TM 5 in NhaA. Unlike the NMR structure, TM 5 in NhaA is a straight helix, with the charged aspartates facing the pore. This could suggest that additional helix-helix interactions in NHE1 may be important in maintaining a more helical structure, and in maintaining the correct orientations of the flexible halves of TM VII. NhaA has a DD motif (residues 163–164) rather than a ND motif (residues 266–267) that is found in NHE1 and related exchangers. These aspartates in NhaA are implicated in direct ion binding (*65*). NhaA does not have an additional residue equivalent to the more distal E262 in NHE1, however its importance in NHE1 could suggest some role in ion binding or activation or alternatively, could reflect differences in the functions of NHE1 and NhaA such as their differing stoichiometry. Alternatively, a nearby glutamate on TM 8 of NhaA could play a role similar to E262 (*68*). Interestingly, the two pore lining leucines identified in NHE1 (L255 and L258) are on the intracellular side of the membrane in both the models of NHE1 topology, yet were found to be accessible to extracellularly applied reagents. This could be similar to the intramembrane loops that are thought to be positioned inside the cell, but are accessible from the outside of the cell (*51*). Their accessibility is also consistent with a role similar to NhaA TM 5 which is critical for the activity of the exchanger. The critical nature of the charged residues and pore lining nature of L255/258 suggest they all lie along the ion translocation pathway. This is supported in the location of TM 5 in the Landau (*66*) model, and these residues lie on one face of the TM in some structures in the NMR ensemble.

TM IX

In DPC micelles the structure of TM IX (residues 338–365) shows two helical regions bent at a right angle to each other around a kink at residue S351 (Figure 1-5, C) (*118*). Mutations to E346, G352, H349, have been found to decrease drug sensitivity (*79*, *119*, *120*). Mutations to H349 showed little effect on activity. E346 and G352 mutations, however, decreased activity. Reddy et al. (*101*) found

that E346 and S351 are pore lining. Mutations to either of these residues also affected extracellular sodium and intracellular proton affinities. Most of the important residues lie in the center of the TM helix, near the kink in the NMR structure where they could play some role in ion transport and inhibitor binding. TM 9 in NhaA forms a long kinked helix. This kink, and residues on the extracellular side of the helix, are thought to be important in pH sensing and the resulting conformational changes. In the model of Landau (*66*), the sequence of TM IX forms two TM helices, TM 7–8, with the central kinked region forming an extracellular loop, and with TM 8 lining the extracellular pore. This could also be consistent with the accessibility and inhibitor binding studies, and activity could be affected by changes to the pH sensitivity of the protein. In NhaA, TM 8 lines the pore and is involved in pH regulation (*121*). It is not clear from current data whether TM IX represents a single helix as predicted by Wakabayashi (*51*), or if it is two TMs as predicted in the Landau topology model (*66*).

Objectives

While there is a large amount of functional and physiological data regarding NHE1, there is still very little known about its structure. Currently, there are two differing topology models for NHE1: one proposed by Wakabayashi et al. based on biochemical evidence, and another by Landau et al., based on evolutionary conservation and homology modelling. They differ in the numbering and positioning of the TM helices between the two models and it would be useful to distinguish which topology model is more correct to help interpret the large body of functional data available as well for comparisons to the data available for NhaA. The NMR structures by Rainey et al. and Reddy et al. provide the only detailed structural information about the transmembrane helices of NHE1 and correlate well with the functional studies. They provide some hint that the structures of NHE1 and NhaA may be similar, however its is unclear which of the topology models is correct and the structural details of the remainder of the protein remain to be determined. The only other structural data on NHE1 membrane domain comes from single particle reconstruction using electron microscopy. The structure and mechanism of regulation of the C-terminal domain is also poorly understood.

The focus of this thesis is the structural and functional investigation of NHE1, specifically, using NMR and the "divide and conquer" approach to look at the transmembrane domain of NHE1. These structural results will be integrated with

the results with the detailed functional data obtained in the Fliegel laboratory. We also attempt to extend the divide and conquer approach to looking at the structures of multiple transmembrane helices, and gain some further insight into the structure, function and folding of NHE1. Some of the goals of this thesis include, firstly, gain structural and functional insights into additional TM helices of NHE1. Secondly, test and compare the two topology models in light of the NMR structures and corresponding functional data. Can we distinguish between the two topologies and choose one over the other? Finally, to what extent can we use the "divide and conquer" approach for studying structure and function of NHE1?

The work presented in this thesis consists primarily of work that has been published collaboratively, combining the structural and functional study of particular regions of NHE1. The methods used in both the structural work using NMR and in vitro cell culture functional work are common throughout the studies, and are detailed in Chapter 2. Additional procedures used only in one or two chapters are detailed in their respective chapters. Chapters 3 and 4 examine the structure and function of two extracellular loops of NHE1, extracellular loop 2 (EL 2) (between TM III–IV) and extracellular loop 4 (EL 4) (between TM VII–VIII). There are few studies on the interhelical loops of NHE1, however, these loops may be important in the function of NHE1, as well as important in interactions with NHE1 inhibitors. We then continue by investigating the structure and function of the transmembrane helices of NHE1. We start by studying TM XI in Chapter 5 and TM VI in Chapters 6 and 7. These helices have been previously shown to be functionally important in NHE1. We show that they adopt interesting structures and show that they are central to the mechanism of the protein. Chapter 8 examines the structure and function of the fourth transmembrane segment of a yeast Na^+/H^+ exchanger, sod2. This exchanger is more closely related to the bacterial NhaA and our results may imply similarity in the structure and function of sod2, NhaA, and NHE1. Chapter 9 attempts to take the divide and conquer approach further, looking at the structure of a larger NHE1 peptide: two linked transmembrane helices, TM VI–VII, connected by the native intracellular loop sequence. The structure of two interacting helices may allow us to build up TM–TM interactions of NHE1, and provide insight into not just the secondary structure, but also the tertiary, three-dimensional structure and the folding of NHE1. Chapter 10 presents preliminary data, where we attempt to look at even larger segments using NMR spectroscopy, such as 3 TM segments of NHE1, TM V–VII and TM X–XII, which builds on the previous work of TM VI and TM VI–VII. We also look at full length *Escherichia coli* NhaA using solid-state

NMR, as a possible model Na^+/H^+ exchanger protein for NMR studies, and which may provide a possible stepping stone to future NMR studies of full length NHE1. Finally, Chapter 11 presents some overall conclusions and future directions from this work. The appendices contain work that does not follow the main topic of this thesis, primarily structural studies of other transmembrane or membrane interacting peptides.

References

1. Krogh, A., Larsson, B., von Heijne, G., and Sonnhammer, E. L. (2001) Predicting transmembrane protein topology with a hidden Markov model: application to complete genomes. *J. Mol. Biol. 305*, 567–580.
2. Yıldırım, M. A., Goh, K.-I., Cusick, M. E., Barabási, A.-L., and Vidal, M. (2007) Drug-target network. *Nat. Biotechnol. 25*, 1119–1126.
3. Kendrew, J. C., Dickerson, R. E., Strandberg, B. E., Hart, R. G., Davies, D. R., Phillips, D. C., and Shore, V. C. (1960) Structure of myoglobin: A three-dimensional Fourier synthesis at 2 Å resolution. *Nature 185*, 422–427.
4. Berman, H. M., Westbrook, J., Feng, Z., Gilliland, G., Bhat, T. N., Weissig, H., Shindyalov, I. N., and Bourne, P. E. (2000) The Protein Data Bank. *Nucleic Acids Res. 28*, 235–242.
5. White, S. Membrane Proteins of Known Structure, `http://blanco.biomol.uci.edu/mpstruc/` (accessed Apr. 1, 2013).
6. Henderson, R., and Unwin, P. N. (1975) Three-dimensional model of purple membrane obtained by electron microscopy. *Nature 257*, 28–32.
7. Deisenhofer, J., Epp, O., Miki, K., Huber, R., and Michel, H. (1985) Structure of the protein subunits in the photosynthetic reaction centre of *Rhodopseudomonas viridis* at 3 Å resolution. *Nature 318*, 618–624.
8. Michel, H., Weyer, K. A., Gruenberg, H., Dunger, I., Oesterhelt, D., and Lottspeich, F. (1986) The 'light' and 'medium' subunits of the photosynthetic reaction centre from *Rhodopseudomonas viridis*: isolation of the genes, nucleotide and amino acid sequence. *EMBO J. 5*, 1149–1158.
9. Sipos, L., and von Heijne, G. (1993) Predicting the topology of eukaryotic membrane proteins. *Eur. J. Biochem. 213*, 1333–1340.
10. Granseth, E. (2010) Prediction of re-entrant regions and other structural features beyond traditional topology models, in *Structural Bioinformatics of Membrane Proteins* (Frishman, D., Ed.), pp 123–136, Springer Vienna, Austria.
11. Screpanti, E., and Hunte, C. (2007) Discontinuous membrane helices in transport proteins and their correlation with function. *J. Struct. Biol. 159*, 261–267.
12. Lee, A. G. (2003) Lipid-protein interactions in biological membranes: a structural perspective. *Biochim. Biophys. Acta, Biomembr. 1612*, 1–40.
13. Lee, A. G. (2011) Lipid-protein interactions. *Biochem. Soc. Trans. 39*, 761–766.
14. Wagner, S., Bader, M. L., Drew, D., and de Gier, J.-W. (2006) Rationalizing membrane protein overexpression. *Trends Biotechnol. 24*, 364–371.
15. Kyte, J., and Doolittle, R. F. (1982) A simple method for displaying the hydropathic character of a protein. *J. Mol. Biol. 157*, 105–132.

16. Engelman, D. M., Steitz, T. A., and Goldman, A. (1986) Identifying nonpolar transbilayer helices in amino acid sequences of membrane proteins. *Annu. Rev. Biophys. Biophys. Chem. 15*, 321–353.

17. Tusnády, G. E., and Simon, I. (2010) Topology prediction of helical transmembrane proteins: how far have we reached? *Curr. Protein Pept. Sci. 11*, 550–561.

18. Bowie, J. U. (2013) Structural biology. Membrane protein twists and turns. *Science 339*, 398–399.

19. van Geest, M., and Lolkema, J. S. (2000) Membrane topology and insertion of membrane proteins: search for topogenic signals. *Microbiol. Mol. Biol. Rev. 64*, 13–33.

20. Sale, K., Faulon, J.-L., Gray, G. A., Schoeniger, J. S., and Young, M. M. (2004) Optimal bundling of transmembrane helices using sparse distance constraints. *Protein Sci. 13*, 2613–2627.

21. Cherezov, V., Rosenbaum, D. M., Hanson, M. A., Rasmussen, S. G. F., Thian, F. S., Kobilka, T. S., Choi, H.-J., Kuhn, P., Weis, W. I., Kobilka, B. K., and Stevens, R. C. (2007) High-resolution crystal structure of an engineered human β_2-adrenergic G protein-coupled receptor. *Science 318*, 1258–1265.

22. Landau, E. M., and Rosenbusch, J. P. (1996) Lipidic cubic phases: a novel concept for the crystallization of membrane proteins. *Proc. Natl. Acad. Sci. U.S.A. 93*, 14532–14535.

23. Williamson, M. P., Havel, T. F., and Wüthrich, K. (1985) Solution conformation of proteinase inhibitor IIA from bull seminal plasma by ^{1}H nuclear magnetic resonance and distance geometry. *J. Mol. Biol. 182*, 295–315.

24. MacKenzie, K. R., Prestegard, J. H., and Engelman, D. M. (1997) A transmembrane helix dimer: structure and implications. *Science 276*, 131–133.

25. Almeida, F. C., and Opella, S. J. (1997) fd coat protein structure in membrane environments: structural dynamics of the loop between the hydrophobic transmembrane helix and the amphipathic in-plane helix. *J. Mol. Biol. 270*, 481–495.

26. Sanders, C. R., and Sönnichsen, F. (2006) Solution NMR of membrane proteins: practice and challenges. *Magn. Reson. Chem. 44*, S24–S40.

27. McDermott, A. (2009) Structure and dynamics of membrane proteins by magic angle spinning solid-state NMR. *Annu. Rev. Biophys. 38*, 385–403.

28. Tugarinov, V., Choy, W.-Y., Orekhov, V. Y., and Kay, L. E. (2005) Solution NMR-derived global fold of a monomeric 82-kDa enzyme. *Proc. Natl. Acad. Sci. U.S.A. 102*, 622–627.

29. Gautier, A., Mott, H. R., Bostock, M. J., Kirkpatrick, J. P., and Nietlispach, D. (2010) Structure determination of the seven-helix transmembrane receptor sensory rhodopsin II by solution NMR spectroscopy. *Nat. Struct. Mol. Biol. 17*, 768–774.

30. Park, S. H., Das, B. B., Casagrande, F., Tian, Y., Nothnagel, H. J., Chu, M., Kiefer, H., Maier, K., De Angelis, A. A., Marassi, F. M., and Opella, S. J. (2012) Structure of the chemokine receptor CXCR1 in phospholipid bilayers. *Nature 491*, 779–783.

31. Sprangers, R., and Kay, L. E. (2007) Quantitative dynamics and binding studies of the 20S proteasome by NMR. *Nature 445*, 618–622.

32. Brett, C. L., Donowitz, M., and Rao, R. (2005) Evolutionary origins of eukaryotic sodium/proton exchangers. *Am. J. Physiol.: Cell Physiol. 288*, C223–C239.

33. Malo, M. E., and Fliegel, L. (2006) Physiological role and regulation of the Na^+/H^+ exchanger. *Can. J. Physiol. Pharmacol. 84*, 1081–1095.

34. Xiang, M., Feng, M., Muend, S., and Rao, R. (2007) A human Na^+/H^+ antiporter sharing evolutionary origins with bacterial NhaA may be a candidate gene for essential hypertension. *Proc. Natl. Acad. Sci. U.S.A. 104*, 18677–18681.

35. Mitchell, P. (2011) Chemiosmotic coupling in oxidative and photosynthetic phosphorylation. 1966. *Biochim. Biophys. Acta, Bioenerg. 1807*, 1507–1538.

36. Mitchell, P., and Moyle, J. (1967) Respiration-driven proton translocation in rat liver mitochondria. *Biochem. J. 105*, 1147–1162.

37. Murer, H., Hopfer, U., and Kinne, R. (1976) Sodium/proton antiport in brush-border-membrane vesicles isolated from rat small intestine and kidney. *Biochem. J. 154*, 597–604.

38. Sardet, C., Franchi, A., and Pouysségur, J. (1989) Molecular cloning, primary structure, and expression of the human growth factor-activatable Na^+/H^+ antiporter. *Cell 56*, 271–280.

39. Alexander, R. T., and Grinstein, S. (2006) Na^+/H^+ exchangers and the regulation of volume. *Acta Physiol. 187*, 159–167.

40. Stock, C., and Schwab, A. (2006) Role of the Na^+/H^+ exchanger NHE1 in cell migration. *Acta Physiol. 187*, 149–157.

41. Pedersen, S. F. (2006) The Na^+/H^+ exchanger NHE1 in stress-induced signal transduction: implications for cell proliferation and cell death. *Pflugers Arch. 452*, 249–259.

42. Fliegel, L. (2009) Regulation of the Na^+/H^+ exchanger in the healthy and diseased myocardium. *Expert Opin. Ther. Targets 13*, 55–68.

43. Cardone, R. A., Casavola, V., and Reshkin, S. J. (2005) The role of disturbed pH dynamics and the Na^+/H^+ exchanger in metastasis. *Nat. Rev. Cancer 5*, 786–795.

44. Zerbini, G., Maestroni, A., Breviario, D., Mangili, R., and Casari, G. (2003) Alternative splicing of NHE-1 mediates Na-Li countertransport and associates with activity rate. *Diabetes 52*, 1511–1518.

45. Kemp, G., Young, H., and Fliegel, L. (2008) Structure and function of the human Na^+/H^+ exchanger isoform 1. *Channels 2*, 329–336.

46. Murphy, E., and Allen, D. G. (2009) Why did the NHE inhibitor clinical trials fail? *J. Mol. Cell. Cardiol. 46*, 137–141.

47. Counillon, L., Pouysségur, J., and Reithmeier, R. A. (1994) The Na^+/H^+ exchanger NHE-1 possesses N- and O-linked glycosylation restricted to the first N-terminal extracellular domain. *Biochemistry 33*, 10463–10469.

48. Wakabayashi, S., Bertrand, B., Shigekawa, M., Fafournoux, P., and Pouysségur, J. (1994) Growth factor activation and "H^+-sensing" of the Na^+/H^+ exchanger isoform 1 (NHE1). Evidence for an additional mechanism not requiring direct phosphorylation. *J. Biol. Chem. 269*, 5583–5588.

49. Sardet, C., Counillon, L., Franchi, A., and Pouysségur, J. (1990) Growth factors induce phosphorylation of the Na^+/H^+ antiporter, glycoprotein of 110 kD. *Science 247*, 723–726.

50. Orlowski, J., Kandasamy, R. A., and Shull, G. E. (1992) Molecular cloning of putative members of the Na^+/H^+ exchanger gene family. cDNA cloning, deduced amino acid sequence, and mRNA tissue expression of the rat Na^+/H^+ exchanger NHE-1 and two structurally related proteins. *J. Biol. Chem. 267*, 9331–9339.

51. Wakabayashi, S., Pang, T., Su, X., and Shigekawa, M. (2000) A novel topology model of the human Na^+/H^+ exchanger isoform 1. *J. Biol. Chem. 275*, 7942–7949.

52. Akabas, M. H., Stauffer, D. A., Xu, M., and Karlin, A. (1992) Acetylcholine receptor channel structure probed in cysteine-substitution mutants. *Science 258*, 307–310.

53. Sato, Y., Ariyoshi, N., Mihara, K., and Sakaguchi, M. (2004) Topogenesis of NHE1: direct insertion of the membrane loop and sequestration of cryptic glycosylation and processing sites just after TM9. *Biochem. Biophys. Res. Commun. 324*, 281–287.

54. Sato, Y., and Sakaguchi, M. (2005) Topogenic properties of transmembrane segments of *Arabidopsis thaliana* NHX1 reveal a common topology model of the Na^+/H^+ exchanger family. *J. Biochem. 138*, 425–431.

55. Wakabayashi, S., Hisamitsu, T., Pang, T., and Shigekawa, M. (2003) Mutations of Arg^{440} and Gly^{455}/Gly^{456} oppositely change pH sensing of Na^+/H^+ exchanger 1. *J. Biol. Chem. 278*, 11828–11835.

56. Rimon, A., Tzubery, T., and Padan, E. (2007) Monomers of the NhaA Na^+/H^+ antiporter of *Escherichia coli* are fully functional yet dimers are beneficial under extreme stress conditions at alkaline pH in the presence of Na^+ or Li^+. *J. Biol. Chem. 282*, 26810–26821.

57. Olami, Y., Rimon, A., Gerchman, Y., Rothman, A., and Padan, E. (1997) Histidine 225, a residue of the NhaA-Na^+/H^+ antiporter of *Escherichia coli* is exposed and faces the cell exterior. *J. Biol. Chem. 272*, 1761–1768.

58. Hunte, C., Screpanti, E., Venturi, M., Rimon, A., Padan, E., and Michel, H. (2005) Structure of a Na^+/H^+ antiporter and insights into mechanism of action and regulation by pH. *Nature 435*, 1197–1202.

59. Pornillos, O., and Chang, G. (2006) Inverted repeat domains in membrane proteins. *FEBS Lett. 580*, 358–362.

60. Appel, M., Hizlan, D., Vinothkumar, K. R., Ziegler, C., and Kühlbrandt, W. (2009) Conformations of NhaA, the Na^+/H^+ exchanger from *Escherichia coli*, in the pH-activated and ion-translocating states. *J. Mol. Biol. 386*, 351–365.

61. Olkhova, E., Hunte, C., Screpanti, E., Padan, E., and Michel, H. (2006) Multiconformation continuum electrostatics analysis of the NhaA Na^+/H^+ antiporter of *Escherichia coli* with functional implications. *Proc. Natl. Acad. Sci. U.S.A. 103*, 2629–2634.

62. Arkin, I. T., Xu, H., Jensen, M. Ø., Arbely, E., Bennett, E. R., Bowers, K. J., Chow, E., Dror, R. O., Eastwood, M. P., Flitman-Tene, R., Gregersen, B. A., Klepeis, J. L., Kolossváry, I., Shan, Y., and Shaw, D. E. (2007) Mechanism of Na^+/H^+ antiporting. *Science 317*, 799–803.

63. Tzubery, T., Rimon, A., and Padan, E. (2004) Mutation E252C increases drastically the K_m value for Na^+ and causes an alkaline shift of the pH dependence of NhaA Na^+/H^+ antiporter of *Escherichia coli*. *J. Biol. Chem. 279*, 3265–3272.

64. Kozachkov, L., Herz, K., and Padan, E. (2007) Functional and structural interactions of the transmembrane domain X of NhaA, Na^+/H^+ antiporter of *Escherichia coli*, at physiological pH. *Biochemistry 46*, 2419–2430.

65. Maes, M., Rimon, A., Kozachkov-Magrisso, L., Friedler, A., and Padan, E. (2012) Revealing the ligand binding site of NhaA Na^+/H^+ antiporter and its pH dependence. *J. Biol. Chem. 287*, 38150–38157.

66. Landau, M., Herz, K., Padan, E., and Ben-Tal, N. (2007) Model structure of the Na^+/H^+ exchanger 1 (NHE1): functional and clinical implications. *J. Biol. Chem. 282*, 37854–37863.

67. Shrode, L. D., Gan, B. S., D'Souza, S. J., Orlowski, J., and Grinstein, S. (1998) Topological analysis of NHE1, the ubiquitous Na^+/H^+ exchanger using chymotryptic cleavage. *Am. J. Physiol. 275*, C431–C439.

68. Schushan, M., Xiang, M., Bogomiakov, P., Padan, E., Rao, R., and Ben-Tal, N. (2010) Model-guided mutagenesis drives functional studies of human NHA2, implicated in hypertension. *J. Mol. Biol. 396*, 1181–1196.

69. Goswami, P., Paulino, C., Hizlan, D., Vonck, J., Yildiz, O., and Kühlbrandt, W. (2011) Structure of the archaeal Na^+/H^+ antiporter NhaP1 and functional role of transmembrane helix 1. *EMBO J. 30*, 439–449.

70. Miyazaki, E., Sakaguchi, M., Wakabayashi, S., Shigekawa, M., and Mihara, K. (2001) NHE6 protein possesses a signal peptide destined for endoplasmic reticulum membrane and localizes in secretory organelles of the cell. *J. Biol. Chem. 276*, 49221–49227.

71. Hu, N.-J., Iwata, S., Cameron, A. D., and Drew, D. (2011) Crystal structure of a bacterial homologue of the bile acid sodium symporter ASBT. *Nature 478*, 408–411.

72. Moncoq, K., Kemp, G., Li, X., Fliegel, L., and Young, H. S. (2008) Dimeric structure of human Na^+/H^+ exchanger isoform 1 overproduced in *Saccharomyces cerevisiae*. *J. Biol. Chem. 283*, 4145–4154.

73. Fafournoux, P., Noël, J., and Pouysségur, J. (1994) Evidence that Na^+/H^+ exchanger isoforms NHE1 and NHE3 exist as stable dimers in membranes with a high degree of specificity for homodimers. *J. Biol. Chem. 269*, 2589–2596.

74. Núñez-Ramírez, R., Sánchez-Barrena, M. J., Villalta, I., Vega, J. F., Pardo, J. M., Quintero, F. J., Martinez-Salazar, J., and Albert, A. (2012) Structural insights on the plant salt-overly-sensitive 1 (SOS1) Na^+/H^+ antiporter. *J. Mol. Biol. 424*, 283–294.

75. Herz, K., Rimon, A., Jeschke, G., and Padan, E. (2009) β-sheet-dependent dimerization is essential for the stability of NhaA Na^+/H^+ antiporter. *J. Biol. Chem. 284*, 6337–6347.

76. Hisamitsu, T., Yamada, K., Nakamura, T. Y., and Wakabayashi, S. (2007) Functional importance of charged residues within the putative intracellular loops in pH regulation by Na^+/H^+ exchanger NHE1. *FEBS J. 274*, 4326–4335.

77. Lacroix, J., Poët, M., Maehrel, C., and Counillon, L. (2004) A mechanism for the activation of the Na/H exchanger NHE-1 by cytoplasmic acidification and mitogens. *EMBO Rep. 5*, 91–96.

78. Murtazina, R., Booth, B. J., Bullis, B. L., Singh, D. N., and Fliegel, L. (2001) Functional analysis of polar amino-acid residues in membrane associated regions of the NHE1 isoform of the mammalian Na^+/H^+ exchanger. *Eur. J. Biochem. 268*, 4674–4685.

79. Khadilkar, A., Iannuzzi, P., and Orlowski, J. (2001) Identification of sites in the second exomembrane loop and ninth transmembrane helix of the mammalian Na^+/H^+ exchanger important for drug recognition and cation translocation. *J. Biol. Chem. 276*, 43792–43800.

80. Wang, J., Sahoo, D., Sykes, B. D., and Ryan, R. O. (1998) NMR evidence for a conformational adaptation of apolipophorin III upon lipid association. *Biochem. Cell Biol. 76*, 276–283.

81. Gebreselassie, D., Rajarathnam, K., and Fliegel, L. (1998) Expression, purification, and characterization of the carboxyl-terminal region of the Na^+/H^+ exchanger. *Biochem. Cell Biol. 76*, 837–842.

82. Hisamitsu, T., Pang, T., Shigekawa, M., and Wakabayashi, S. (2004) Dimeric interaction between the cytoplasmic domains of the Na^+/H^+ exchanger NHE1 revealed by symmetrical intermolecular cross-linking and selective co-immunoprecipitation. *Biochemistry 43*, 11135–11143.

83. Nørholm, A.-B., Hendus-Altenburger, R., Bjerre, G., Kjaergaard, M., Pedersen, S. F., and Kragelund, B. B. (2011) The intracellular distal tail of the Na^+/H^+ exchanger NHE1 is intrinsically disordered: implications for NHE1 trafficking. *Biochemistry 50*, 3469–3480.

84. Mishima, M., Wakabayashi, S., and Kojima, C. (2007) Solution structure of the cytoplasmic region of Na^+/H^+ exchanger 1 complexed with essential cofactor calcineurin B homologous protein 1. *J. Biol. Chem. 282*, 2741–2751.

85. Ben Ammar, Y., Takeda, S., Sugawara, M., Miyano, M., Mori, H., and Wakabayashi, S. (2005) Crystallization and preliminary crystallographic analysis of the human calcineurin homologous protein CHP2 bound to the cytoplasmic region of the Na^+/H^+ exchanger NHE1. *Acta Crystallogr., Sect. F: Struct. Biol. Cryst. Commun. 61*, 956–958.

86. Köster, S., Pavkov-Keller, T., Kühlbrandt, W., and Yildiz, Ö. (2011) Structure of human Na^+/H^+ exchanger NHE1 regulatory region in complex with calmodulin and Ca^{2+}. *J. Biol. Chem. 286*, 40954–40961.

87. Li, X., Ding, J., Liu, Y., Brix, B. J., and Fliegel, L. (2004) Functional analysis of acidic amino acids in the cytosolic tail of the Na^+/H^+ exchanger. *Biochemistry 43*, 16477–16486.

88. Li, X., Khan, M. F., Schriemer, D. C., and Fliegel, L. (2013) Structural changes in the C-terminal regulatory region of the Na^+/H^+ exchanger mediate phosphorylation induced regulation. *J. Mol. Cell. Cardiol.* In press.

89. Bordag, N., and Keller, S. (2010) α-helical transmembrane peptides: a "divide and conquer" approach to membrane proteins. *Chem. Phys. Lipids 163*, 1–26.

90. Popot, J. L., and Engelman, D. M. (1990) Membrane protein folding and oligomerization: the two-stage model. *Biochemistry 29*, 4031–4037.

91. Singer, S. J. (1990) The structure and insertion of integral proteins in membranes. *Annu. Rev. Cell Biol. 6*, 247–296.

92. White, S. H., Ladokhin, A. S., Jayasinghe, S., and Hristova, K. (2001) How membranes shape protein structure. *J. Biol. Chem. 276*, 32395–32398.

93. Katragadda, M., Alderfer, J. L., and Yeagle, P. L. (2001) Assembly of a polytopic membrane protein structure from the solution structures of overlapping peptide fragments of bacteriorhodopsin. *Biophys. J. 81*, 1029–1036.

94. Katragadda, M., Chopra, A., Bennett, M., Alderfer, J. L., Yeagle, P. L., and Albert, A. D. (2001) Structures of the transmembrane helices of the G-protein coupled receptor, rhodopsin. *J. Pept. Res. 58*, 79–89.

95. Katragadda, M., Alderfer, J. L., and Yeagle, P. L. (2000) Solution structure of the loops of bacteriorhodopsin closely resembles the crystal structure. *Biochim. Biophys. Acta, Biomembr. 1466*, 1–6.

96. Potetinova, Z., Tantry, S., Cohen, L. S., Caroccia, K. E., Arshava, B., Becker, J. M., and Naider, F. (2012) Large multiple transmembrane domain fragments of a G protein-coupled receptor: biosynthesis, purification, and biophysical studies. *Biopolymers 98*, 485–500.

97. Cohen, L. S., Arshava, B., Neumoin, A., Becker, J. M., Güntert, P., Zerbe, O., and Naider, F. (2011) Comparative NMR analysis of an 80-residue G protein-coupled receptor fragment in two membrane mimetic environments. *Biochim. Biophys. Acta, Biomembr. 1808*, 2674–2684.

98. Naider, F., Arshava, B., Ding, F. X., Arevalo, E., and Becker, J. M. (2001) Peptide fragments as models to study the structure of a G-protein coupled receptor: the α-factor receptor of *Saccharomyces cerevisiae*. *Biopolymers 60*, 334–350.

99. Slepkov, E. R., Rainey, J. K., Li, X., Liu, Y., Cheng, F. J., Lindhout, D. A., Sykes, B. D., and Fliegel, L. (2005) Structural and functional characterization of transmembrane segment IV of the NHE1 isoform of the Na^+/H^+ exchanger. *J. Biol. Chem. 280*, 17863–17872.

100. Ding, J., Rainey, J. K., Xu, C., Sykes, B. D., and Fliegel, L. (2006) Structural and functional characterization of transmembrane segment VII of the Na^+/H^+ exchanger isoform 1. *J. Biol. Chem. 281*, 29817–29829.

101. Reddy, T., Ding, J., Li, X., Sykes, B. D., Rainey, J. K., and Fliegel, L. (2008) Structural and functional characterization of transmembrane segment IX of the NHE1 isoform of the Na^+/H^+ exchanger. *J. Biol. Chem. 283*, 22018–22030.

102. Lindhout, D. A., Thiessen, A., Schieve, D., and Sykes, B. D. (2003) High-yield expression of isotopically labeled peptides for use in NMR studies. *Protein Sci. 12*, 1786–1791.

103. Melnyk, R. A., Partridge, A. W., Yip, J., Wu, Y., Goto, N. K., and Deber, C. M. (2003) Polar residue tagging of transmembrane peptides. *Biopolymers 71*, 675–685.

104. Henry, G. D., and Sykes, B. D. (1994) Methods to study membrane protein structure in solution. *Methods Enzymol. 239*, 515–535.

105. Counillon, L., Franchi, A., and Pouysségur, J. (1993) A point mutation of the Na^+/H^+ exchanger gene (NHE1) and amplification of the mutated allele confer amiloride resistance upon chronic acidosis. *Proc. Natl. Acad. Sci. U.S.A. 90*, 4508–4512.

106. Counillon, L., Noël, J., Reithmeier, R. A., and Pouysségur, J. (1997) Random mutagenesis reveals a novel site involved in inhibitor interaction within the fourth transmembrane segment of the Na^+/H^+ exchanger-1. *Biochemistry 36*, 2951–2959.

107. Touret, N., Poujeol, P., and Counillon, L. (2001) Second-site revertants of a low-sodium-affinity mutant of the Na^+/H^+ exchanger reveal the participation of TM4 into a highly constrained sodium-binding site. *Biochemistry 40*, 5095–5101.

108. Pedersen, S. F., King, S. A., Nygaard, E. B., Rigor, R. R., and Cala, P. M. (2007) NHE1 inhibition by amiloride- and benzoylguanidine-type compounds. Inhibitor binding loci deduced from chimeras of NHE1 homologues with endogenous differences in inhibitor sensitivity. *J. Biol. Chem. 282*, 19716–19727.

109. Slepkov, E., Ding, J., Han, J., and Fliegel, L. (2007) Mutational analysis of potential pore-lining amino acids in TM IV of the Na^+/H^+ exchanger. *Biochim. Biophys. Acta, Biomembr. 1768*, 2882–2889.

110. Slepkov, E. R., Chow, S., Lemieux, M. J., and Fliegel, L. (2004) Proline residues in transmembrane segment IV are critical for activity, expression and targeting of the Na^+/H^+ exchanger isoform 1. *Biochem. J. 379*, 31–38.

111. Slepkov, E. R., Rainey, J. K., Sykes, B. D., and Fliegel, L. (2007) Structural and functional analysis of the Na^+/H^+ exchanger. *Biochem. J. 401*, 623–633.

112. Aurora, R., and Rose, G. D. (1998) Helix capping. *Protein Sci. 7*, 21–38.

113. Padan, E., Kozachkov, L., Herz, K., and Rimon, A. (2009) NhaA crystal structure: functional-structural insights. *J. Exp. Biol. 212*, 1593–1603.

114. Cordes, F. S., Bright, J. N., and Sansom, M. S. P. (2002) Proline-induced distortions of transmembrane helices. *J. Mol. Biol. 323*, 951–960.

115. Yohannan, S., Faham, S., Yang, D., Whitelegge, J. P., and Bowie, J. U. (2004) The evolution of transmembrane helix kinks and the structural diversity of G protein-coupled receptors. *Proc. Natl. Acad. Sci. U.S.A. 101*, 959–963.

116. Reddy, T., Li, X., Fliegel, L., Sykes, B. D., and Rainey, J. K. (2010) Correlating structure, dynamics, and function in transmembrane segment VII of the Na^+/H^+ exchanger isoform 1. *Biochim. Biophys. Acta, Biomembr. 1798*, 94–104.

117. Ding, J., Ng, R. W. P., and Fliegel, L. (2007) Functional characterization of the transmembrane segment VII of the NHE1 isoform of the Na^+/H^+ exchanger. *Can. J. Physiol. Pharmacol. 85*, 319–325.

118. Lee, B. L., Li, X., Liu, Y., Sykes, B. D., and Fliegel, L. (2009) Structural and functional analysis of transmembrane XI of the NHE1 isoform of the Na^+/H^+ exchanger. *J. Biol. Chem. 284*, 11546–11556.

119. Noël, J., Germain, D., and Vadnais, J. (2003) Glutamate 346 of human Na^+/H^+ exchanger NHE1 is crucial for modulating both the affinity for Na^+ and the interaction with amiloride derivatives. *Biochemistry 42*, 15361–15368.

120. Wang, D., Balkovetz, D. F., and Warnock, D. G. (1995) Mutational analysis of transmembrane histidines in the amiloride-sensitive Na^+/H^+ exchanger. *Am. J. Physiol. 269*, C392–C402.

121. Diab, M., Rimon, A., Tzubery, T., and Padan, E. (2011) Helix VIII of NhaA Na^+/H^+ antiporter participates in the periplasmic cation passage and pH regulation of the antiporter. *J. Mol. Biol. 413*, 604–614.

Chapter 2

Methods

Portions of this chapter have been published elsewhere in modified form:

- Lee, B. L., Li, X., Liu, Y., Sykes, B. D., and Fliegel, L. (2009) Structural and functional analysis of extracellular loop 2 of the Na^+/H^+ exchanger. *Biochim. Biophys. Acta, Biomembr. 1788*, 2481–2488.
- Tzeng, J., Lee, B. L., Sykes, B. D., and Fliegel, L. (2011) Structural and functional analysis of critical amino acids in TM VI of the NHE1 isoform of the Na^+/H^+ exchanger. *Biochim. Biophys. Acta, Biomembr. 1808*, 2327–2335.

The NMR and structural methods were written by BLL and BDS, and the functional methods were written by YL, XL, JT, and LF.

Introduction

The experimental procedures used in Chapters 3–7 describing the structural and functional analysis of the single TM helices and extracellular loops are similar. To avoid repetition, these methods are detailed in this chapter. The first half describes the functional analysis of mutations to NHE1 in cells. The second half describes the procedures for the NMR structural analysis of peptides representing fragments of NHE1 TMs and extracellular loops. Figure 2-1 shows a flowchart of the general methods used in studying the transmembrane helices of NHE1. Some additional methods are described in Chapters 6 and 7 that are used specifically in those chapters. The procedures for the expression and purification of peptides fused to maltose binding protein are described in Chapters 8 and 9, and are also used for peptides in Chapter 10 and Appendix D.

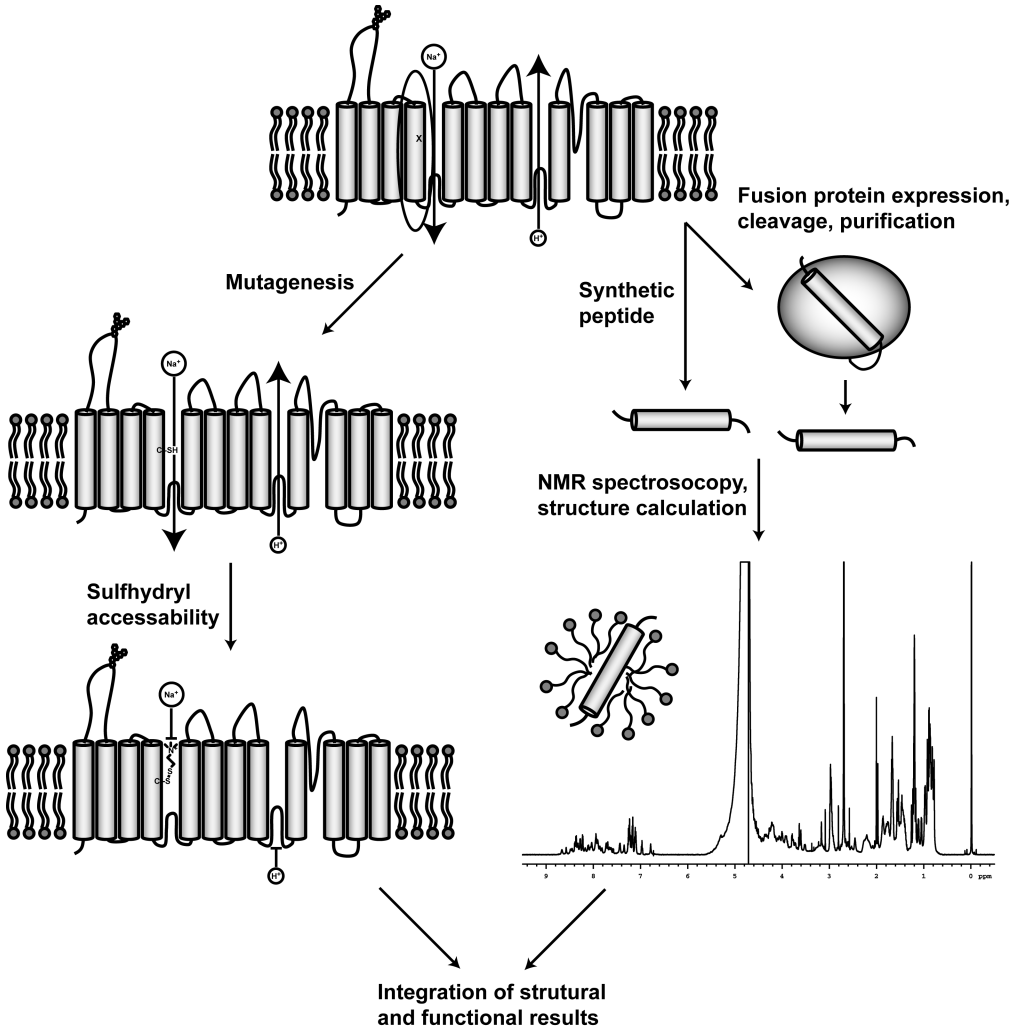

Figure 2-1. Flow chart of the structural and functional analysis of NHE1.

Functional methods

The function of NHE1 was investigated through site directed mutagenesis and characterization of mutant NHE1 exchangers in cultured cells. Individual amino acids were usually mutated to cysteine, which also allowed for cysteine accessibility assays, or alanine, as a more non-disruptive mutation. Occasionally other amino acids mutations were tested as well. The activity of the mutants were determined by examining the recovery of the cells from an acute acid load. Since mutations could affect not only the activity but the correct folding and processing of NHE1, western blots were used to quantify the amounts of total and plasma membrane localized protein, and the activity normalized against these values. In addition to the basal activity of the mutants, changes in activity with or without inhibitors suggest roles for the mutated residue in inhibitor binding. Changes in activity upon the addition of the sulfhydryl reactive compounds MTSET or MTSES to cysteine mutants can suggest a pore lining location for those residues.

Site-directed mutagenesis

Mutations were made to an expression plasmid (pYN4+) containing a hemagglutinin (HA)-tagged human NHE1 isoform of the Na^+/H^+ exchanger. The plasmid contained the cDNA for the entire coding region of the Na^+/H^+ exchanger and it has been previously demonstrated that the tagged expressed protein functions normally (*1*). The plasmid also contains an ampicillin resistance gene for bacterial selection and a neomycin resistance gene for mammalian cell culture selection. Studies in which amino acids were mutated to cysteine utilized a cysteine-less NHE1 protein which had all of the native cysteines mutated to serine (*2*). The activity of the cysteine-less protein was not found to be significantly different from the activity of the wild-type protein. Studies in which mutations were made to alanine or other amino acids utilized the wild-type NHE1 sequence containing cysteines. The specific mutations and the primers used are listed in tables in the respective chapters. Site-directed mutagenesis was performed using PCR amplification by PWO DNA polymerase (Roche Molecular Biochemicals) and using the Stratagene (La Jolla, CA) QuikChange™ site-directed mutagenesis kit. Mutations created or deleted a restriction enzyme site and the fidelity of DNA amplification was confirmed by DNA sequencing.

Cell culture and stable transfection

Stable cell lines of all mutants were made as described earlier (*1*) via transfection with Lipofectamine™ 2000 Reagent (Invitrogen Life Technologies, Carlsbad, CA, USA). (Lipofectamine™ forms cationic liposomes that aid in the passage of the negatively charged nucleic acids through the negatively charged plasma membrane (*3*).) AP-1 cells are a Chinese hamster ovary cell line that lacks an endogenous Na^+/H^+ exchanger. They were used to examine NHE1 activity and were routinely grown in a humidified atmosphere of 5% CO_2 and 95% air in α-MEM supplemented with 10% (v/v) bovine growth serum, 25 mM HEPES, penicillin (100 U/mL) and streptomycin (100 µg/mL), pH 7.4 at 37 °C. The transfection and selection of stable cell lines was carried out as described previously and transfection was done with Lipofectamine™ 2000 Reagent (*2*). Briefly, 1.0×10^6 cells were seeded in 60 mm Petri dish, in 4 mL of growth media. Cells were grown until 90% confluent and transfected with 10 µg of wild type or mutant plasmids. Post transfection, cells were trypsinized, diluted 10 or 100 times with α-MEM medium and plated in 100 mm dishes in α-MEM media containing 800 µg/mL geneticin (G418) that was used to maintain selection pressure without acute acid load selection. pYN4+ plasmid encoded a neomycin resistance gene, which allowed the selection of transfected cells using geneticin (G418) antibiotics. After the initial selection, single clones of transfected cells were obtained and stable cell lines were maintained in 400 µg/mL G418 and were regularly re-established from frozen stocks at passage numbers between 5 and 15. Results shown are from at least two independently obtained clones for each mutant cell line.

SDS-PAGE and immunoblotting

Cells were cultured in 60 or 35 mm dishes until 80–90% confluent, and then were harvested as described earlier (*4*). Growth medium was removed by aspiration and cell monolayers were washed with 4 °C phosphate-buffered saline. Plates were kept on ice to reduce protein degradation. RIPA Lysis buffer (1% NP-40, 0.25% sodium deoxycholate, 0.1% Triton X-100, 5 mM EGTA, 0.1 mM phenylmethylsulfonyl fluoride, 0.1 mM benzamidine, protease inhibitor cocktail) was added to AP-1 cells for 1–3 min. Cell debris were removed by centrifugation at 14,000 rpm for 5 min at 4 °C. Supernatants were kept in clean eppendorf tubes and they were either frozen for −80 °C storage or prepared for SDS-PAGE. Cell lysates containing NHE1 were resolved on 10% SDS/polyacrylamide gels. For Western blot analysis

equal amounts of up to 100 µg of each cell lysate sample was resolved on 10% SDS-polyacrylamide gels. Proteins were transferred onto nitrocellulose membrane (BioRad) and detected using anti-HA monoclonal antibody. The secondary antibody was peroxidase-conjugated goat anti-mouse antibody. NHE1 was visualized by enhanced chemiluminescence (Amersham enhanced chemiluminescence Western blotting and detection system), and X-ray films (Fuji medical X-ray film) were processed by Kodak XOMAT 2000 M35 processor. ImageJ software (National Institutes of Health, Bethesda, MD, USA) was used to quantify band intensities.

Cell surface expression

Targeting of NHE1 to the cell surface was examined essentially as described earlier (*2*, *4*). Cells were grown to 50–70% confluence in 60 mm dishes. The plates were placed on ice, washed once with 4 °C PBS followed by a second wash with 4 °C borate buffer pH 9 (154 mM NaCl, 7.2 mM KCl, 1.8 mM $CaCl_2$, 10 mM boric acid). 3 mL of freshly made sulpho-NHS-SS-Biotin (Pierce Chemical Company, Rockford, IL, USA), which reacts with primary amine groups and interacts with streptavidin resin, at a concentration of 0.5 mg/mL in borate buffer was added to each plate and cells were incubated for 30 min at 4 °C. Cells were then washed 3 times with cold quenching buffer pH 8.3 (192 mM glycine, 25 mM Tris) on ice. Solubilization of cells was achieved by addition of 500 µL IP lysis buffer pH 7.5 (1% (w/v) deoxycholic acid, 1% (w/v) Triton X-100, 0.1% (w/v) SDS, 150 mM NaCl, 1 mM EDTA, 10 mM Tris/Cl, 0.1 mM phenylmethylsulfonyl fluoride, 0.1 mM benzamidine, and lab-made protease inhibitor cocktail). Cell debris was removed by centrifugation at $16{,}000 \times g$ at 4 °C for 20 min. Supernatants were transferred into two equal 200 µL fractions in eppendorf tubes, to a "Total" fraction and an "Unbound" fraction. We have found (*2*, *4*) that bound labelled NHE1 does not reliably elute from streptavidin resin so we examined total and unbound fractions. In the unbound fraction, 50 µL of immobilized streptavidin resin was added to bind the biotin labelled proteins. Unbound fractions were then incubated at 4 °C overnight with gentle rocking. The supernatant containing unbound NHE1 were collected the following day by centrifugation at $16{,}000 \times g$ for 2 min to pellet the bound NHE1. 25 µL of the total fraction and 28 µL of unbound fraction were loaded on 10% acrylamide gels for SDS-PAGE. NHE1 was detected by western blotting. Calculations of surface targeting and corrections for activity were for the fully glycosylated protein.

Na^+/H^+ exchange activity

NHE1 activity was measured using a PTI Deltascan spectrofluorometer as described earlier (*4*). Stably transfected cells were seeded on glass coverslips (2×10^5 cells per coverslip) and grown until they reached 80–90% confluency. The coverslip was then transferred to a cuvette holder with constant stirring at 37 °C. The cells were loaded with 0.15 µg/mL 2′,7′-bis-(2-carboxyethyl)-5(6)-carboxyfluorescein acetoxymethyl ester (BCECF-AM) as a fluorescent pH indicator and incubated in "Normal buffer" (135 mM NaCl, 5 mM KCl, 1 mM $MgCl_2$, 1.8 mM $CaCl_2$, 5.5 mM glucose, and 10 mM HEPES, pH 7.4) at 37 °C. Normal buffer is nominally bicarbonate free. BCECF-AM is uncharged and can penetrate the cell membrane. Intracellular esterases cleave the AM group, trapping the now charged molecule inside the cell. Intracellular acidosis was induced by NH_3/NH_4^+ prepulse/withdrawal: incubation for 3 min in "Normal buffer" supplemented with 50 mM NH_4Cl, pH 7.4, followed by incubation for 30 sec in "Na^+-free buffer" (135 mM N-methyl-D-glucamine, 5 mM KCl, 1.8 mM $CaCl_2$, 1 mM $MgCl_2$, 5.5 mM glucose, and 10 mM HEPES, pH 7.4). An equilibrium of $NH_3 + H^+ \rightleftharpoons NH_4^+$ is established across the membrane via the uncharged and membrane permeable NH_3 species. Entry of NH_3 into the cell and equilibration with NH_4^+ transiently increases intracellular pH. Removal of NH_3/NH_4^+ from the extracellular side results in rapid exit of NH_3 and intracellular acidification due to excess H^+ left within the cell. Intracellular pH (pH_i) recovery and fluorescence measurement was in "Normal buffer" allowing the cells to recover for at least 3 min. There were no differences in buffering capacities of stable cell lines. Following pH_i recovery for every experiment, a three-point pH calibration curve was made using the K^+/nigericin method with Na^+-free calibration buffers (5 mM *N*-methyl-D-glucamine, 135 mM KCl, 1.8 mM $CaCl_2$, 1 mM $MgSO_4$, 5.5 mM glucose, 10 mM HEPES, at pH 6, 7, and 8) and 10 µM nigericin (*5*). Buffering capacity of cells was determined as described earlier (*5*, *6*) and proton flux via NHE1 was determined using the slope of the first 20 seconds of the recovery period. Other kinetic parameters of the Na^+/H^+ exchanger were determined essentially as described earlier (*5*, *6*). Because we earlier found that growth conditions affect the absolute level of NHE1 activity, experiments comparing the activities of wild type and NHE1 mutants were done in pairs or groups, so that all comparisons of activity were done with cells grown to the same confluence and with the same media.

For some experiments, Na^+ and Li^+ concentrations were varied while maintaining osmolarity with *N*-methyl-D-glucamine. In other experiments we investigated

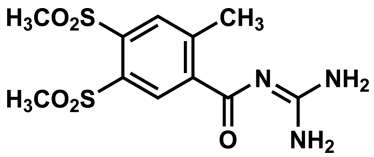

Figure 2-2. NHE1 inhibitor EMD87580.

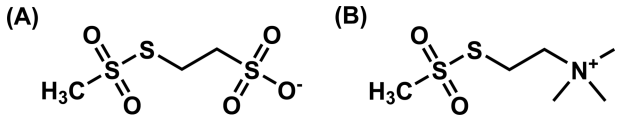

Figure 2-3. Sulfhydryl reactive reagents. (A) 2-Sulfonatoethyl methanethiosulfonate (MTSES). (B) (2-(Trimethylammonium)ethyl) methanethiosulfonate (MTSET).

the inhibitor sensitivity of some mutants. Cells were treated with the highly selective NHE1 inhibitor EMD87580 (Figure 2-2) at varying concentrations (*7*). EMD87580 was dissolved in water and the inhibitory effect of EMD87580 was measured using a dual-pulse acidification assay. In this assay, cells were treated with ammonium chloride two times as described above and allowed to recover in NaCl containing medium following each pulse. The first pulse and recovery is in the absence of EMD87580 while the second pulse recovery is in the presence of inhibitor. To calculate residual activity during recovery from acidosis the following formula was used:

$$\%\text{Residual activity} = \frac{\text{Proton flux with reagent}}{\text{Proton flux without reagent}} \times 100\%$$

The rate of recovery from acid load is compared $\pm$ inhibitor. Results are shown as mean $\pm$ S.E. and statistical significance was determined using a Wilcoxon-Mann-Whitney Rank Sum test. IC_{50} values were calculated as described earlier (*8*). Differences between the IC_{50} values of mutants was determined by a Holm-Sidak post hoc test. The extracellular accessibility of cysteine mutants to the sulfhydryl reactive reagents (2-(trimethylammonium)ethyl) methanethiosulfonate (MTSET) or 2-sulfonatoethyl methanethiosulfonate (MTSES) (Figure 2-3) were also performed using the two pulse acidification assay. After recovery from the first pulse, the cells are incubated with 10 mM MTSET or MTSES in Normal buffer for 10 min, then the second pulse was performed as above.

Structural methods

We adopted the "divide and conquer" approach to investigating the structure of NHE1. Chemically synthesized peptides were purchased in the case of smaller

or difficult to express peptides. Larger peptides were overexpressed in *E. coli*, by fusion to a larger, soluble protein which can help to prevent peptide degradation, aid in solubility and purification. Expression in bacteria also allows for ^{15}N, ^{13}C, and/or ^{2}H isotopic labelling for NMR studies. The fusion protein expression is detailed in later chapters. The purified transmembrane peptides were dissolved in conditions that would mimic the hydrophobic environment of a lipid bilayer, such as organic solvents or detergent micelles. The structures of the peptides could then be determined using standard solution state NMR methods.

Peptide synthesis and purification

Peptides representing the transmembrane segment or extracellular loop of interest was purchased from GI Biochem (Shanghai) Ltd. or the Alberta Peptide Institute (for EL 2) crude or at ∼95% purity. Crude peptide was purified at the Institute for Biomolecular Design at the University of Alberta using HPLC. Peptide purity and identity was assessed with HPLC, matrix-assisted laser desorption ionization mass spectrometry and assignment of the NMR spectra. The peptide sequences were initially based on the sequences predicted by the topology model of Wakabayashi et al. (*9*), and were sometimes lengthened to include charged residues which more clearly signified the end of a transmembrane helix. The boundaries of the TM helices studied in this thesis were approximately the same in both the Wakabayashi (*9*) and Landau (*10*) models. For the hydrophobic transmembrane sequences, additional lysine residues were added to each termini as this has been shown to improve solubility and handling during purification (*11*, *12*). The extracellular loop peptides did not contain lysine tags but instead contained an N-terminal acetyl group and a C-terminal amide group to remove the positive and negative charges from the termini that would not be found in the native, full length sequence.

NMR sample preparation and spectroscopy

Samples for NMR spectroscopy were prepared by dissolving 1–2 mM lyophilized transmembrane peptide in DPC-d_{38} in 95% H_2O, 5% D_2O to provide a deuterium signal for the spectrometer frequency lock, and 0.25 mM deuterated 2,2-dimethyl-2-silapentane-5-sulfonic acid (DSS-d_6) (Chenomx Inc.) as an internal NMR standard. The amount of membrane mimetic detergent used was calculated such that the sample had the same or greater *micellar* concentration compared to peptide concentration. Assuming 50–75 molecules of DPC (dodecylphosphocholine)

detergent per micelle, this resulted in a 1:75 molar ratio of peptide to detergent. Larger amounts of detergent were used for SDS (sodium dodecylsulfate) samples (primarily TM V–VII) and DMPC (dihexanoyl phosphatidylcholine) samples (attempted with TM VI–VII) due to their higher critical micellar concentrations (CMC) (8–15 mM vs. 1 mM for DPC), whose amount does not contribute to the micelles. Deuterated DPC and SDS were used for non-labelled peptides to suppress strong ^{1}H detergent signals that would otherwise interfere in ^{1}H 1D and ^{1}H-^{1}H 2D NMR experiments. Water soluble peptide samples such as for EL 2 contained 95% H_2O, 5% D_2O, 0.35 mM DSS-d_6, 150 mM KCl or NaCl, and between 2–20 mM imidazole as a pH buffer and a NMR-based pH indicator (*13*). The pH of the samples were adjusted to 5 without consideration of the deuterium effects on the glass pH electrode. Samples in organic solvents or solvent-water mixtures contained at least one deuterated organic solvent for the spectrometer lock (usually $CDCl_3$ or isopropanol-d_8 (IPA-d_8)) with the remainder of the solvent components non-deuterated. Some peptide samples were made in neat DMSO-d_6. Organic solvent mixtures containing volatile solvents could be exchanged by evaporation under dry $N_{2(g)}$ or $Ar_{2(g)}$ and/or lyophilization, from which the recovered peptide could be redissolved in different membrane mimetics or organic solvents. Total volumes of the NMR samples ranged from 0.5–0.7 mL for a standard thin-walled 5 mm NMR tube or 0.32 mL for 5 mm Shigemi tubes.

Spectra for peptides were routinely obtained on spectrometers with a ^{1}H frequency of 500 or 600 MHz, while additional 2D or 3D NOESY spectra were often acquired on a cold-probe equipped 800 MHz spectrometer for improved resolution and sensitivity. Initial characterization of the samples used one-dimensional ^{1}H NMR spectra for unlabelled samples or two-dimensional ^{1}H-^{15}N heteronuclear single quantum correlation (HSQC) spectra for ^{15}N labelled samples, primarily looking at the lineshape and chemical shift dispersion of the backbone amide peaks. The peaks in the amide region ($\sim$7–9 ppm) should be sharp and well defined, indicating structural homogeneity in the sample, and well dispersed (> 0.5 ppm), indicating folding of the peptide. Spectra acquired for assignment and structure calculation included two-dimensional ^{1}H-^{1}H double quantum filtered correlation spectroscopy (DQF-COSY), total correlation spectroscopy (TOCSY) (60 ms mixing times), and nuclear Overhauser effect spectroscopy (NOESY) (150–250 ms mixing times) experiments for unlabelled samples. Three-dimensional ^{1}H-^{1}H-^{15}N TOCSY-HSQC and NOESY-HSQC could also be obtained for ^{15}N labelled samples. Experiments were acquired at a temperature of 30 °C. Spectra for EL 2 were acquired at 10 °C. Spectra

were processed using NMRPipe (*14*) and analyzed in NMRView (*15*). The identification and assignment of peaks was performed manually in NMRView. Sequential assignment was performed using acquired spectra using standard methods (*16*). For ^{15}N labelled peptides, 3D HNHA spectra were sometimes acquired to obtain $^{3}J_{\mathrm{HNH}\alpha}$ coupling constants which can be related to the peptide backbone phi dihedral angles.

The peptides used for NMR structure determination were usually chemically synthesized, and were not labelled with ^{13}C or ^{15}N, due to the high cost of labelled amino acids. As such, only homonuclear 1D ^{1}H spectra and 2D ^{1}H-^{1}H correlation spectra could be used. Some peptides were expressed biosyntheically, in *E. coli* as fusion proteins, which allowed for ^{15}N labelling at only a modest increase in cost. Isotopic labelling can provide a additional spectral dimension to resolve crowded regions in the homonuclear spectra. ^{15}N labelling, for example, can can be used to obtain 2D ^{1}H-^{15}N HSQC spectra, which can more clearly resolve the amide peaks compared to ^{1}H-only spectra, and provide a clearer indication of the quality of the protein and NMR sample. Each peak represents an individual amide ^{1}H-^{15}N pair in the sample. The number, dispersion, and width of the peaks can indicate the purity, degree of structuring, or aggregation state of the protein. Isotopic labelling also allows for the acquisition of the 3D analogues to the 2D homonuclear spectra for assignment and structure determination used above, again, to take advantage of the better resolution of peaks the additional ^{15}N or ^{13}C dimension can provide. Many additional experiments have also been developed around isotopically labelled samples. The motional properties of the peptide can be characterized by various ^{15}N relaxation experiments, which are all based on the 2D HSQC experiment, for example.

NMR structure calculations

Structure calculations were performed using the Python scripting interface in Xplor-NIH (*17*) based on the peptide structure calculation protocol developed Rainey et al. (*18*, *19*). NOE restraints for structure calculation were generated within NMRView by calibrating restraints by peak intensity and sorting them into distance ranges of strong (1.8–2.8 Å), medium (1.8–3.4 Å), or weak (1.8–5.0 Å). Some restraints were extended into a very weak category (1.8–6.0 Å) as needed during refinement. Calibrated distances for TM VI–VII were not binned but rather the calibrated distance ranges were used directly. Comparison of the chemical shifts of the peptide to random coil chemical shifts (*20*, *21*) were used to predict regions containing alpha-helical secondary structure. Helical dihedral angle restraints

($\phi = -60 \pm 30^\circ$ and $\psi = -40 \pm 40^\circ$) were added to regions that were helical based on both structure calculation and chemical shifts. A soft square-well potential was used for the restraining function in structure calculation to allow for some error in the peak assignments and distance calibration. Ambiguous restraints used the "sum" averaging method in Xplor-NIH (*18*, *22*) to allow for the restraint to match the distance either one or the other of the ambiguous pairs of protons, rather than match some averaged distance between both pairs of protons. In each round of structure calculation, an extended polypeptide was generated and subjected to simulated annealing using the distance restraints and dihedral dihedral angle restraints, with 50 structures generated for each round. After each round, violating restraints were examined and either lengthened or removed. Restraints were increased up to the next binned distance range or increased based on the average magnitude of the violation and the number of structures violating. Initially, violations > 0.5 Å in $> 50\%$ of structures were examined. Refinement of restraints gradually increased in stringency, to where violations > 0.1 Å in $> 10\%$ of structures were examined. Initial structure calculation runs did not include dihedral angle restraints in the helical regions so as not to bias the structure calculations. Later runs included dihedral angle restraints either at a fixed strength or gradually increased then decreased in strength over the course of the iterative runs. 50 structures were calculated in each run and for the final run, the structures were sorted by overall energy and the lowest 50% or more of the structures were kept for analysis.

References

1. Slepkov, E. R., Chow, S., Lemieux, M. J., and Fliegel, L. (2004) Proline residues in transmembrane segment IV are critical for activity, expression and targeting of the Na^+/H^+ exchanger isoform 1. *Biochem. J. 379*, 31–38.
2. Slepkov, E. R., Rainey, J. K., Li, X., Liu, Y., Cheng, F. J., Lindhout, D. A., Sykes, B. D., and Fliegel, L. (2005) Structural and functional characterization of transmembrane segment IV of the NHE1 isoform of the Na^+/H^+ exchanger. *J. Biol. Chem. 280*, 17863–17872.
3. Dalby, B., Cates, S., Harris, A., Ohki, E. C., Tilkins, M. L., Price, P. J., and Ciccarone, V. C. (2004) Advanced transfection with Lipofectamine 2000 reagent: primary neurons, siRNA, and high-throughput applications. *Methods 33*, 95–103.
4. Ding, J., Rainey, J. K., Xu, C., Sykes, B. D., and Fliegel, L. (2006) Structural and functional characterization of transmembrane segment VII of the Na^+/H^+ exchanger isoform 1. *J. Biol. Chem. 281*, 29817–29829.
5. Murtazina, R., Booth, B. J., Bullis, B. L., Singh, D. N., and Fliegel, L. (2001) Functional analysis of polar amino-acid residues in membrane associated regions of the NHE1 isoform of the mammalian Na^+/H^+ exchanger. *Eur. J. Biochem. 268*, 4674–4685.
6. Silva, N. L., Wang, H., Harris, C. V., Singh, D., and Fliegel, L. (1997) Characterization of the Na^+/H^+ exchanger in human choriocarcinoma (BeWo) cells. *Pflugers Arch. 433*, 792–802.
7. Chen, L., Chen, C. X., Gan, X. T., Beier, N., Scholz, W., and Karmazyn, M. (2004) Inhibition and reversal of myocardial infarction-induced hypertrophy and heart failure by NHE-1 inhibition. *Am. J. Physiol.: Heart Circ. Physiol. 286*, H381–H387.
8. Slepkov, E., Ding, J., Han, J., and Fliegel, L. (2007) Mutational analysis of potential pore-lining amino acids in TM IV of the Na^+/H^+ exchanger. *Biochim. Biophys. Acta, Biomembr. 1768*, 2882–2889.
9. Wakabayashi, S., Pang, T., Su, X., and Shigekawa, M. (2000) A novel topology model of the human Na^+/H^+ exchanger isoform 1. *J. Biol. Chem. 275*, 7942–7949.
10. Landau, M., Herz, K., Padan, E., and Ben-Tal, N. (2007) Model structure of the Na^+/H^+ exchanger 1 (NHE1): functional and clinical implications. *J. Biol. Chem. 282*, 37854–37863.
11. Cano-Sanchez, P., Severino, B., Sureshbabu, V. V., Russo, J., Inui, T., Ding, F.-X., Arshava, B., Becker, J., and Naider, F. (2006) Effects of N- and C-terminal addition of oligolysines or native loop residues on the biophysical properties of transmembrane domain peptides from a G-protein coupled receptor. *J. Pept. Sci. 12*, 808–822.

12. Melnyk, R. A., Partridge, A. W., Yip, J., Wu, Y., Goto, N. K., and Deber, C. M. (2003) Polar residue tagging of transmembrane peptides. *Biopolymers 71*, 675–685.

13. Baryshnikova, O. K., Williams, T. C., and Sykes, B. D. (2008) Internal pH indicators for biomolecular NMR. *J. Biomol. NMR 41*, 5–7.

14. Delaglio, F., Grzesiek, S., Vuister, G. W., Zhu, G., Pfeifer, J., and Bax, A. (1995) NMRPipe: a multidimensional spectral processing system based on UNIX pipes. *J. Biomol. NMR 6*, 277–293.

15. Johnson, B. A. (2004) Using NMRView to visualize and analyze the NMR spectra of macromolecules. *Methods Mol. Biol. 278*, 313–352.

16. Wüthrich, K. (1986) *NMR of Proteins and Nucleic Acids*, John Wiely & Sons, New York, NY.

17. Schwieters, C. D., Kuszewski, J. J., Tjandra, N., and Clore, G. M. (2003) The Xplor-NIH NMR molecular structure determination package. *J. Magn. Reson. 160*, 65–73.

18. Rainey, J. K., Fliegel, L., and Sykes, B. D. (2006) Strategies for dealing with conformational sampling in structural calculations of flexible or kinked transmembrane peptides. *Biochem. Cell Biol. 84*, 918–929.

19. Wang, J., Hodges, R. S., and Sykes, B. D. (1995) Generating multiple conformations of flexible peptides in solution on the basis of NMR nuclear Overhauser effect data: application to desmopressin. *J. Am. Chem. Soc. 117*, 8627–8634.

20. Wishart, D. S., Sykes, B. D., and Richards, F. M. (1992) The chemical shift index: a fast and simple method for the assignment of protein secondary structure through NMR spectroscopy. *Biochemistry 31*, 1647–1651.

21. Wishart, D. S., Bigam, C. G., Holm, A., Hodges, R. S., and Sykes, B. D. (1995) ^{1}H, ^{13}C and ^{15}N random coil NMR chemical shifts of the common amino acids. I. Investigations of nearest-neighbor effects. *J. Biomol. NMR 5*, 67–81.

22. Brünger, A. T. (1992) *X-PLOR (Version 3.1) A System for X-ray Crystallography and NMR*, Yale University Press, New Haven, CT.

Chapter 3

Structural and functional analysis of extracellular loop 2 of the Na^+/H^+ exchanger

A version of this chapter has been published as:

- Lee, B. L., Li, X., Liu, Y., Sykes, B. D. and Fliegel, L. (2009) Structural and functional analysis of extracellular loop 2 of the exchanger. *Biochim. Biophys. Acta, Biomembr. 1788*, 2481–2488.

BLL performed the NMR, and XL and YL performed the functional experiments. BDS and LF helped edit the manuscript.

Summary

The extracellular regions of the NHE1 membrane domain are believed to contribute to cation coordination, transport and sensitivity to inhibitors. In this study we characterized the structure and function of extracellular loop 2 (EL 2). Mutation of residues P153, P154 and F155 demonstrated that these residues were critical for efficient NHE1 function. Mutations to Ala resulted in decreases in cation affinity and in decreases in activity of the protein, these were more marked in both P154 and F155. NMR spectroscopy was used to characterize the solution structure of a peptide NAc-G150–F155-NH_2. The peptide showed at least three different conformers in solution due to cis–trans isomerization of the T152–P153 and P153–P154 peptide bonds. The trans-trans conformation appeared to be in an extended conformation, whereas the cis-trans conformation showed a propensity to form a beta turn. Our results show that the EL 2 region is critical to NHE1 function and that a peptide of the EL 2 region can adopt different structures in solution potentially forming a beta turn that is important in function of the full protein. Mutation of P154 could disrupt the beta turn, affecting helix packing and the protein structure and function.

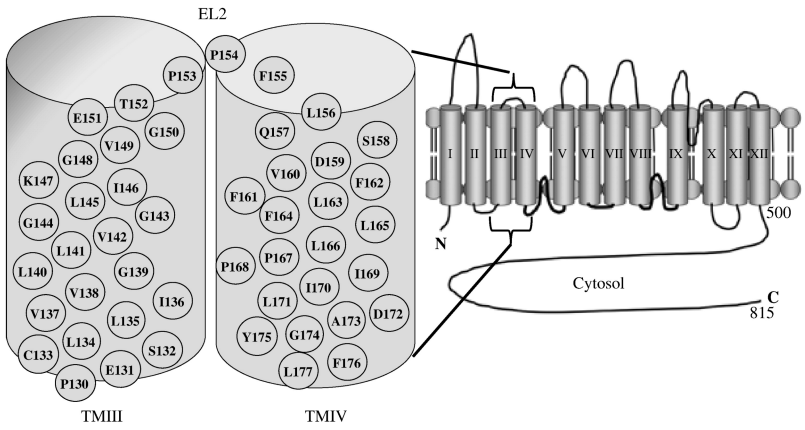

Figure 3-1. Model of the NHE1 isoform of the Na^+/H^+ exchanger. The right panel indicates the topology of the Na^+/H^+ exchanger isoform 1 (*13*) while the left side is an enlargement of illustrating amino acids of TM III–EL 2–TM IV.

Introduction

Mammalian NHE1 plays a key role in regulation of cell pH, cell volume, and cell proliferation; and in metastasis of certain kinds of tumour cells (*1*, *2*). It also promotes cell growth and differentiation (*3*), is critical to cell motility in some cell types (*4*), and regulates sodium fluxes and cell volume after challenge by osmotic shrinkage (*5*). The Na^+/H^+ exchanger also plays a critical causal role in heart hypertrophy and in the damage that occurs during heart ischemia and reperfusion. Inhibition of the exchanger with Na^+/H^+ exchanger inhibitors protects the myocardium (*6–8*).

Although the exact mechanisms of transport and inhibitor binding by NHE1 are not known, specific residues within several regions of the membrane domain as well as several extracellular loops and membrane-associated segments of NHE1 have been implicated as being important for ion binding and transport (reviewed in (*9*)). The membrane-associated segment, extracellular loop (EL) 5 is involved in the drug sensitivity and cation binding and transport (*9*, *10*). Loop regions between α-helices can influence their arrangements and packing (*11*) and extracellular loops of membrane proteins have been shown to modulate their function (*12*).

TM IV immediately follows EL 2 (Figure 3-1). Numerous residues of TM IV have been implicated in NHE1 function and the extramembrane loops at either end of TM IV contain residues that are important for NHE1 function. Early experiments showed that three residues of EL 2 affect both the drug sensitivity and the activity of the exchanger (*14*). Intracellular loop (IL) 2, at the C-terminal end of TM IV, contains residues that may line the ion-transport pore and when mutated to Cys.

Mutation	Oligonucleotide sequence	Restriction site
P153A	5′-GGTGTAGGCGAGAC**ggCgCC**CTTCCTGCAGTCCGAC-3′	NarI
P154A	5′-GGTGTAGGCGAGAC**gCCggCC**TTCCTGCAGTCCGACGTCTTC-3′	NaeI
F155A	5′-GGTGTAGGCGAGACACCCCCCgcC**CTaCAG**TCCGACGTCTTCTTCCTC-3′	(PstI)

Table 3-1. Oligonucleotide primers for site-directed mutagenesis. Mutated nucleotides are in lower case letters. Mutated codons are indicated in bold. Restriction sites removed (in parentheses) or added are in bold. In each case the forward direction of the primer pair is illustrated.

R180 and Q181 are accessible by externally applied MTSET (*13*). Recently, we determined the structure of TM IV which was predominantly not alpha helical, though structured (*15*). F161, in the extracellular side of the bilayer, was a pore lining residue and Pro residues in the middle of the bilayer were critical to function (*15*, *16*). However, in those studies we did not examine the preceding EL 2. In this study we characterize EL 2 in detail. We examined individual amino acids of this extracellular loop and their contribution to differential drug cation sensitivity and cation coordination. In addition we present the first NMR solution structure of an extracellular loop of a mammalian Na^+/H^+ exchanger.

Methods

Mutagenesis was performed as described in Chapter 2. Primers used for mutations are described in Table 3-1. For NMR structural studies, an EL 2 peptide consisting of amino acids G150 to F155 of human NHE1 (sequence, GETPPF; acetyl-capped N-terminus, amide-capped C-terminus) was synthesized by the Alberta Peptide Institute at $> 95\%$ purity. NMR spectroscopy and structure calculation were performed essentially as described, however a 2D ROESY experiment was obtained instead of the 2D NOESY experiment.

Results

Figure 3-1 illustrates a general model of the Na^+/H^+ exchanger (*13*) and an enlargement of TM III–EL 2–TM IV is also shown. Based on our and other reports of the importance of TM IV we conducted further investigation of this region. In particular, we characterized amino acids P153, P154 and F155 of the extracellular loop 2. Prolines may be particularly important in membrane proteins, disrupting α-helices, and introducing flexibility (*16*, *17*). Mutations were made to an expression plasmid containing a full length, tagged human NHE1 isoform of the Na^+/H^+ exchanger. Initially, experiments determined whether these mutant forms

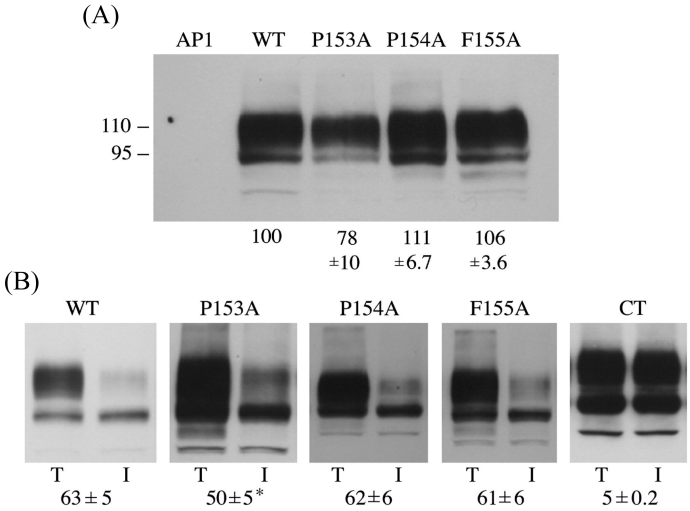

Figure 3-2. Western blot analysis of cell extracts from stable cell lines expressing wild type and mutants of NHE1. (A) Western blot of cell extracts from AP-1 cells transfected with HA-tagged wild-type NHE1 (WT) or transfected with NHE1 mutants P153A (P153A), P154A (P154A) and F155A (F155A). Anti-HA antibody was used to detect tagged NHE1 protein and the amount of NHE1 protein was quantified. Numbers underneath the lanes indicate the mean value ($\pm$ S.D.) of the sum of densitometric scans of both 110 kDa and 95 kDa bands relative to wild-type NHE1 for at least three experiments. (B) Plasma membrane targeting of the Na^+/H^+ exchanger in AP-1 cells transfected with wild-type NHE1 (WT) and with the NHE1 mutants P153A (P153A), P154A (P154A) and F155A (F155A). Sulfo-NHS-SS-biotin-treated cells were lysed and their proteins were solubilized and subsequently treated with streptavidin agarose to bind labelled protein as described in the Methods. Equal samples of total lysates (T) and unbound (representing intracellular) lysates (I) were run on SDS-PAGE and blotted with anti-HA antibody to identify NHE1 protein. Non-specific (CT) refers to an experiment in which non-specific binding to streptavidin-agarose beads was measured by following the standard procedure without labelling cells with biotin. The percent of the total NHE1 protein localized to the plasma membrane is indicated. The results are mean $\pm$ standard error for at least 4 determinations. * indicates significantly reduced plasma membrane targeting in comparison to wild type NHE1 ($p < 0.05$).

of the Na^+/H^+ exchanger expressed and targeted properly. Western blotting using anti tag (HA) antibodies was used to characterize the proteins expression (Figure 3-2, A). AP1 cells transfected with plasmid containing the HA-tagged wild type NHE1 resulted in the presence of an immunoreactive species of 110 kDa, plus a smaller band at 95 kDa that represents an immature form of the exchanger that is not fully glycosylated (*15*). Untransfected cells (Lane 1, AP1) show no such immunoreactivity. The level of expression relative to the wild type Na^+/H^+ exchanger is shown below each mutant. The P153A mutant had significantly decreased expression ($p < 0.05$), 78% of the wild type, while the protein level of P154 and F155A mutants was not significantly different than that of wild type.

Mutation of membrane associated amino acids can affect surface targeting of the Na^+/H^+ exchanger (*15*). Therefore, we examined intracellular targeting of the NHE1 expressing cell lines. After cells were treated with sulfo-NHS-SS-biotin, labelled proteins of lysates were bound to streptavidin-agarose beads. To identify NHE1 protein, we used Western blotting with anti-HA antibody and examined equal amounts of total cell lysates and unbound lysates. This revealed the relative amounts of tagged intracellular NHE1 protein. Figure 3-2, B, illustrates examples of the results and a summary of at least 4 experiments. A majority of the wild-type NHE1 protein was present on the plasma membrane, P154A and F155A proteins had similar level of plasma membrane localization in comparison with the wild type protein. However, P153A did have slightly, but significantly reduced plasma membrane targeting compared to the wild-type NHE1 protein. We noted that non-specific binding of proteins to streptavidin agarose beads was approximately 5%, therefore, our values of NHE1 on the cell surface are an overestimate by this amount. We also analyzed the subcellular distribution of the fully glycosylated and partially or de-glycosylated forms of NHE1 separately (Table 3-S2). This analysis showed that the partially glycosylated form of NHE1 was mostly intracellular and the surface targeting of fully glycosylated NHE1 was therefore 5–10% higher than the values given in Figure 3-2, B. The P153A mutant, was still significantly decreased in its targeting relative to the other mutants.

Since we observed that these mutations did not greatly impair expression or surface targeting of the protein, we examined the activity of the mutant exchangers in comparison with the wild type protein. Figure 3-3 shows both the uncorrected activity (grey bars) and the activity corrected for expression and surface processing (black bars) relative to wild-type NHE1 for the three mutants. All three mutants had significantly decreased activity relative to wild-type NHE1. The P153A mutant

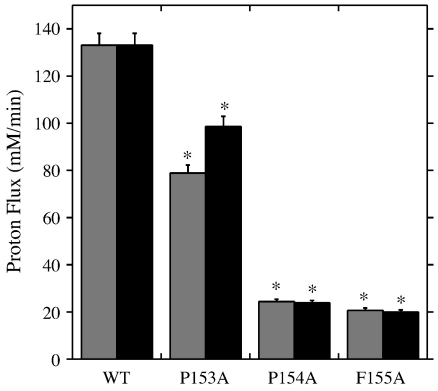

Figure 3-3. Na^+/H^+ exchanger activity of AP1 cells stably transfected with control and NHE1 mutants. NHE activity was measured in 135 mM NaCl as described in Methods in stable cell lines expressing wild type NHE1 (WT) and NHE1 mutant proteins P153A (P153A), P154A (P154A) and F155A (F155A). Initial pH's of the mutant cells after acidification were 6.04, 6.06, 6.07 and 6.07 for the mutant cell lines, respectively, and were not significantly different from one another. Grey bars indicated uncorrected values of NHE1 activity. Black bars indicate activity after correction for the level of expression and surface targeting relative to the WT. Results are relative to the value of the wild type NHE1 protein and are the mean $\pm$ S.E. for 5–7 determinations from two independently made cell lines. * indicates significantly different from the wild type at $p < 0.01$.

was decreased the least of these mutants. When correcting for expression levels and targeting this decrease was reduced.

EMD87580 is a potent and selective NHE1 inhibitor (*18*). Alterations in sensitivity to inhibition have been reported earlier upon mutation of amino acids in transmembrane segments of NHE1 and may indicate important alterations in cation binding or coordination by the protein (*19*, *20*). To determine whether alterations in NHE1 inhibitor sensitivity occurred with the amino acids mutated in this study, we initially tested the effect of 0.7 μM EMD87580 on the mutants. We have earlier determined that this concentration of EMD87580 inhibits approximately 40–50% of the activity of the NHE1 protein (*9*, *21*). The initial pH of recovery varied nominally by an average of less than 0.04 pH units between wild type and mutants. The difference between the starting pH of the first and second pulse varied nominally by an average of 0.009 pH units. Figure 3-4 shows the results comparing the rate of proton flux of the second pulse in the presence of EMD87580 with that of the proton flux in the absence of EMD87580. The P154A mutant had decreased level of inhibition by EMD87580 in comparison to the wild type. To further investigate these results in more detail we characterized the effectiveness of a wide range of

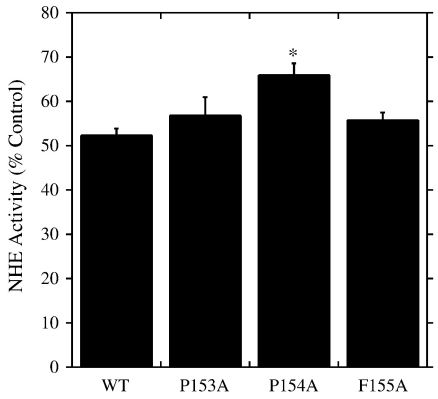

Figure 3-4. Effect of EMD87580 on activity of wild type and NHE1 mutant proteins. NHE1 activity was determined in 135 mM NaCl. The activity was determined in a dual pulse assay in which cells were acidified twice and allowed to recover twice. The relative rates of proton flux were determined and the second pulse in the presence of 0.7 μM EMD87580, was compared to the first. NHE1 (WT); P153A (P153A); P154A (P154A); F155A (F155A). The results are the mean ± S.E. of at least 12 determinations. * indicates significantly different from the wild type at $p < 0.05$.

concentrations of EMD87580 on the mutant NHE1 proteins relative to the control (not shown). In these tests there was also no significant difference in the starting pH_i of recovery or between the starting pH_i in the first and second pulse of recovery. The value of wild type NHE1 IC_{50} was 0.64 μM. The IC_{50} values of P153A and P155A were 0.84 and 0.83 μM respectively, which were not significantly different from the wild type. The resistance of the P154A mutant was increased more than that of the others and it had an IC_{50} of 1.27 μM, a two-fold increase over that of the wild type and was the only statistically significant change ($p < 0.05$).

To gain insights into the nature of the effects of the mutations, we examined their affinity for Na^+ or Li^+ relative to that of the wild type. Ammonium chloride was used to induce acidification and varying levels of NaCl or LiCl were used to allow recovery. Differences in activity between the groups were not due to differences in initial pH following acidification induced by ammonium chloride. Figure 3-5, A, illustrates the effects of altering the Na^+ levels on the activity of the protein. All the mutants had less activity than wild type. The P153A had the most activity of the mutants while the P154A and F155A mutants were reduced more in activation in comparison with the wild type. The K_m for the wild type, P153A, P154A and F155A was 73.3, 74.2, 66.6, and 72.3 mM respectively, which indicated that the affinity for Na^+ was not greatly altered compared to the wild type. The V_{max} values of the wild type and P153A, P154A and F155A mutants were 196, 138, 111 and 56

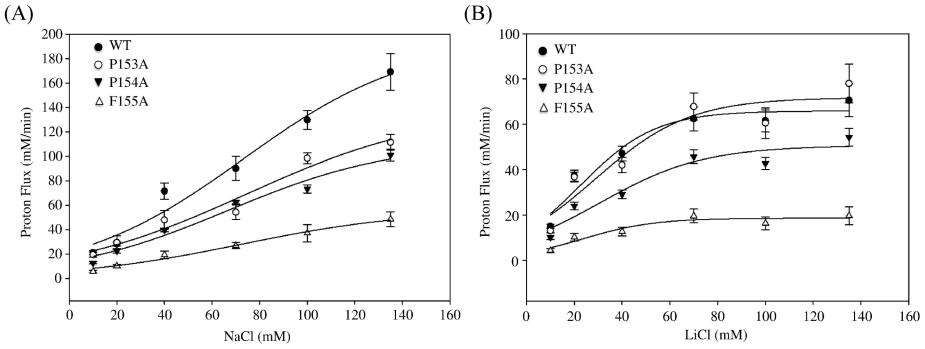

Figure 3-5. Effect of different Na^+ and Li^+ concentration on activity of wild type and NHE1 mutant proteins. NHE1 activity was determined as described in the "Methods" and is shown without correction for expression levels or targeting. (A) Effect of different Na^+ concentrations (10, 20, 40, 70, 100 and 135 mM) on NHE1 activity. (B) Effect of different Li^+ concentrations (10, 20, 40, 70, 100 and 135 mM) on NHE1 activity. All the results are the mean ± S.E. of at least 8 determinations.

mM/min, respectively, suggesting substantial apparent decreases for the mutants. It should be noted that saturating concentrations of NaCl were not necessarily reached due to osmotic considerations with the cells, so the V_{max} values should be noted as estimates only.

Similar experiments were done using LiCl instead of NaCl (Figure 3-5, B). In this case, the proton transport rates were much lower than that of Na^+. The V_{max} for wild type, P153A, P154A and F155A mutants was 66, 71, 51 and 19 mM/min, respectively, indicating a possible decrease in the V_{max} of transport for the P154A mutant and a reduction in activity in the F155A mutant. The K_m for these proteins was 22, 29, 30 and 23 mM, respectively, which again illustrated that the Li^+ transport affinity of the P154A mutant was not greatly altered. It was noted that for the wild type NHE1 protein and the three mutants, by the LiCl concentration of 70 mM activity was maximal and further increases in LiCl did not stimulate NHE1 activity further. It has been previously reported that lower concentrations of LiCl are required for activation of NHE1 in comparison to NaCl concentrations (*9*, *22*).

The peptide representing the predicted extracellular loop 2 of NHE1 was synthesized with N-terminal acetate and C-terminal amide caps to remove charges at the peptide termini that would not be present in the full protein. NMR spectra were acquired with a sample containing 0.1 M KCl; however, the extracellular loop would normally be exposed to a higher concentration of Na^+ compared to K^+ in its native environment. The 1D NMR spectra of a sample in 0.1 M NaCl was the same as spectra in 0.1 M KCl (data not shown), so the KCl sample was used for analysis.

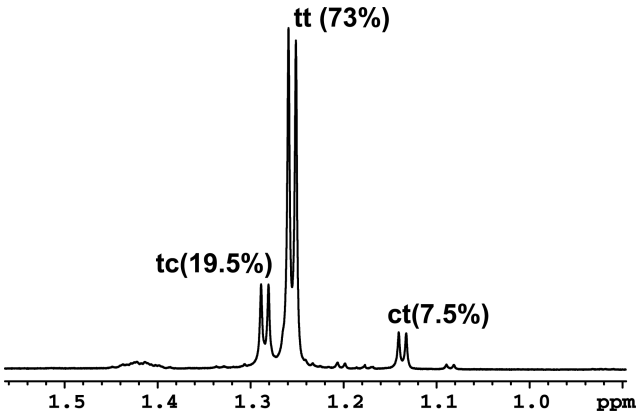

Figure 3-6. Region of 1D NMR spectrum showing cis–trans isomerization in the EL 2 peptide. The threonine methyl region from the 1D spectrum of the EL 2 peptide is shown, with the methyl peaks labelled with the conformation of the peptide it belongs to: trans-trans (tt), trans-cis (tc), or cis-trans (ct). The relative percentages of each from integration of the peaks are shown in brackets.

Trial 1D NMR spectra were acquired at 10, 20, and 30 °C. Spectra acquired at 10 °C allowed for better resolution of peaks near the water peak, and the 2D spectra for analysis were obtained at this temperature. It is also expected that lower temperatures would stabilize any nascent structure in the peptide. Due to the small molecular weight of the peptide (∼700 Da), NOESY spectra crosspeaks would have intensities near zero, and so a ROESY spectrum was obtained instead.

Sequential assignment was performed using the TOCSY and ROESY spectra. Spectra showed triplicate peaks from all of the residues except the N-terminal glycine, resulting from the slow cis–trans isomerization of the peptide bonds preceding the two prolines. Figure 3-6 shows a portion of the 1D spectrum containing the Thr methyl peaks from the three conformations. Integration of the threonine methyl peaks in the 1D spectrum gives percentages of about 73, 19.5, and 7.5% for the three conformations. X–Pro peptide bond conformations were determined from the X-Hα to Pro-Hα or Pro-Hδ connectivities. The major conformation was identified as trans-trans, and the second as trans-cis. The third conformation (cis-trans) was not investigated further due to spectral overlap and the low intensity of the peaks. A cis-cis conformation could not be seen.

Contacts from the ROESY spectra between P153 and F155 suggest a beta turn in the trans-cis conformation. A strong Pro Hα–Phe HN contact can be seen, which would suggest a beta-turn at residues T152–F155. Other contacts, between the Pro and Phe rings, suggest there could be an interaction between them, possibly a CH$\cdots\pi$ interaction, which could help stabilize the cis bond and promote turn

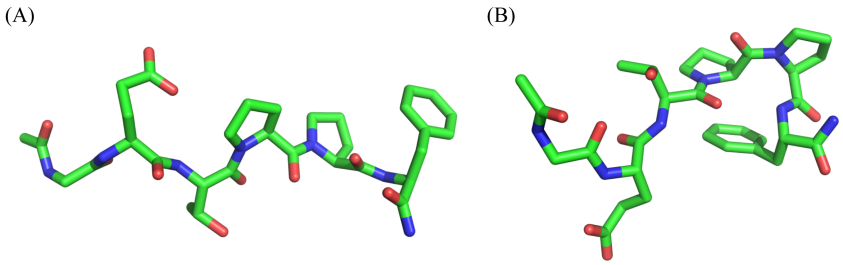

Figure 3-7. Structures of EL 2 peptide calculated from ROESY distance restraints. Single structures from the ensembles of structures calculated for the (A) trans-trans and (B) trans-cis conformation of the peptide.

formation (*23*). There are also weak contacts between the Phe and Glu residues, which could result from the turn formation. The interaction of the Phe and Pro rings is supported by the splitting of the Phe Hβ proton peak, from which 2 different values of the $^{3}J_{\mathrm{H}\alpha\mathrm{H}\beta}$ coupling constants can be measured ($\sim$ 5 and 12 Hz), suggesting restricted movement of the side chain. In contrast, the trans-trans conformation has only a single peak with a $^{3}J_{\mathrm{H}\alpha\mathrm{H}\beta}$ of $\sim$7.6 Hz. There do not appear to be any contacts in the trans-trans conformation that support formation of any secondary structure.

Structures were calculated separately for the trans-trans and trans-cis conformations. Structures for the third conformation were not calculated, due to the lack of interresidue restraints. Secondary structure assignment using the PROMOTIF v2.0 (*24*) suggests that beta-turns occur in some of the structures calculated in both the trans-trans and trans-cis peptides. 35 of 46 trans-cis peptide structures contained beta-turns at T152–F155, with some structures showing close contacts between the Phe and Pro rings. The flexible nature of a small peptide would allow it to sample a large number of conformations, with the result that the spectra would show an average of these conformations. The restraints obtained from the ROESY spectrum are thus also an average of the conformations the peptide is experiencing. The variation in the structures could be reflective of this flexibility, or of the low number of intermolecular restraints available for structure calculation, but the presence of crosspeaks in the ROESY still suggest that a turn is being formed. 24 of the 44 structures in the trans-trans conformer contained beta-turns at G150–P153, however, due to a lack of appropriate interresidue contacts, it is unlikely that a stable turn is being formed. Figure 3-7 shows a calculated structure for each conformation.

```
148 GVGET PPF LQSDV 160   Human             (32)
148 GVGEK PPF LQSEV 160   Rabbit            (33)
148 AVGET PPF LQSEV 160   Porcine           (34)
148 GVGET PPI LQSEV 160   Bovine            (#Q28036)
156 GVGET PPV LHSDT 168   Amphiuma          (35)
139 AIGEK APV LHYEL 151   Flounder          (36)
221 GVGES PPL LQSDI 233   Ornithorhynchus   (XM_001518234)
129 AVGET PPV LNSDV 141   Xenopus           (37)
115 VIGEE PPV LDSQL 128   Oncorhyncus       (38)
140 AVGEK PPI LKSDI 152   Coturnix          (ABJ88911)
154 GSWKR EEV FSPMG 166   Drosophila        (NM 134647)
```

Figure 3-8. Alignment of amino acid sequences of EL 2 and surrounding region of various NHE1 proteins. The alignment was made either manually or using the program "DNA Strider." The EL 2 region is shaded where identical to that of human NHE1. References (*32–38*) are indicated and where they were not available the accession number of the protein sequence was given.

Discussion

Studies on the membrane domain of the NHE1 isoform of the Na^+/H^+ exchanger have suggested that specific amino acids of the TM segments IV, VII, IX and XI are critical in the function of the protein (*19*, *21*, *25*, *26*). Specific mutations of TM IV in particular can alter the Na^+ affinity and sensitivity to inhibition (*19*, *27*). It is known that the loop regions at either end of transmembrane segments also contain residues that are important for NHE1 function (*14*, *19*, *28*). In K^+ channels and in the *E. coli* Na^+/H^+ antiporter NhaA, residues extending past the plane of the lipid bilayer have also been suggested to be important in attraction of cations, facilitating their transport (*29*, *30*). Studies have suggested TM IV and associated amino acids are important in cation coordination and inhibitor efficacy (*14*, *15*, *22*, *27*, *31*). In the present study we therefore further characterized three residues of the extracellular loop 2 involved in the NHE1 structure, function and drug recognition.

Of the amino acids 153–155 it was clear that both P154 and F155 are critical to NHE1 function. Though mutation of either residue did not cause a great aberration in either targeting or expression of the protein, mutation of either causes nominally larger decreases in activity than mutation of P153. The only significant effects on resistance to inhibition by EMD87580 were via mutation of P154, further suggesting it had a critical role in NHE1 function. Figure 3-8 shows a comparison of the amino acid sequences of EL 2 and nearby sequences of TM III and IV. P154 was completely conserved in all vertebrate species examined while F155 was more variable and P153 was usually, but not always, conserved. F155 was not well conserved, though a bulky hydrophobic residue was always present in this position. Neither EL 2 nor

this general region were conserved at all in invertebrate species such as *Drosophila*. It is generally agreed that conservation of a particular region or of an amino acid is suggestive of a more critical function, which is in agreement with our results. Of the other amino acids studied, the P153A mutation decreased both the protein expression level and the surface targeting comparing with the wild type. This result indicated that although P153 is not as critical to NHE1 activity as P154 and F155, its mutation affects NHE1 expression levels and targeting.

In the case of F155A mutation, there were no significant changes among the protein expression level and surface targeting however, activity was reduced and EMD87580 sensitivity was slightly decreased. Thus the F155 residue was not essential for NHE1 structure and function but mutation to Ala resulted in a decrease in activity of NHE1. It may be that a bulky hydrophobic residue is required at this position for full function (Figure 3-8).

An earlier report demonstrated that in rat NHE1, the dual mutation P157S/ P158F (corresponding to human P153/P154) markedly reduced the sensitivity to another NHE1 inhibitor EIPA, 7 fold (*14*). We observed that mutation of either residue had a smaller affect on inhibitor sensitivity than that study. This could be due to either the different inhibitor used, EMD87580 vs. EIPA, or because we mutated individual amino acids and not both prolines simultaneously. The dual P157S/P158F reported earlier (*14*) did not affect Na^+ affinity but did affect maximal activity of the protein. Our study found that mutation of P154 had a marked inhibitory effect on cation affinity in addition to transport rate, while mutation of P153 did not. Our results therefore suggest the second Pro of the pair in EL 2 is more important than the first in determining vertebrate NHE1 function.

Because Pro residues are known to significantly influence the secondary conformations of proteins, they may contribute to the differential drug sensitivity of the NHE isoforms. Prolines tend to be helix breakers (*17*, *39*) within TM segments. In addition it has been suggested that membrane proteins accumulate Pro residues at the end of their TM segments in order to expose select amino acids at the interface of molecular recognition events, while allowing stable association and native folding (*40*). It is also interesting to note that TM IV itself has a pair of Pro residues, P167 and P168 that are critical to function of the protein (*16*). However in contrast to these prolines, the requirement for a Pro at position 153 and 154 is not absolute. Substitutions could be made that retained NHE1 activity.

Proline residues have a high preference of forming the cis isomer of the peptide bond preceding it due to the cyclic nature of proline, relative to other amino

acids, which are mainly in the trans form (*41*). Three conformations of the peptide could be observed in solution due to the cis–trans isomerization of the peptide bonds preceding the proline residues, with a possible fourth conformation not observed, due to a low population and/or peak overlap. When in the trans-cis conformation, the peptide is able to form a beta turn, and this suggests that the sequence in the full protein could also adopt a turn. Also, the sequence involved appears to be favourable in forming a turn with a cis-peptide bond (*42*). The formation of a turn would support its predicted location in the topology model of NHE1, as a short loop between two transmembrane helices. The beta-turn structure allows for a 180-degree reversal of peptide backbone facilitating re-entry into the membrane bilayer. A short peptide would be quite flexible, with a large population of the peptide in a trans-trans and extended conformation, so the actual conformation in the protein would likely also depend on the distances between the ends of the two connecting helices as well as its interactions other nearby residues.

The ability of the peptide sequence to adopt a beta-turn might explain the results in the mutagenesis experiments. If the sequence forms a turn in the full protein, then the mutation of the critical P154 to Ala could make the formation of the turn less favourable, due to the decreased preference for the cis bond previous to the mutated residue. Conformational changes in the TM helix packing have been implicated in the bacterial Na^+/H^+ exchanger activation (*43*, *44*) and dynamics simulations suggest that the sequences of interhelical loops may be involved in stabilizing helix interactions (*45*). The change from a beta-turn to an extended conformation in the extracellular loop could affect the packing of the transmembrane helices, which could result in a less active protein. The observed decrease in inhibition by EMD87580 could be due to a decrease in binding of the inhibitor, due to a change in structure of its binding pocket on mutation of the loop region. The drug could be binding in a pocket that includes the loop, so that a mutation would change the structure of the binding pocket, or the drug could bind in a pocket which is indirectly affected by mutations in the loop which could affect the helix packing.

In summary our results show that EL 2 is important in NHE1 function, likely playing a role in maintaining appropriate conformation of the protein, possibly by influencing helix packing. P154 and F155 are both critical residues of this extracellular loop though significant function of the protein still remained after their mutation. Future studies will characterize the role of other extracellular loops of the protein.

Acknowledgements

We are grateful to Kathy Trieber (University of Alberta, Dept. of Biochemistry) for her assistance in statistical analysis of samples.

Supplementary Materials

Protein	WT	P153A	P154A	F155A	CT
NHE	69±1	*58±1	72±2	67±4	2±1
dNHE1	15±3	17±3	11±1	17±2	5±1

Table 3-S2. Analysis of plasma membrane targeting of the Na^+/H^+ exchanger in AP-1 cells transfected with wild-type NHE1 (WT) and with the NHE1 mutants P153A (P153A), P154A (P154A) and F155A (F155A). Experiments were carried out as described in Figure 3-2, B, and the distribution of the fully glycosylated (NHE1) or partially/de- glycosylated NHE1 (dNHE1) was analyzed separately. The percent of the total NHE1 protein localized to the plasma membrane is indicated. The results are mean ± S.E. for at least 4 determinations. * indicates significantly reduced plasma membrane targeting in comparison to wild type NHE1 ($p < 0.05$). Non-specific (CT) refers to an experiment in which non-specific binding to streptavidin-agarose beads was measured by following the standard procedure without labelling cells with biotin.

References

1. Fliegel, L. (2008) Molecular biology of the myocardial Na^+/H^+ exchanger. *J. Mol. Cell. Cardiol. 44*, 228–237.
2. Cardone, R. A., Casavola, V., and Reshkin, S. J. (2005) The role of disturbed pH dynamics and the Na^+/H^+ exchanger in metastasis. *Nat. Rev. Cancer 5*, 786–795.
3. Grinstein, S., Rotin, D., and Mason, M. J. (1989) Na^+/H^+ exchange and growth factor-induced cytosolic pH changes. Role in cellular proliferation. *Biochim. Biophys. Acta, Rev. Biomembr. 988*, 73–97.
4. Denker, S. P., and Barber, D. L. (2002) Cell migration requires both ion translocation and cytoskeletal anchoring by the Na^+/H^+ exchanger NHE1. *J. Cell Biol. 159*, 1087–1096.
5. Shrode, L., Cabado, A., Goss, G., and Grinstein, S. (1996) Role of the Na^+/H^+ antiporter isoforms in cell volume regulation, in *The Na^+/H^+ Exchanger* (Fliegel, L., Ed.), pp 101–122, R. G. Landes Co., Austin, TX.
6. Malo, M. E., and Fliegel, L. (2006) Physiological role and regulation of the Na^+/H^+ exchanger. *Can. J. Physiol. Pharmacol. 84*, 1081–1095.
7. Karmazyn, M., Liu, Q., Gan, X. T., Brix, B. J., and Fliegel, L. (2003) Aldosterone increases NHE-1 expression and induces NHE-1-dependent hypertrophy in neonatal rat ventricular myocytes. *Hypertension 42*, 1171–1176.
8. Mentzer, R. M., Jr, Lasley, R. D., Jessel, A., and Karmazyn, M. (2003) Intracellular sodium hydrogen exchange inhibition and clinical myocardial protection. *Ann. Thorac. Surg. 75*, S700–S708.
9. Slepkov, E. R., Rainey, J. K., Sykes, B. D., and Fliegel, L. (2007) Structural and functional analysis of the Na^+/H^+ exchanger. *Biochem. J. 401*, 623–633.
10. Murtazina, R., Booth, B. J., Bullis, B. L., Singh, D. N., and Fliegel, L. (2001) Functional analysis of polar amino-acid residues in membrane associated regions of the NHE1 isoform of the mammalian Na^+/H^+ exchanger. *Eur. J. Biochem. 268*, 4674–4685.
11. Muñoz, V., Blanco, F. J., and Serrano, L. (1995) The hydrophobic-staple motif and a role for loop-residues in α-helix stability and protein folding. *Nat. Struct. Biol. 2*, 380–385.
12. Zhao, M. M., Gaivin, R. J., and Perez, D. M. (1998) The third extracellular loop of the β_2-adrenergic receptor can modulate receptor/G protein affinity. *Mol. Pharmacol. 53*, 524–529.
13. Wakabayashi, S., Pang, T., Su, X., and Shigekawa, M. (2000) A novel topology model of the human Na^+/H^+ exchanger isoform 1. *J. Biol. Chem. 275*, 7942–7949.

14. Khadilkar, A., Iannuzzi, P., and Orlowski, J. (2001) Identification of sites in the second exomembrane loop and ninth transmembrane helix of the mammalian Na^+/H^+ exchanger important for drug recognition and cation translocation. *J. Biol. Chem. 276*, 43792–43800.

15. Slepkov, E. R., Rainey, J. K., Li, X., Liu, Y., Cheng, F. J., Lindhout, D. A., Sykes, B. D., and Fliegel, L. (2005) Structural and functional characterization of transmembrane segment IV of the NHE1 isoform of the Na^+/H^+ exchanger. *J. Biol. Chem. 280*, 17863–17872.

16. Slepkov, E. R., Chow, S., Lemieux, M. J., and Fliegel, L. (2004) Proline residues in transmembrane segment IV are critical for activity, expression and targeting of the Na^+/H^+ exchanger isoform 1. *Biochem. J. 379*, 31–38.

17. Sansom, M. S. (1992) Proline residues in transmembrane helices of channel and transport proteins: a molecular modelling study. *Protein Eng. 5*, 53–60.

18. Chen, L., Chen, C. X., Gan, X. T., Beier, N., Scholz, W., and Karmazyn, M. (2004) Inhibition and reversal of myocardial infarction-induced hypertrophy and heart failure by NHE-1 inhibition. *Am. J. Physiol.: Heart Circ. Physiol. 286*, H381–H387.

19. Slepkov, E., Ding, J., Han, J., and Fliegel, L. (2007) Mutational analysis of potential pore-lining amino acids in TM IV of the Na^+/H^+ exchanger. *Biochim. Biophys. Acta, Biomembr. 1768*, 2882–2889.

20. Harris, C., and Fliegel, L. (1999) Amiloride and the Na^+/H^+ exchanger protein: mechanism and significance of inhibition of the Na^+/H^+ exchanger (review). *Int. J. Mol. Med. 3*, 315–321.

21. Ding, J., Rainey, J. K., Xu, C., Sykes, B. D., and Fliegel, L. (2006) Structural and functional characterization of transmembrane segment VII of the Na^+/H^+ exchanger isoform 1. *J. Biol. Chem. 281*, 29817–29829.

22. Orlowski, J. (1993) Heterologous expression and functional properties of amiloride high affinity (NHE-1) and low affinity (NHE-3) isoforms of the rat Na^+/H^+ exchanger. *J. Biol. Chem. 268*, 16369–16377.

23. Dasgupta, B., Chakrabarti, P., and Basu, G. (2007) Enhanced stability of *cis* Pro-Pro peptide bond in Pro-Pro-Phe sequence motif. *FEBS Lett. 581*, 4529–4532.

24. Hutchinson, E. G., and Thornton, J. M. (1996) PROMOTIF—a program to identify and analyze structural motifs in proteins. *Protein Sci. 5*, 212–220.

25. Reddy, T., Ding, J., Li, X., Sykes, B. D., Rainey, J. K., and Fliegel, L. (2008) Structural and functional characterization of transmembrane segment IX of the NHE1 isoform of the Na^+/H^+ exchanger. *J. Biol. Chem. 283*, 22018–22030.

26. Lee, B. L., Li, X., Liu, Y., Sykes, B. D., and Fliegel, L. (2009) Structural and functional analysis of transmembrane XI of the NHE1 isoform of the Na^+/H^+ exchanger. *J. Biol. Chem. 284*, 11546–11556.

27. Counillon, L., Noël, J., Reithmeier, R. A., and Pouysségur, J. (1997) Random mutagenesis reveals a novel site involved in inhibitor interaction within the fourth transmembrane segment of the Na^+/H^+ exchanger-1. *Biochemistry 36*, 2951–2959.

28. Wakabayashi, S., Hisamitsu, T., Pang, T., and Shigekawa, M. (2003) Mutations of Arg^{440} and Gly^{455}/Gly^{456} oppositely change pH sensing of Na^+/H^+ exchanger 1. *J. Biol. Chem. 278*, 11828–11835.

29. Hunte, C., Screpanti, E., Venturi, M., Rimon, A., Padan, E., and Michel, H. (2005) Structure of a Na^+/H^+ antiporter and insights into mechanism of action and regulation by pH. *Nature 435*, 1197–1202.

30. Doyle, D. A., Morais Cabral, J., Pfuetzner, R. A., Kuo, A., Gulbis, J. M., Cohen, S. L., Chait, B. T., and MacKinnon, R. (1998) The structure of the potassium channel: molecular basis of K^+ conduction and selectivity. *Science 280*, 69–77.

31. Pedersen, S. F., King, S. A., Nygaard, E. B., Rigor, R. R., and Cala, P. M. (2007) NHE1 inhibition by amiloride- and benzoylguanidine-type compounds. Inhibitor binding loci deduced from chimeras of NHE1 homologues with endogenous differences in inhibitor sensitivity. *J. Biol. Chem. 282*, 19716–19727.

32. Sardet, C., Franchi, A., and Pouysségur, J. (1989) Molecular cloning, primary structure, and expression of the human growth factor-activatable Na^+/H^+ antiporter. *Cell 56*, 271–280.

33. Tse, C. M., Brant, S. R., Walker, M. S., Pouyssegur, J., and Donowitz, M. (1992) Cloning and sequencing of a rabbit cDNA encoding an intestinal and kidney-specific Na^+/H^+ exchanger isoform (NHE-3). *J. Biol. Chem. 267*, 9340–9346.

34. Reilly, R. F., Hildebrandt, F., Biemesderfer, D., Sardet, C., Pouysségur, J., Aronson, P. S., Slayman, C. W., and Igarashi, P. (1991) cDNA cloning and immunolocalization of a Na^+/H^+ exchanger in LLC-PK1 renal epithelial cells. *Am. J. Physiol. 261*, F1088–F1094.

35. McLean, L. A., Zia, S., Gorin, F. A., and Cala, P. M. (1999) Cloning and expression of the Na^+/H^+ exchanger from *Amphiuma* RBCs: resemblance to mammalian NHE1. *Am. J. Physiol. 276*, C1025–C1037.

36. Pedersen, S. F., King, S. A., Rigor, R. R., Zhuang, Z., Warren, J. M., and Cala, P. M. (2003) Molecular cloning of NHE1 from winter flounder RBCs: activation by osmotic shrinkage, cAMP, and calyculin A. *Am. J. Physiol.: Cell Physiol. 284*, C1561–C1576.

37. Busch, S. (1997) Cloning and sequencing of the cDNA encoding for a Na^+/H^+ exchanger from *Xenopus laevis* oocytes (X1-NHE). *Biochim. Biophys. Acta, Biomembr. 1325*, 13–16.

38. Borgese, F., Sardet, C., Cappadoro, M., Pouyssegur, J., and Motais, R. (1992) Cloning and expression of a cAMP-activated Na^+/H^+ exchanger: evidence that the cytoplasmic domain mediates hormonal regulation. *Proc. Natl. Acad. Sci. U.S.A. 89*, 6765–6769.

39. Barlow, D. J., and Thornton, J. M. (1988) Helix geometry in proteins. *J. Mol. Biol. 201*, 601–619.

40. Orzáez, M., Salgado, J., Giménez-Giner, A., Pérez-Payá, E., and Mingarro, I. (2004) Influence of proline residues in transmembrane helix packing. *J. Mol. Biol. 335*, 631–640.

41. MacArthur, M. W., and Thornton, J. M. (1991) Influence of proline residues on protein conformation. *J. Mol. Biol. 218*, 397–412.

42. Pal, D., and Chakrabarti, P. (1999) Cis peptide bonds in proteins: residues involved, their conformations, interactions and locations. *J. Mol. Biol. 294*, 271–288.

43. Olkhova, E., Padan, E., and Michel, H. (2007) The influence of protonation states on the dynamics of the NhaA antiporter from *Escherichia coli*. *Biophys. J. 92*, 3784–3791.

44. Kozachkov, L., Herz, K., and Padan, E. (2007) Functional and structural interactions of the transmembrane domain X of NhaA, Na^+/H^+ antiporter of *Escherichia coli*, at physiological pH. *Biochemistry 46*, 2419–2430.

45. Ulmschneider, M. B., Sansom, M. S. P., and Di Nola, A. (2005) Properties of integral membrane protein structures: derivation of an implicit membrane potential. *Proteins 59*, 252–265.

Chapter 4

Structural and functional analysis of extracellular loop 4 of the NHE1 isoform of the Na^+/H^+ exchanger

A version of this chapter has been published as:

- Lee, B. L., Liu, Y., Li, X., Sykes, B. D. and Fliegel, L. (2012) Structural and functional analysis of extracellular loop 4 of the NHE1 isoform of the Na^+/H^+ exchanger. *Biochim. Biophys. Acta, Biomembr. 1818*, 2783–2790.

BLL performed the NMR, and YL and XL performed the functional experiments. BDS and FL helped edit the manuscript.

Summary

The mammalian Na^+/H^+ exchanger isoform 1 (NHE1) is a ubiquitously expressed plasma membrane protein. It regulates intracellular pH by removing a single intracellular H^+ in exchange for one extracellular Na^+. The membrane domain of NHE1 comprises the 500 N-terminal amino acids and is made of 12 transmembrane segments. The extracellular loops of the transmembrane segments are thought to be involved in cation coordination and inhibitor sensitivity. We have characterized the structure and function of amino acids 278–291 representing extracellular loop 4. When mutated to Cys, residues F277, F280, N282 and E284 of EL 4 were sensitive to mutation and reaction with MTSET inhibiting NHE1 activity. In addition they were found to be accessible to extracellular applied MTSET. A peptide of the amino acids of EL 4 was mostly unstructured suggesting that it does not provide a rigid structured link between TM VII and TM VIII. Our results suggest that EL 4 makes an extension upward from TM VII to make up part of the mouth of the NHE1 protein and is involved in cation selectivity or coordination. EL 4 provides

a flexible link to TM VIII which may either allow movement of TM VII or allow TM VIII to not be adjacent to TM VII.

Introduction

The mammalian NHE1 protein is believed to consist of 12 transmembrane (TM) segments that comprise the N-terminal 500 amino acids. These are connected by a series of extra membrane segments which form intracellular and extracellular loops (EL). Loops between α-helices can influence their arrangements and packing (*1*) and can modulate protein function (*2*). For NHE1, EL 5 may be involved in drug sensitivity and cation binding (*3*, *4*). EL 2 links TM segments III and IV and mutation of residues of EL 2 affects both the drug sensitivity and the activity of NHE1 (*5*, *6*). Two models of the topology of NHE1 are in question with two different models, one model is based on cysteine accessibility studies (*7*) and a second being based on computational comparison with the deduced structure of the *Escherichia coli* Na^+/H^+ exchanger NhaA suggested (*8*). Although significant variation in the predictions occurs after amino acid 315, prior to this region the models are essentially identical with the exception of the latter model predicting that the first two transmembrane segments are cleaved free of the protein. Amino acids 278–290 are predicted to form an EL in both models. They form EL 4 connecting TM VII and VIII in the model of Wakabayashi et al. (*7*) and are predicted to form the same loop in the model of Landau et al. (*8*) connecting the same two transmembrane segments that are numbered V and VI in that model. Little is known about this particular loop connecting TM VII (amino acids 251–273) and VIII (amino acids 291–311) in terms of its functional role and contribution by the amino acids present in it. We have earlier examined the structure and function of TM VII. We found that TM VII is a predominantly α-helical segment, that is critical to NHE1 function and that it contained pore lining residues (*9*, *10*).

ELs of transporters are often critical to their function. For example in the serotonin transporter, the glutamate transporter and the glycine transporter (*11*–*13*) ELs play key roles in function. For Na^+/K^+ ATPase the second EL is a major determinant of extracellular cation affinity (*14*, *15*). Amino acids of the acetylcholine receptor (*16*, *17*) and NhaA (*18*) ELs are also involved in the attraction of cation to the extracellular surface. In this study we examined the role of EL 4 (amino acids 274–290) of the NHE1 isoform of the mammalian Na^+/H^+ exchanger. We also used NMR to characterize the structure of synthetic peptides representing EL 4.

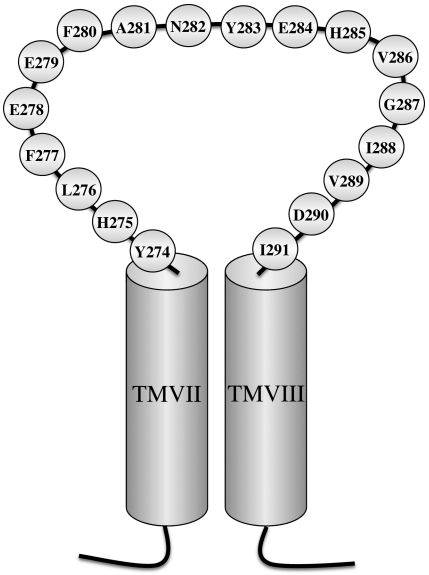

Figure 4-1. Models of EL 4 of the NHE1 isoform of the Na^+/H^+ exchanger. Topological model of the EL 4 of the transmembrane domain of the NHE1 isoform of the Na^+/H^+ exchanger. TM segment numbering is based on cysteine accessibility studies (*7*).

Methods

Both the functional characterization of NHE1 and structural characterization of an EL 4 peptide were carried out as described in Chapter 2. Mutants are listed in Table 4-S1. For NMR spectroscopy, linear and cyclic peptides representing EL 4 (sequence acetyl-YHLFEEFANYEHVGIVDI-amide, and disulfide-cyclicized acetyl-CGYHLFEEFANYEHVGIVDIFLGFLC-amide), were purchased from GL Biochem (Shanghai) Ltd. The samples were dissolved in DMSO-d_6. NMR spectra for the linear and cyclic peptide samples were obtained at temperatures of 30 °C and 35 °C, respectively.

Results

Characterization of EL 4 mutants

Figure 4-1 illustrates a model of EL 4 and shows the amino acids present. EL 4 consists of residues Y274–I291. It contains several acidic residues and a mixture of hydrophilic and hydrophobic amino acids. EL 4 was initially studied by a combination of site specific mutagenesis and cysteine scanning mutagenesis. The acidic residues of EL 4, E278, E279, E284 and D290, were changed to their corre-

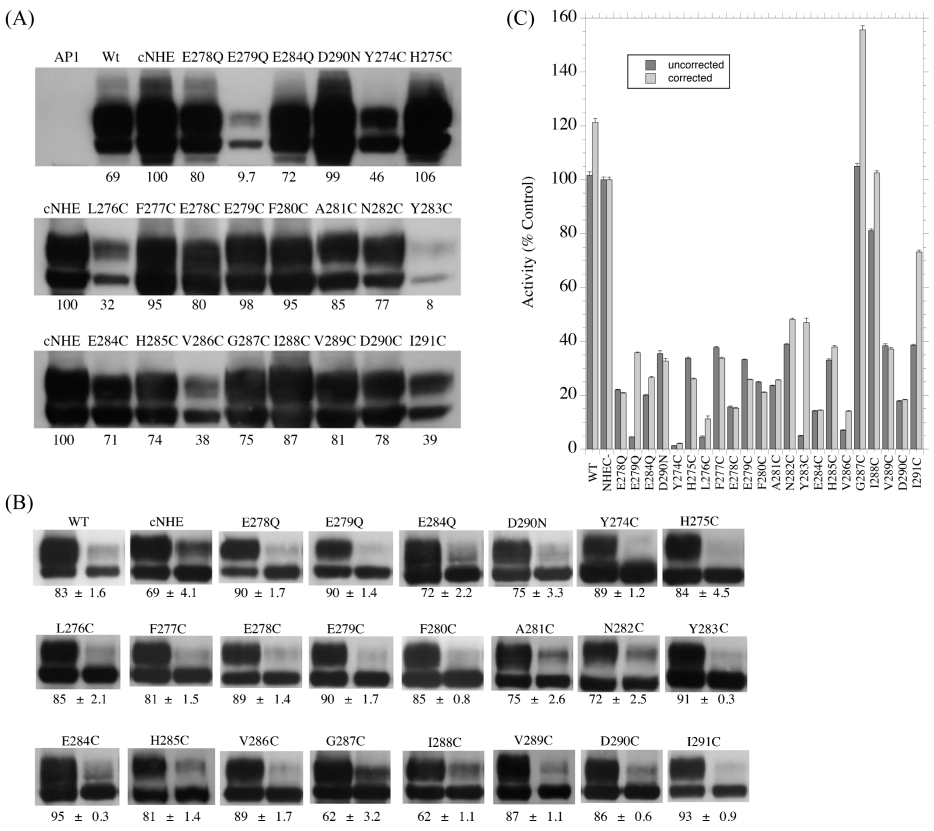

Figure 4-2. Analysis of wild type NHE1 and mutant EL 4 proteins. (A) Western blot of whole cell lysates of stable cell lines expressing Na^+/H^+ exchanger EL 4 mutants or control protein. Mutations are as indicated. 100 µg of total protein was loaded in each lane. Numbers below the lanes indicate the amount of NHE1 protein relative to wild type NHE. Mean values ($n = 3$ to 4) were obtained from densitometric scans of both the 110 and 95 kDa bands. AP-1 refers to AP-1 cells mock transfected. Wt, and cNHE1 refer to cells stably expressing wild type Na^+/H^+ exchanger protein and the cysteineless NHE1, respectively. (B) Surface localization of NHE1 in AP-1 cells expressing control and EL 4 mutants. Equal amounts of total cell lysate (left lane) and unbound intracellular lysate (right lane) were examined by Western blotting with anti-HA antibody to identify NHE1 protein. WT and cNHE1 are cell lines stably expressing wild type NHE1 and cysteineless NHE1, respectively. The percent of the total NHE1 protein found on the plasma membrane is indicated for each mutant. For Ct this indicates the amount of non-specific binding to streptavidin-agarose beads. Results are the mean ± S.E., with $n \geq 4$ determinations. Autoradiography exposure times were increased for mutants expressing lower levels of protein. (C) Summary of the rate of recovery after an acute acid load of AP-1 cells transfected with wild type NHE1, cNHE, and EL 4 Na^+/H^+ exchanger mutants. The mean activity of cNHE1 stably transfected with NHE1 was 1.7 ΔpH/min, and this value was set to 100% and other activities are a percent of those of cNHE. Values are the mean ± S.E. of 6–10 determinations. Results are shown for mean activity of both uncorrected (black) and normalized for surface processing and expression levels (gray).

sponding non-charged amino acids, E to Q and D to N in individual mutant proteins. Also, all the amino acids of EL 4 were changed to cysteine in the background of the cysteineless NHE1 (cNHE1) protein. We first determined the expression levels, targeting and activity of the mutant NHE1 proteins. Figure 4-2, A–C, illustrates these results. Expression levels were determined by western blotting with antibody against the HA tag on the Na^+/H^+ exchanger protein. Figure 4-2, A, demonstrates that all the mutant proteins were expressed. As shown earlier (*19*), NHE1 was expressed as a fully glycosylated and a partial or de-glycosylated protein and these two immunoreactive bands were present in all stable cell lines. Expression of several of the mutants was reduced. Most notably, the E279Q and Y283C protein levels were less than 10% of the level of cNHE1. The mutants Y274C, L276C, V286C and I291C also had reduced expression that was between 50 and 30% of cNHE1. Most other mutants had some slight decrease in expression compared to controls, though a few (D290N, H275C, F277C, E279C, F280C) were equivalent to cNHE1. For both the E279Q and the V286C mutants, aside from their lower levels of expression, it was notable that a larger percentage of the expressed protein was present as the unglycosylated form.

We next examined the targeting of the mutant proteins to the cell surface. Cell surface biotinylation experiments were done as described earlier (*9*). The results are shown in Figure 4-2, B. The mutant proteins targeted well to the cell surface. Though minor variations occurred in the efficiency of targeting, these were not nearly as large as we have observed earlier with mutations of transmembrane regions of the NHE1 protein (*19*, *20*).

Determination of the activity of the EL 4 mutants showed that most of the mutants had reduced activity relative to either the wild type or cysteineless NHE1 protein. With the exception of the G287C and I288C mutants, all of the activity was less than half of that of the control (Figure 4-2, C). The uncorrected activity of the E279Q, Y274C, L276C, Y283C and V286C mutants was less than 10% of the control level and these mutants were considered inactive or nearly so, and were not used for further study. For the E279Q and the Y283C much of the decrease in measurable activity was due to a decrease in the expression level of the protein, though the residual activity was too low for further characterization.

We determined the effect of MTSET and MTSES on the activity of the remaining active cysteine mutants. The results are shown in Figure 4-3. Mutant F277C was exquisitely sensitive to inhibition by positively charged MTSET, but not to inhibition by negatively charged MTSES. Mutants F280C, N282C and E284C

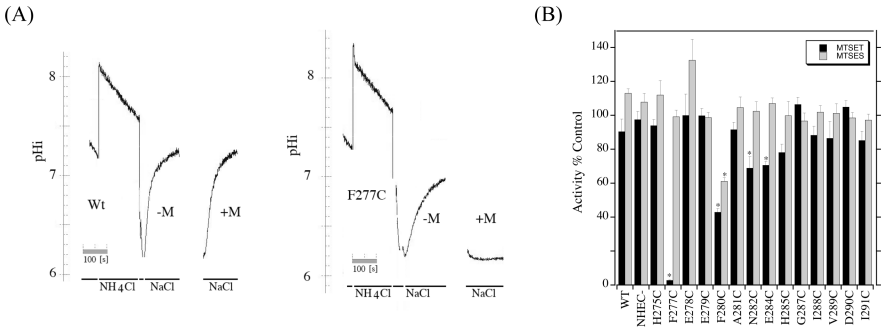

Figure 4-3. Effect of sulphydryl reactive compounds, MTSET and MTSES, on activity of cNHE1 and single cysteine NHE1 mutant containing cell lines. (A) Example of results of effect of MTSET on activity of cNHE1 and F277C NHE1 mutant. NHE1 protein activity was assayed in stably transfected AP-1 cells as described in the "Methods." Activity was measured after two acid pulses. The first pulse illustrated was in the absence of MTSET. For ease of viewing, only the recovery from acidosis is shown for the second pulse, in which cells were treated with MTSET. NH_4Cl, treatment with ammonium chloride. After NH_4Cl treatment, there was a brief Na^+ free treatment to induce acidosis. NaCl, time when recovery from acidosis was in NaCl containing buffer, for the second pulse this contained MTSET as indicated and cells were pretreated with MTSET for 10 min prior to NH_4Cl induced acid load. (B) Summary of effects of MTSET and MTSES on NHE activity of EL 4 mutants. Activity was measured after dual ammonium chloride pulses as described in the "Methods." The second acidification was after cells were treated with 10 mM MTSET or MTSES. Results are presented as the percent of activity of the second acid load, relative to the first. * indicates that the second recovery from acid load was significantly lower than the first at $p < 0.05$. Solid filled bars represent MTSET treatments and hatched bars are MTSES treatments.

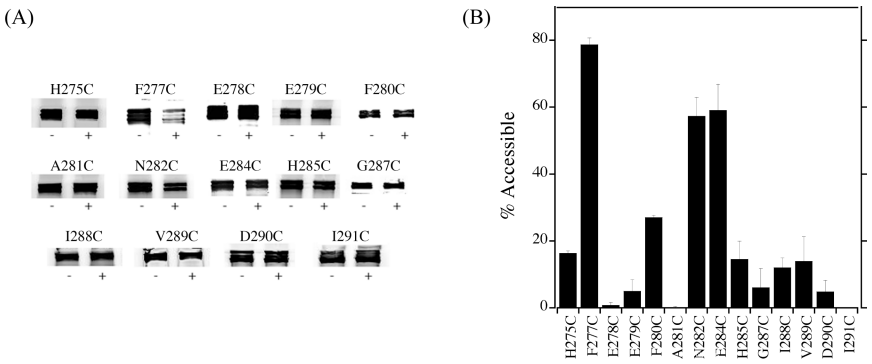

Figure 4-4. Accessibility of residues of EL 4 to reactivity with MTSET. The accessibility of the residues of EL 4 to reactivity with MTSET was measured as described in the "Methods." (A) Examples of results illustrated MTSET blocking of reactivity with IRDye800-maleimide. Prior reaction with MTSET blocks the reactivity with IRDye800-maleimide. + indicates reacted with MTSET prior to reaction with IRDye800-maleimide. (B) Summary of the results illustrating calculated accessibility of residues of EL 4. Results are the mean ± S.E. of at least 3 experiments.

were all also partially sensitive to inhibition by MTSET while only mutant F280C was partially sensitive to inhibition by MTSES.

It is possible that some Cys residues were reactive with MTSES or MTSET but that this was not inhibitory to NHE1 activity. We therefore measured the accessibility of the active cysteine mutants. The results are shown in Figure 4-4. Residues that were inhibited by MTSET when changed to Cys (F277, F280, N282, E284) were more accessible to MTSET and incubation with MTSET blocked reactivity with IRDye800-maleimide. The F280C mutant protein was less accessible than the F277C, N282C and E284C containing proteins, but was more accessible than other residues.

Characterization of EL 4 peptide

We purchased two chemically synthesized peptides containing the EL 4 sequence for high-resolution NMR spectroscopy. The first peptide was a linear peptide containing Y274–I291 of EL 4, with N-terminal acetyl and C-terminal amine caps to remove the charges at the peptide termini. A second peptide of the sequence acetyl-CG-Y274-L296-C-amine was also synthesized. Additional residues on the C-terminal end of this second peptide corresponded to the slight difference in prediction of the locations of the transmembrane helices between the topology models proposed by (*7*) and (*8*). The peptide also contained disulfide-linked cysteines at the termini

to produce a cyclic peptide, which may restrict the conformations adopted by the extracellular loop, and a glycine spacer at the N-terminal end to increase the distance between the ends of EL 4. These were designed to link the N and C-terminals of the peptide, mimicking a putative association between transmembrane segments VII and VIII.

1D ^{1}H NMR spectra were used to judge the quality of the samples of solubilized EL 4 for structure determination. Spectra of the linear peptide in aqueous buffer (50 mM imidazole, 100 mM KCl, 10% D_2O, 0.25 mM DSS-d_6) suggested that the peptide was unstructured in aqueous solution. HN and Hα peaks in the 1D spectra were distributed over a very narrow range, 8.0–8.4 ppm and 4.1–4.3 ppm, respectively. Addition of up to 20% TFE-d_3 did not affect the dispersion of the HN and Hα peaks and again suggested that the peptide was unstructured. The peptide sample was lyophilized and reconstituted in DMSO-d_6, where there appeared to be an improvement in the dispersion of the peaks, suggesting it may be more structured in DMSO. 2D NMR spectra were then acquired for assignment and structure determination. The cyclic peptide was found to be insoluble in H_2O and TFE/H_2O, but was soluble in DMSO. NMR spectra were also acquired for this peptide in DMSO.

Differences in the quality of the spectra could be observed between the linear and cyclic peptides. Spectra of the linear peptide contained relatively narrow peaks, while the spectra of the cyclic peptide contained broad peaks as shown by the amide regions of the 1D NMR spectra (Figure 4-5). Both peptides could be fully assigned. The cyclic peptide also contains additional unassigned peaks that may have been either impurities or minor conformations of the peptide.

The NMR spectra suggest that despite the increased dispersion of the peaks in DMSO compared to aqueous solution, the peptide is still mostly unstructured in DMSO. There is poor chemical shift dispersion in the Hα dimension, as shown by the 2D DQF-COSY spectra (Figure 4-5) with the non-glycine Hα peaks limited to 4.1–4.6 ppm in both the linear and cyclic peptides. The NOESY spectra of both peptides contained weak intraresidue HN-Hα peaks and strong sequential Hα-HN connectivities, and generally lack medium and long range connectivities, also indicative of poorly structured peptides. A comparison of Hα chemical shift values with published random coil chemical shift values measured in H_2O (*21*) and DMSO (*22*) also suggest that the peptides are relatively unstructured in solution (Figure 4-6). Continuous regions of large negative chemical shift differences suggest alpha-helical content, while positive values would suggest beta-sheet content. Neither of the

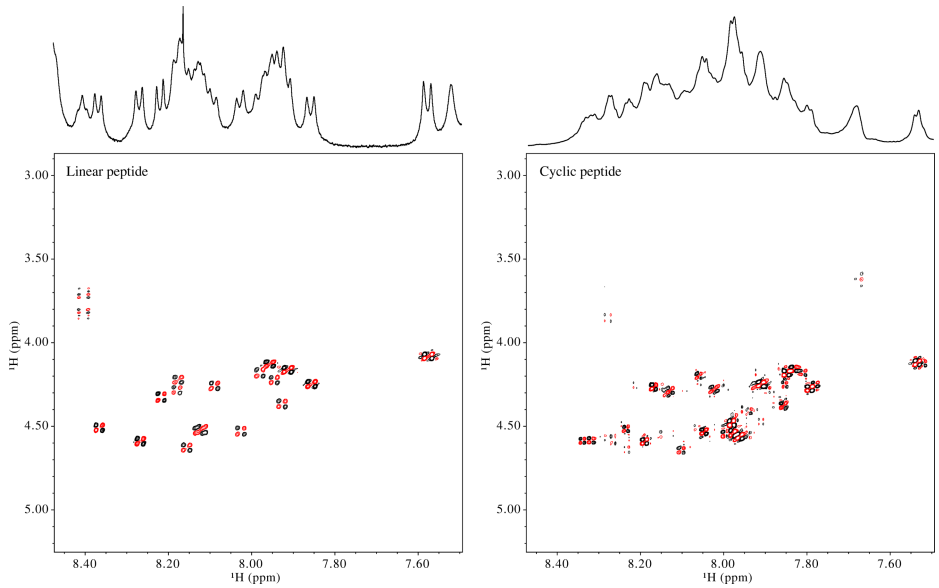

Figure 4-5. 1D ^{1}H and 2D ^{1}H-^{1}H DQF-COSY spectra of the linear and cyclic EL 4 peptides in DMSO. The HN-Hα "fingerprint" region of the 2D DQF-COSY spectra of the linear and cyclic peptides is shown. Above are the corresponding HN regions of the 1D NMR spectra of the peptides. Spectra for the linear peptide were acquired at 500 MHz and 30 °C, and 800 MHz and 35 °C for the cyclic peptide, and referenced to the DMSO peak at 2.50 ppm.

peptides shows any contiguous segments with either strong negative or positive values, again suggesting that the peptides are relatively unstructured. The similarities in the chemical shifts and chemical shift differences between the linear and cyclic peptides suggest that they may also be adopting similar, if relatively unstructured, conformations, despite the restraint provided by the disulfide bond in the cyclic peptide.

Discussion

Functional investigation of EL 4

In this study we examined EL 4 of the NHE1 isoform of the Na^{+}/H^{+} exchanger, examining the residues critical in function, their accessibility and the structure of EL 4. There has been some previous related work (*7*) that examined the topology of NHE1 and the accessibility of a few residues of EL 4. Mutation of amino acids E278 to H285 to Cys resulted in a protein in which all these mutants were all shown to be accessible extracellularly. In addition that study examined the effect of external MTSET on NHE1 activity. They found some similar but some

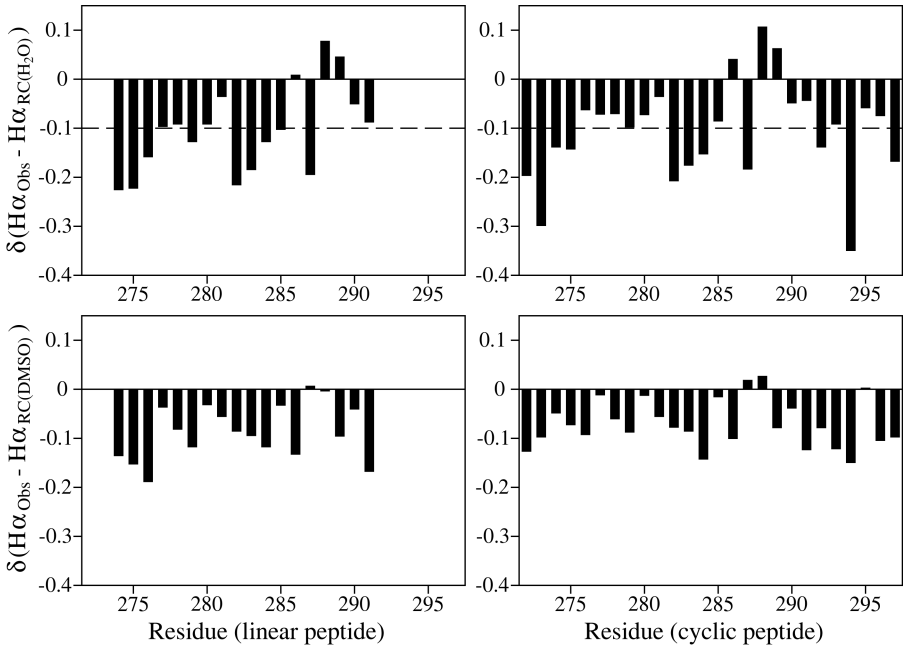

Figure 4-6. Chemical shift index values for the linear and cyclic EL 4 peptides in DMSO. Differences in Hα chemical shift between observed Hα values for the peptides and published random coil Hα chemical shifts in water (*21*) and DMSO (*22*) are shown per residue. Contiguous regions of large negative secondary shifts suggest helical content while large positive secondary shifts suggest beta sheet content. Regions exceeding the cutoff value of -0.1 ppm (dotted line) when using random coil values determined in water suggest helical content (*23*).

different results from our study. Similar to their study, we found slight inhibitory effects of MTSET on the N282C mutant protein. However, we found many other differences. In contrast to their results, we found no significant inhibitory effect of MTSET on the A281C mutant. It should be noted that the effect of MTSET that was found earlier was very small. Another difference between their study and ours is that we found significant effects of MTSET on the E284C protein and of both MTSET and MTSES on the F280C protein which was not shown earlier. Further, we found that the F277C mutant protein (which was not examined in that study) was inhibited most strongly by MTSET. Why they did not detect effects of MTSET on the F280C protein is uncertain at this time. However we found a significant, reproducible inhibitory effect of MTSET and in addition, this residue was accessible to MTSET. We noted that accessibility of the F280C mutant protein was temperature sensitive, and was greatly reduced at 30 °C (not shown). It should be noted that the earlier study examined NHE1 activity using a radioisotope assay examining Na^+ uptake. The present assay, examining rapid kinetics of NHE1 in a dual pulse system, would likely have greater time-resolution and detect changes in activity that might not be detectable using a radioisotope assay. Of note, we found that the F277C mutant protein was the most reactive protein with MTSET, in our accessibility assay (Figure 4-4), further confirming the results of the activity measurements.

We also found that with the exception of mutant F280C, positively charged MTSET was inhibitory while negatively charged MTSES was without effect. If EL 4 is an external region of the NHE1 protein involved in cation coordination, it would appear reasonable that addition of a positively charged compound would be more inhibitory, possibly repelling a cation at the mouth of the protein. In the case of the F280C mutant protein, while MTSET was greatly inhibitory, negatively charged MTSES was also strongly inhibitory, though not as much as MTSET. In this case, effects on ion passage by MTSES are likely due to a steric hindrance caused by the addition of the bulky compound and are not charge related. Another mutant protein, the F277C mutant, was the most strongly inhibited by MTSET. We suggest that this side chain of this amino acid was more directly pointing toward the mouth of the extracellular cation funnel of the NHE1 protein. Therefore, its linkage to the positively charged MTSET more effectively caused inhibition of cation coordination in the mouth of the NHE1 protein. Overall, our study suggests that the residues F277, F280, N282 and E284 form an important part of the extracellular pore of NHE1. Mutation of the adjacent residues L276 and Y283 to Cys caused an inactive protein, suggesting they may also play an important part of the extracellular pore of NHE1.

While further study of these residues is called for, clearly the side chain of these amino acids must be within certain constraints that were not met by substitution to Cys.

We also made mutations to eliminate the negative charge on amino acids E278, E279, E284 and D290. In all cases activity was reduced but not eliminated. For the mutant protein with the E279Q mutation, the decrease in activity was largely due to a reduction in the level of protein expression. We had hypothesized that having negatively charged side chains, these amino acids might be critical in cation attraction. However for these amino acids this does not appear to be the case. Nevertheless, it is apparent that only amino acid E279 is important of these, and the effects were mainly on protein expression. An effect on protein conformation or processing may occur.

Analysis of EL 4 structure and function

High-resolution NMR analysis of the linear and cyclic EL 4 peptides suggests that both peptides adopt mostly random-coil conformations in DMSO. DMSO has an intermediate dielectric constant ($\sim$46) (*24*) similar to the membrane interface (*25*), making it a reasonable mimetic of the environment experienced by the loop. A study by Katragadda et al. (*26*) showed that the NMR structures of isolated loops from bacteriorhodopsin in DMSO adopt structures equivalent to the known crystal structure of the protein. Other studies (*27–29*) including our own on EL 2 of NHE1 (*30*), have also found structures in interhelical loops in aqueous solution or DMSO. However, this was not the case for EL 4 of NHE1. It is unlikely that the length of the peptides we studied is the reason for the lack of structure, as the other studies on isolated loops have used peptides of similar lengths. The lack of structure could suggest that the loop is flexible, which could be important in the function of NHE1. Alternatively, the loop may only be structured in the full protein, where interactions with other extracellular regions of the protein and with the membrane bilayer could restrict the conformation of the loop. However to address this possibility we examine the EL 4 peptide with its ends tethered by a disulfide bond. Even in this case we did not find a structured peptide. In the three-dimensional model of NHE1 proposed by Landau et al. (*8*) EL 4 connects the transmembrane helices 5 and 6 of this model (corresponding to TM VII and TM VIII of the Wakabayashi model (*7*)). The Landau et al. model does not suggest any interactions between the transmembrane segments. The lack of structure in the loop could be to allow the helices to be some distance apart from each other.

Our data are somewhat contradictory to a recent 3D model which did not place VII and VIII surrounding the catalytic core of the protein (*31*). However, that model did not directly provide evidence for the location of these transmembrane segments and was largely based on homology modelling. We have earlier demonstrated that TM VII possesses several amino acids that when changed to Cys, are sensitive to derivatization with MTSET and affect protein function (*9*, *10*). In addition, mutation of residues of TM VII altered sensitivity to NHE1 specific inhibitors (*9*). Additionally, E262 of TM VII is exquisitely sensitive to mutation and changing that residue to an Asp, alters the affinity of the NHE1 protein to Li^+ but not for Na^+, suggesting that this amino acid is involved in cation coordination (*4*). TM VII also has a flexible middle region from amino acids G261–S263 which may allow conformation changes associated with movement during transport (*9*, *32*). These data all support a role for this transmembrane segment in NHE1 function which is consistent with a functional role for EL 4 in the pore of the NHE1 protein.

Conclusions

Overall, our results support a model in which TM VII is important in the catalytic core of the protein and amino acids 274–284 of EL 4 make an extension upward from TM VII to make up part of the mouth of the protein. A flexible connection from TM VII to TM VIII may allow TM VII to make conformational changes associated with its postulated role in transport (*32*). F277, F280, N282, E284 are in particular shown to be critical as demonstrated by the inhibitory effect shown when mutated to Cys and reacted with positively charged MTSET.

Supplementary Materials

Mutation	Oligonucleotide Sequence	Restriction Site
E278Q	5′-CCTGTATCACCTCTTTcAG**GAaTTc**GCCAACTACGAAC-3′	EcoRI
E279Q	5′-CCTGTATCACCTCTT**cGAGcAGTTTGC**CAACTACG-3′	BcgI
E284Q	5′-GAGTTTGCCAACTA**CcAACACGTtGG**CATCGTGGACATC-3′	BstXI
D290N	5′-CACGTGGGCATCGT**GaACATCTTC**CTCGGCTTC-3′	XmnI
Y274C	5′-GACGCCGTCACTGT**aGTaCT**GTgTCACCTCTTTGAGG-3′	ScaI
H275C	5′-GACGCCGTCACTGT**aGTaCT**GTATtgCCTCTTTGAGGAGTTT-3′	ScaI
L276C	5′-GTGGTCCTGTATCACtgCTTTGAG**GAaTTc**GCCAACTACGAAC-3′	EcoRI
F277C	5′-GTCCTGTATCACCTCTgTGAG**GAaTTc**GCCAACTACGAACAC-3′	EcoRI
E278C	5′-CCTGTATCACCTCTTTtgc**GAaTTc**GCCAACTACGAACAC-3′	EcoRI
E279C	5′-CCTGTATCACCTCTTTGAGtgTT**TcGCgA**ACTACGAACACGTGGGC-3′	NruI
F280C	5′-CCTGTATCACCTCTT**cGAGGAGTgTGC**CAACTACGAACAC-3′	BcgI
A281C	5′-CACCTCTTTGAG**GAaTTc**tgCAACTACGAACACGTGG-3′	EcoRI
N282C	5′-CCTCTTTGAGGAGTTT**GCatgC**TACGAACACGTGGGC-3′	SphI
Y283C	5′-GAGGAGTTTGC**CAAtTg**CGAACACGTGGGCATC- 3′	MfeI
E284C	5′-GGAGTTTGCCAACTAC**tgcCACGTGGGC**ATCGTGG- 3′	BglI
H285C	5′-GAGTTTGCCAACTAC**GAAtgC**GTGGGCATCGTGGAC- 3′	BsmI
V286C	5′-GCCAACTACGAACACtgcGGCATC**GTcGAC**ATCTTCCTCGGC- 3′	SalI
G287C	5′-CCAACTACGAACACGTGtGCATC**GTcGAC**ATCTTCCTCGGC- 3′	SalI
I288C	5′-CTACGAACACGTGGGCtgC**GTcGAC**ATCTTCCTCGGC- 3′	ScaI
V289C	5′-CTACGAACACGTGGG**CATatg**cGACATCTTCCTCGGC-3′	NdeI
D290C	5′-AACTACGAACACGTGGGCATCGT**atgCAT**CTTCCTCGGCTTC-3′	NsiI
I291C	5′-GAACACGTGGGCATC**GTcGAC**tgCTTCCTCGGCTTCCTG-3′	SalI

Table 4-S1. Oligonucleotides used for site-directed mutagenesis of EL 4. Mutated nucleotides are in lower case, restriction sites are in bold.

References

1. Muñoz, V., Blanco, F. J., and Serrano, L. (1995) The hydrophobic-staple motif and a role for loop-residues in α-helix stability and protein folding. *Nat. Struct. Biol. 2*, 380–385.
2. Zhao, M. M., Gaivin, R. J., and Perez, D. M. (1998) The third extracellular loop of the β_2-adrenergic receptor can modulate receptor/G protein affinity. *Mol. Pharmacol. 53*, 524–529.
3. Slepkov, E., Ding, J., Han, J., and Fliegel, L. (2007) Mutational analysis of potential pore-lining amino acids in TM IV of the Na^+/H^+ exchanger. *Biochim. Biophys. Acta, Biomembr. 1768*, 2882–2889.
4. Murtazina, R., Booth, B. J., Bullis, B. L., Singh, D. N., and Fliegel, L. (2001) Functional analysis of polar amino-acid residues in membrane associated regions of the NHE1 isoform of the mammalian Na^+/H^+ exchanger. *Eur. J. Biochem. 268*, 4674–4685.
5. Lee, B. L., Li, X., Liu, Y., Sykes, B. D., and Fliegel, L. (2009) Structural and functional analysis of transmembrane XI of the NHE1 isoform of the Na^+/H^+ exchanger. *J. Biol. Chem. 284*, 11546–11556.
6. Khadilkar, A., Iannuzzi, P., and Orlowski, J. (2001) Identification of sites in the second exomembrane loop and ninth transmembrane helix of the mammalian Na^+/H^+ exchanger important for drug recognition and cation translocation. *J. Biol. Chem. 276*, 43792–43800.
7. Wakabayashi, S., Pang, T., Su, X., and Shigekawa, M. (2000) A novel topology model of the human Na^+/H^+ exchanger isoform 1. *J. Biol. Chem. 275*, 7942–7949.
8. Landau, M., Herz, K., Padan, E., and Ben-Tal, N. (2007) Model structure of the Na^+/H^+ exchanger 1 (NHE1): functional and clinical implications. *J. Biol. Chem. 282*, 37854–37863.
9. Ding, J., Rainey, J. K., Xu, C., Sykes, B. D., and Fliegel, L. (2006) Structural and functional characterization of transmembrane segment VII of the Na^+/H^+ exchanger isoform 1. *J. Biol. Chem. 281*, 29817–29829.
10. Ding, J., Ng, R. W. P., and Fliegel, L. (2007) Functional characterization of the transmembrane segment VII of the NHE1 isoform of the Na^+/H^+ exchanger. *Can. J. Physiol. Pharmacol. 85*, 319–325.
11. Mitchell, S. M., Lee, E., Garcia, M. L., and Stephan, M. M. (2004) Structure and function of extracellular loop 4 of the serotonin transporter as revealed by cysteine-scanning mutagenesis. *J. Biol. Chem. 279*, 24089–24099.
12. Grunewald, M., Menaker, D., and Kanner, B. I. (2002) Cysteine-scanning mutagenesis reveals a conformationally sensitive reentrant pore-loop in the glutamate transporter GLT-1. *J. Biol. Chem. 277*, 26074–26080.

13. López-Corcuera, B., Núñez, E., Martínez-Maza, R., Geerlings, A., and Aragón, C. (2001) Substrate-induced conformational changes of extracellular loop 1 in the glycine transporter GLYT2. *J. Biol. Chem. 276*, 43463–43470.

14. Capendeguy, O., Chodanowski, P., Michielin, O., and Horisberger, J.-D. (2006) Access of extracellular cations to their binding sites in Na,K-ATPase: role of the second extracellular loop of the α subunit. *J. Gen. Physiol. 127*, 341–352.

15. Capendeguy, O., and Horisberger, J.-D. (2005) The role of the third extracellular loop of the Na^+,K^+-ATPase α subunit in a luminal gating mechanism. *J. Physiol. 565*, 207–218.

16. Unwin, N. (1995) Acetylcholine receptor channel imaged in the open state. *Nature 373*, 37–43.

17. Miyazawa, A., Fujiyoshi, Y., and Unwin, N. (2003) Structure and gating mechanism of the acetylcholine receptor pore. *Nature 423*, 949–955.

18. Hunte, C., Screpanti, E., Venturi, M., Rimon, A., Padan, E., and Michel, H. (2005) Structure of a Na^+/H^+ antiporter and insights into mechanism of action and regulation by pH. *Nature 435*, 1197–1202.

19. Slepkov, E. R., Rainey, J. K., Li, X., Liu, Y., Cheng, F. J., Lindhout, D. A., Sykes, B. D., and Fliegel, L. (2005) Structural and functional characterization of transmembrane segment IV of the NHE1 isoform of the Na^+/H^+ exchanger. *J. Biol. Chem. 280*, 17863–17872.

20. Slepkov, E. R., Chow, S., Lemieux, M. J., and Fliegel, L. (2004) Proline residues in transmembrane segment IV are critical for activity, expression and targeting of the Na^+/H^+ exchanger isoform 1. *Biochem. J. 379*, 31–38.

21. Wishart, D. S., Bigam, C. G., Holm, A., Hodges, R. S., and Sykes, B. D. (1995) ^1H, ^{13}C and ^{15}N random coil NMR chemical shifts of the common amino acids. I. Investigations of nearest-neighbor effects. *J. Biomol. NMR 5*, 67–81.

22. Bundi, A., Grathwohl, C., Hochmann, J., Keller, R. M., Wagner, G., and Wüthrich, K. (1975) Proton NMR of the protected tetrapeptides TFA-Gly-Gly-L-X-L-Ala-OCH_3, where X stands for one of the 20 common amino acids. *J. Magn. Reson. 18*, 191–198.

23. Wishart, D. S., Sykes, B. D., and Richards, F. M. (1992) The chemical shift index: a fast and simple method for the assignment of protein secondary structure through NMR spectroscopy. *Biochemistry 31*, 1647–1651.

24. Haynes, W. M., Ed. (2011) *CRC Handbook of Chemistry and Physics*, 92nd ed., CRC Press, Boca Raton, FL.

25. Bordag, N., and Keller, S. (2010) α-helical transmembrane peptides: a "divide and conquer" approach to membrane proteins. *Chem. Phys. Lipids 163*, 1–26.

26. Katragadda, M., Alderfer, J. L., and Yeagle, P. L. (2000) Solution structure of the loops of bacteriorhodopsin closely resembles the crystal structure. *Biochim. Biophys. Acta, Biomembr. 1466*, 1–6.

27. Bennett, M., Yeagle, J. A., Maciejewski, M., Ocampo, J., and Yeagle, P. L. (2004) Stability of loops in the structure of lactose permease. *Biochemistry 43*, 12829–12837.

28. Wu, J., Feng, M., and Ruan, K.-H. (2008) Assembling NMR structures for the intracellular loops of the human thromboxane A_2 receptor: implication of the G protein-coupling pocket. *Arch. Biochem. Biophys. 470*, 73–82.

29. Ruan, K.-H., Wu, J., So, S.-P., Jenkins, L. A., and Ruan, C.-H. (2004) NMR structure of the thromboxane A_2 receptor ligand recognition pocket. *Eur. J. Biochem. 271*, 3006–3016.

30. Lee, B. L., Li, X., Liu, Y., Sykes, B. D., and Fliegel, L. (2009) Structural and functional analysis of extracellular loop 2 of the Na^+/H^+ exchanger. *Biochim. Biophys. Acta, Biomembr. 1788*, 2481–2488.

31. Nygaard, E. B., Lagerstedt, J. O., Bjerre, G., Shi, B., Budamagunta, M., Poulsen, K. A., Meinild, S., Rigor, R. R., Voss, J. C., Cala, P. M., and Pedersen, S. F. (2011) Structural modeling and electron paramagnetic resonance spectroscopy of the human Na^+/H^+ exchanger isoform 1, NHE1. *J. Biol. Chem. 286*, 634–648.

32. Reddy, T., Li, X., Fliegel, L., Sykes, B. D., and Rainey, J. K. (2010) Correlating structure, dynamics, and function in transmembrane segment VII of the Na^+/H^+ exchanger isoform 1. *Biochim. Biophys. Acta, Biomembr. 1798*, 94–104.

Chapter 5

Structural and functional analysis of transmembrane region XI of the NHE1 isoform of the Na^+/H^+ exchanger

A version of this chapter has been published as:

- Lee, B. L., Li, X., Liu, Y., Sykes, B. D., Fliegel, L. (2009) Structural and functional analysis of transmembrane XI of the NHE1 isoform of the Na^+/H^+ exchanger. *J. Biol. Chem. 284*, 11546–11556.

BLL and XL contributed equally to this work. BLL performed and analyzed the NMR experiments. XL and YL performed the mutagenesis and accessibility experiments. The manuscript was written by BLL, XL, LF, and BDS.

Summary

We characterized structural and functional aspects of the critical transmembrane (TM) segment XI (residues 449–470) of the Na^+/H^+ exchanger isoform 1 (NHE1) by using cysteine scanning mutagenesis and high resolution NMR. Each residue of TM XI was mutated to cysteine in the background of the cysteine-less protein and the sensitivity to water-soluble sulfhydryl reactive compounds MTSET and MTSES was determined for those residues with at least moderate activity remaining. Of the residues tested, only proteins with mutations L457C, I461C, and L465C were inhibited by MTSET. The activity of the L465C mutant was almost completely eliminated, whereas that of the L457C and I461C mutants was partially affected. The structure of a peptide representing TM XI (residues K447–K472) was determined using high resolution NMR spectroscopy in dodecylphosphocholine (DPC) micelles. The structure consisted of helical regions between D447–Y454 and F460–K471 at the N- and C-termini of the peptide, respectively, connected by a

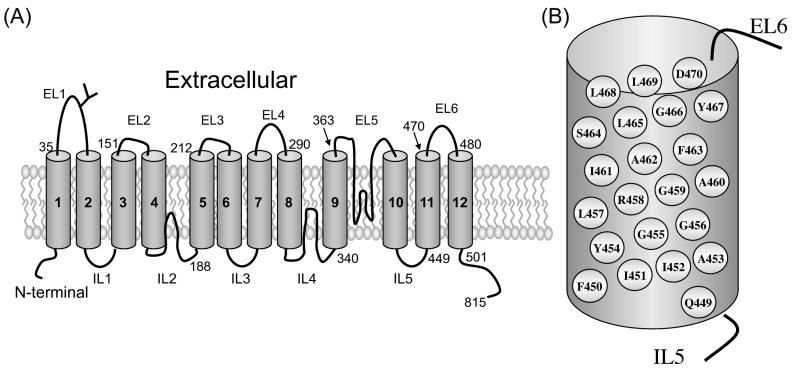

Figure 5-1. Models of the Na^+/H^+ exchanger. (A) Simplified topological model of the transmembrane domain of the NHE1 isoform of the Na^+/H^+ exchanger as described earlier (*1*). EL, extracellular loop; IL, intracellular loop. (B) Model of amino acids present in TM XI.

region with poorly defined, irregular structure consisting of residues G455–G459. TM XI of NHE1 had a structural similarity to TM XI of the *Escherichia coli* Na^+/H^+ exchanger NhaA. The results suggest that TM XI is a discontinuous helix, with residue L465 contributing to the pore.

Introduction

The membrane domain of human Na^+/H^+ exchanger isoform 1 (NHE1) contains 500 amino acids and is thought to consist of 12 transmembrane (TM) helices as determined by cysteine scanning accessibility mutagenesis by Wakabayashi et al. (Figure 5-1, A) (*1*). The membrane domain is responsible for ion movement across the membrane. The mechanism of transport of the membrane domain is of great interest both from a scientific viewpoint and in the design of improved NHE1 inhibitors that may be necessary for clinical use (*2*). In this regard, we have recently characterized the functionally important residues and the structure of TM IV, TM VII, and TM IX (*3–5*).

Several different lines of evidence have suggested that TM XI is also critical to NHE1 function. A recent study generated chimeras of NHE1 from various species and found that a region including TM XI was important in determining NHE1 inhibitor sensitivity (*6*). More specifically, mutagenesis of several amino acids of TM XI has shown that it is likely involved in either ion transport or proper targeting to the plasma membrane. Two mutants in TM XI, Y454C and R458C, are retained in the endoplasmic reticulum (*7*). In addition, mutation of G455 and G456 in TM XI shift the pH_i dependence of the exchanger to the alkaline side, whereas

mutation of R440 in intracellular loop 5 at the N-terminal end of TM XI shifts the pH_i dependence to make it more acidic (*8*, *9*). Also, the structure of the bacterial Na^+/H^+ exchanger NhaA has been elucidated. Both TM IV and TM XI play a critical role forming an assembly that cross, with each being a helix, an extended polypeptide and a short helix (*10*). We found that TM IV of NHE1 has a similar structure and function to that of TM IV of NhaA (*3*, *11*), leaving open the possibility that TM XI of NHE1 is also similar in structure and function to TM XI of NhaA.

For these reasons, we undertook a systematic examination of the structural and functional aspects of TM XI of the NHE1 isoform of the Na^+/H^+ exchanger. In this study we use cysteine scanning mutagenesis and site-specific mutagenesis to identify and characterize critical pore lining residues of the protein. We also use nuclear magnetic resonance (NMR) spectroscopy to characterize the structure of a synthetic peptide representing TM XI in dodecylphosphocholine (DPC) micelles. Evidence has suggested that TM segments of membrane proteins possess all the structural information required to form their higher order structures in their amino acid sequence (*12*). This has been demonstrated in earlier studies on membrane protein segments such as the cystic fibrosis transmembrane conductance regulator (*13*), a fungal G-protein coupled receptor (*14*), bacteriorhodopsin (*15*, *16*), and rhodopsin (*17*), where it was shown that isolated TM segments from membrane proteins had structures in good agreement with the segments of the entire protein. Also, the use of DPC micelles has been shown to be an excellent membrane mimetic environment for these studies (*18*, *19*). Our study identifies L465 as contributing to the pore of the protein and shows that the structure of TM XI consists of two helices corresponding to D447–Y454 and F460–K471 at the N- and C-termini, respectively, connected by a flexible region at residues G455–G459. The structure of TM XI was similar to the x-ray structure of TM XI of NhaA.

Experimental procedures

Experiments were performed essentially as described earlier in Chapter 2. Residues were mutated to cysteine in a cysteine-less NHE1 plasmid construct. The primers used for site directed mutagenesis are listed in Table 5-1. Based on the cysteine scanning results, additional mutations of L465 to alanine, lysine and aspartate were also made, and these primers are listed in Table 5-2. Transfection, characterization and cysteine accessibility were performed as described. A peptide representing TM XI (sequence KDQFIIAYGGLRGAIAFSLGYLLDKK, acetyl-

Mutation	Oligonucleotide sequence	Restriction site
Gln449	5′-GTATCGTG**AAGCTt**ACCCCCAAGGACtgcTTCATCATCGCC-3′	HindIII
Phe450	5′-CCCCCAAGGACCA**AtgcAT**CATCGCCTATGG-3′	SstI
Ile451	5′-CCCAAGGACCAGTTCtgcATCG**CaTATG**GGGGCCTGCGAG-3′	NdeI
Ile452	5′-GGACCAGTTCATC**tgcGCa**TATGGGGGCCTGC-3′	FspI
Ala453	5′-CCAGTTCATCATCtgcTATGG**aGGCCT**GCGAGGGGC-3′	StuI
Tyr454	5′-CAGTTCATCATC**GCatgc**GGGGGCCTGCGAGG-3′	SphI
Gly455	5′-CATCATCGCCTATtgcGG**CttaaG**AGGGGCCATCGCC-3′	AflII
Gly456	5′-CATCGCCTATGGGtgc**ttaaG**AGGGGCCATCGCC-3′	AflII
Leu457	5′-GCCTATGGGGGCtg**cCGcGG**GGCCATCGCCTTC-3′	SacII
Arg458	5′-CATCGCCTATGG**aGGCCT**GtgtGGGGCCATCGCC-3′	StuI
Gly459	5′-GGGGGCCTGCGA**tgcGCA**ATCGCCTTCTCTC-3′	FspI
Ala460	5′-GGGGCCTGCGAGG**atgCAT**CGCCTTCTCTC-3′	NsiI
Ile461	5′-GGCCTGCGAGGG**GCATGC**GCCTTCTCTCTGGG-3′	SphI
Ala462	5′-CTGCGAGGGGC**CATatg**CTTCTCTCTGGGC-3′	NdeI
Phe463	5′-GAGGGGCCATC**GCatgc**TCTCTGGGCTACC-3′	SphI
Ser464	5′-GGCCATCGCCTTCTg**cCTaGG**CTACCTCCTGG-3′	AvrII
Leu465	5′-CATCGCCTTCTCTtgcG**GgTACC**TCCTGGACAAG-3′	KpnI
Gly466	5′-CGCCTTCTCTCTGtGCTACCT**tCTaGA**CAAGAAGCACTTC-3′	XbaI
Tyr467	5′-CCTTCTCTCTGGGCT**gtCTaC**TGGACAAGAAGCAC-3′	AccI
Leu468	5′-CTCTCTGGGCTACtg**tCTaGA**CAAGAAGCACTTC-3′	XbaI
Leu469	5′-GCCTTCTCTCTGG**GaTAtC**TCtgcGACAAGAAGCACTTC-3′	EcoRV
Asp470	5′-GGGCTACCTCCTGtgcAAaAAGCACTTCCCCATG-3′	(XmnI)

Table 5-1. Oligonucleotides used for site-directed mutagenesis of TM XI. Mutated nucleotides are in lower case lettering, restriction sites are bold. Restriction sites deleted are indicated in parentheses. Oligonucleotides used for cysteine scanning mutagenesis are shown. All mutations were to Cys.

Mutation	Oligonucleotide sequence	Restriction site
L465A	5′-GCCATCGCCTTCTCTgcGG**GgTACC**TCCTGGACAAG-3′	KpnI
L465K	5′-GCCATCGCCTTCTCTaaGG**GgTACC**TCCTGGACAAG-3′	KpnI
L465D	5′-GCCATCGCCTTCTCTgatG**GgTACC**TCCTGGACAAG-3′	KpnI

Table 5-2. Synthetic oligonucleotides used for mutagenesis of L465 to Ala, Lys, or Asp.

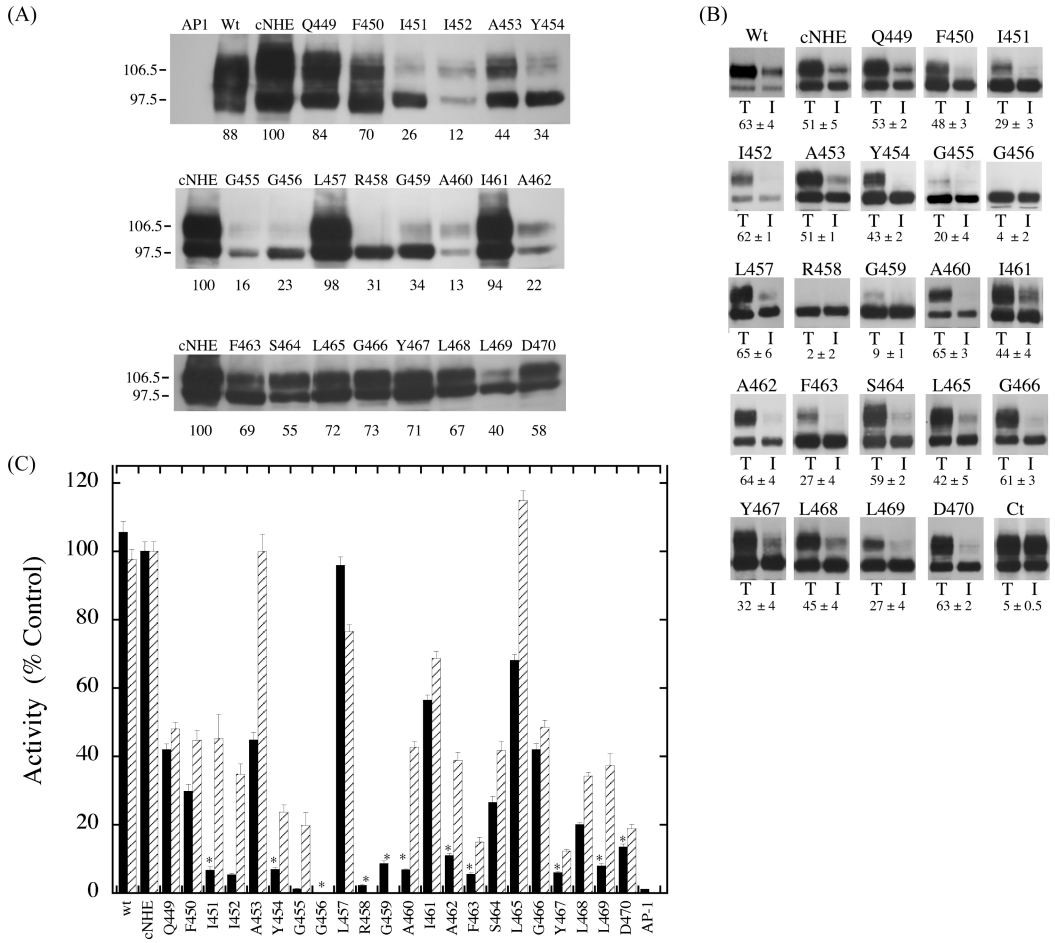

Figure 5-2. Analysis of wild type and mutant NHE1 proteins. (Continued on page 89.)

capped N-terminus, amide-capped C-terminus) was purchased from GI Biochem (Shanghai) Ltd. at ∼95% purity. An ∼5% impurity was identified in the ^{1}H NMR spectra (see below). NMR and structure calculation were also performed as described. In addition to the 2D COSY, TOCSY and NOESY homonuclear spectra, a 2D ^{13}C-^{1}H natural abundance HSQC was also obtained at 500 MHz. The ensemble of NMR structures and the structure calculation restraints have been deposited in the Protein Data Bank and Biological Magnetic Resonance Bank (PDB code 2KBV, BMRB accession number 16056).

Results

Figure 5-1, A, shows a general model of the NHE1 isoform of the Na^{+}/H^{+} exchanger based on the topology deduced by cysteine scanning accessibility studies (*1*). Figure 5-1, B, shows a schematic model illustrating the amino acids of TM XI.

Figure 5-2. (Continued from page 88.) (A) Western blot of cell extracts of AP-1 cells containing stably transfected Na^+/H^+ exchanger mutants or control. In all mutations the amino acid indicated was changed to cysteine. 100 μg of total protein was loaded in each lane. Numbers below the lanes indicate the values obtained from densitometric scans of both the 110 and 95 kDa bands relative to wild type NHE. Results are typical of three to five measurements. AP1 refers to mock transfected AP-1 cells. Wt, refers to cells stably transfected with wild type Na^+/H^+ exchanger protein. (B) Subcellular localization of control and TM XI mutants in AP-1 cells. Sulfo-NHS-SS-biotin-treated cells were lysed and streptavidin-agarose beads were used to bind labelled proteins as described under "Experimental Procedures." Equal amounts of total cell lysate (T) and unbound intracellular lysate (I) were run on SDS-PAGE and Western blotting with anti-HA antibody identified NHE1 protein. Wt, refers to cells stably transfected with wild type Na^+/H^+ exchanger protein. Ct refers to a control experiment in which nonspecific binding to streptavidin-agarose beads was carried out following the standard procedure but without labelling cells with biotin. The percent of the total NHE1 protein found within the plasma membrane is indicated for each mutant. For Ct, the numbers indicate the amount of nonspecific binding to streptavidin-agarose beads. Results are the mean ± S.E. of at least three determinations. (C) Rate of recovery from an acid load by AP-1 cells stably transfected with cNHE1, and TM XI Na^+/H^+ exchanger mutants. Na^+/H^+ exchanger activity was measured after transient induction of an acid load as described under "Experimental Procedures." The activity of cNHE1 stably transfected with NHE1 was 0.036 ΔpH/s, and this value was set to 100%. All mutations to cysteine were done in the background of the cysteine-less NHE1 and activities are percent of those of cNHE. Mutations were in the cNHE1 and results are expressed as mean ± S.E. of 8–16 determinations. Results are shown for mean activity of both uncorrected (black) and normalized for surface processing and expression levels (hatched). * indicates mutants with uncorrected activity that is less than 20% of cNHE1.

To examine which amino acids of TM XI are pore-lining, we used the cysteine-less Na^+/H^+ exchanger (cNHE1). Each residue in TM XI of cNHE1 was mutated to a cysteine residue. Initial experiments examined whether these mutant forms of the Na^+/H^+ exchanger were active enough for further study. Figure 5-2, A–C, examines the expression, targeting, and activity of the wild type and mutant TM XI mutants. Expression levels of several of the mutants were greatly decreased in comparison to the controls. Changing I452, G455, or A460 to Cys decreased expression to less than 20% of that of cNHE1. Eight other mutant Na^+/H^+ exchangers, I451C, A453C, Y454C, G456C, R458C, G459C, A462C, and L469C, also had expression reduced to levels 22–45% that of cNHE1. All the mutants with reduced expression of NHE1 showed a great reduction in the level of mature, fully glycosylated protein. In some of these mutants (I451C, Y454C, G455C, G456C, R458C, G459C, and L469C) expression was predominantly of the lower molecular weight form of the Na^+/H^+ exchanger, which represents protein with reduced levels of glycosylation. We have earlier shown that unglycosylated Na^+/H^+ exchanger may be functional (*20*), therefore the unglycosylated protein was included in analysis of the levels of protein expression.

We have previously (*3*) demonstrated that the mutation of amino acids of transmembrane segments in the Na^+/H^+ exchanger can affect the plasma membrane targeting of the protein. Therefore, we examined intracellular targeting of the NHE1 TM XI expressing cell lines. Cells were treated with sulfo-NHS-SS-biotin and then lysed and solubilized as described under "Experimental Procedures." Labelled proteins were bound to streptavidin-agarose beads and equal amounts of total cell lysates and unbound lysates (representing intracellular protein) were separated by size using SDS-PAGE. Western blotting with anti-HA antibody identified the tagged NHE1 protein. Figure 5-2, B, illustrates examples of the results and a summary of quantification of both the 106 and 97 kDa bands. The immature form of the protein was included because we previously noted that there can be some leak of this protein to the cell surface (*21*). A number of the mutants had reduced targeting to the cell surface, in comparison to cNHE1. Less than 10% of G456C, R458C, and G459C were targeted to the cell surface, and because the nonspecific was $\sim$5%, the results suggest that these proteins were mostly, if not all, retained within the cell. A second class of mutant was targeted about half as well as the cysteine-less NHE1, with $\sim$20–30% targeted to the cell surface. This consisted of I451C, G455C, F463C, Y467C, and L469C. The balance of the mutants were similar to cNHE1 in their targeting efficiency.

We determined how mutations of TM XI affected the activity of the protein. The rate of recovery from an acute acid load was determined as described earlier (*21*). Figure 5-2, C, illustrates the rate of recovery from an acute acid load by stable cell lines transfected with either wild type Na^+/H^+ exchanger or mutants of TM XI. The rate of recovery is also shown when corrected for both the level of expression and surface targeting for most mutants. The mutants fell into several general categories. One mutant A453C had less than 50% of the cNHE activity, but the activity was near normal when correcting for expression levels and surface targeting, suggesting that the protein itself was fully functional but the mutations were affected for expression levels and surface targeting. L465C was similar to A453C but with higher uncorrected NHE1 activity. In both cases this was due to a combination of effects on expression levels and surface targeting. Mutants L457C and I461C retained over 50% of cNHE1 activity and had relatively normal surface targeting and expression levels. The balance of the mutants had quite reduced activity, less than 50% of the cNHE1 level. Q449C, F450C, S464C, and G466C had 25–45% of cNHE1 activity and this was only slightly improved by correcting for expression levels and surface targeting. This indicated that these proteins themselves were at least partially defective in Na^+/H^+ exchange activity. A number of other mutants had quite low activity relative to cNHE1, less than 20% of uncorrected values. This included I451C, I452C, Y454C, G455C, G456C, R458C, G459C, A460C, A462C, F463C, Y467C, L468C, L469C, and D470C. For most of these mutants correcting for expression levels and surface targeting increased activity although this was always well below that of cNHE1, suggesting that the effects were at least in part due to direct effects on the activity of the protein. It was not possible to accurately determine the corrected activity for many of these mutants because of their variability, low expression levels, and poor surface targeting. This included G456C, R458C, and G459C.

We examined the sensitivity to MTSET or MTSES of the mutant Na^+/H^+ exchangers that had greater than 20% residual activity of cNHE1 (Figure 5-3, A and B). Of the active Na^+/H^+ exchangers, only L465C was greatly affected by treatment with positively charged MTSET. This resulted in elimination of most of the activity of the protein. Two other mutants, L457C and I461C, were partially inhibited by MTSET. Negatively charged MTSES had no effect on any of the mutant proteins. Mutants G459C and A460C are not illustrated in the inhibition results due to their low activity, but were also tested. Experiments indicated that they were not inhibited by addition of MTSES or MTSET.

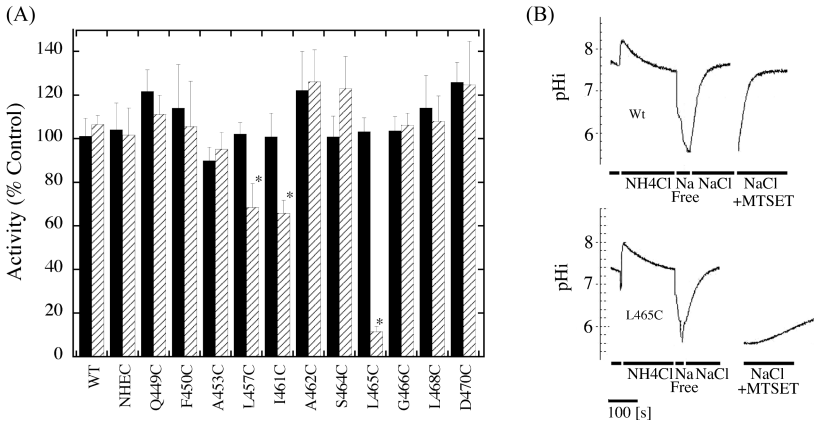

Figure 5-3. Effect of MTSET and MTSES on activity of cNHE1 and single cysteine TM XI mutant NHE1 containing cell lines. (A) Summary of results of Na^+/H^+ exchanger assays of active TM XI mutants. Activity was measured after two pulses of transient induction of an acid load as described under "Experimental Procedures." The first activity was in the absence of MTSES or MTSET, the second was when cells were treated with 10 mM reagent before transient acidification. Results illustrated represent the percentage of activity of the second acid load, in comparison to the first. * indicates that the second recovery from acid load was significantly lower than the first at $p < 0.01$, Mann-Whitney U test. Solid filled bars represent MTSES treatments and hatched bars represent MTSET treatments. (B) Example of results of effect of MTSET on activity of wild type and L465C mutant. Wild type (Wt) and L465C NHE1 protein activity was assayed in stably transfected AP-1 cells as described under "Experimental Procedures." Activity was measured after two acid pulses as described in (A). The first pulse in the absence of MTSET is shown. For ease of viewing, only the recovery from acidosis is shown for the second pulse, in which cells were treated with MTSET. NH_4Cl, treatment with ammonium chloride; sodium free, treatment with Na^+ free buffer to induce acidosis; NaCl, recovery from acidosis in NaCl containing buffer, for the second pulse this contained MTSET and cells were pretreated with MTSET for 10 min prior to NH_4Cl-induced acid load.

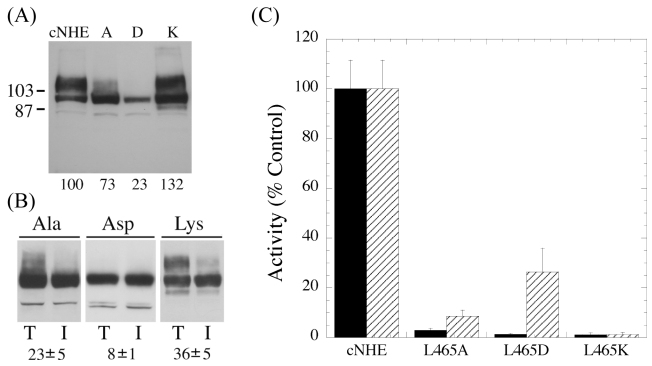

Figure 5-4. Characterization of site-specific mutants of L465. (A) Western blot of cell extracts of AP-1 cells containing stably transfected Na^+/H^+ exchanger mutants or control. Samples were analyzed as described in the legend to Figure 5-2, A. Numbers below the lanes indicate the values obtained from densitometric scans of both the 110 and 95 kDa bands relative to wild type NHE1. Results are typical of three to five measurements. cNHE refers to cysteine-less NHE1. A, D, and K refer to mutant cell lines containing cNHE1 with the L465 mutations to Ala, Asp, and Lys respectively. (B) Subcellular localization of TM XI mutants in AP-1 cells. Mutants contained the NHE1 L465 mutations to Ala, Asp, and Lys as indicated. Sulfo-NHS-SS-biotin-treated cells were lysed and streptavidin-agarose beads were used to bind labelled proteins as described under "Experimental Procedures." Equal amounts of total cell lysate (T) and unbound intracellular lysate (I) were run on SDS-PAGE and Western blotting with anti-HA antibody identified the NHE1 protein. The percent of the total NHE1 protein found within the plasma membrane is indicated for each mutant. Results are the mean ± S.E. of at least three determinations. (C) Rate of recovery from an acid load by AP-1 cells stably transfected with cNHE, and TM XI Na^+/H^+ exchanger L465 mutations to Ala, Asp, and Lys. Na^+/H^+ exchanger activity was measured after transient induction of an acid load as described in the legend to Figure 5-2, C. All mutations to cysteine were done in the background of the cysteine-less NHE1 and activities are percent of those of cNHE. Mutations were in the cNHE1 and results are expressed as mean ± S.E. of 8–16 determinations. Results are shown for mean activity of both uncorrected (black) and normalized for surface processing and expression levels (hatched).

Because of the strong effect that we observed of MTSET on L465C, we conducted a series of experiments in which we mutated that amino acid to a neutral residue (Ala), to a negatively charged residue (Asp), and to a positively charged residue (Lys). We then determined effects on activity, surface processing, and expression of the intact NHE1 protein. The results are shown in Figure 5-4. Western blotting (Figure 5-4, A) against the anti-HA tag of the NHE1 mutant proteins showed varying effects dependent on the mutation. Mutation of L465 to Asp resulted in a large decrease in the amount of protein expressed and in addition, virtually all of the protein expressed was of the unglycosylated or partially glycosylated form. Similarly, mutation to Ala reduced the amount of protein expressed and reduced the amount of fully glycosylated protein, but not to as great an extent. Mutation of L465 to Lys did not reduce the amount of NHE1 expressed. There was also a significant amount of fully glycosylated protein although the amount relative to the de-glycosylated protein was somewhat reduced. In all three cases, targeting to the cell surface was low (Figure 5-4, B). This was especially true for the L465D mutant. Activity of the three mutants was greatly reduced (Figure 5-4, C). In all cases the raw activity we observed for the mutants was only a small fraction of the control level. It was of interest that for the L465A and L465D mutants, there was a significant amount of activity present, when correcting for aberrant surface targeting and expression levels. In contrast, the L465K protein was well expressed and targeted to the cell surface, but the change to a positively charged residue completely eliminated activity of the protein.

We used NMR spectroscopy to determine the structure of a TM XI peptide. Cationic residues at the termini of peptides have been shown to aid in their purification and maintenance of transbilayer orientation (*22*). For this reason, the ends of the peptide were chosen to be K447 and K472, which provides cationic residues at both ends of the peptide and include the predicted TM XI sequence. The N- and C-terminal acetyl and amide caps, respectively, remove charges at the peptide termini that would not be present in the full protein.

The peptide was readily solubilized in the presence of DPC, which acts as a membrane mimetic, and provided a sample that was stable for months at room temperature. Previous structural studies of transmembrane helices from NHE1 also found DPC micelles to be effective for solubilization and sample stability (*5*, *23*). An examination of the two-dimensional ^{1}H-^{1}H NMR spectra showed additional peaks that could not be assigned to the major conformation of the TM XI peptide. Adjusting sample conditions such as peptide concentration and the peptide-to-lipid

Unique NOE restraints	
Total	548
Intraresidue	195
Sequential	195
Medium range ($i+2$ to $i+4$)	156
Long range ($\geq i+5$)	2
Ambiguous	47
Ramachandran plot statistics	
Core	72.0%
Allowed	26.0%
Generously allowed	1.0%
Disallowed	1.0%
XPLOR-NIH energies (kcal/mol)	
Total	16.78 ± 2.44
NOE	0.89 ± 1.03
NOE violations	
0.1–0.2 Å	6
0.2–0.3 Å	2
> 0.3 Å	1

Table 5-3. NMR structural statistics for the 40 structures retained out of 50 structures calculated.

ratio did not affect intensity of these peaks in the DQF-COSY NMR spectra, and therefore they were assumed to be an impurity ($\sim$5% based upon the area of the NMR peaks) in the synthetic TM XI peptide and not a minor conformation in slow exchange. The sample for structure determination contained $\sim$2 mM TM XI peptide and $\sim$150 mM DPC in 95% H_2O, 5% D_2O with 0.25 mM deuterated 2,2-dimethyl-2-silapentane-5-sulfonic acid as a chemical shift and intensity standard. Concentrations of 1 mM peptide and 75 mM DPC were used in previous studies (*4*, *5*); however, we decided to use concentrations of 2 and 150 mM for an increased signal to noise ratio in the NMR spectra. There were no noticeable differences in the spectra at the higher concentration. Spectra were taken at 30 °C, which gave good one-dimensional ^{1}H NMR spectral characteristics.

Sequential assignment using two-dimensional ^{1}H-^{1}H DQF-COSY, TOCSY, and NOESY NMR spectra allowed all of the hydrogen atoms in the peptide to be assigned except for Phe Hζ and Tyr Hη. Assignments for carbon atoms using the natural abundance ^{13}C-^{1}H HSQC NMR spectrum were incomplete because of the limited chemical shift dispersion. The predominantly α-helical nature of the peptide, resulting in limited chemical shift dispersion, and the relatively broad line widths in the spectra, meant some of the NOE assignments were ambiguous. The impurities were $\sim$5% of the concentration of the TM XI peptide, and any impurities from the NOE, similarly reduced, were unlikely to be a concern for assignment. Nonetheless, a soft-well potential function was used during structure calculation to allow for any ambiguous or erroneous assignments. Dihedral angle restraints

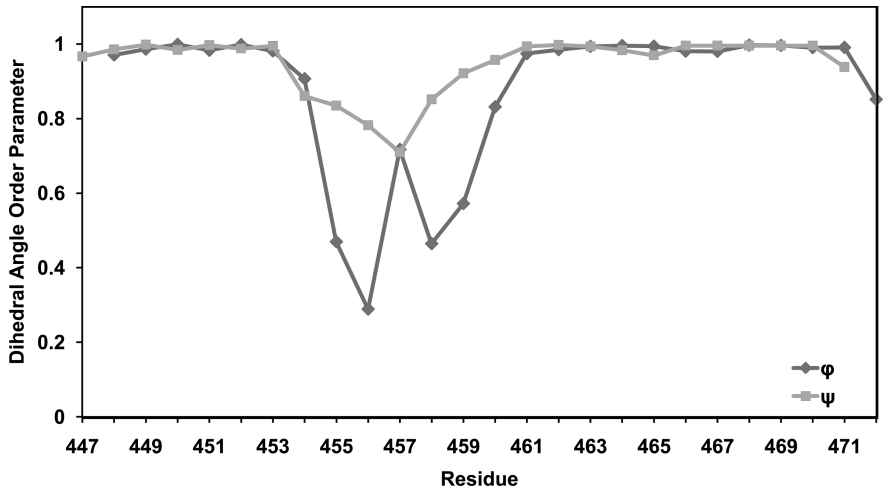

Figure 5-5. Dihedral angle order parameters for the final 40 ensemble members. Order parameters are calculated as in reference (*23*). An order parameter of 1 indicates the particular angle is the same for all members in the ensemble, and is 0 when the angles are completely random.

were not initially applied during structure calculation to allow the structure to be based mainly on the observed NOE distance restraints. Chemical shift prediction of secondary structure (*24*, *25*) (Figure 5-S1) and NOE connectivities ($i+3$ and $i+4$) (Figure 5-S2) suggested helical regions at approximately residues 449–453 and 461–469. Therefore, the phi and psi angles in these regions were restricted to $-60\pm30^\circ$ and $-40\pm40^\circ$, respectively, for additional rounds of annealing and refinement. After refinement, a total of 548 unique restraints were used for the final structure calculation. The 40 lowest energy structures of the 50 calculated were retained, which satisfied restraints with minimal NOE and dihedral angle violations. Structure calculation statistics are summarized in Table 5-3 and Figure 5-S2.

It was not possible to superimpose the entire ensemble of NMR structures over the full-length of the peptide. The pair wise backbone r.m.s. deviation for each of the ensemble members compared with the average structure ranged from 1.81 Å to 4.36 Å. Superposition of the ensemble members was done using the method of Kabsch (*26*), as implemented in LSQKAB in the CCP4 suite. To look for regions of fixed structure, segments of the peptide 4 to 15 residues long were superimposed, and contiguous segments of residues obtained from the superimpositions with an r.m.s. deviation less than 1.0 Å were examined based on the length and r.m.s. deviation of the segments.

Residues K447–G454 at the N-terminus and A460–K471 at the C-terminus best indicated a region of fixed structure from the r.m.s. deviation analysis and

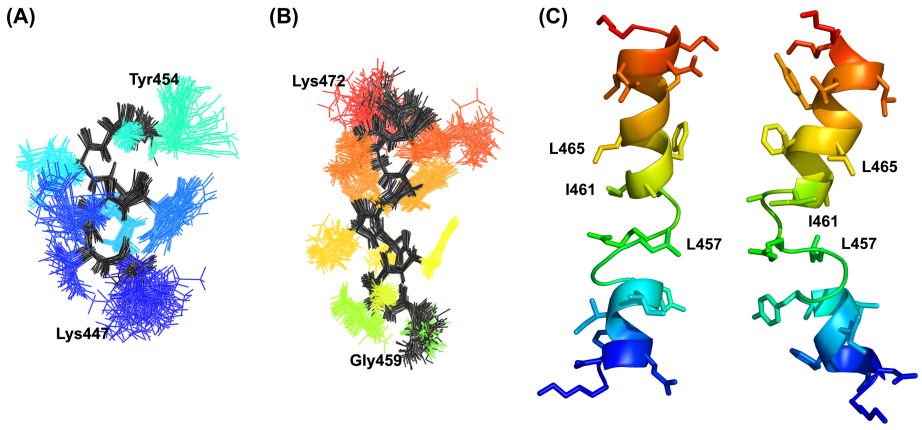

Figure 5-6. NMR structure of TM XI in DPC micelles. Superimposition of structurally conserved regions of the TM XI peptide structure. Superimposition of the backbone atoms of the structurally conserved regions (A) K447–G454 and (B) G460–K471. The backbone is shown in black, side chains are shown in color. (C) Two views of a single ensemble member with MTSET-sensitive residues labelled.

are mainly helical. The relative orientation of these two regions vary with respect to each other among the ensemble members around a structurally variable central region consisting of residues G455–G459. The dihedral order parameters (*23*) (Figure 5-5) for the N- and C-terminal regions are close to unity, indicating strongly conserved dihedral angles in these regions across the ensemble, whereas the order parameter for the central region shows large variation in the dihedral angles for those residues. A plot of the averaged backbone r.m.s. deviations per residue versus the average structure, for superimposition of residues 447–454 and 460–471, is shown in Figure 5-S3. The two superimposed regions show low r.m.s. deviations, which increase in toward the extended region. The superimposition of the C-terminal helix (Figure 5-S3, diamonds) shows an increase in r.m.s. deviation at residues L465–G466. This is reflected in the structures as a slight bend in the helix at these residues. Superimposition of residues A460–L465 and G466–K471 separately give better r.m.s. deviation values than for the entire C-terminal helix, and show that there is some slight variability between the two halves of the helix at this bend. Residues F461–K471 and D448–Y453 fall within the helical region of the Ramachandran plot and show good clustering of the dihedral angles, and so can be assigned as α-helical. Superimposition of the structurally conserved regions at the N- and C-termini are shown in Figure 5-6, A and B. Figure 5-6, C, shows a schematic of an ensemble member from two views, which shows the general structure of the peptide: two helices connected by an extended segment.

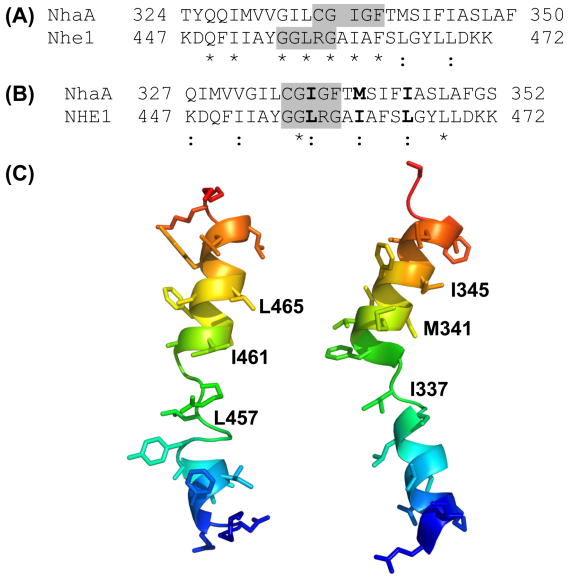

Figure 5-7. Comparison of TM XI of NHE1 with TM XI of NhaA. (A) SEQSEE based (*27*) alignment of the amino acid sequences of TM XI of NhaA and NHE1. (B) Alignment of the sequences based on optimal structural alignment of the extended regions (highlighted) of NHE1 TM XI (G455–G459) and NhaA TM XI. Colon indicates replacement by similar amino acid and asterisk indicates amino acid identity. MTSET-sensitive residues, and the corresponding residues in NhaA are shown in bold. (C) Comparison of the NMR structure of TM XI of NHE1 in DPC micelles with that of TM XI in the x-ray structure of NhaA. Amino acids 447–472 of NHE1 and amino acids 327–352 of NhaA are included. The ensemble member of the NMR structures chosen for comparison had the lowest backbone r.m.s. deviation compared with the corresponding region in NhaA for the superimposition of the extended regions, and with arbitrary rotation of the two helices around the flexible G455 and G459 to match the helices of NhaA.

The region between the two helices does not superimpose well. At best, G455–R458 superimposes poorly, with an r.m.s. deviation of 0.8 Å, and shows decreased dihedral angle order parameters compared with the helical regions. The large variation in dihedral angles over this segment and variation in the relative orientation of the helices in the ensemble could suggest that this region is flexible. It should be noted, however, that variability seen in the structure could be a result of a lack of NOE restraints to constrain the structure of that region, instead of actual flexibility in the structure. Glycine residues have fewer NOE restraints compared with other residues (Figure 5-S2) due to the lack of side chain contacts, and could explain the variability in the structures because much of the flexibility in the structure occurs around Gly residues, 455, 456, 459, and 466.

A comparison of the NMR structure of TM XI of NHE1 in DPC micelles

with the structure of TM XI in the x-ray structure of NhaA is presented in Figure 5-7. Figure 5-7, A, shows an alignment of the TM XI sequences from NhaA and NHE1 using SEQSEE (*27*), which shows reasonable sequence similarity but a poor alignment of the helical and central regions that are predicted by the x-ray and NMR structures. Attempting to align the structures of the extended region to the x-ray structure of TM XI of NhaA results in reasonable backbone superimposition of residues 455–459 of NHE1 on to residues 335–339 of NhaA, with the orientations of both the N- and C-terminal helices around this segment varying. Using this central region to align the sequences of NHE1 and NhaA TM XI (Figure 5-7, B) suggests that the MTSET-sensitive residues L457, I461, and L465 identified in this article would correspond to I337, M341, and I345, respectively. Figure 5-7, C, shows a comparison of structures of NhaA and NHE1 TM XI with arbitrary rotation of the helices around the variable G455 and G459 residues in the NMR structure to better match the orientation of the NhaA helical regions. Clearly the general structure of the two peptides is similar for the two proteins; although this cannot be taken as proof that the NMR structure in DPC micelles is equivalent to that of the full-length protein in vivo.

Discussion

In this study we examined the structural and functional characteristics of TM XI of the NHE1 isoform of the Na^+/H^+ exchanger. A number of studies (*6*, *8*, *9*) have suggested that this transmembrane segment is critical in activity of the protein. When we replaced amino acids of TM XI with cysteines we found that it was quite sensitive to this substitution. Of the 22 amino acids mutated, 14 had activity severely reduced. Several others also had activity reduced to a lesser degree. We found earlier that the susceptibility to mutation was high in some transmembrane segments such as TM IV, whereas other TM segments such as TM IX appear more tolerant of changes. We noted this variability earlier (*5*) and it has been found in other proteins (*28*). This could reflect a more critical role of a particular TM segment, in function. Of note, amino acids 454–463 were all greatly reduced in activity, with the exception of L457 and I461. Most of the mutations made resulted in decreased activity of the product protein that were often caused at least partially by effects on targeting and expression levels. R458 and Y454 of this region have previously (*7*) been suggested to be retained in the endoplasmic reticulum when mutated to cysteine. In our hands, proteins with these mutations showed little activity. We found

that R458 was retained in an intracellular location, however, targeting of Y454 was only slightly reduced below that of the cysteine-less protein. It was not possible to test either mutant protein for the effects of sulfhydryl reactive reagents on activity.

When we examined the remaining active mutants for sensitivity to sulfhydryl reactive reagents, we found that only the L465C mutant was strongly affected by positively charged MTSET. It was unaffected by negatively charged MTSES. This suggested that this residue is likely a pore lining residue of the protein. That the positively charged compound would inhibit activity, but not the negatively charged one, could be due to direct electrostatic repulsion of a transported cation. MTSES would not provide any such repulsion. This concept is supported by site-specific mutagenesis studies of this amino acid. The L465K mutant was totally inactive despite being well expressed and targeted to the plasma membrane. The L465D mutant, whereas reduced in activity and not well targeted or expressed, was still functional. Mutation of L465 to Ala resulted in a protein with minimal activity, possibly due to structural effects of expression of the smaller amino acid. The L465A protein was poorly expressed and targeted.

We also found that MTSET treatment resulted in reduction of activity of two other amino acids, L457 and I461. We suggest that their side chains may be near and partially accessible to the protein translocation pore, but likely are not directly pointing to the pore. This is supported by the structural analysis of the protein. TM XI was found to be comprised of two helical segments, with an intervening more extended region. The location of the pore lining residues in the peptide structure is shown in Figure 5-6, C. Both L465 and I461 are on the same side of the C-terminal helix. Looking down the helical axis, the two residues are $\sim 40^{\circ}$ offset from each other, such that L465 could be pointing into the pore, whereas I461 is not directly pointing toward the pore, but is at an orientation in agreement with the idea that it could be close to the pore. The side chain of L457 is located in the structurally variable region, so no conclusion can be drawn about its orientation from the peptide structure. Further insights into its orientation must await elucidation of the structure of the intact protein and its presence in a variable region is likely a limitation in the present analysis imposed by examining the peptide in DPC micelles. In the full protein, the extended region would likely be more rigid and L457 in a different position due to the environment and interactions provided by the surrounding TM helices in the intact protein.

It is important to note that recently, there has been disagreement on the proposed topology of the NHE1 protein. An earlier model (*7*) used substituted

cysteine accessibility studies to predict a 12-TM protein with an internal C-terminus and several membrane-associated segments (Figure 5-1, A). More recently, Landau et al. (*29*) proposed a different topology using the crystal structure of *Escherichia coli* NhaA as a template for bioinformatics and computational analysis for fold alignment algorithms to propose a new topology. Although several of the TM segments differed between the two models, TMs X–XII were essentially unaltered. This supports the assignment of these amino acids as TM XI in our study.

We found that TM XI consisted of two helical regions, comprising amino acids 447–453 and 460–471 connected by an extended region from amino acids 455–459. In their study, Landau et al. (*29*) made several predictions about the structure of TM XI. They suggested that G455 and G456 would facilitate unwinding of that region of the TM XI helix. Our results agree with their predictions as these two amino acids were within the extended region of amino acids 455–459. The fact that there were only two amino acids that retained good functional activity within the 454–463 sequence supports the concept that this is a domain critical to function of the protein. Unfortunately mutant proteins containing these amino acids did not retain enough activity to be examined functionally.

G455 and G456 have been shown to be critical in affecting the set point of the NHE1 protein and have been suggested to constitute important elements of the pH sensor of NHE1 (17, 18). Their presence in a conserved extended region of the protein would support this hypothesis. It should be noted, however, that in NhaA, Arkin et al. (*30*) favour a model of pH regulation by which protonation-deprotonation of a single carboxyl of an acidic residue affects protein structure and regulates pH sensitivity. If this were true for NHE1, then changes to G455 and G456 would likely affect NHE1 function through alterations in structure, which secondarily alter the pH sensor of the protein or regulation by the pH sensor. We found that mutation of these two residues resulted in both reduced expression and glycosylation of the protein. In addition, targeting of the protein was mostly aberrant. This, plus their presence in, and possible mediation of the structure of the extended region supports the concept that they are critical for the structure of the protein.

Because TM IV of NHE1 has a similar structure and function to TM IV of NhaA (*11*), we examined the possibility that TM XI of NHE1 has a similar structure and function to TM XI of NhaA. Although the two proteins have poor primary amino acid sequence conservation, we have earlier suggested that they may have similar three-dimensional structures and might conserve key residues important in function (*31*). We therefore compared our structure of TM XI of NHE1 with the

NhaA crystal structure (*10*). The equivalent of the MTSET-sensitive residues L465 and I461 of NHE1 in the NhaA structure would be I345 and M341, respectively, based on the alignment shown in Figure 5-7, B. Residues 345 and 341 in NhaA are on the C-terminal helix of TM XI, on the periplasmic side of the pore. If the corresponding residues in NHE1 are in a similar location, near the extracellular pore, this would account for them being MTSET accessible. Residue I337 of NhaA, equivalent to residue L457 in NHE1, does not appear to be accessible from the pore and points toward the cytoplasmic side. The crystal structure is of an inactive state of NhaA, however; conformational changes suggested to occur with activation (*32*, *33*) may allow access to this region.

In summary, we have shown that TM XI of NHE1 is critical to function of the protein and possesses a pore lining residue at amino acid L465. The structure of TM XI is that of a helix with an intervening interrupted irregular structure consisting of residues G455–G459. It has an overall similarity to the structure of TM XI of the *E. coli* antiporter NhaA. Future experiments will further compare the structure and function of NHE1 with that of NhaA in an effort to further elucidate the mechanism of function of the mammalian Na^+/H^+ exchanger. Solving the structure of the full-length protein will provide more details of transmembrane segment overall structure and elucidate the precise location of any residues that are in variable regions of peptide segments.

Supplementary Materials

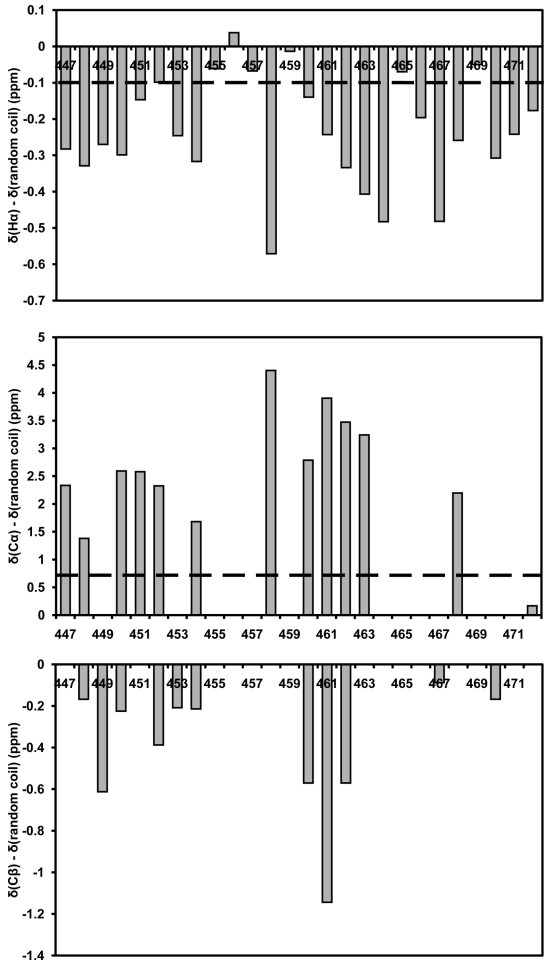

Figure 5-S1. Chemical shift index prediction of secondary structure. Difference between observed and random coil chemical shifts (*25*) for each residue in the TM XI peptide for Hα (top), Cα (center), and Cβ (bottom) chemical shifts. Contiguous segments showing upfield shifts for Hα (< -0.1 ppm, dotted line) and Cβ atoms and downfield shifts for Cα atoms (> 0.7 ppm) from random coil values indicate helical character. Unassigned Cα and Cβ atoms are given a value of zero in the figure.

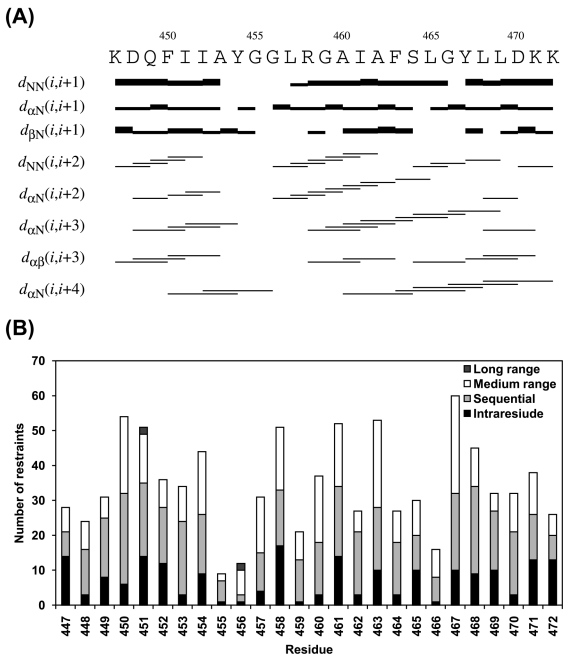

Figure 5-S2. NOE restraints used in the final TM XI structure calculation. (A) A summary of the NOE restraints between particular HN, Hα, Hβ atoms, modified from CYANA output (L.A. Systems, Inc.). (B) Summary of the number of NOE restraints per residue classified as intraresidue, sequential, medium range ($i+2$ to $i+4$), and long range ($> i+4$).

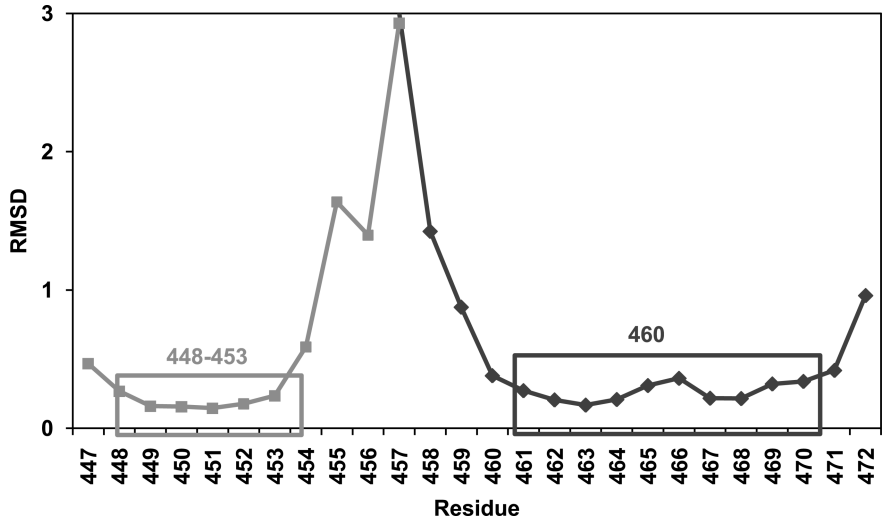

Figure 5-S3. Per residue RMSD values for the optimal superimpositions of the N- and C- terminal helices. Superposition and RMSD calculations were performed with LSQKAB from the CCP4 suite, and with custom scripts. Regions of the calculated ensemble of the peptide were iteratively superimposed, and the resulting segments with RMSD less than 1.0 Å were further sorted by size and RMSD over the segment to find the optimal regions for superimposition. Per-residue RMSDs are shown for the superimpositions of the backbone atoms of K447–G454 (squares) and G460–K471 (diamonds).

References

1. Wakabayashi, S., Pang, T., Su, X., and Shigekawa, M. (2000) A novel topology model of the human Na^+/H^+ exchanger isoform 1. *J. Biol. Chem. 275*, 7942–7949.
2. Karmazyn, M., Sawyer, M., and Fliegel, L. (2005) The Na^+/H^+ exchanger: a target for cardiac therapeutic intervention. *Curr. Drug Targets: Cardiovasc. & Haematol. Disord. 5*, 323–335.
3. Slepkov, E. R., Rainey, J. K., Li, X., Liu, Y., Cheng, F. J., Lindhout, D. A., Sykes, B. D., and Fliegel, L. (2005) Structural and functional characterization of transmembrane segment IV of the NHE1 isoform of the Na^+/H^+ exchanger. *J. Biol. Chem. 280*, 17863–17872.
4. Ding, J., Rainey, J. K., Xu, C., Sykes, B. D., and Fliegel, L. (2006) Structural and functional characterization of transmembrane segment VII of the Na^+/H^+ exchanger isoform 1. *J. Biol. Chem. 281*, 29817–29829.
5. Reddy, T., Ding, J., Li, X., Sykes, B. D., Rainey, J. K., and Fliegel, L. (2008) Structural and functional characterization of transmembrane segment IX of the NHE1 isoform of the Na^+/H^+ exchanger. *J. Biol. Chem. 283*, 22018–22030.
6. Pedersen, S. F., King, S. A., Nygaard, E. B., Rigor, R. R., and Cala, P. M. (2007) NHE1 inhibition by amiloride- and benzoylguanidine-type compounds. Inhibitor binding loci deduced from chimeras of NHE1 homologues with endogenous differences in inhibitor sensitivity. *J. Biol. Chem. 282*, 19716–19727.
7. Wakabayashi, S., Pang, T., Su, X., and Shigekawa, M. (2000) Second mutations rescue point mutant of the Na^+/H^+ exchanger NHE1 showing defective surface expression. *FEBS Lett. 487*, 257–261.
8. Wakabayashi, S., Hisamitsu, T., Pang, T., and Shigekawa, M. (2003) Mutations of Arg^{440} and Gly^{455}/Gly^{456} oppositely change pH sensing of Na^+/H^+ exchanger 1. *J. Biol. Chem. 278*, 11828–11835.
9. Wakabayashi, S., Hisamitsu, T., Pang, T., and Shigekawa, M. (2003) Kinetic dissection of two distinct proton binding sites in Na^+/H^+ exchangers by measurement of reverse mode reaction. *J. Biol. Chem. 278*, 43580–43585.
10. Hunte, C., Screpanti, E., Venturi, M., Rimon, A., Padan, E., and Michel, H. (2005) Structure of a Na^+/H^+ antiporter and insights into mechanism of action and regulation by pH. *Nature 435*, 1197–1202.
11. Slepkov, E. R., Rainey, J. K., Sykes, B. D., and Fliegel, L. (2007) Structural and functional analysis of the Na^+/H^+ exchanger. *Biochem. J. 401*, 623–633.
12. Cunningham, F., and Deber, C. M. (2007) Optimizing synthesis and expression of transmembrane peptides and proteins. *Methods 41*, 370–380.

13. Oblatt-Montal, M., Reddy, G. L., Iwamoto, T., Tomich, J. M., and Montal, M. (1994) Identification of an ion channel-forming motif in the primary structure of CFTR, the cystic fibrosis chloride channel. *Proc. Natl. Acad. Sci. U.S.A. 91*, 1495–1499.

14. Naider, F., Khare, S., Arshava, B., Severino, B., Russo, J., and Becker, J. M. (2005) Synthetic peptides as probes for conformational preferences of domains of membrane receptors. *Biopolymers 80*, 199–213.

15. Hunt, J. F., Earnest, T. N., Bousché, O., Kalghatgi, K., Reilly, K., Horváth, C., Rothschild, K. J., and Engelman, D. M. (1997) A biophysical study of integral membrane protein folding. *Biochemistry 36*, 15156–15176.

16. Katragadda, M., Alderfer, J. L., and Yeagle, P. L. (2001) Assembly of a polytopic membrane protein structure from the solution structures of overlapping peptide fragments of bacteriorhodopsin. *Biophys. J. 81*, 1029–1036.

17. Yeagle, P. L., Choi, G., and Albert, A. D. (2001) Studies on the structure of the G-protein-coupled receptor rhodopsin including the putative G-protein binding site in unactivated and activated forms. *Biochemistry 40*, 11932–11937.

18. Damberg, P., Jarvet, J., and Gräslund, A. (2001) Micellar systems as solvents in peptide and protein structure determination. *Methods Enzymol. 339*, 271–285.

19. Henry, G. D., and Sykes, B. D. (1994) Methods to study membrane protein structure in solution. *Methods Enzymol. 239*, 515–535.

20. Haworth, R. S., Fröhlich, O., and Fliegel, L. (1993) Multiple carbohydrate moieties on the Na^+/H^+ exchanger. *Biochem. J. 289 (Pt 3)*, 637–640.

21. Li, X., Ding, J., Liu, Y., Brix, B. J., and Fliegel, L. (2004) Functional analysis of acidic amino acids in the cytosolic tail of the Na^+/H^+ exchanger. *Biochemistry 43*, 16477–16486.

22. Davis, J. H., Clare, D. M., Hodges, R. S., and Bloom, M. (1983) Interaction of a synthetic amphiphilic polypeptide and lipids in a bilayer structure. *Biochemistry 22*, 5298–5305.

23. Rainey, J. K., Fliegel, L., and Sykes, B. D. (2006) Strategies for dealing with conformational sampling in structural calculations of flexible or kinked transmembrane peptides. *Biochem. Cell Biol. 84*, 918–929.

24. Wishart, D. S., Sykes, B. D., and Richards, F. M. (1992) The chemical shift index: a fast and simple method for the assignment of protein secondary structure through NMR spectroscopy. *Biochemistry 31*, 1647–1651.

25. Wishart, D. S., Bigam, C. G., Holm, A., Hodges, R. S., and Sykes, B. D. (1995) ^1H, ^{13}C and ^{15}N random coil NMR chemical shifts of the common amino acids. I. Investigations of nearest-neighbor effects. *J. Biomol. NMR 5*, 67–81.

26. Kabsch, W. (1976) A solution for the best rotation to relate two sets of vectors. *Acta Crystallogr., Sect. A: Cryst. Phys., Diffr., Theor. Gen. Crystallogr. 32*, 922–923.

27. Wishart, D. S., Boyko, R. F., Willard, L., Richards, F. M., and Sykes, B. D. (1994) SEQSEE: a comprehensive program suite for protein sequence analysis. *CABIOS, Comput. Appl. Biosci. 10*, 121–132.

28. He, M. M., Sun, J., and Kaback, H. R. (1996) Cysteine-scanning mutagenesis of transmembrane domain XII and the flanking periplasmic loop in the lactose permease of *Escherichia coli*. *Biochemistry 35*, 12909–12914.

29. Landau, M., Herz, K., Padan, E., and Ben-Tal, N. (2007) Model structure of the Na^+/H^+ exchanger 1 (NHE1): functional and clinical implications. *J. Biol. Chem. 282*, 37854–37863.

30. Arkin, I. T., Xu, H., Jensen, M. Ø., Arbely, E., Bennett, E. R., Bowers, K. J., Chow, E., Dror, R. O., Eastwood, M. P., Flitman-Tene, R., Gregersen, B. A., Klepeis, J. L., Kolossváry, I., Shan, Y., and Shaw, D. E. (2007) Mechanism of Na^+/H^+ antiporting. *Science 317*, 799–803.

31. Dibrov, P., and Fliegel, L. (1998) Comparative molecular analysis of Na^+/H^+ exchangers: a unified model for Na^+/H^+ antiport? *FEBS Lett. 424*, 1–5.

32. Olkhova, E., Padan, E., and Michel, H. (2007) The influence of protonation states on the dynamics of the NhaA antiporter from *Escherichia coli*. *Biophys. J. 92*, 3784–3791.

33. Kozachkov, L., Herz, K., and Padan, E. (2007) Functional and structural interactions of the transmembrane domain X of NhaA, Na^+/H^+ antiporter of *Escherichia coli*, at physiological pH. *Biochemistry 46*, 2419–2430.

Chapter 6

Structural and functional analysis of transmembrane segment VI of the NHE1 isoform of the Na^+/H^+ exchanger

A version of this chapter has been published:

- Tzeng, J., Lee, B. L., Sykes, B. D. and Fliegel, L. (2010) Structural and functional analysis of transmembrane segment VI of the NHE1 isoform of the Na^+/H^+ exchanger. *J. Biol. Chem. 285*, 36656–36665.

BLL and JT contributed equally to this work. BLL performed and analyzed the NMR experiments. JT performed the mutagenesis and accessibility experiments. The manuscript was written by BLL, JT, LF, and BDS.

Summary

The Na^+/H^+ exchanger isoform 1 is a ubiquitously expressed integral membrane protein. It resides on the plasma membrane of cells and regulates intracellular pH in mammals by extruding an intracellular H^+ in exchange for one extracellular Na^+. We characterized structural and functional aspects of the transmembrane segment (TM) VI (residues 227–249) by using cysteine scanning mutagenesis and high resolution NMR. Each residue of TM VI was mutated to cysteine in the background of the cysteineless NHE1 protein, and the sensitivity to water-soluble sulfhydryl-reactive compounds (2-(trimethylammonium)ethyl) methanethiosulfonate (MTSET) and 2-sulfonatoethyl methanethiosulfonate (MTSES) was determined for those residues with significant activity remaining. Three residues were essentially inactive when mutated to Cys: D238, P239, and E247. Of the remaining residues, proteins with the mutations N227C, I233C, and L243C were strongly inhibited by MTSET, whereas amino acids F230, G231, A236, V237, A244, V245, and E248

were partially inhibited by MTSET. MTSES did not affect the activity of the mutant NHE1 proteins. The structure of a peptide representing TM VI was determined using high resolution NMR spectroscopy in dodecylphosphocholine (DPC) micelles. TM VI contains two helical regions oriented at an approximate right angle to each other (residues 229–236 and 239–250) surrounding a central unwound region. This structure bears a resemblance to TM IV of the *Escherichia coli* protein NhaA. The results demonstrate that TM VI of NHE1 is a discontinuous pore-lining helix with residues N227, I233, and L243 lining the translocation pore.

Introduction

NHE1 consists of an N-terminal membrane domain of ∼500 amino acids and a C-terminal regulatory domain of ∼315 amino acids (*1*, *2*). The membrane domain is responsible for ion movement. Two models of the topology of NHE1 exist. An analysis of topology by cysteine scanning accessibility suggested that NHE1 has three membrane-associated re-entrant segments and 12 integral transmembrane segments (*3*). A different model of the topology of NHE1 was more recently suggested (*4*). It was based on computational methods, including evolutionary conservation analyses and fold alignment methods with NhaA, a partially homologous bacterial Na^+/H^+ antiporter whose crystal structure has been determined (*5*). A comparison of the models shows some similarities and some differences (*6*). Amino acids 227–249 are predicted to form a transmembrane segment with the same orientation in both models and were initially referred to as TM VI in the topology model of Wakabayashi et al. (*3*).

The mechanism of transport of the membrane domain is both of great interest from a scientific viewpoint and potentially helpful in the design of improved NHE1 inhibitors for clinical use (*6*). In this regard, we have recently characterized the functionally important residues and the structure of TM IV (residues 155–180), TM VII (residues 250–275), TM IX (residues 338–365), and TM XI (residues 447–472), as well as the second extracellular loop (residues 153–155).

TM VI of NHE1 has not been well studied. In the proposed new topology of NHE1 suggested by Landau et al. (*4*), TM VI (amino acids 227–249) is renumbered as TM IV. This region corresponds to TM IV of the bacterial antiporter NhaA. In the high resolution structure of NhaA, TM IV was an important part of a novel fold of two TMs that crossed each other in the center of the membrane and played a key role in ion binding and transport (*5*). It was proposed that amino acids 227–249 of NHE1

provide an equivalent role for this protein, forming part of the TM 4–TM 11 assembly (*4*). We therefore decided to investigate TM VI (amino acids 227–249) of NHE1 in detail. We used cysteine scanning mutagenesis to identify and characterize critical pore-lining residues of the protein. We also used nuclear magnetic resonance (NMR) spectroscopy to characterize the structure of a synthetic peptide representing TM VI in dodecylphosphocholine (DPC) micelles, including paramagnetic relaxation NMR experiments (*7*, *8*) to examine the location of the peptide in the micelle and its interaction with a cation. Studies have shown that TMs of membrane proteins possess all of the structural information required to form their higher order structures in their amino acid sequence (*9*). This has been demonstrated in earlier studies on membrane protein segments, such as the cystic fibrosis transmembrane conductance regulator (*10*), bacteriorhodopsin (*11*, *12*), a fungal G-protein-coupled receptor (*13*), and rhodopsin (*14*). The use of DPC micelles has also been shown to be an excellent membrane mimetic environment for these studies (*15*, *16*).

Our results identify TM VI as a critical pore-lining segment of NHE1. Three residues were identified as lining the pore, and several others were affected by changing them to Cys and reacting with MTSET. We also demonstrate that TM VI is an interrupted helix with a similarity to TM IV of NhaA.

Experimental procedures

Mutagenesis and NMR experiments were performed as described in Chapter 2. The primers used in site-directed mutagenesis are listed in Table 6-S1. For NMR experiments, a synthetic peptide representing TM VI (sequence acetyl-KKKD-NLLFGSIISAVDPVAVLAVFEEIHKKK-amide) was purchased from GI Biochem (Shanghai) Ltd.

Paramagnetic relaxation experiments

Paramagnetic relaxation enhancement (PRE) rates were measured by titrating a $MnCl_2$ stock solution into an NMR sample of TM VI in DPC to concentrations of 0, 0.1, 0.2, 0.5, and 1.0 mM Mn^{2+} and measuring proton T_1 relaxation rates at each titration point using a series of two-dimensional ^{1}H-^{1}H NOESY spectra with a saturation recovery sequence at the beginning (*8*). The saturation recovery sequence at the beginning of each NOESY utilized the gradient homospoil option built into the Varian tnnoesy pulse sequence. The relaxation delays were 200, 314, 493, 775, 1216, 1910, and 3000 ms for the series of NOESY experiments at each titration point.

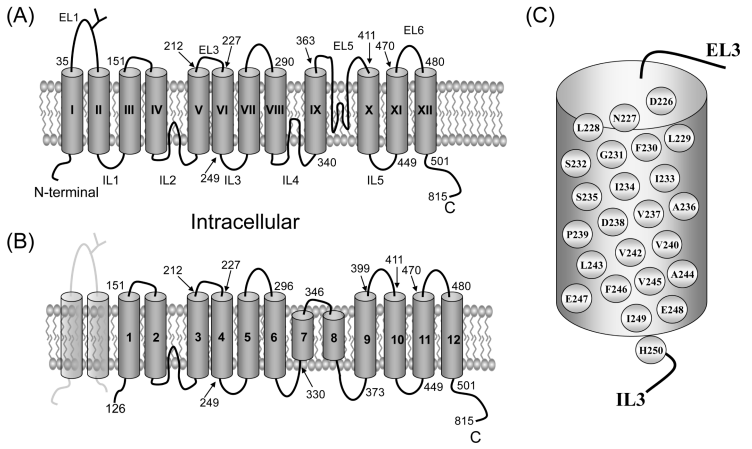

Figure 6-1. Models of NHE1 isoform of the Na^+/H^+ exchanger. (A) Topological model of the transmembrane domain of the NHE1 isoform of the Na^+/H^+ exchanger based on cysteine accessibility studies (*3*). (B) Topological model of NHE1 based on comparison with crystal structure of bacterial homologue NhaA (*4*). (C) Schematic diagram of amino acids present in TM VI.

NMRView (*17*) was used for peak assignment and intensity measurement. Curve fitting was performed using the program Xcrvfit (Version 4.0.12; R. Boyko and B. D. Sykes) for determining T_1 and PRE values.

Results

Figure 6-1 shows models of the NHE1 isoform of the Na^+/H^+ exchanger. Figure 6-1, A, is a schematic based on the topology deduced by cysteine scanning accessibility studies (*3*), whereas Figure 6-1, B, is a model of NHE1 based on homology modelling with bacterial NhaA (*4*). Residues corresponding to TM VI in Figure 6-1, A, are predicted to be in the same orientation and relative position in Figure 6-1, B. The first two TMs are believed to be cleaved and removed in this model; therefore, TM VI is relabelled TM IV. Figure 6-1, C, shows a schematic model illustrating the amino acids of this TM (herein referred to as TM VI based on (*3*)). To examine which amino acids of TM VI are lining the protein cation pore, we performed a cysteine scanning accessibility study of this TM. Each residue in TM VI of cysteineless Na^+/H^+ exchanger (cNHE1) was mutated to a cysteine residue. Initially, we determined whether these mutant forms of the Na^+/H^+ exchanger were active enough to permit functional analysis. Figure 6-2, A–C, illustrates the results of experiments determining expression, targeting, and activity levels of the wild type and TM VI mutant NHE1 proteins. Expression levels (Figure 6-2, A) of some of the TM VI Cys scanning mutants decreased greatly. N227C and A236C mutations

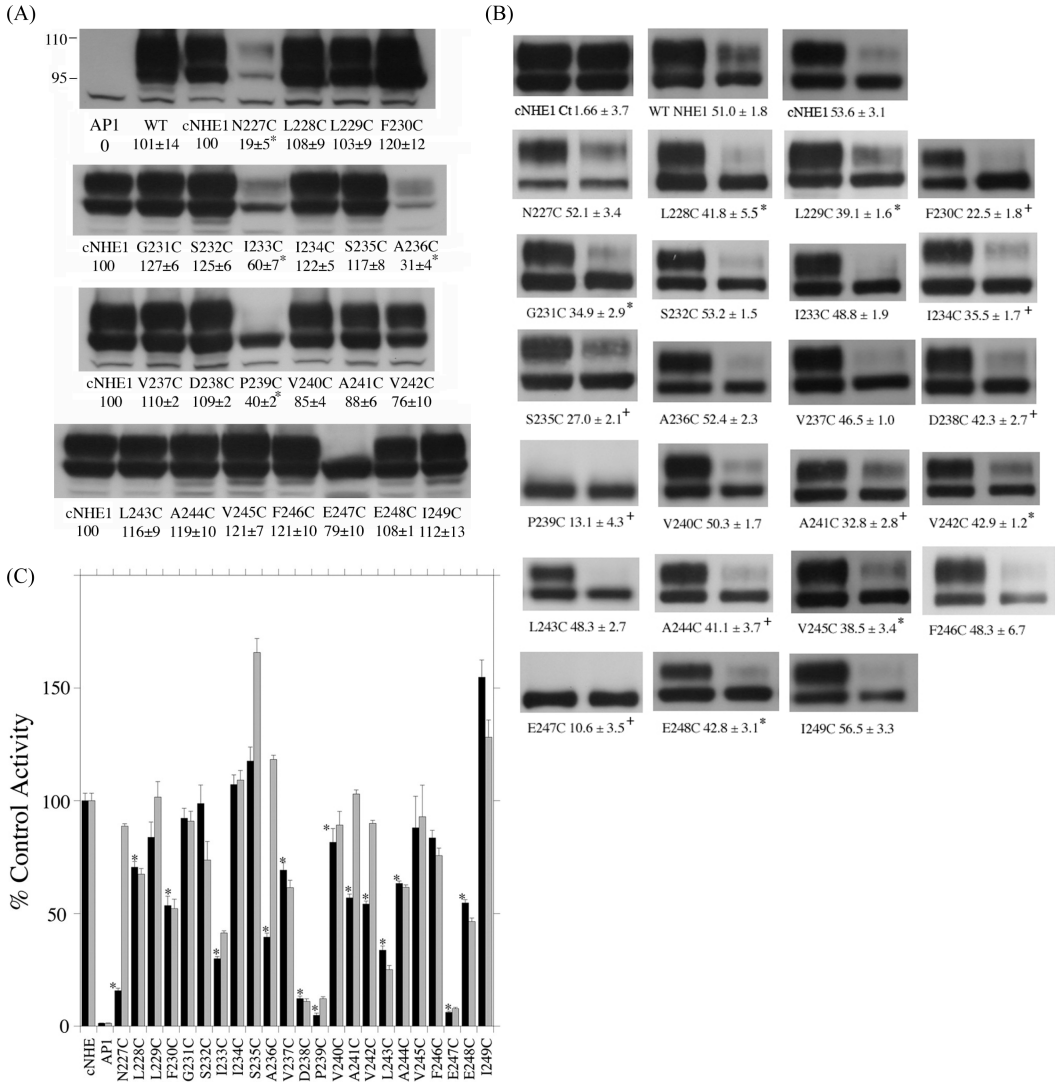

Figure 6-2. Analysis of wild type and mutant NHE1 proteins. (Continued on page 114.)

Figure 6-2. (Continued from page 113.) (A) Western blot of whole cell extracts of stable transfectants expressing Na^+/H^+ exchanger TM VI mutants or control proteins. All mutations were to cysteine. 75 µg of total protein was loaded in each lane. The numbers below the lanes indicate the mean values ($n = 3$ to 4) obtained from densitometric scans of both the 110 and 95 kDa bands relative to wild type NHE1. AP-1, mock-transfected AP-1 cells. Wt and cNHE1, cells stably expressing wild type Na^+/H^+ exchanger protein and the cysteineless NHE1, respectively. *, significantly different from cNHE1 at $p < 0.05$. (B) Surface localization of cells expressing control and TM VI mutants, as described under "Experimental Procedures." Equal amounts of total cell lysate (left lane) and unbound intracellular lysate (right lane) were examined by Western blotting with anti-HA antibody to identify NHE1 protein. cNHE1 Ct, a control experiment in which nonspecific binding to streptavidin-agarose beads was carried out following the standard procedure but without labelling cells with biotin. The percentage of the total NHE1 protein found on the plasma membrane is indicated for each mutant; calculations were based on the fully glycosylated protein only. For the control experiment, this indicates the amount of nonspecific binding to streptavidin-agarose beads. Results are the means ± S.E. ($n \geq 6$ determinations. Autoradiography exposure times were increased for mutants expressing lower levels of protein. +, significantly different from that of cNHE1 at $p < 0.01$. (C) Summary of the rate of recovery from an acute acid load of AP-1 cells transfected with cNHE and TM VI Na^+/H^+ exchanger mutants. The mean activity of cNHE1 stably transfected with NHE1 was 0.01 ΔpH/s, and this value was set to 100%. Activities are a percentage of those of cNHE1. Values are the mean ± S.E. (error bars) of 6–10 determinations. Results are shown for mean activity, both uncorrected (black) and normalized for surface processing (of glycosylated protein) and expression levels (gray). Mutants P239C and E247C were not corrected for surface targeting. *, mutants with uncorrected activity that is significantly different from that of cNHE1 at $p < 0.001$.

decreased expression to less than one-third of control. The mutants I233C and P239C had expression reduced to 60 and 40% of the cNHE1 protein, respectively. In all cases in the mutants with reduced NHE1 expression, there was a great reduction in the level of mature, fully glycosylated protein. It was also noticeable that in the P239C and E247C mutants, expression was almost exclusively of the lower molecular weight, partial or deglycosylated form of the NHE1 protein.

Mutation of amino acids of TMs of NHE1 can cause intracellular retention of the NHE1 protein (*18*). We wanted to determine if changes in NHE1 activity that we observed were due to effects on the protein itself or were due in whole or in part to intracellular retention of the protein. We therefore examined intracellular targeting of the NHE1 TM VI-expressing mutant cell lines as described under "Experimental Procedures." Sulfo-NHS-SS-biotin cell surface-labelled proteins were bound to streptavidin-agarose beads, and equal amounts of total cell lysates and unbound lysates (representing intracellular protein) were examined by using SDS-PAGE. Western blotting against the anti-HA tag identified the relative amount of NHE1 protein in the total and intracellular fractions (Figure 6-2, B). Table 6-S2 shows a summary of the plasma membrane localization of the glycosylated and unglycosylated proteins. Although some of this unglycosylated protein may be functional (*19*) and may still target to the cell surface (*20*), a majority of the surface protein is of the glycosylated protein (*21*), so the activity was corrected for surface-localized glycosylated NHE1 protein. The results are shown in Figure 6-2, B, and Table 6-S2. The fully glycosylated protein is more highly targeted to the cell surface, relative to the partial or deglycosylated protein. The relative amounts of the partial or deglycosylated protein targeted to the plasma membrane varied from $\sim$30 to 15% of the fully glycosylated levels. This was noticeably decreased for mutants F230C and D238C, although the significance of this observation is not yet clear. A number of the mutants (L229C, I234C, S235C, P239C, A241C, V242C, V245C, and E247C) had significantly less targeting of the fully glycosylated protein to the cell surface. For some of the mutants, the difference between the cNHE1 targeting and the mutants was not very large (L229C, I234C, S235C, A241C, V242C, and V245C); however, for other mutants, the amount of glycosylated protein targeted to the surface was negligible (P239C and E247C). For mutants I233C and L243C, surface targeting of the glycosylated band was slightly increased, although the significance of this observation is not yet clear.

We also determined the Na^+/H^+ exchanger activity of the NHE1 TM VI mutants. An acute acid load was induced as described earlier (*21*), and the rate of

recovery from the acute acid load was determined in stable cell lines transfected with either wild type Na^+/H^+ exchanger or mutants of TM VI. To determine if decreased activity was due to effects on the protein itself or due to changes in surface targeting or expression, the rate of recovery was also corrected for both of these values, relative to cNHE1 (Figure 6-2, C, and Table 6-S3). Several of the mutants (D238C, P239C, and E247C) had greatly reduced activity that was less than 15% of the control levels. It was not possible to accurately work with them for further experiments. Several other mutants (N227C, I233C, A236C, L243C, and E248C) had activity from 15 to 40% that of cNHE1. Their activity, although reduced, was still substantial enough for further experimentation. It was notable that for the mutants N227C, A236C, A241C, and V242C, the NHE1 activity was essentially equivalent to controls when corrected for effects on surface processing and expression levels. This indicated that the protein functioned normally but that the reduced activity we observed was due to decreased expression or targeting of the protein. The N227C and A236C mutants had large decreases in expression levels but normal surface targeting. (Both the A241C and V242C mutants had significant decreases in surface targeting and minor decreases in expression levels.) Two mutants, S235C and I249C, had somewhat elevated levels of NHE1 activity. The significance of this observation is not yet clear, although for I249C it may reflect a higher level of surface targeting.

We next determined the sensitivity of the Cys mutants to MTSET or MTSES. Figure 6-3, A, illustrates one example of the findings with a mutant that is sensitive to MTSET, and Figure 6-3, B, shows a summary of the results of the various mutants tested. Of the active Na^+/H^+ exchangers, N227C, I233C, and L243C were very sensitive to MTSET treatment. This resulted in elimination of most of the activity of the protein. Seven other mutants, F230C, G231C, A236C, V237C, A244C, V245C, and E248C, were partially inhibited by MTSET although to a more limited extent. Negatively charged MTSES had no effect on any of the mutant proteins. As a control, we examined the sensitivity of an F161C mutant that we have previously determined was sensitive to both MTSET and MTSES (*18*). This mutant was again inhibited by both MTSET and MTSES.

NMR spectroscopy was used to determine the structure of a peptide containing the TM VI sequence. The peptide included residues D226–H250, which encompasses the predicted transmembrane helix in both models of the NHE1 topology (Figure 6-1, A–C). We added cationic lysine residues at the termini of this peptide as we have earlier (*20*) because this aids in their purification and in the maintenance of correct transbilayer orientation (*22*). N- and C-terminal acetyl and

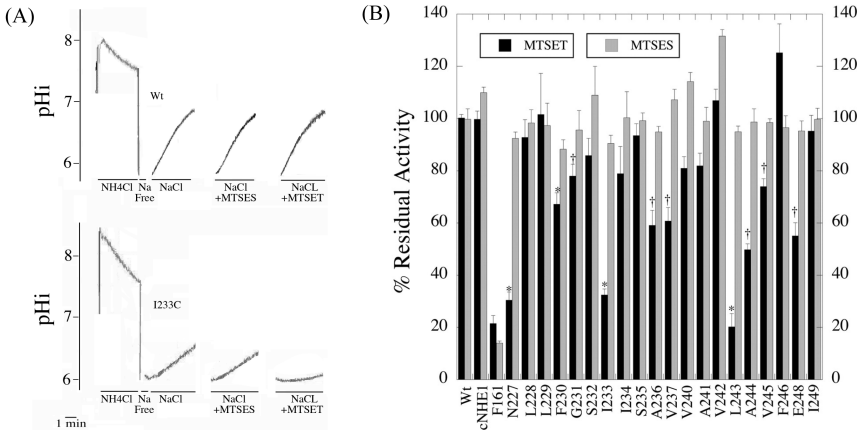

Figure 6-3. Effect of sulfhydryl-reactive compounds, MTSET and MTSES, on activity of cNHE1 and single cysteine NHE1 mutant-containing cell lines. (A) Example of results of the effect of MTSET or MTSES on activity of cNHE1 and I233C mutant. cNHE and I233C NHE1 protein activity was assayed in stably transfected AP-1 cells as described under "Experimental Procedures." Activity was measured after two acid pulses. The first pulse in the absence of MTSET is shown. For ease of viewing, only the recovery from acidosis is shown for the second pulse, in which cells were treated with MTSES or MTSET. NH_4Cl, treatment with ammonium chloride; Na Free, treatment with Na^+-free buffer to induce acidosis; NaCl, recovery from acidosis in NaCl-containing buffer (for the second pulse, this contained MTSET/MTSES, and cells were pretreated with MTSET/MTSES for 10 min prior to NH_4Cl-induced acid load). (B) Summary of results of mutant and control activities of TM VI mutants. Activity was measured after two ammonium chloride pulses as described under "Experimental Procedures." The second acidification was after cells were treated with 10 mM reagent. Results are presented as the percentage of activity of the second acid load relative to the first. * or †, the second recovery from acid load was significantly lower than the first at $p < 0.01$ or $p < 0.05$, respectively. Solid filled bars, MTSET treatments; lightly shaded bars, MTSES treatments.

amide caps, respectively, were added to remove charges at the peptide termini similar to our earlier procedure (*20*) to better represent the full-length protein. We have previously used DPC to act as a membrane mimetic for transmembrane segments of NHE1 (*20*, *23*). TM VI peptide was solubilized by a similar procedure and provided a stable, well behaved sample suitable for structure determination by NMR. A one-dimensional ^{1}H NMR spectrum of the peptide in DPC showed relatively narrow lines and reasonable spectral dispersion, indicative of structure formation in the peptide (results not shown).

Sequential assignment of the peptide was accomplished using two-dimensional ^{1}H-^{1}H double-quantum filtered correlation spectroscopy (DQF-COSY), total correlation spectroscopy (TOCSY), and nuclear Overhauser effect spectroscopy (NOESY) using standard procedures (*24*). The assignment of the peptide was complete except for some Lys Hε atoms. Strong NOE peaks observed between D238 Hα and P239 Hδ indicate a trans conformation for the peptide bond between D238 and P239. Additional resonances that would correspond to a cis peptide bond conformation were not detected, suggesting that the dominant conformation is the trans-proline conformation. Distance restraints for structure calculation were obtained from the two-dimensional NOESY spectrum acquired at 800 MHz. Distances were calibrated using peak intensity rather than peak volume to compensate for peak overlap. A soft square well potential was used for the NOE potential to compensate for possible erroneous assignments or overrestrained distances. Structures were initially calculated without dihedral angle restraints, so the structure would be influenced primarily by the NOE distance restraints. Dihedral angle restraints were added in at a later stage of refinement. NOE restraints and chemical shift index prediction of secondary structure (*25*) (Figure 6-S1) suggested that the peptide was helical at approximately residues L229–A236 and V240–K251. Helical dihedral angle restraints for phi ($60 \pm 30^{\circ}$) and psi ($40 \pm 40^{\circ}$) dihedral angles were applied to these residues for several further rounds of calculation. The 40 lowest energy structures of the 50 structures of the final structure calculation were kept for analysis, and the structure calculation statistics are summarized in Table 6-S4.

The ensemble of peptide structures do not superimpose particularly well with each other over the entire length of the peptide. Attempts to superimpose small regions of the ensemble of structures show two overlapping segments of the peptide at residues L228–D238 and V237–K253, which superimpose well, where the average root mean square deviation per residue over the ensemble of structures is less than 1 Å (Figure 6-4 and Figure 6-S2). Superimposition was performed using

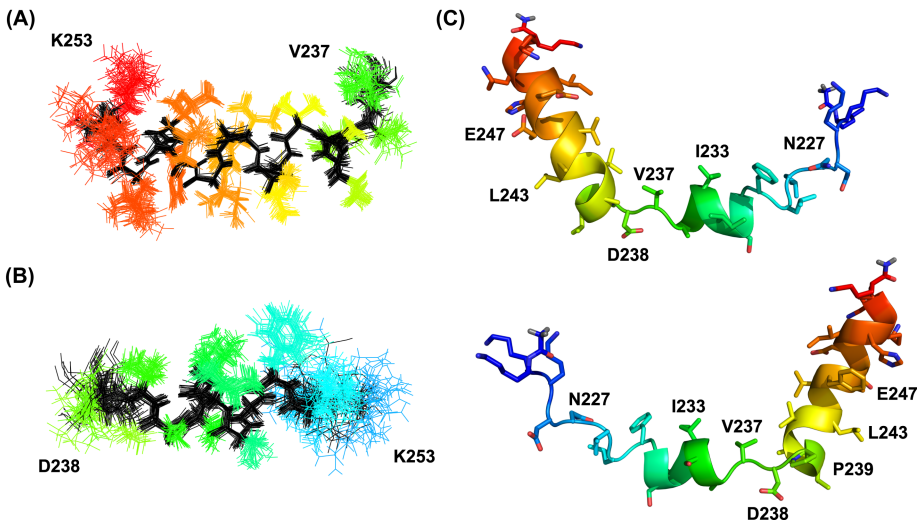

Figure 6-4. NMR structure of TM VI in DPC micelles. Shown is superimposition of structurally conserved regions of the TM VI peptide structure. Superimposition of the backbone atoms of the structurally conserved regions 228–238 (A) and 237–253 (B) is shown. The backbone is shown in black, and side chains are shown in color. (C) Views of a single ensemble member with MTSET-sensitive residues labelled shown from two sides.

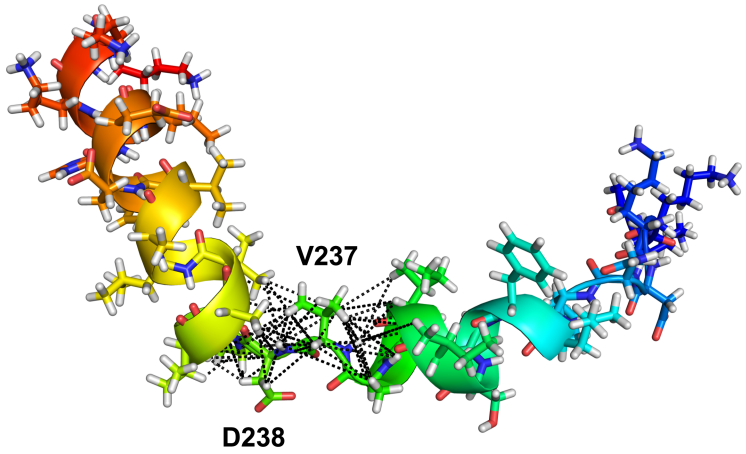

Figure 6-5. Distance restraints maintaining the kinked structure of TM VI. The lowest energy ensemble member is shown in both a schematic diagram and a stick representation. Distance restraints to and from atoms in residues V237 and D238 to other atoms are shown in black dotted lines.

the method of Kabasch (*26*), as implemented in the CCP4 suite (*27*). The lowest energy structure is shown in Figure 6-4, C. The two structurally conserved regions contain two α-helices at residues L229–A236 and P239–K252, based on the dihedral angles in that region, and are maintained at approximately right angles to each other primarily due to restraints from V237–D238 in the extended region to residues in the helices on either side (Figure 6-5). This extended segment allows for some variation in the relative orientations of the two helices among the ensemble members (Figure 6-S2). A plot of the dihedral angle order parameters (*28*) (Figure 6-S3) also shows the two structured regions of the peptide, corresponding to the helices, and a short, more structurally variable region, corresponding to the extended region. The N-terminal end of the peptide, K223–L228, appears to be unstructured, as shown by the lack of NOE contacts in that region and by chemical shift index values suggesting random coil conformations. The C-terminal helix is slightly curved, which could reflect the peptide's conformation in the micelle or the smaller number of NOE contacts between the residues that are located on the outside of the curve.

A crystal structure of an *E. coli* Na^+/H^+ antiporter, NhaA, has been determined (*5*). NHE1 and NhaA share similar activities and are distantly related; therefore, it is possible that they have similar structures, as has been suggested earlier (*4*). Pairwise alignment of TM VI of NHE1 onto the sequence of NhaA suggests that TM VI aligns with TM VI of NhaA (residues 180–200); this alignment is shown in Figure 6-6, A. TM VI in NhaA is a straight helix and primarily hydrophobic, located on the periphery of the protein in the NhaA crystal structure. This alignment does not support the critical role of NHE1 TM VI found in this paper. Using more advanced alignment and structure prediction techniques, Landau et al. (*4*) suggest that the sequence of TM VI of NHE1 is equivalent to TM IV of NhaA. A SEQSEE (*29*) alignment of these two helices (not shown) suggests that the P239 in NHE1 lines up with the D133 in NhaA. This is close to the alignment proposed in the Landau model that aligns NHE1 D238 and NhaA D133. The latter alignment is shown in Figure 6-6, B, and is used for superimposition of the NMR structure of TM VI with the structure of TM IV from NhaA (Figure 6-6, C).

No member of the ensemble of structures of the entire length of TM VI, determined by NMR, superimposed well onto the entire structure of TM IV from NhaA. The L-shaped conformation of the NMR structure inhibits superimposition of the entire structure onto NhaA TM IV, which has a more linear conformation. Differences in the conformations of the helical regions also prevent a reasonable superimposition (root mean square deviation < 1 Å) of the helices between NHE1

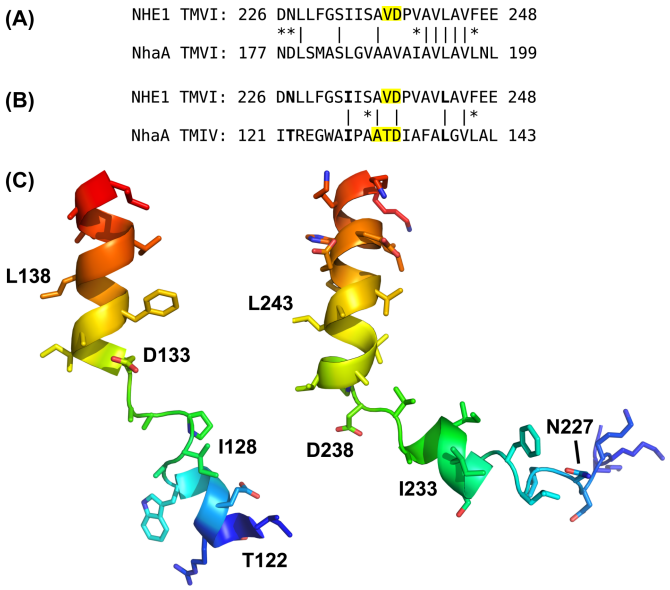

Figure 6-6. Comparison of TM VI of NHE1 with TM IV of NhaA. (A) Region identified using the SEQSEE program (*29*) for the optimal pairwise alignment of the sequence of NHE1 TM VI against the entire NhaA sequence. (B) Alignment of the sequences of NHE1 TM VI and NhaA TM IV, as suggested by Landau et al. (*4*), with the extended regions highlighted. A vertical bar indicates amino acid identity. *, similar amino acids. MTSET-sensitive residues and the corresponding residues in NhaA are shown in boldface type. (C) Comparison of a representative NMR structure of TM VI of NHE1 (right) with that of TM IV of NhaA (left). Amino acids 223–253 of NHE1 and amino acids 121–143 of NhaA are shown. The conserved Asp residue and MSTET-sensitive residues in NHE1 and the corresponding residues in NhaA are labelled.

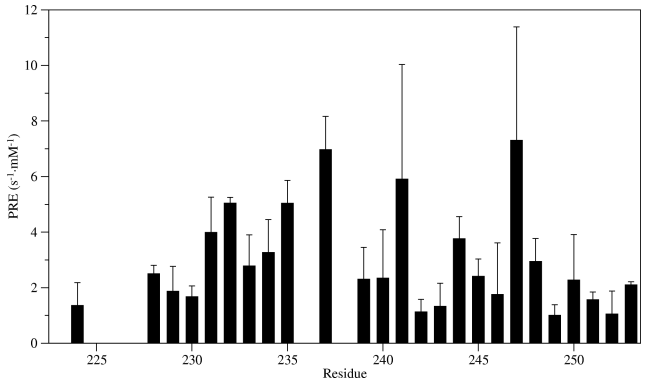

Figure 6-7. Paramagnetic relaxation enhancement rates for TM VI in DPC micelles. Backbone Hα PRE values are shown for TM VI. Higher PRE values represent a greater change in the measured T_1 relaxation rates with respect to Mn^{2+} concentration and consequently represent regions of the peptide that are closer to the surface of the detergent micelle that are more accessible to the water-soluble Mn^{2+} ions.

TM VI and NhaA TM IV. However, smaller, overlapping segments of the NMR structure of TM VI of NHE1 can superimpose well onto the crystal structure of TM IV of NhaA, covering the two helical regions in the structures. The central extended region in the NMR structure does not superimpose particularly well with the extended region in the crystal structure of TM IV of NhaA. At best, A130–D133 of NhaA and S235–D238 of NHE1 align structurally, with root mean square deviations of about 1–2 Å. Despite the poor superimposition of the NMR and crystal structures, there is nevertheless a qualitative resemblance between them. The lowest energy ensemble member of the TM VI NMR structure and the structure of TM IV from NhaA are shown in Figure 6-6, C. Both contain two α-helices at each end separated by an extended region of two or three residues in the middle. Both the NMR structure of NHE1 TM VI and the crystal structure of NhaA TM IV contain an evolutionarily conserved Asp residue at the beginning of the C-terminal helix. This seems to support the sequence alignment and three-dimensional structural model of NHE1 proposed by Landau et al. (*4*). The residues identified in NHE1 TM VI that are most sensitive to MTSET, N227, I233, and L243, correspond to T122, I128, and L138, respectively, based on this alignment.

To determine the location of the TM VI peptide within the DPC micelles, we measured the paramagnetic relaxation enhancement rates for the peptide in the presence of Mn^{2+}. Broadening and overlap of peaks in the one-dimensional NMR spectra prevent accurate measurement of relaxation times. In the absence of isotopic labelling, such as for synthetic peptides, homonuclear two-dimensional spectra have

been used to resolve peaks and measure the relaxation rates of samples (*8*, *30*). We used a two-dimensional NOESY with a saturation recovery pulse sequence to measure the T_1 relaxation times of the peptide. Only resolved peaks were used for curve fitting to determine T_1 times. PRE values are determined by linear fitting of $1/T_1$ versus Mn^{2+} concentrations. PRE values were averaged together in the case of multiple measurable peaks representing the same proton. PRE values for backbone Hα atoms are shown in Figure 6-7. The regions of the peptide that were determined to be helical in the NMR structure show a periodic variation in PRE values, with maxima at G231–S232, V237, A241, A244, and E247. PRE values increase dramatically at residues within or near the extended region of the NMR structure, A236–D238. Values for A236 and D238 were similar to or higher than V237 but could not be fitted accurately and are not shown. Due to overlap of peaks even in the two-dimensional spectra, only a few peaks from the terminal lysines could be used for measurement. The terminal Lys Hα appear to have relatively low PRE values compared with the rest of the peptide. The PRE measurements (Figure 6-7) provided additional details about the structure of the peptide and its interactions with the micelle (see "Discussion").

Discussion

In this work, we characterized both the structural and functional characteristics of amino acids 228–249 of the NHE1 isoform of the Na^+/H^+ exchanger. These residues are purported to be either TM VI (*3*) or TM IV (*4*) of the protein. This TM has not been well studied earlier, but molecular modelling by Landau et al. (*4*) and our own (not shown) suggested that it may be an important pore-lining segment, critical in activity of the protein. Initial experiments therefore used cysteine scanning mutagenesis to examine if this segment was pore-lining. All of the amino acids of the segment from N227 to I249 were mutated to Cys in the background of the cysteineless protein that we have earlier shown is fully functional (*18*, *20*). With mutation to Cys, the activity of many residues was reduced. For the amino acids D238, P239, and E247, the activity was reduced so greatly that it was not possible to assay these mutants further. For 12 other mutants, the activity was reduced but was sufficient for measurement. We have found that some TMs (TM IV (*18*) and TM IX (*23*)) are more tolerant of mutations to Cys. Others, such as TM XI (*20*), appear to be intolerant of changes, and this differential sensitivity has been noted in other proteins (*31*). In several cases (N227, A236, A241, and V242), partially decreased

activity was due to decreased levels of expression or targeting of the protein. This indicated that these proteins were functional but were not processed properly.

When mutated to Cys, amino acids of TM VI (amino acids 228–249) were exquisitely sensitive to reaction with MTSET. Of the 20 mutant locations that were active and were changed to Cys residues, treatment with MTSET resulted in inhibition in 10 amino acid positions. This made TM VI more susceptible than any of TM IV, IX, or XI. Three of the mutants (at amino acids N227, I233, and L243) were greatly inhibited by MTSET, whereas seven others were inhibited to a lesser degree. In no cases did reactivity with MTSES cause any inhibition with the amino acids of TM VI. A positive control, F161 of TM IV, was inhibited by both MTSES and MTSET. Positively charged MTSET may be inhibitory because of direct electrostatic repulsion of a Na^+ or H^+. These results suggested that many residues of TM VI were pore-lining and that this segment plays an important role in forming the pore of the NHE1 protein. Although the residues strongly inhibited by MTSET (N227, I233, and L243) are strong candidates for pore-lining residues, those partially inhibited (F230, G231, A236, V237, A244, V245, and E248) are less clear cases. Residues A244 and V245 are next to L243 and may have partial access to the pore. We have previously found a similar phenomenon; in TM IX, residues adjacent to strongly inhibited residues also tended to be partially inhibited (*20*). E248 is on a similar face of TM VI as A244 (Figure 6-4), which may explain its partial accessibility. Residues N227, F230, A236, and V237 also are on the same face of the peptide as N227 (Figure 6-4), which may again account for their partial accessibility.

The structure of TM VI was that of two α-helices between residues L229 and A236 and residues P239 and K252, separated by an extended region at V237–D238. We have also found that in the cases of TM XI of NHE1 (*20*) and TM IV of NHE1 (*18*), the TM is not a continuous unbroken helix. Recent structures of membrane proteins have suggested that this is not an uncommon occurrence. For example, TMs of rhodopsin are interrupted or kinked at multiple sites (*32*). Up to 40% of TM helices contain kinks or other distortions from an ideal helix conformation, and these residues tend to be highly conserved and often directly involved in the function of transporters and channels (*33*). These regions also tend to have an increased incidence of glycine or prolines (*33*), and we found that the extended region of V237–D238 was immediately upstream of P239. Proline residues are considered to be helix breakers because they lack an amide hydrogen and cause a kink of $\sim 26^\circ$ in the α-helix (*34*, *35*). This causes the $(i-4)$ backbone carbonyl to not have its normal

hydrogen bond donor and prevents formation of the $(i-3)$-carbonyl–$(i+1)$-amide backbone hydrogen bond (*34*). With each proline, the α-helix also has two free backbone carbonyls that could coordinate cations or interact with inhibitors (*35*). All three residues upstream of P239 (A236, V237, and D238) were important in activity or expression and, when mutated, resulted in decreases in NHE1 activity. In addition, the A236C and V237C mutants were partially inhibited by reactivity with MTSET, suggesting that they are accessible from the cell exterior and pore lining or at least partially accessible to the pore. This extended region of TM VI appears to be critical to NHE1 function.

The crystal structure of the *E. coli* Na^+/H^+ antiporter NhaA revealed a novel fold consisting of two TMs, TMs IV and XI, that were assembled to form crossed extended chains (*5*). Modelling of NHE1 based on the structure of NhaA suggested that residues of TM VI (amino acids 227–249) might play a role equivalent to TM IV of NhaA. A comparison of these two segments is shown in Figure 6-6. Although the two segments are not identical, they were similar in overall structure. It was proposed that D238 of NHE1 could play a critical role in stabilizing helix dipoles (*4*) similar to D133 of NhaA. When we mutated D238 to Cys, NHE1 was essentially inactive, supporting this suggestion. The location of D238, at the end of a helix, is also similar to that of D133 of NhaA (Figure 6-6). One possibility is that P239 maintains the extended structure of this region by breaking the helix and allowing dipole formation, whereas D238 stabilizes the helix dipole that forms. Supporting this suggestion is the fact that TM VI of NHE1 is similar to that of TM IV of NhaA, more so than to other TMs of NhaA, including TM VI. A comparison of alignments between TM VI of NHE1 with TMs VI and IV of NhaA is shown in Figure 6-6, A and B. Although the alignment of TM VI of NHE1 with TM VI of NhaA shows more sequence identity, alignment with TM IV of NhaA lines up the critical D238 residue and the extended regions from the structures of the two TMs. Further experiments are necessary to test if P239 and D238 are critical to formation of an extended helix and to dipole stabilization.

Comparison of the structure of NHE1 TMs with NhaA further supports the conclusion that TM VI of NHE1 is similar to TM IV of NhaA. TM IV of NHE1 (amino acids 155–177) has a general structure somewhat similar to that of TM IV of NhaA (*18*, *36*), with an extended region followed by a helix; however, the extended region is not preceded by a helical region. Furthermore, unlike TM VI of NHE1 and TM IV of NhaA, TM IV of NHE1 does not contain a charged residue in the extended region of the NMR structure. Thus, TM IV of NHE1 does not compare

as well to TM IV of NhaA as TM VI of NHE1 (Figure 6-6, C). TM VI of NhaA also does not compare well with TM VI of NHE1. TM VI of NhaA is an unbroken helix and is not similar to the structure of TM VI of NHE1 (*4*). It does not have an extended region similar to TM VI of NHE1, and these extended regions of TMs of NhaA are believed to be critical in protein function (see above).

We have earlier shown that TM XI plays a critical role in NHE1 function (*20*). Landau et al. (*4*) suggest that TM VI (amino acids 227–249, referred to as TM IV by them) plays a role equivalent to that of the TM IV–TM XI assembly in NhaA. These helices are suggested to form the core of the alternating access mechanism. Our results for both TMs are in agreement with their suggestion. We found that both of these TMs have a helix-extended-helix conformation, that is capable of forming dipoles similar to the TM IV–TM XI assembly in NhaA. Therefore, TM VI (amino acids 227–249) and TM XI may form the core of an alternating access mechanism, similar to TM IV and TM XI of NhaA. However, further experiments are necessary to test this hypothesis.

Figure 6-4 illustrates the structure of TM VI of NHE1 with highlighting of some of the MTSET-reactive positions and D238. Some of the MTSET-reactive residues (N227, I233, and V237) align along a similar face that is perhaps pore-lining. D238 does not, but it may be more involved in helix stabilization, as suggested above. Although the residues L243 and E247 line up on the same face of the C-terminal helix, they do not align on the same face as the N-terminal MTSET-reactive residues, although it must be remembered that they are separated from the more N-terminal amino acids by the extended flexible region. In addition, the TM probably has different positions in different parts of the reaction cycle, and it is unknown in which position the present segment is maintained.

The alignment of the sequences of TM VI of NHE1 and TM IV of NhaA might suggest that the residues found to be pore lining in NHE1 may also be pore-lining in NhaA (Figure 6-6, B). Residues L243 and E247 in NHE1 would correspond to L138 and an A142 in NhaA based on this alignment. In agreement with the MTSET results in NHE1, these corresponding residues in NhaA are also pore-lining. This also supports the suggestion that these two helices play similar roles in each protein. The situation is less clear for the N-terminal region of the peptide. Residues N227 and I233 in NHE1 would correspond to T122 and I128 in NhaA. Both of these residues in the NhaA crystal structure are pointing away from the predicted pore region. However, conformational changes or flexibility in the protein (*37*, *38*) may allow for access to these residues in NhaA, and this might also occur for NHE1.

The results from the paramagnetic relaxation experiments (Figure 6-7) provide additional detail about the structure of the peptide and its interactions with the micelle. The periodic nature of the PRE values confirms the two helical regions in the NMR structure and suggests that they have one side facing the solvent and one side facing the micelle, with the smaller and more polar residues facing the solvent. There are two topologies of the peptide that might give these results: one where the peptide is lying on the surface of the micelle or one where two or more peptides interact to form a solvent-accessible pore within the micelle. Our experiments do not distinguish between these two possibilities. Hα PRE values for the Lys termini of the peptide are low. This could be a result of burial of the Lys residues in the micelle or the electrostatic repulsion of the Mn^{2+} by the positively charged side chains. The large increase in PRE values in the extended region of the peptide suggests that the region is binding Mn^{2+}, probably through the attraction of Mn^{2+} by some combination of the negatively charged D238, exposed carbonyl groups, and a helix dipole (Figure 6-5). This emphasizes the important role of this region in the function of NHE1. The results may also be reflective of the important role of this TM, which might be equivalent to the role of TM IV in NhaA in cation binding and transport (*4*, *5*). There is some correlation between the functional data and the PRE data. Some of the Mn^{2+}-accessible residues (G231, A236, D238, A244, and E247) in the NMR studies are also accessible to MTSET when mutated to Cys or are critical in NHE1 function in the full length protein. Other MTSET-accessible residues appear to be adjacent to the Mn^{2+}-accessible regions. It is uncertain at this time whether the Mn^{2+} accessibility reflects a role for Na^+ or H^+ coordination, but the possibility is intriguing. Further experimentation is necessary to determine if these NMR studies can be used to predict pore-lining residues in a TM.

Overall, our results have shown that TM VI (amino acids 227–249) is a pore-lining TM that is critical to NHE1 function. It has a characteristic helix–extended region–helix conformation that is conducive to formation of dipoles, with the extended middle region that is typically important in the function of transport proteins. The structure of TM VI of NHE1 has an overall similarity to that of TM IV of NhaA. Residue D238 has a location within the TM similar to that of the critical D133 of NhaA. We have recently developed an expression system for overproduction of the entire full-length NHE1 protein (*39*). Solving the structure of the full length protein will provide more details of the TM and its position within the entire protein.

Supplementary Materials

Mutation	Oligonucleotide sequence	Restriction Site
N227	5′-CAACAACATCGGCCT**tCTaGA**CtgCCTGCTCTTCGGCAGC-3′	XbaI
L228	5′-CGGCCTCCTGGAC**AAttgc**CTCTTCGGCAGCATC-3′	MfeI
L229	5′-CTCCTGGACAACCTGtgCTTCGG**atcgAT**CATCTCGGCCGTG-3′	ClaI
F230	5′-CTGGACAACCTGCTCTgC**GGatcC**ATCATCTCGGCCGTG-3′	BamHI
G231	5′-GACAACCTGCTCTTCtGCAGCATCATCT**CcGCgG**TGGACCCCGTGGCG-3′	SacII
S232	5′-CAACCTGCTCTTCGG**atGCAT**CATCTCGGCCGTG-3′	NsiI
I233	5′-CTGCTCTTCGG**CAGCtg**CATCTCGGCCGTGGAC-3′	PvuII
I234	5′-GCTCTTCGGCAG**CATatg**CTCGGCCGTGGACCC-3′	NdeI
S235	5′-CTTCGGCAGCAT**CATaTg**cGCCGTGGACCCCGTG-3′	NdeI
A236	5′-GGCAGCATCATCTCGtg**CGTcGAC**CCCCGTGGCGG-3′	SalI
V237	5′-CAGCATCATCTCG**GCatgc**GACCCCGTGGCGG-3′	SphI
D238	5′-CGGCAGCATCATCT**CcGCgG**TGtgCCCCGTGGCGGTTC-3′	SacII
P239	5′-CATCATCTCGGCC**GTcGAC**tgCGTGGCGGTTCTGG-3′	SalI
V240	5′-TCGGCCGTGGACCCC**tgcGCa**GTTCTGGCTGTCTTTG-3′	FspI
A241	5′-GCCGTGGACCCCGTGtgcGT**gCTaGC**TGTCTTTGAGG-3′	NheI
V242	5′-CGTGGACCCCGTG**GCatgc**CTGGCTGTCTTTGAG-3′	SphI
L243	5′-GACCCCGTGGCGGTT**tgcGCa**GTCTTTGAGGAAATTC-3′	FspI
A244	5′-CGTGGACCCCGTGGC**aGTaCT**GtgTGTCTTTGAGGAAATTC-3′	ScaI
V245	5′-CGTGGCGGTTCTG**GCatgC**TTTGAGGAAATTC-3′	SphI
F246	5′-GCGGTTCTGGCTGTCTgTGAGGA**gATTCACATC**AATGAG-3′	BsaBI
E247	5′-GTTCTGGCTGTCTTTtgcG**AgATTCACATC**AATGAG-3′	BsaBI
E248	5′-TCTGGCTGTCTTTGA**atgcAT**TCACATCAATGAG-3′	NsiI
I249	5′-GCTGTCTTTGAG**GAAtgc**CACATCAATGAGCTG-3′	BsmI

Table 6-S1. Oligonucleotides used for site-directed mutagenesis of TM VI. Mutated nucleotides are lower case, restriction sites are bold.

Cell line	%NHE1 plasma membrane		
	Total	Glycosylated	Unglycosylated
cNHE1 Ct	1.66±3.7	0±3.6	5.5±3.0
WT NHE1	51.0±1.8	67.3±2.4	21.1±3.1
cNHE1	53.6±3.1	72.8±3.3	17.9±2.9
N227C	52.1±3.4	67.4±4.2	17.8±4.6
L228C	41.8±5.5	70.8±4.1	9.2±8.3
L229C	39.1±1.6	58.3±1.9	5.0±1.2
F230C	22.5±1.8	62.4±1.4	0±2.3
G231C	34.9±2.9	58.2±2.9	8.3±2.8
S232C	53.2±1.5	78.0±0.9	10.2±1.9
I233C	48.8±1.9	87.3±1.9	3.4±4.1
I234C	35.5±1.7	58.8±1.7	4.8±1.0
S235C	27.0±2.1	44.0±2.1	3.8±3.1
A236C	52.4±2.3	77.4±2.1	13.1±3
V237C	46.5±1.0	74.3±3.3	9.1±1.1
D238C	42.3±2.7	74.5±2.0	2.9±3.6
P239C	13.1±4.3	0	13.1±4.3
V240C	50.3±1.7	78.0±2.2	10.5±2.3
A241C	32.8±2.8	45.6±4.0	15.4±2.8
V242C	42.9±1.2	57.9±0.9	18.0±1.2
L243C	48.3±2.7	84.9±2.1	9.2±3.4
A244C	41.1±3.7	62.8±5.7	6.7±1.7
V245C	38.5±3.4	57.2±3.8	8.2±4.3
F246C	48.3±6.7	66.4±6.7	15.7±6.6
E247C	10.6±3.5	0	10.6±3.5
E248C	42.8±3.1	79.7±2.2	13.7±3.9
I249C	56.5±3.3	78.6±2.3	16.9±2.8

Table 6-S2. Surface localization of total, glycosylated and unglycosylated NHE1 protein. Surface localization of the cNHE1 and the indicated mutants was measured as described in the "Materials and Methods." The percentage of NHE1 on the plasma membrane is indicated for both the fully glycosylated, partial (or unglycosylated) protein and for both together (total). cNHE1Ct is a control experiment to determine background signal without treatment of cell surfaces with sulfo-NHS-SS-biotin.

Cell lines	Activity	Expression	Activity corrected for expression	Surface localized glycosylated NHE1	Activity corrected for surface localization	Activity corrected for expression and surface localization
cNHE1	100.0	100.0	100.0	72.8	100.0	100.0
N227C	15.8	19.2	82.1	67.4	17.0	88.7
L228C	70.6	107.5	65.6	70.8	72.5	67.4
L229C	83.8	103.0	81.3	58.3	104.7	101.6
F230C	53.6	119.8	44.7	62.4	62.5	52.2
G231C	92.3	126.8	72.7	58.2	115.4	91.0
S232C	98.8	125.0	79.0	78.0	92.2	73.7
I233C	30.0	60.4	49.6	87.3	25.0	41.4
I234C	107.2	121.6	88.2	58.8	132.7	109.2
S235C	117.6	117.5	100.1	44.0	194.7	165.7
A236C	39.5	31.4	125.9	77.4	37.2	118.4
V237C	69.2	110.3	62.7	74.3	67.8	61.5
D238C	12.3	109.3	11.2	74.5	12.0	11.0
P239C	4.9	40.0	12.1	0.0	N/A	12.1
V240C	81.6	85.3	95.7	78.1	76.1	89.3
A241C	56.9	88.3	64.5	45.6	91.0	103.0
V242C	54.2	75.7	71.5	57.9	68.1	90.0
L243C	33.8	115.7	29.2	84.9	29.0	25.1
A244C	63.4	119.2	53.1	62.8	73.4	61.6
V245C	88.0	120.6	73.0	57.2	112.1	92.9
F246C	83.5	121.0	69.0	66.4	91.6	75.6
E247C	6.2	79.1	7.8	0.0	N/A	7.8
E248C	54.7	107.6	50.8	79.7	50.0	46.5
I249C	154.8	111.9	138.3	78.6	143.4	128.2

Table 6-S3. Activity of cNHE1 and TM VI mutants corrected with protein expression and surface localization. The NHE activity, expression levels and surface localization of the cNHE1 and the indicated mutants was measured as described in the "Materials and Methods." The correction for surface localization was made using values of surface processing for the fully glycosylated NHE1 protein.

Unique NOE restraints	
Total	750
Intraresidue	194
Sequential	199
Medium range ($i+2$ to $i+4$)	201
Long range ($\geq i+5$)	4
Ambiguous	152
Ramachandran plot statistics	
Core	61.4%
Allowed	33.4%
Generously allowed	3.6%
Disallowed	0.6%
Xplor-NIH energies (kcal/mol)	
Total	25.31 ± 2.28
NOE	1.97 ± 0.73
NOE violations	
0.1–0.2 Å	13
0.2–0.3 Å	5
> 0.3 Å	0

Table 6-S4. NMR structural statistics for the 40 structures retained out of 50 structures calculated.

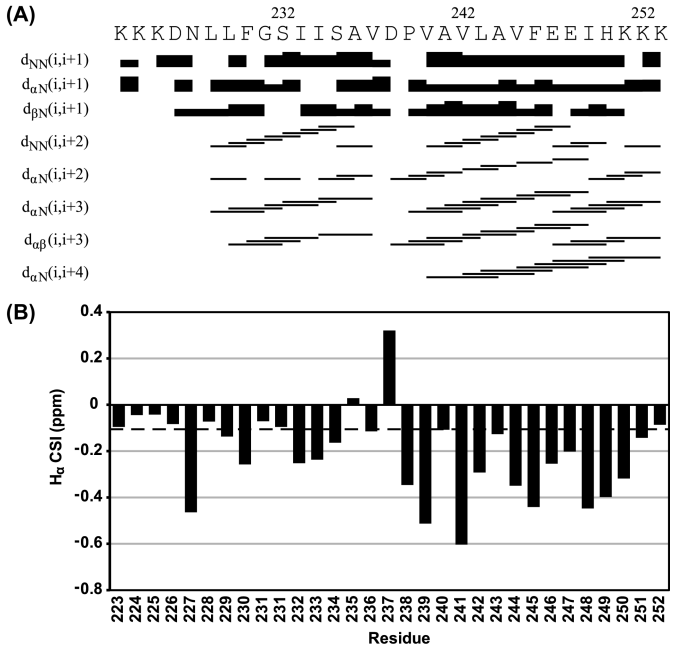

Figure 6-S1. NOE distance restraints and chemical shift index predictions of secondary structure in TM VI. (A) NOE distance restraints used in structure calculation that are indicative of helical secondary structure are shown. (B) Chemical shift index prediction of secondary structure (*25*). Differences in chemical shift between the experimental data and random coil chemical shifts ≤ -0.1 ppm (dotted line) are indicative of helical structure.

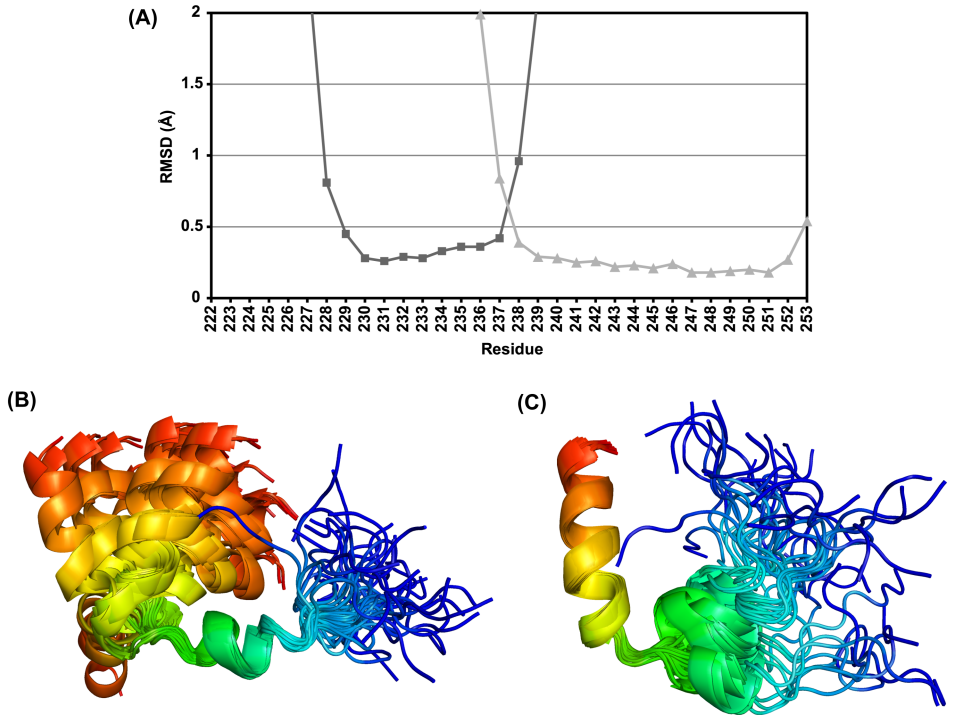

Figure 6-S2. Superimposition of NMR ensemble of TM VI. (A) Per-residue RMSD values for superimposition of the structurally homogeneous regions of the NMR ensemble. Squares, superimposition over residues L228–D238. Triangles, superimposition over residues V237–K253. Values are pairwise RMSD values between each ensemble member and an average structure, and averaged over the entire ensemble. (B) TM VI NMR ensemble superimposed over residues L228–D238. (C) superimposition over residue V273–K253.

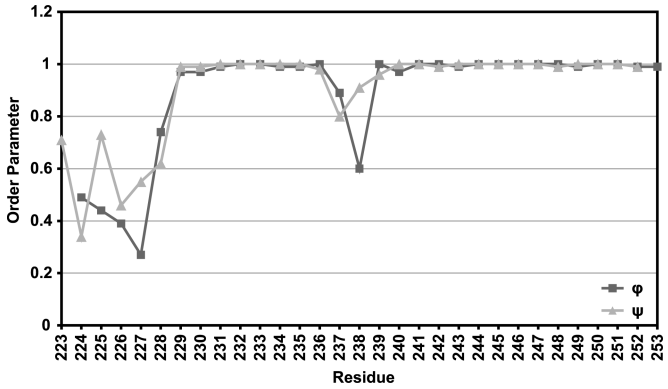

Figure 6-S3. Dihedral angle order parameters for the final 40 ensemble members of the TM VI peptide structure. Order parameters were calculated as in (*28*). The order parameter is 1 for a dihedral angle that is identical across the ensemble of structures, and is 0 when the angle is completely random.

References

1. Karmazyn, M., Sawyer, M., and Fliegel, L. (2005) The Na^+/H^+ exchanger: a target for cardiac therapeutic intervention. *Curr. Drug Targets: Cardiovasc. & Haematol. Disord. 5*, 323–335.
2. Fliegel, L. (2001) Regulation of myocardial Na^+/H^+ exchanger activity. *Basic Res. Cardiol. 96*, 301–305.
3. Wakabayashi, S., Pang, T., Su, X., and Shigekawa, M. (2000) A novel topology model of the human Na^+/H^+ exchanger isoform 1. *J. Biol. Chem. 275*, 7942–7949.
4. Landau, M., Herz, K., Padan, E., and Ben-Tal, N. (2007) Model structure of the Na^+/H^+ exchanger 1 (NHE1): functional and clinical implications. *J. Biol. Chem. 282*, 37854–37863.
5. Hunte, C., Screpanti, E., Venturi, M., Rimon, A., Padan, E., and Michel, H. (2005) Structure of a Na^+/H^+ antiporter and insights into mechanism of action and regulation by pH. *Nature 435*, 1197–1202.
6. Kemp, G., Young, H., and Fliegel, L. (2008) Structure and function of the human Na^+/H^+ exchanger isoform 1. *Channels 2*, 329–336.
7. Zamoon, J., Mascioni, A., Thomas, D. D., and Veglia, G. (2003) NMR solution structure and topological orientation of monomeric phospholamban in dodecylphosphocholine micelles. *Biophys. J. 85*, 2589–2598.
8. Zangger, K., Respondek, M., Göbl, C., Hohlweg, W., Rasmussen, K., Grampp, G., and Madl, T. (2009) Positioning of micelle-bound peptides by paramagnetic relaxation enhancements. *J. Phys. Chem. B 113*, 4400–4406.
9. Cunningham, F., and Deber, C. M. (2007) Optimizing synthesis and expression of transmembrane peptides and proteins. *Methods 41*, 370–380.
10. Oblatt-Montal, M., Reddy, G. L., Iwamoto, T., Tomich, J. M., and Montal, M. (1994) Identification of an ion channel-forming motif in the primary structure of CFTR, the cystic fibrosis chloride channel. *Proc. Natl. Acad. Sci. U.S.A. 91*, 1495–1499.
11. Hunt, J. F., Earnest, T. N., Bousché, O., Kalghatgi, K., Reilly, K., Horváth, C., Rothschild, K. J., and Engelman, D. M. (1997) A biophysical study of integral membrane protein folding. *Biochemistry 36*, 15156–15176.
12. Katragadda, M., Alderfer, J. L., and Yeagle, P. L. (2001) Assembly of a polytopic membrane protein structure from the solution structures of overlapping peptide fragments of bacteriorhodopsin. *Biophys. J. 81*, 1029–1036.
13. Naider, F., Khare, S., Arshava, B., Severino, B., Russo, J., and Becker, J. M. (2005) Synthetic peptides as probes for conformational preferences of domains of membrane receptors. *Biopolymers 80*, 199–213.

14. Yeagle, P. L., Choi, G., and Albert, A. D. (2001) Studies on the structure of the G-protein-coupled receptor rhodopsin including the putative G-protein binding site in unactivated and activated forms. *Biochemistry 40*, 11932–11937.

15. Damberg, P., Jarvet, J., and Gräslund, A. (2001) Micellar systems as solvents in peptide and protein structure determination. *Methods Enzymol. 339*, 271–285.

16. Henry, G. D., and Sykes, B. D. (1994) Methods to study membrane protein structure in solution. *Methods Enzymol. 239*, 515–535.

17. Johnson, B. A. (2004) Using NMRView to visualize and analyze the NMR spectra of macromolecules. *Methods Mol. Biol. 278*, 313–352.

18. Slepkov, E. R., Rainey, J. K., Li, X., Liu, Y., Cheng, F. J., Lindhout, D. A., Sykes, B. D., and Fliegel, L. (2005) Structural and functional characterization of transmembrane segment IV of the NHE1 isoform of the Na^+/H^+ exchanger. *J. Biol. Chem. 280*, 17863–17872.

19. Haworth, R. S., Fröhlich, O., and Fliegel, L. (1993) Multiple carbohydrate moieties on the Na^+/H^+ exchanger. *Biochem. J. 289 (Pt 3)*, 637–640.

20. Lee, B. L., Li, X., Liu, Y., Sykes, B. D., and Fliegel, L. (2009) Structural and functional analysis of transmembrane XI of the NHE1 isoform of the Na^+/H^+ exchanger. *J. Biol. Chem. 284*, 11546–11556.

21. Li, X., Ding, J., Liu, Y., Brix, B. J., and Fliegel, L. (2004) Functional analysis of acidic amino acids in the cytosolic tail of the Na^+/H^+ exchanger. *Biochemistry 43*, 16477–16486.

22. Davis, J. H., Clare, D. M., Hodges, R. S., and Bloom, M. (1983) Interaction of a synthetic amphiphilic polypeptide and lipids in a bilayer structure. *Biochemistry 22*, 5298–5305.

23. Reddy, T., Ding, J., Li, X., Sykes, B. D., Rainey, J. K., and Fliegel, L. (2008) Structural and functional characterization of transmembrane segment IX of the NHE1 isoform of the Na^+/H^+ exchanger. *J. Biol. Chem. 283*, 22018–22030.

24. Wüthrich, K. (1986) *NMR of Proteins and Nucleic Acids*, John Wiely & Sons, New York, NY.

25. Wishart, D. S., Sykes, B. D., and Richards, F. M. (1992) The chemical shift index: a fast and simple method for the assignment of protein secondary structure through NMR spectroscopy. *Biochemistry 31*, 1647–1651.

26. Kabsch, W. (1976) A solution for the best rotation to relate two sets of vectors. *Acta Crystallogr., Sect. A: Cryst. Phys., Diffr., Theor. Gen. Crystallogr. 32*, 922–923.

27. Collaborative Computational Project, Number 4 (1994) The CCP4 suite: programs for protein crystallography. *Acta Crystallogr., Sect. D: Biol. Crystallogr. 50*, 760–763.

28. Rainey, J. K., Fliegel, L., and Sykes, B. D. (2006) Strategies for dealing with conformational sampling in structural calculations of flexible or kinked transmembrane peptides. *Biochem. Cell Biol. 84*, 918–929.

29. Wishart, D. S., Boyko, R. F., Willard, L., Richards, F. M., and Sykes, B. D. (1994) SEQSEE: a comprehensive program suite for protein sequence analysis. *CABIOS, Comput. Appl. Biosci. 10*, 121–132.

30. Arseniev, A., Sobol, A., and Bystrov, V. (1986) T_1 relaxation measurement by two-dimensional NMR spectroscopy. *J. Magn. Reson. 70*, 427–435.

31. He, M. M., Sun, J., and Kaback, H. R. (1996) Cysteine-scanning mutagenesis of transmembrane domain XII and the flanking periplasmic loop in the lactose permease of *Escherichia coli*. *Biochemistry 35*, 12909–12914.

32. Sakmar, T. P., Menon, S. T., Marin, E. P., and Awad, E. S. (2002) Rhodopsin: insights from recent structural studies. *Annu. Rev. Biophys. Biomol. Struct. 31*, 443–484.

33. Kauko, A., Illergård, K., and Elofsson, A. (2008) Coils in the membrane core are conserved and functionally important. *J. Mol. Biol. 380*, 170–180.

34. Barlow, D. J., and Thornton, J. M. (1988) Helix geometry in proteins. *J. Mol. Biol. 201*, 601–619.

35. Sansom, M. S. (1992) Proline residues in transmembrane helices of channel and transport proteins: a molecular modelling study. *Protein Eng. 5*, 53–60.

36. Slepkov, E. R., Rainey, J. K., Sykes, B. D., and Fliegel, L. (2007) Structural and functional analysis of the Na^+/H^+ exchanger. *Biochem. J. 401*, 623–633.

37. Appel, M., Hizlan, D., Vinothkumar, K. R., Ziegler, C., and Kühlbrandt, W. (2009) Conformations of NhaA, the Na^+/H^+ exchanger from *Escherichia coli*, in the pH-activated and ion-translocating states. *J. Mol. Biol. 386*, 351–365.

38. Arkin, I. T., Xu, H., Jensen, M. Ø., Arbely, E., Bennett, E. R., Bowers, K. J., Chow, E., Dror, R. O., Eastwood, M. P., Flitman-Tene, R., Gregersen, B. A., Klepeis, J. L., Kolossváry, I., Shan, Y., and Shaw, D. E. (2007) Mechanism of Na^+/H^+ antiporting. *Science 317*, 799–803.

39. Moncoq, K., Kemp, G., Li, X., Fliegel, L., and Young, H. S. (2008) Dimeric structure of human Na^+/H^+ exchanger isoform 1 overproduced in *Saccharomyces cerevisiae*. *J. Biol. Chem. 283*, 4145–4154.

Chapter 7

Structural and functional analysis of critical amino acids in TM VI of the NHE1 isoform of the Na^+/H^+ exchanger

A version of this chapter has been published as:

- Tzeng, J., Lee, B. L., Sykes, B. D. and Fliegel, L. (2011) Structural and functional analysis of critical amino acids in TM VI of the NHE1 isoform of the exchanger. *Biochim. Biophys. Acta, Biomembr. 1808*, 2327–2335.

BLL performed the modelling, and JT performed the functional experiments. The manuscript was written by BLL and JT, and edited by BDS and FL.

Summary

The mammalian Na^+/H^+ exchanger isoform 1 (NHE1) resides on the plasma membrane and exchanges one intracellular H^+ for one extracellular Na^+. It maintains intracellular pH and regulates cell volume, and cell functions including growth and cell differentiation. Previous structural and functional studies on TM VI revealed several amino acids that are potentially pore lining. We examined these and other critical residues by site-directed mutagenesis substituting N227 to Ala, Asp, and Arg; I233 to Ala; L243 to Ala; E247 to Asp and Gln; and E248 to Asp and Gln. Mutant NHE1 proteins were characterized in AP-1 cells, which do not express endogenous NHE1. All the TM VI critical amino acids were highly sensitive to substitution and changes often lead to a dysfunctional protein. Mutations of N227 to Ala, Asp, and Arg; I233 to Ala; L243 to Ala; E247 to Asp; and E248 to Gln yielded significant reduction in NHE1 activity. Mutants of N227 demonstrated defects in protein expression, targeting and activity. Substituting N227 to Arg and I233 to Ala decreased the surface localization and expression of NHE1 respectively. The pore

lining amino acids I233 and L243 were both essential for activity. E247 was not essential, but the size of the residue at this location was important while the charge on residue E248 was more critical to NHE1 function. Limited trypsin digestion on L243 to Ala and E248 to Gln revealed that they had increased susceptibility to proteolytic attack, indicating an alteration in protein conformation. Modelling of TM VI with TM XI suggests that these TM segments form part of the critical fold of NHE1 with I233 and L465 of TM XI forming a critical part of the extracellular facing ion conductance pathway.

Introduction

As part of a series of studies analyzing the structure and function of transmembrane regions of NHE1 (*1–4*) we recently analyzed the peptide structure of TM VI (N227–I249) of NHE1 in DPC micelles, and analyzed the functional contribution of amino acids of that segment by using the cysteine scanning accessibility method (*5*). Many amino acid residues of TM VI (transmembrane segment VI) were sensitive to mutation to Cys and reaction with external sulfhydryls indicating that TM VI was a critical pore lining segment. Interestingly, TM VI had a structure consisting of a helix, an extended region, followed by another helix. This was similar in structure to the critical TM IV of the *Escherichia coli* Na^+/H^+ exchanger NhaA (*6*) and we proposed that it serves a similar critical role in NHE1 activity. In this study we further characterized this key transmembrane segment. Of the residues in TM VI that maintained sufficient NHE1 activity when substituted to Cys, the key pore lining amino acids of TM VI were N227, I233 and L243. Several other residues had partially depressed activity when substituted to cysteine including, E247 and E248. Moreover, the E248 to Cys mutant was partially inhibited by MTSET treatment (*5*).

Here we further characterized the functional importance of critical amino acids in TM VI. Applying site-directed mutagenesis methods, N227, I233, L243, E247, and E248 of TM VI were substituted into N227 to Ala, Asp, and Arg; I233 to Ala; L243 to Ala; R247 to Asp and Gln; and R248 to Asp and Gln. These mutant NHE1 proteins were assessed for their protein expression, activity, and surface localization. Limited digestion with trypsin was used to examine protein conformational changes caused by mutations. Additional structural modelling was performed based on previous NMR studies of TM VI and XI to investigate their assembly in the cation translocation pore. Our results demonstrate that TM VI forms a critical part of the cation access pathway along with TM XI. N227 and I233 form

Mutation	Oligonucleotide sequence	Restriction site
N227A	5′-CAACAACATCGGCCT**tCTaGA**CgcCCTGCTCTTCGGCAGC-3′	XbaI
N227D	5′-CAACAACATCGGCCT**tCTaGA**CgACCTGCTCTTCGGCAGC-3′	XbaI
N227R	5′-CAACAACATCGGCCT**tCTaGA**CcgCCTGCTCTTCGGCAGC-3′	XbaI
I233A	5′-CTGCTCTTC**GGatcC**gcCATCTCGGCCGTGGAC-3′	BamHI
L243A	5′-GACCCCGTGGCGGTTg**ccGCgG**TCTTTGAGGAAATT-3′	SacII
E247D	5′-GTTCTGGCTGTCTTTGAcGA**gAT**TCAC**ATC**AATGAG-3′	BsaBI
E247Q	5′-GTTCTGGCTGTCTTTcAGGA**gAT**TCAC**ATC**AATGAG-3′	BsaBI
E248D	5′-TCTGGCTGTC**TTcGAa**GAcATTCACATCAATGAG-3′	BstBI
E248Q	5′-TCTGGCTGTC**TTcGAacAA**ATTCACATCAATGAG-3′	BstBI

Table 7-1. Oligonucleotides used for site-directed mutagenesis of TM VI. Nucleotides mutated are indicated in lower case, and restriction sites introduced are indicated in bold.

part of the extracellular facing pore while L243, E247 and E248 form critical parts of the intracellular fold of the coordination pathway.

Methods

Functional characterization of NHE1 mutants were performed essentially as described in Chapter 2. Mutations made and primers used are listed in Table 7-1. In addition, limited trypsin digestion of NHE1 and modelling of TM VI-XI complex was also performed and are detailed below.

Limited trypsin digestion

Limited trypsin digestion of NHE1 was used to determine changes in the conformation of the protein as described earlier (*7*). Cell lysates were prepared as described above using RIPA lysis buffer, with the exception that proteinase inhibitors phenylmethylsulfonyl fluoride, benzamidine and protease cocktail were not added. Trypsin (phenylalanyl chloromethyl ketone-trypsin, Sigma, St., Louis, MO) was prepared and dissolved in TE buffer. Equal amounts of proteins (100 µL) from cell lysates were treated with trypsin at different trypsin:protein ratios (1:1500, 1:2000, 1:2500, 1:3000) and incubated at 37 °C for 5 min. The reaction was terminated by addition of SDS-PAGE loading buffer followed by boiling at 100 °C for 5 min. Samples were resolved by SDS-PAGE and NHE1 detected by western blot analysis. Quantification of the band intensity was done using ImageJ 1.35 software (National Institutes of Health, Bethesda, MD, USA). To minimize variation we compared the level of fully glycosylated NHE1 protein in mutant proteins to that of the wild type protein treated simultaneously and run on the same gel.

Modelling of the predicted functional assembly of NHE1

Restraints defining the secondary structure of both TM VI and TM XI were obtained from the previously published NMR structures of synthetic peptides representing TM VI and TM XI in dodecylphosphocholine micelles (*4*, *5*). Additional restraints defining the interaction between TM VI and TM XI were measured from the three dimensional model of NHE1 by Landau et al. (*8*) which proposes that TM VI and TM XI are equivalent to the discontinuous helices TM IV and TM XI found in the crystal structure of NhaA (*6*). All interhelical distances between protons less than 4 Å were used. These distances were converted to restraints with a range of 1.8–4.0 Å for the calculation of the model. Calculation of the final model structure used the distance and dihedral restraints from the NMR structure calculation of TM VI and TM XI combined with the interhelical distance restraints obtained from the model of Landau et al. (*8*). An ensemble of 50 structures were calculated, from which the 25 lowest energy structures were used to calculate an average structure. Calculation of the model was performed using simulated annealing in Xplor-NIH 2.26 (*9*) through the Python scripting interface.

Results

Analysis of amino acids of TM VI critical for NHE1 activity

We have previously (*5*) demonstrated that TM VI of NHE1 is a pore lining segment with several specific amino acids of TM VI identified as pore lining residues and with other residues having depressed NHE1 activity when mutated to Cys. We therefore decided to further investigate the characteristics of the critical pore lining residues N227, I233, L243, and other residues (E247 and E248) important for activity. Nine mutations of various types were made to replace these residues in the background of wild type NHE1 protein. Hydrophilic N227 was mutated to an Ala with a small side chain group, to a Gln with longer hydrophilic side chain, and to a positively charged Arg. I233 and L243 were mutated to Ala to remove the contribution of their long hydrophobic side chains. E247 and E248 were mutated into the similarly charged, but smaller Asp and to a polar Gln side chain that does not have a free carboxyl. All TM VI mutant plasmids were successfully transfected in AP-1 cells and the expressed NHE1 protein was detected by SDS-PAGE and subsequent western blotting against the HA tag. Initial experiments determined the expression levels of each TM VI mutant protein (Figure 7-1). NHE1 has two

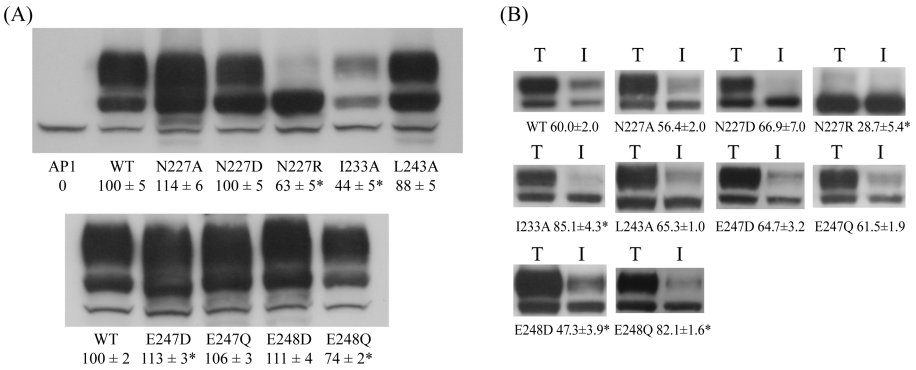

Figure 7-1. Characterization of expression of NHE1 mutant proteins. (A) NHE1 expression levels of mutants of critical residues in TM VI. Western blot analysis of whole cell extracts of WT NHE1, and TM VI mutants. Each lane contained 75 µg of total protein. The specific mutations are indicated. AP1 indicates untransfected-control cell lysates. NHE1 expression levels were examined using anti-HA antibody. Numbers underneath the lanes indicate the mean value ($\pm$ S.E.) of the sum of densitometric scans of both 110 kDa and 95 kDa bands relative to wild-type NHE1 for at least three experiments. * indicates mutants with significantly different expression than WT NHE1 at $p < 0.05$. (B) Surface localization of NHE1 proteins with mutations in critical residues of TM VI. Sulfo-NHS-SS-biotin treated cells were lysed and their proteins were solubilized and subsequently treated as described in the "Methods." Equal samples of total lysates (T) and unbound (representing intracellular) lysates (I) were resolved on SDS-PAGE and probed with anti-HA antibody to identify NHE1 protein. The amount of surface localized fully glycosylated NHE1 was calculated from densitometric analysis by taking $(\text{Total protein}) - (\text{Unbound protein}) = (\text{Membrane surface localized protein})$. The percent of the total NHE1 protein localized to the plasma membrane is indicated. Results are mean $\pm$ S.E., $n \geq 6$ experiments. * Indicates significantly reduced plasma membrane targeting in comparison to wild type (WT) NHE1 ($p < 0.05$).

forms: the mature NHE1 is glycosylated and has a higher molecular weight at around 105–110 kDa, whereas the immature form of NHE1 is partially or non-glycosylated with a molecular weight around 85–95 kDa. Both forms were present in our stably expressing cells. Some of the mutants expressed reduced amounts of NHE1 protein. L243A and E248Q had expression reduced to ∼90% and ∼75% of control NHE1 respectively. I233A displayed the lowest expression of NHE1 expression at only 44% of wild type. Mutation of N227 to Arg reduced expression of the mature form of NHE1 drastically and the immature protein made up the majority of NHE1 expressed. We have previously found that mutation of some other residues of NHE1 had the same effect including the mutations I145C, Y4554C and G459C (*4*).

The surface localization of TM VI mutants was investigated. Membrane proteins are usually synthesized in the endoplasmic membrane destinations. Previous studies have found that mutations in NHE1 may interrupt the synthesis and transport network, which causes intracellular retention of the mutant protein and is reflected in impaired restoration of acidified pH_i (*4*, *10*, *11*). Surface targeting experiments were carried out as described in the "Methods." The total and unbound (intracellular) fractions of cell lysates were examined by SDS-PAGE and western blotting, and the amount of fully glycosylated and partially/non-glycosylated NHE1 were measured. The results are shown in Figure 7-1, B and Table 7-S2. Examination of the fully glycosylated NHE1 protein demonstrated that the amount of NHE1 targeted to the cell surface declined significantly for both N227R and E248D mutants (Figure 7-1, B). N227R targeted to the cell surface about half as well as the control. I233A and E248Q displayed ∼20% higher localization of mature glycosylated NHE1 protein to the cell surface. There was also an ∼10% significant reduction in the glycosylated form of the E248D mutant on the plasma membrane. The mature fully glycosylated NHE1 protein generally targeted to the membrane surface, whereas the immature partially glycosylated NHE1 largely remained mainly intracellular (Table 7-S2). However significant amounts of partially- or un-glycosylated NHE1 protein were also present on the cell surface similar to results we have observed earlier (*5*). Examination of the individual plasma membrane targeting of the fully glycosylated and partially or de-glycosylated forms of the mutants showed that targeting was impaired in several other cases, this included in all N227 mutants and in L243A and E248D (Table 7-S2).

The cation transport activity of NHE1 TM VI mutant stable cell lines was examined by assessing their ability to recover from a transient intracellular acidification. The results are shown in Figure 7-2. Figure 7-2, A, illustrates an example of a

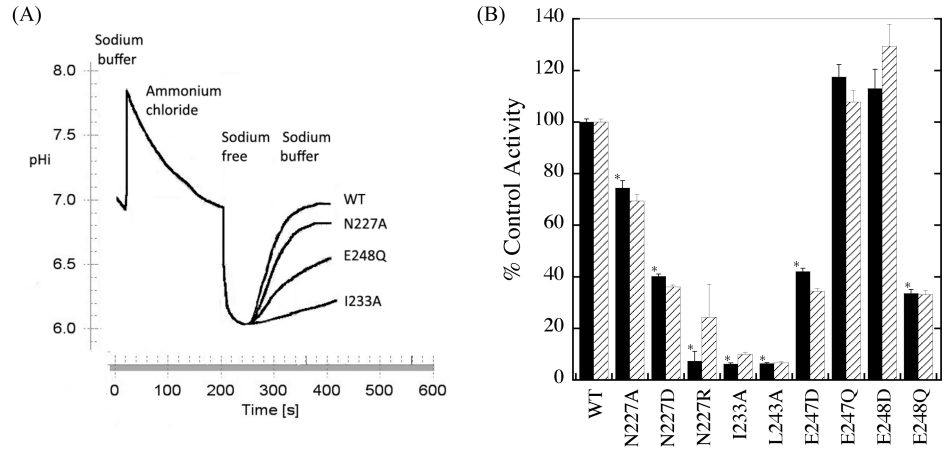

Figure 7-2. Characterization of NHE1 activity for mutations of critical residues in TM VI. (A) Example of activity traces of wild type and mutant NHE1 proteins. The activity of WT NHE1 protein is shown. For clarity, only the pH_i recovery after acidosis is illustrated for the mutant proteins N227A, I233A, and E248Q. (B) Summary of NHE activity of mutant NHE1 proteins. The activities of NHE1 WT control, and TM VI mutants were determined as described in "Methods." The rate of recovery in WT NHE1 was set to 100% and mutants' recovery rates were expressed as a percent of WT. Results are mean $\pm$ S.E. ($n \geq 6$ determinations). Solid bars are NHE1 activities as measured, not corrected for the level of protein expressed or surface targeting. Hatched bars indicate NHE1 activity corrected for expression levels and surface targeting. * indicates uncorrected TM VI mutant activities that are significantly lower than that of WT NHE1 at $p < 0.05$.

time course of transient intracellular acidifications followed by recoveries. The graph in Figure 7-2, B, indicates the uncorrected NHE1 activities in black bars and hatched bars are activities normalized with expression levels and levels of surface localization of the mature form of NHE1. Table 7-S2 illustrates the raw NHE1 activities prior to correction with protein expression levels and surface expression. Some mutant NHE1 proteins had nearly no signs of pH_i recovery after intracellular acidification (N227R, I233A, and L243A). N227A exhibited ~75% of control activity. N227D and E248Q had less than 40% of control activity. Correcting the raw activities for protein expression and localization, did not revert activity back to wild type NHE1 levels indicating that the effect of the mutations on activity were due to effects on actual activity of the NHE1 proteins, and not due to aberrant targeting or expression levels.

Of the nine TM VI mutations four residues, I233A, L243A, E247D, and E248Q were chosen for further investigation to determine the nature of the defect in NHE1 activity. Limited trypsin digestions were carried out to determine if there were changes in protein conformation (*7*, *12*). Cell lysates were treated with trypsin for 5 min and at different ratios of trypsin:protein (1:1500 to 1:3000 as indicated) to produce fragments of NHE1 protein. Control digestions of wild type NHE1 protein were always done simultaneously with the mutants to make experimental results more uniform. The results (Figure 7-3, A–E) showed that there was no significant difference between the digestion pattern of NHE1 control, E247D and I233A mutant proteins. E248Q displayed a higher sensitivity to trypsin than the wild type, and most of the immunoreactive NHE1 bands disappeared even at the lowest trypsin:protein ratio of 1:3000. Other mutants were slightly more susceptible to trypsin hydrolysis compared to WT NHE1. For L243A, most of the bands were digested in the L243A mutant at 1:2000 trypsin:protein ratio treatment. There was no appearance of additional bands due to trypsin digestion. Western blot analysis was done using the HA-tag at the C-terminal tail of NHE1.

Molecular modeling of TM VI and TM XI

NhaA, a bacterial homologue to the human Na^+/H^+ exchanger NHE1, contains two discontinuous helices, TM IV and TM XI (*6*). These helices are thought to be central to the alternating-exchange mechanism in the transporter. In the model of NHE1 developed by Landau et al. (*8*), they suggested that TM VI and XI are functionally and structurally equivalent to TM IV and XI, respectively, of NhaA. We previously determined the structure of peptides of TM VI and TM XI using

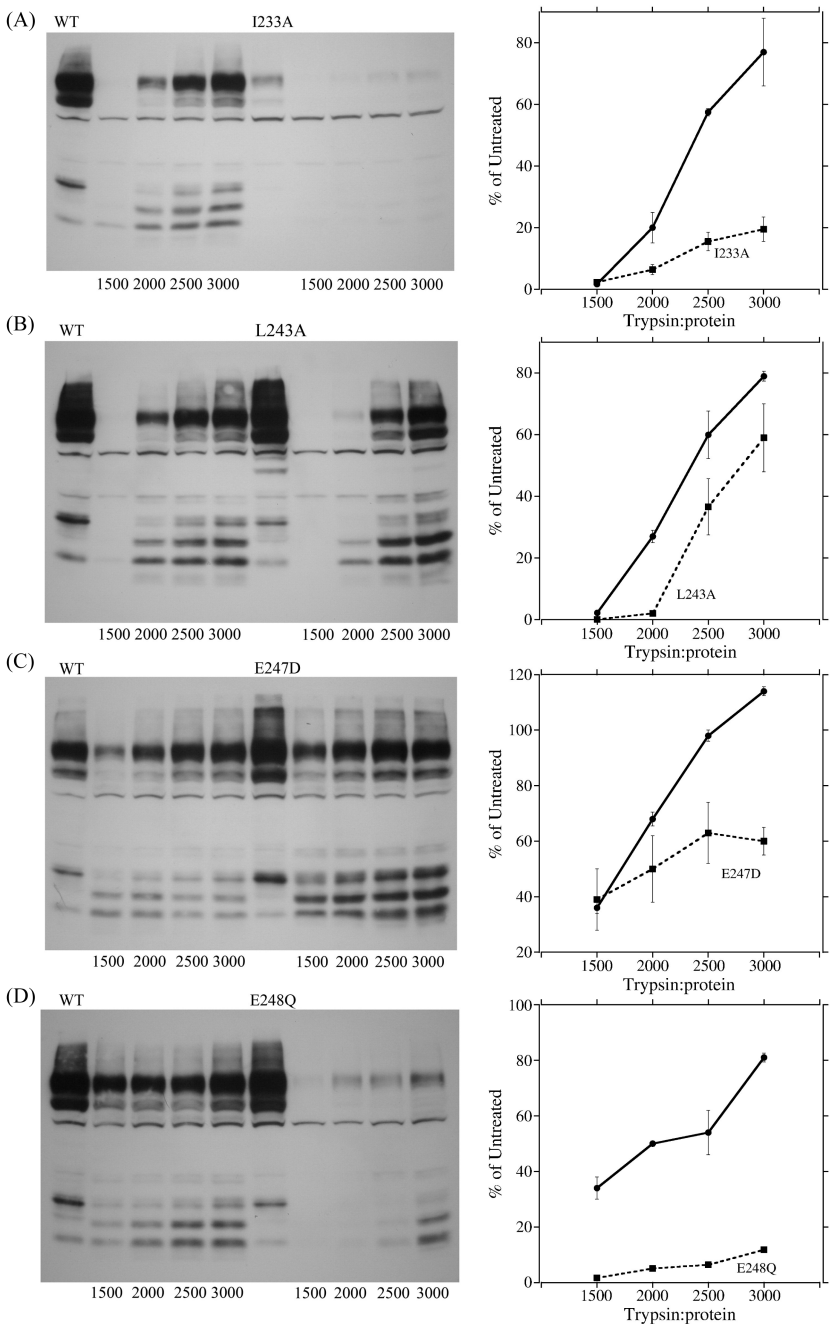

Figure 7-3. Limited trypsin digestion of selected TM VI mutants. (A–D) Representative Western blots (left side) of WT NHE1, E247D, E248Q, L243A, and I233A whole cell lysates treated with trypsin:protein ratios of 0:1, 1:1500, 1:2000, 1:2500, and 1:3000 as indicated. The pattern of NHE1 digestion was detected using anti-HA antibodies. Similar results were reproduced at least two times. (Right side) Summary of results of digestion of WT and mutant NHE1. The relative levels of fully glycosylated NHE1 were compared for WT and mutant NHE1 proteins. The levels of each mutant are compared with that of the WT done simultaneously and run on the same gel.

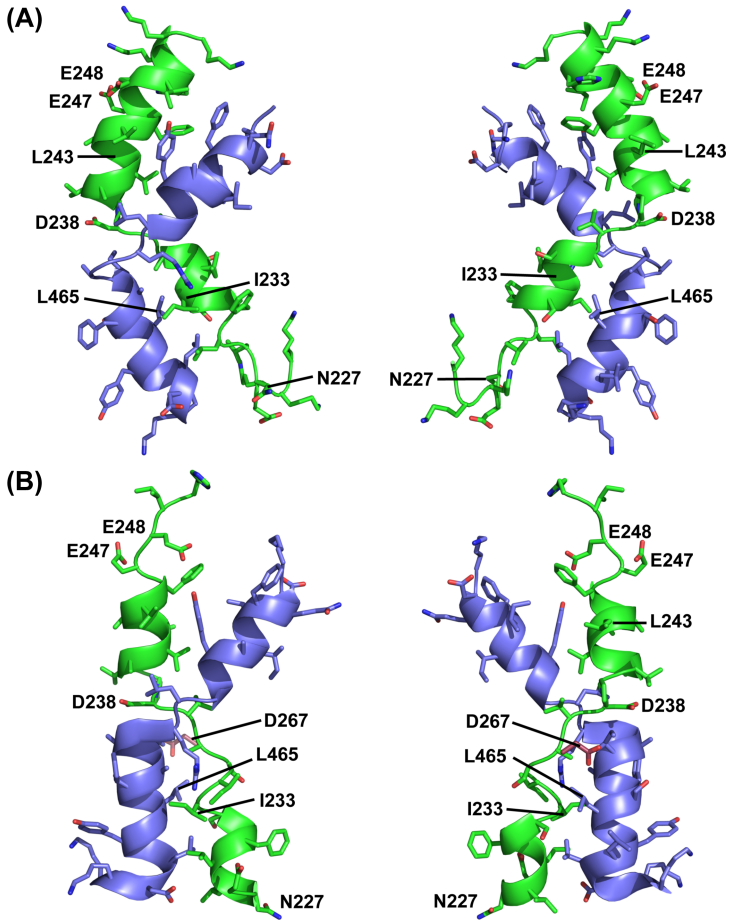

Figure 7-4. Model of TM VI/TM XI assembly. (A) Model of discontinuous helix assemblies in NHE1 using NMR and artificial restraints. The model was generated using NMR restraints from the structure determination of the individual helices TM VI (residues 226–250) and TM XI (residues K447–K472) combined with distances from the model determined by Landau et al. (*8*). Additional terminal lysine tags present in the TM VI peptide structure, but not in the native sequence, are included. TM VI is shown in green, and TM XI is shown in blue. Residues in TM VI which were mutated in this study are labelled. The right diagram is a 180° rotation of the structure. (B) Model of discontinuous helices in NHE1 determined by Landau et al. (*8*). The diagram shows the predicted structure of TM VI and TM XI as determined by Landau et al. (*8*) (who describe them as TM 4 and TM 11 respectively). TM VI (TM 4) (residues D226–H250) is shown in green and TM XI (TM 11) (residues K447–K472) is shown in blue. Residues in TM VI which were mutated in this study are labelled. The right diagram is a 180° rotation of the structure. The side chain of D267 from TM VII (TM 5) (residues 253–273) is shown in red.

high-resolution solution-state NMR in dodecylphosphocholine micelles and found that TM XI of NHE1 is similar in structure to TM XI of NhaA (*4*), and that TM VI of NHE1 is similar in structure to TM IV of NhaA (*5*). Both TM VI and TM XI contained two helical regions connected by a flexible, extended region, similar to the structure of the discontinuous helices of TM IV and XI NhaA (*6*), suggesting we could model our NMR structures into a similar conformation. To generate a model of the NMR structures of interacting TM VI and TM XI, experimental NMR restraints from the individual helices were combined with restraints based on the Landau 3D model of NHE1. Restraints defining the structure of each of the TMs were defined by the previously published NMR distance and dihedral restraints (*4*, *5*). Restraints for the interaction between the TMs were obtained from the Landau model (*8*), with inter-TM proton-proton distances less than 4 Å set as distance restraints with a range of 1.8–4.0 Å. These restraints were combined and used to generate 50 structures. An average structure calculated from the 25 lowest energy structures is shown in Figure 7-4, A.

The secondary structures of TM VI and TM XI in this model are the same as in the NMR structures. TM VI consists of two helical regions, at residues 229–236 and 239–250, separated by a short extended region at residues 237–238. Residues 223–228 are flexible in the model as in the NMR structure. TM XI has a similar structure, with two helical regions at residues 447–454 and 460–471, with an extended region at residues 455–459. The orientation of the helices in TM VI is also approximately the same as the earlier published NMR structure (*5*), with the two helical regions at right angles to each other. TM XI, which had much variability in the orientation of its helices in the NMR structure (*4*), also adopts a right angled conformation, likely adopting to the conformation of TM VI.

TM VI and TM XI from the model of Landau et al. (*8*) are shown in Figure 7-4, B. The helical regions for TM XI in the Landau model are almost the same as the NMR model (residues 448–454 and 460–470). The N-terminal helix in TM VI is different. Residues 227–232 form a helix, while 233–236 form a distorted helix. This difference in structure results in many restraint violations in this region in the NMR model shown in Figure 7-4, A. In the C-terminal helix, residues 240–246 in the Landau model are helical, making this shorter than in the NMR based model. The lysine tags in the NMR based model are not present in the native protein structure or in the model of Landau et al. (*8*). In Figure 7-4, B, it can be seen that the axes of the C-terminal helices of TM VI and TM XI are parallel, while in Figure 7-4, A, they are tilted away from vertical, towards the N-terminal helices of TM VI and TM XI.

The interhelical restraints result in the orientation of side chains in the interface of the NMR model to be generally similar in the Landau model, while the orientation of side chains away from the interface tends towards the results obtained with NMR measurements.

We examined the relative position of the mutated amino acids of TM VI in two model structures of TM VI. The amino acids mutated in this study are indicated. In Figure 7-4, A, N227 which was essential for activity, is on the extracellular face of the membrane, possibly on the extracellular loop, and could be part of the mouth or funnel of the protein. I233 is in close association with TM XI, perhaps mediating inter-TM associations but also possibly lining a potential pore region. It is near to L465 which was a pore lining residue of TM XI (*4*, *5*). The essential amino acid L243 is facing slightly away from region between the two TM segments but points along the same face as L465. Both E247 and E248 are in or near the cytosolic face of the protein. The charge on E248 was essential for activity and it is interesting that it faces away from the direction of the side chain of L243. E247 is on a similar side as L243 and L465.

Figure 7-4, B, illustrates a model of TM VI and TM XI based upon the predictions of Landau et al. (*8*). There are similarities and some differences from Figure 7-4, A, in the position of the mutated amino acids. N227 is on the extracellular side but points more away from a putative extracellular funnel region. I233 is pointing more towards the inter-TM VI-XI space, still in association with L465. Amino acid L243 is in a similar position as in Figure 7-4, A. The acidic amino acids E247 and E248 face in near opposite directions to each other. E247 is in a similar position as in Figure 7-4, A, while the relative position of E248 has changed markedly, now on the intracellular loop rather than part of the TM helix, and it points more towards the space between the TM segments. Both residues are on the cytosolic side of the membrane.

Discussion

TM VI in NHE1 function

The mechanism of Na^+/H^+ exchange is a question of significant interest both as a basic biological problem, and because of the critical role that the NHE1 protein plays in both heart disease, cell growth and differentiation, and in metastasis of tumour cells. In the *E. coli* Na^+/H^+ exchanger, NhaA, TMs IV and XI play a

critical role in Na^+/H^+ exchange. Both these helices are discontinuous, interrupted by an extended segment and the discontinuous helices form mid-membrane dipoles. The ion binding site of NhaA is formed around the extended segments of TMs IV and XI and includes a cluster of amino acids (D164, D163, D133 and T132) (*6*, *13*). We recently examined the structure and properties of TM VI of NHE1. We showed that it is a critical TM segment containing the pore lining amino acids N227, I233 and L243 that are accessible from the extracellular aqueous phase. TM VI had an architecture similar to that of TM IV of NhaA, with two helical parts being interrupted by an extended mid membrane segment (*5*). TM IV of NHE1 had a smaller amount of similarity to TM IV of NhaA. It had only one helical region consisting of amino acids 169–176 (*1*). We also found that another TM fragment of NHE1, TM XI, had the helix-discontinuous region-helix structure, similar to that of TM XI of NhaA. It also possesses pore lining residues (*4*).

Functional analysis

In the present study, we further characterized some of the critical amino acids of TM VI. As noted above, amino acids N227, I233 and L243 were earlier shown to be pore lining amino acids, being reactive with MTSET applied from the extracellular surface. In addition, we earlier found that mutation of amino acids E247 and E248 to Cys resulted in an inactive and partially active protein respectively. The E248C mutant was also partially inhibited with externally applied MTSET (*5*). We therefore further characterized these five amino acids in efforts to determine what role they played in NHE1 function. N227 was substituted to Ala, Asp, and Arg. I233 and L243 were mutated to Ala and E247 and E248 were mutated to Asp and Gln respectively. N227 is clearly an important though not essential amino acid. None of the mutations in N227 were very well tolerated; N227C (*5*) and N227R (present study) expressed reduced amounts of NHE1 and only the immature form of NHE1 respectively. N227A and N227D exhibited diminished NHE1 activity and had some mistargeting. Asn contains an uncharged polar side chain, and substitution to alanine had the least effect on NHE1 activity. When N227 was mutated into negatively charged Asp, the activity of NHE1 dropped to 40% of control. Substituting positively charged Arg for N227 seemed to be the most unfavourable. It resulted in virtual elimination of activity, mistargeting of the protein and decreased expression. The positive charge introduced by Arg could affect sodium coordination, or could destabilize other balancing electrostatic forces within the membrane. This could lead to conformational changes in the protein

which led to loss of production of the fully glycosylated protein. Overall, our results with this amino acid suggest that it is pore lining, though not absolutely essential.

I233 and L243 were also shown earlier to be important pore lining amino acids (*5*). For both of these amino acids, mutation to Ala eliminated NHE1 activity. The decrease in activity was not accounted for by decreased protein expression levels or by decreased targeting to the cell surface. These results demonstrate that these amino acids are not only pore lining, but their side chain is critical to the maintenance of NHE1 activity. That mutation to the small uncharged Ala caused so dramatic an effect on activity, further indicates that these amino acids are critical in NHE1 function. Limited digestions with trypsin did suggest a possible change in the conformation of the I233A mutant, though this analysis was not as clear because of the lower expression level of this protein. The L243A mutant protein did show a slight change in accessibility to trypsin, indicating a change in protein conformation. We suggest that mutation of this pore lining amino acid to a smaller one affects the protein folding or stability, which affects its accessibility to trypsin and also affects ion binding and transport. It should be pointed out that our analysis of changes in protein conformation was done using the C-terminal HA tag. Thus it is possible that other changes in the N-terminal region were not detected by our assay and new fragments not containing the HA tag would not be detected.

Analysis of amino acids E247 and E248 was quite revealing. We earlier demonstrated that mutation of these residues to Cys compromised NHE1 activity and that E248 was at least partially pore lining (*5*). These results were intriguing and partially led to the decision to further investigate these amino acids. Also, we have earlier (*14*) suggested that the negative charge that these side chains impart, could aid in cation coordination. Therefore, we investigated the effect of neutralizing and modifying the charge in these positions. We obtained different results with these two amino acids. Neutralizing the charge on E247 had no effect on NHE1 activity, while changing to the smaller Asp residue noticeably inhibited activity. In contrast, changing E248 to Asp, had no effect on NHE1 activity while changing to Gln, caused a precipitous decline in NHE1 activity that was accompanied by a change in conformation of the protein. These results demonstrate that the charge on E247 is unimportant in activity, while the location and size of the amino acid is more critical. At position 248, the charge is critical and a small change in the position of the carboxyl group was not of great significance. We suggest that at amino acid 248, the carboxyl is involved in cation coordination and/or maintenance of the coordination structure or sphere of the NHE1 protein. A mutation at this

amino acid, neutralizing the carboxyl group, destabilized the conformation of the protein.

Structure and function of the critical fold of NHE1

As noted above, TM VI of NHE1 resembles TM IV of NhaA, more so than does TM IV. It also has more pore lining amino acids, as determined by cysteine scanning mutagenesis (*5*). In addition, we earlier noted that TM XI of NHE1 is similar to TM XI of NhaA (*4*). We therefore suggest that TM VI and TM XI constitute the critical catalytic fold of NHE1, similar to TM IV and TM XI of NhaA. Landau et al. (*8*) have also suggested that TM VI and TM XI play the equivalent role to TM IV and XI of NhaA. Their model suggests that the amino acids of "TM VI" are actually TM IV, (the first two TM segments of NHE1 being removed as a signal sequence) and thus they propose a critical TM IV–TM XI structure. Recently Nygaard et al. (*15*) modelled the NHE1 protein. Their modelling suggests that TM IV (amino acids 160–179) and TM XI are the critical fold in NHE1 and are similar to TM IV and TM XI of NhaA. Their modelling also suggested that D172 of TM IV and R425 of TM X have dipole masking functions. However, we have shown that the charge on D172 is unnecessary for NHE1 function (*16*). Mutation of this residue to Gln did not affect NHE1 activity and mutation to Asn only slightly reduced activity (*16*). Thus, the charge at this amino acid is not necessary to NHE1 function and it is unlikely to have a dipole masking function. In addition, as noted above, TM VI of NHE1 is much more similar to TM IV of NhaA, than is TM IV of NHE1. Thus we suggest that TM VI and TM XI are much more likely candidates for the critical fold mediating NHE1 transport.

We therefore examined the putative structure of the TM VI and TM XI region and the location of the critical amino acids of TM VI. The entire structure of the NHE1 protein is unavailable; however, we have earlier (*4*, *5*) determined the structure of peptides representing TM VI and TM XI, and Landau et al. (*8*) have modelled this region based on comparison with NhaA. Figure 7-4 depicts two models of the TM VI/XI assembly, the one from this study based on the NMR derived structures of the TM segments (Figure 7-4, A) and one from the model of Landau et al. (*8*) (Figure 7-4, B). The positions of N227, I233, L243, E247 and E248 are indicated as well as some other critical nearby amino acids. In general the overall architecture of the model based on the determined NMR structures and the model base on that of Landau et al. (*8*) are similar but there are differences in the position of the side chains as noted below. Both Figure 7-4, A, and Figure 7-4, B, illustrate that D238 lies

between the assembly of discontinuous helices TM VI/XI, and it may compensate for the positive polarity contributed by the N-terminal ends. Previously we demonstrated that substituting D238 with Cys resulted in a dysfunctional NHE1 protein (*5*). When considered in the context of the whole model (*8*), Figure 7-4, B, shows that the side chain of L243 is pointing towards the same face of the membrane as a putative protonation site at D267. This position is similar in the empirically based NMR model (Figure 7-4, A). D267 is also located in close proximity to the pore lining residues I233 and L465, which might explain their sensitivity to mutation (*4*, *5*, *8*). Given that L465, I233 were pore lining, and that D267 is the putative protonation site, it appears as though this region defines at least part of the channel and transport site of the protein. Clearly mutation or derivation of amino acids in this region is detrimental to the function of NHE1 as demonstrated by mutation to amino acids D267, I233 and L465 (*2*, *4*, *5*). Furthermore, studies in NhaA suggest that movement occurs in this region during activation and transport, which could also explain the pore accessibility we observed (*17*, *18*).

While it is uncertain which model is closer to the true structure of NHE1, some features of each model correlate better with the data we obtained. The charge on E247 was not essential while that on E248 was. In addition we (*5*) found that when E248 was mutated to Cys, reaction with MTSET partially inhibited the protein, suggesting it is at least partially pore lining. In the NMR structure based model E248 points more away from a putative coordination sphere and is in a helical region while in the model of Landau et al. (*8*), E248 is part of a flexible loop and appears to point more towards the putative cytoplasmic coordination sphere, which could be important in attraction of protons for transport and is more in accordance with our effects on function. Conversely, N227 was intolerant of mutation and clearly an important amino acid. Mutation to a positively charged amino acid was most detrimental, in keeping with a putative role in a coordination sphere of a cation. In Figure 7-4, B, N227 points further away from a coordination sphere while in the NMR based model (Figure 7-4, A), it is part of a flexible region possibly in the extracellular loop, where it could be more oriented towards a putative coordination region, which is in greater accordance with its function. Other amino acids have less variation in their position between the two models. It should be noted that overall, both models were quite similar and differences could represent a limitation in solving the structures of single isolated helices or different conformations of the protein during the reaction cycle.

Conclusion

In conclusion, the critical amino acids of TM VI, N227, I233, L243, E247 and E248, contribute significantly to the normal function of NHE1. N227 is essential in protein expression, processing and activity. The pore lining I233 may locate close to D267 and L265 and is essential for NHE1 activity, perhaps forming part of a narrowing cation access channel or a trimming region. L243 is another pore lining residue that contributes to Na^+/H^+ transport and protein stability/conformation. E247 and E248 are most likely involved in cation transport or protein stability as well, with E248 important in protein stability and conformational folding and the charge on E248 being critical in protein function. We suggest that TM VI makes up part of a critical fold of NHE1, similar to that which occurs in NhaA. A full length high resolution structure of NHE1 is desirable to confirm these observations and solve the mechanism of mammalian Na^+/H^+ translocation.

Supplementary Materials

Cell Line	Activity (ΔpH/min)	S.E.
WT	0.87	0.010
N227A	0.65	0.025
N227D	0.35	0.007
N227R	0.06	0.033
I233A	0.05	0.004
L243A	0.05	0.003
E247D	0.36	0.011
E247Q	1.02	0.041
E248D	0.98	0.064
E248Q	0.29	0.014

Table 7-S2. Raw NHE activity of WT (control) and TM VI mutants was determined as described in the "Materials and Methods." Results are mean $\pm$ S.E. ($n \geq 6$ determinations.

References

1. Slepkov, E. R., Rainey, J. K., Li, X., Liu, Y., Cheng, F. J., Lindhout, D. A., Sykes, B. D., and Fliegel, L. (2005) Structural and functional characterization of transmembrane segment IV of the NHE1 isoform of the Na^+/H^+ exchanger. *J. Biol. Chem. 280*, 17863–17872.
2. Ding, J., Rainey, J. K., Xu, C., Sykes, B. D., and Fliegel, L. (2006) Structural and functional characterization of transmembrane segment VII of the Na^+/H^+ exchanger isoform 1. *J. Biol. Chem. 281*, 29817–29829.
3. Reddy, T., Ding, J., Li, X., Sykes, B. D., Rainey, J. K., and Fliegel, L. (2008) Structural and functional characterization of transmembrane segment IX of the NHE1 isoform of the Na^+/H^+ exchanger. *J. Biol. Chem. 283*, 22018–22030.
4. Lee, B. L., Li, X., Liu, Y., Sykes, B. D., and Fliegel, L. (2009) Structural and functional analysis of transmembrane XI of the NHE1 isoform of the Na^+/H^+ exchanger. *J. Biol. Chem. 284*, 11546–11556.
5. Tzeng, J., Lee, B. L., Sykes, B. D., and Fliegel, L. (2010) Structural and functional analysis of transmembrane segment VI of the NHE1 isoform of the Na^+/H^+ exchanger. *J. Biol. Chem. 285*, 36656–36665.
6. Hunte, C., Screpanti, E., Venturi, M., Rimon, A., Padan, E., and Michel, H. (2005) Structure of a Na^+/H^+ antiporter and insights into mechanism of action and regulation by pH. *Nature 435*, 1197–1202.
7. Murtazina, R., Booth, B. J., Bullis, B. L., Singh, D. N., and Fliegel, L. (2001) Functional analysis of polar amino-acid residues in membrane associated regions of the NHE1 isoform of the mammalian Na^+/H^+ exchanger. *Eur. J. Biochem. 268*, 4674–4685.
8. Landau, M., Herz, K., Padan, E., and Ben-Tal, N. (2007) Model structure of the Na^+/H^+ exchanger 1 (NHE1): functional and clinical implications. *J. Biol. Chem. 282*, 37854–37863.
9. Schwieters, C. D., Kuszewski, J. J., Tjandra, N., and Clore, G. M. (2003) The Xplor-NIH NMR molecular structure determination package. *J. Magn. Reson. 160*, 65–73.
10. Wakabayashi, S., Pang, T., Su, X., and Shigekawa, M. (2000) Second mutations rescue point mutant of the Na^+/H^+ exchanger NHE1 showing defective surface expression. *FEBS Lett. 487*, 257–261.
11. Hisamitsu, T., Ben Ammar, Y., Nakamura, T. Y., and Wakabayashi, S. (2006) Dimerization is crucial for the function of the Na^+/H^+ exchanger NHE1. *Biochemistry 45*, 13346–13355.
12. Ndayizeye, M., Touret, N., and Fliegel, L. (2009) Proline 146 is critical to the structure, function and targeting of sod2, the Na^+/H^+ exchanger of *Schizosaccharomyces pombe*. *Biochim. Biophys. Acta, Biomembr. 1788*, 983–992.

13. Padan, E. (2008) The enlightening encounter between structure and function in the NhaA Na^+/H^+ antiporter. *Trends Biochem. Sci. 33*, 435–443.

14. Dibrov, P., and Fliegel, L. (1998) Comparative molecular analysis of Na^+/H^+ exchangers: a unified model for Na^+/H^+ antiport? *FEBS Lett. 424*, 1–5.

15. Nygaard, E. B., Lagerstedt, J. O., Bjerre, G., Shi, B., Budamagunta, M., Poulsen, K. A., Meinild, S., Rigor, R. R., Voss, J. C., Cala, P. M., and Pedersen, S. F. (2011) Structural modeling and electron paramagnetic resonance spectroscopy of the human Na^+/H^+ exchanger isoform 1, NHE1. *J. Biol. Chem. 286*, 634–648.

16. Slepkov, E., Ding, J., Han, J., and Fliegel, L. (2007) Mutational analysis of potential pore-lining amino acids in TM IV of the Na^+/H^+ exchanger. *Biochim. Biophys. Acta, Biomembr. 1768*, 2882–2889.

17. Olkhova, E., Padan, E., and Michel, H. (2007) The influence of protonation states on the dynamics of the NhaA antiporter from *Escherichia coli*. *Biophys. J. 92*, 3784–3791.

18. Appel, M., Hizlan, D., Vinothkumar, K. R., Ziegler, C., and Kühlbrandt, W. (2009) Conformations of NhaA, the Na^+/H^+ exchanger from *Escherichia coli*, in the pH-activated and ion-translocating states. *J. Mol. Biol. 386*, 351–365.

Chapter 8

Structural and functional analysis of transmembrane segment IV of the salt tolerance protein sod2

A version of this chapter has been submitted for publication as:

- Ullah, A., Kemp, G., Lee, B. L., Alves, C., Young, H., Sykes, B. D., and Fliegel, L. Structural and functional analysis of transmembrane segment IV of the salt tolerance protein sod2. *J. Biol. Chem.*, in press.

AU performed mutation and functional analysis of sod2, AU and CA performed cloning and expression of the peptide, GK performed expression and purification of the peptide as well as the sod2 modelling, and BLL performed the NMR experiments. Each also helped write the manuscript, with HY, BDS, and LF editing.

Summary

Sod2 is the plasma membrane Na^+/H^+ exchanger of fission yeast *S. pombe*. It provides salt tolerance by removing excess intracellular sodium (or lithium) in exchange for protons. We examined the role of amino acid residues of transmembrane segment IV (TM IV) (residues F126–I152) in activity by using alanine scanning mutagenesis and examining salt tolerance in sod2-deficient *S. pombe*. Two amino acids were critical for function. Mutations T144A and V147A resulted in defective proteins that did not confer salt tolerance when re-introduced into *S. pombe*. Sod2 protein with other alanine mutations in TM IV, had little or no effects. T144D and T144K mutant proteins were inactive, however a T144S protein was functional and provided lithium, but not sodium, tolerance and transport. Analysis of sensitivity to trypsin indicated that the mutations caused a conformational change in the sod2 protein. We expressed and purified TM IV (amino acids 125–154). NMR analysis

yielded a model with two helical regions (amino acids 128–142 and 147–154) separated by unwound region (amino acids 143–146). Molecular modelling of sod2 suggested TM IV has a structure similar to that deduced by NMR analysis and an overall structure similar to that of *E. coli* NhaA. TM IV of sod2 has similarities to TM V of the *Zygosaccharomyces rouxii* Na^+/H^+ exchanger and TM VI of isoform 1 of mammalian Na^+/H^+ exchanger. TM IV of sod2 is critical to transport and may be involved in cation binding or conformational changes of the protein.

Introduction

Under normal physiological conditions, plants, yeast and mammalian cells have relatively low Na^+ concentrations in their cytosol. Since the external Na^+ is much higher than internal Na^+, this leads to an accumulation of intracellular Na^+. Organisms respond to this salt stress in several ways. Plants and yeast deal with these excess "toxic" levels of intracellular Na^+ primarily by either extruding it, or by sequestering it into vacuoles, thereby reducing the cytosolic concentration. This process is mediated by transporters and other regulatory proteins. In the fission yeast *Schizosaccharomyces pombe*, the Na^+/H^+ antiporter (sod2) is responsible for most of the salt removal from the cytosol (*1*). This protein functions by using the external proton gradient to pump out internal sodium ions. Disruption of this gene results in a reduced extrusion of cytoplasmic Na^+ and a decreased tolerance of external Na^+ (*1*). Sod2 removes both Na^+ and Li^+ from the cytosol using the proton gradient created by the plasma membrane ATPase (*1*, *2*). We have previously (*3*, *4*) used *S. pombe* with a knockout of the sod2 gene to study the effects of mutation of amino acids in this protein. Because of the limited number of other salt tolerance mechanisms in this species, removal of this gene results in a severe salt tolerance phenotype (*1*, *3*, *4*). This makes *S. pombe* a very useful organism for the study of salt tolerance proteins.

Sod2 belongs to the class of Na^+/H^+ exchanger membrane proteins that exchange Na^+ for H^+ across lipid bilayers. The eukaryotic and prokaryotic genes that encode the members of this monovalent cation/proton antiporter superfamily have been reviewed (*5*). Briefly, the superfamily includes three families, the cation/proton antiporter 1 family, cation proton/antiporter 2 family and the sodium-transporting carboxylic acid decarboxylase family, each of which has unique bacterial ancestors. The cation/proton antiporter 1 family includes many well studied Na^+/H^+ exchangers including from fungi, plants and mammals, and includes the human

NHE1–NHE9 isoforms. The cation/proton antiporter 2 family includes *S. pombe* sod2 and shares its origins with prokaryotic NhaA, the *E. coli* antiporter, for which a crystal structure has been deduced (*6*). This family also includes two relatively recently characterized forms of human Na^+/H^+ exchangers, HsNHA1 and HsNHA2, that may be involved in hypertension (*5*, *7*, *8*). The sodium-transporting carboxylic acid decarboxylase family is a smaller family that mediates transmembrane export of 1–2 Na^+ in exchange for an extracellular H^+ (*5*), and contains the mammalian sperm-specific Na^+/H^+ exchangers.

The mechanism of transport of Na^+/H^+ exchangers is of great interest both because of the potential to improve salt tolerance in plants and make salt resistant phenotypes, but also as a fundamental scientific problem. Significant progress has been made in the understanding of bacterial transport by NhaA (*6*). However eukaryotic transporters are not as well understood, and have a different exchange stoichiometry, and are activated by different physiological conditions. NHE1 is the most well characterized mammalian Na^+/H^+ exchanger and we have determined the structure and critical residues of several membrane associated fragments of NHE1 (*9–15*). One of the critical TM segments is TM IV, which has been compared to the important TM IV of *E. coli* NhaA (*9*, *16*). We have earlier examined several key residues of sod2 in different transmembrane segments of the protein (*3*, *4*, *17*, *18*). In this study we examine the structure and function of a transmembrane segment of this yeast salt tolerance protein. Our results demonstrate that TM IV of sod2 is critical to sod2 function with amino acids 144–147 comprising part of a region critical for transport. This study is the first structural and functional characterization of an entire transmembrane segment of a yeast salt tolerance membrane protein and demonstrates that this region is critical for cation selectivity and salt tolerance.

Experimental procedures

Materials

Restriction enzymes were obtained from New England Biolabs, Inc. (Mississauga ON, Canada). PWO DNA polymerase was obtained from Roche Applied Science (Roche Molecular Biochemicals, Mannheim, Germany).

Strains and media

S. pombe bearing the sod2 gene disruption (sod2::ura4) was used for all transformations and as a control where indicated (*3*). It was maintained on low sodium minimal KMA medium or yeast extract adenine (YEA) using methods described earlier (*1*, *3*). KMA medium was used where indicated and contains (per 1 L): potassium hydrogen phthalate, 3 g; K_2HPO_4, 3 g; yeast nitrogen base without amino acids, 7 g; glucose, 20 g; and adenine, 200 mg. Leucine at 200 mg/L was added to maintain the sod2::ura4 leu1-32 strain where indicated and all media was buffered using 50 mM MES/Citrate and adjusted to pH 5.0 with KOH. Wherever indicted NaCl or LiCl was added to the media. For growth curves in liquid media 5×10^6 cells from an overnight exponentially growing culture were inoculated into 2.5 mL of fresh liquid media. *S. pombe* containing the pREP-41sod2GFP plasmid (and mutant derivatives) were routinely grown in medium in the absence of thiamine. Cultures were grown at 30 °C with constant agitation using a rotary shaker. The A_{600} was determined at the various times indicated. Growth curves were determined a minimum of three times and results are mean ± S.E. The plasmid pREP-41sod2GFP was used for sod2 expression and has been described earlier (*19*). pREP-41sod2GFP contains the entire sod2 gene plus a C-terminal GFP tag separated by a nine amino acid Gly-Ala spacer. The GFP has the S65T mutation and an NdeI site was removed by silent mutation to assist in cloning.

Growth on plates was supplemented with NaCl or LiCl at the indicated concentrations in KMA medium with leucine agar. The plasmid pREP-41sod2GFP without any mutations (*19*), was used as a control.

Sod2 TM IV (see below) was expressed in XL1-Blue cells as a maltose binding protein fusion using a modified pMAL-c2x containing a tobacco etch virus (TEV) protease cleavage site between maltose binding protein and the peptide of interest. Expression was induced with IPTG in either LB (for unlabelled peptide) or M9 (for labelled samples) media. Expression conditions were: LB, 0.6 mM IPTG, 37 °C, 24 h; and M9, 1 mM IPTG, 22 °C, 48 h. LB media contains: tryptone, 1% w/v; yeast extract, 0.5% w/v; NaCl, 1% w/v. M9 media contains: $(^{15}NH_4)_2SO_4$, 7.5 mM; glucose, 28 mM; thiamine, 30 µM; [Na_2HPO_4, 47 mM; KH_2PO_4, 22 mM; NaCl, 8.5 mM]; [$MnSO_4 \cdot 1H_2O$, 30 µM; $FeSO_4 \cdot 7H_2O$, 3.3 µM; $MgSO_4 \cdot 7H_2O$, 203 µM; $CaCl_2 \cdot 2H_2O$, 3.4 µM]; [K_2HPO_4, 60 mM; KH_2PO_4, 36 mM; pH adjusted to 7.5 with KOH]; where the individual components or mixtures contained within the square brackets were autoclaved separately and combined afterwards.

Site-directed mutagenesis

Mutations to sod2 were made to the pREP-41sod2GFP plasmid directly. The mutations created or removed a restriction enzyme site as described earlier (*20*). Table 8-S1 summarizes the mutations made to the sod2 gene. DNA sequencing was used to confirm the accuracy of the mutations and fidelity of DNA amplification.

Western blotting of sod2

Western blot analysis was used to compare levels of sod2 expression (*20*). Cell lysates were made from 50 mL cultures of yeast transformed with wild type and mutant pREP-41sod2GFP. Yeast cells grown in KMA medium to an OD_{600} of 2 at 30 °C. Cells were pelleted ($3500 \times g$, 10 min) and washed with double distilled water and resuspended in lysis buffer (50 mM Tris-HCl, pH 8.0, 5 mM EDTA, protease inhibitor cocktail (*21*), and 1 mM dithiothreitol). Cells were then lysed using a Bullet Blender® using 0.5 mm zirconium oxide beads at a speed of 10 for 40 minutes. In some cases they were passed through an Emulsiflex homogenizer at a pressure of 25000 psi. Unbroken cells were pelleted by centrifugation at $3500 \times g$ for 5 min, and the supernatant was centrifuged at $14000 \times g$ for 10 min. Enriched membranes of the supernatant were then pelleted at $100000 \times g$ for 1 h, and resuspended in a small volume of the same buffer. Equal amounts of up to 25 µg of each sample were resolved on a 10% SDS/polyacrylamide gel. Nitrocellulose transfers were immunostained using a primary antibody of anti-GFP polyclonal antibody (A generous gift of Dr. Luc Berthiaume, Dept. of Cell Biology, University of Alberta). The secondary antibody was IRDye 680-conjugated goat anti-rabbit polyclonal antibody (Bio/Can, Mississauga, ON, Canada). The Odyssey scanning system was used for Western detection (LI-COR Biosciences, USA). Immediately after transfer and prior to immunostaining, nitrocellulose transfers were stained with Ponceau S to ensure equivalent loading and transfer of samples (*22*).

Trypsin treatment of microsomal membranes

Yeast cell membranes were prepared as described above and were made to a concentration of 2 mg/mL in 1 mM EDTA, adjusted to pH 7.4 with Tris-HCl. Trypsin (phenylalanyl chloromethyl ketone-trypsin, Sigma, St. Louis, MO) was added to give a trypsin:protein ratio (1:200) and the samples were incubated at 30 °C, for the times indicated. The reaction was terminated by the addition of SDS-PAGE sample buffer and samples were resolved on 12% SDS-polyacrylamide gels. Western

blotting against the sod2 GFP tag was performed to examine the degree of protein fragmentation (*4*).

Microscopy and indirect immunofluorescence

Confocal imaging of *S. pombe* containing GFP tagged sod2 was performed on an Olympus IX81 microscope equipped with a Nipkow spinning-disk optimized by Quorum Technologies (Guelph, ON, Canada). Images were acquired with the 60× objective on a Hamamatsu EM-CCD camera (Hamamatsu, Japan) using the software Volocity (Improvision Inc., Lexington, MA). Yeast cells were either fixed in 4% formaldehyde prior to imaging or for live cell imaging, confocal microscopy was used examining the GFP tag on sod2 essentially as described earlier (*19*).

Indirect immunofluoresence was performed using an antibody cross reactive against the plasma membrane H^+-ATPase of *S. pombe* and originally made against Neurospora H^+-ATPAse (a generous gift of Dr. C. Slayman, Yale School of Medicine). Cells were prepared for immunofluorescence by treatment with zymolase essentially as described earlier (*23*). Labelling was performed with rabbit anti-H^+-ATPase antibody at a dilution of 1:1000. Visualization used Cy3 conjugated donkey anti rabbit antibody (Jackson Immunochemicals, West Grove PA, USA) at a 1:250 dilution.

Atomic absorption spectrophotometry

To determine the ability of wild type and mutant sod2 proteins to remove intracellular Na^+ or Li^+, various strains were grown in KMA medium to an OD_{600} of approximately 0.4. Cells were harvested by centrifugation and washed and were then incubated in KMA medium supplement with either 100 mM NaCl or 10 mM LiCl for 1 h to load the cells with the appropriate cation. Cells were then harvested and were washed two times with 20 mM MES, pH 7.0 and resuspended in 10 mL buffer containing 20 mM MES pH 5.5, 0.1 mM $MgCl_2$ and 2% glucose at 30 °C. Samples were taken at various intervals up to 2 h and Na^+ or Li^+ content were determined by atomic absorption spectrophotometry as described earlier (*4*). Results from at least three independent experiments are shown.

Sod2 TM IV peptide purification

Amino acids 125–154 (sequence LFPQINFLGSLLIAGCITSTDPVLSALIVG) of sod2 were expressed as a fusion protein with maltose binding protein. The

design was such that we also introduced 3 additional N- and C-terminal lysines to the peptide. This was done to aid in the solubility of the peptide, as described earlier (*11*, *15*). The primers SodMBPf (5′-CATGGGATCCAAAAAAAAATTGTTTC-CACAAATTAACTTTTTAGG-3′) and SodMBPr (5′-CCGGGAATTCTCATTT-CTTTTTTCCTACAATCAATGCTGATAG-3′) were used to amplify the DNA of sod2 while adding the terminal lysines. They were designed to allow for in frame expression with MBP in a modified pMal-c2X plasmid (*24*) which also has a tobacco etch virus (TEV) protease site upstream of the insert to allow for cleavage from the MBP. PCR was performed using the pREP-41sod2GFP plasmid as a template and the PCR product contained the TM IV sequence with the modified termini flanked by a 5′ BamHI restriction endonuclease site and a 3′ EcoRI site. After cloning into the modified pMal-c2X vector mentioned above, the plasmid construction was confirmed by DNA sequencing.

The *E. coli* strain XL1 blue was used for expression. Expression and purification were similar to the procedures used by Douglas et al. (*24*). After induction cells were pelleted by centrifugation at $4000 \times g$ and were stored at -20 °C. For purification cell pellets were suspended in 100 mL of purification buffer (PB) containing (per 1 L): 10 mM sodium phosphate buffer, pH 7; 60 mM NaCl; 0.5 mM EDTA; 20% v/v glycerol; 0.02% NaN_3 plus added HALT protease inhibitor cocktail (EDTA-free) (Thermo Scientific, Rockford, IL, USA). The cells were lysed using either ultrasonication (Branson Sonifier, Emerson Industrial Automation, Danbury, CT, USA) or high-pressure homogenization (Emulsiflex-C3, Avestin Inc., Ottawa, Canada). They were then clarified by centrifugation at $50000 \times g$ for 30 min at 4 °C. The supernatant containing MBP-sod2 fusion protein was loaded onto an amylose-affinity column (NEB, Mississauga, ON, Canada) and allowed to incubate with agitation for 1–2 h at 4 °C. The resin was washed with 3 column volumes of cold PB and the fusion protein eluted in cold elution buffer (PB + 60 mM maltose). For efficient cleavage of the maltose binding protein tag, the eluent was concentrated to > 5 mg/mL and 1 mM DTT was added. The sod2 fragment was cleaved free of the MBP using TEV protease at 10 U/mg of fusion protein. TEV cleavage was at 16 °C for 48–72 hours. The protein was then precipitated by the addition of trichloroacetic acid (1.5 g per 100 mg fusion protein) and pelleted by centrifugation. After brief washes with water to remove residual TCA the pellet was subjected to liquid-liquid extraction with $CHCl_3$:2-propanol:water (ratio 5:5:1). First the organic solvents were mixed and added to the pellet. Gentle scrapping was used to break the pellet up into small pieces before homogenization with a glass Dounce homogenizer.

After most of the pellet was pulverized the appropriate amount of water was added to the homogenizer and homogenization continued. When the remaining insoluble material appeared quite "fibrous" the mixture was added into a separatory funnel and shaken intermittently throughout the day then left to separate overnight. In the morning the organic (bottom) layer was removed and put in a clean separatory funnel. One volume of fresh water was added and the extraction repeated. The resulting organic layer was then used directly for NMR studies. Most complete extraction of the hydrophobic peptide was achieved at 1 vol = 1 mL, per 30 mg fusion protein (i.e. 5 mL $CHCl_3$, 5 mL 2-propanol, and 1 mL water per 30 mg fusion protein. For studies of unlabelled peptide, deuterated solvents (Cambridge Isotope Laboratories, Andover, MA) were used and the extraction was carried out at higher protein concentrations (i.e. 1 vol per 100 mg fusion protein). For ^{15}N labelled samples $CDCl_3$ and undeuterated 2-propanol were used. The identity of the purified peptide was confirmed by MALDI-TOF mass spectrometry. The purity of the sod2 TM IV peptide was estimated at over 95%.

NMR spectroscopy

Peptide samples obtained from liquid-liquid extraction were used for high-resolution NMR spectroscopy. After testing with various membrane mimetics, examination of 1D ^1H NMR and 2D ^{15}N HSQC NMR spectra indicated that the best solvent for sod2 TM IV was $CDCl_3$/IPA-d_8. By drying the organic extract under a gentle stream of nitrogen gas an adequately concentrated sample for structure determination was obtained. $CDCl_3$ in the extract was used as a lock solvent and spectra were referenced to tetramethylsilane added to the solvent.

All NMR spectra were acquired at 500 MHz and 30 °C. 2D ^{15}N HSQC (*25*), 3D ^{15}N NOESY-HSQC (150 ms mixing time) (*26*), TOCSY-HSQC (50 ms mixing time) (*26*), and HNHA (*27*, *28*) spectra were collected with VnmrJ (Varian Inc.) and processed in NMRPipe (*29*). Resonance assignment and analysis was performed in NMRViewJ (*30*). Xplor-NIH (*31*) was used to model the secondary structure of the peptide.

Homology modelling

A homology model of sod2 was created with the program Modeller (*32*) using the crystal structure of *Escherichia coli* NhaA (PDB entry: 1ZCD). *Arabidopsis thaliana* SOS1 was used as a mediator to align sod2 and NhaA using Clustal

Omega (*33*) on the EMBL-EBI server (*34*). The alignment was refined by using the TMHMM2 secondary structure prediction algorithm (*35*) to predict the location of α-helical transmembrane segments and the JPred3 algorithm (*36*) to further support the regions of predicted α-helical secondary structure in sod2. These data, along with the known position of transmembrane helices in NhaA, were used to adjust the alignment to best reflect the most likely position of transmembrane segments in sod2. Short helical restraints ($<$ 10 residues) were given to Modeller, in regions where longer helices was predicted. The validity of the model was analyzed using a protein validation software suite (*37*) and the ConSurf method (*38*, *39*) on the online server (*40*).

Results

We examined amino acids thought to be important in activity of a transmembrane segment of the yeast *S. pombe* salt tolerance protein sod2. While the transmembrane segment assignments are not certain, amino acids 126–151 were assigned as TM IV based on previously published (*41*) model of the protein (Figure 8-1, A) based on hydrophobicity analysis. This segment (FPQINFLGSLLIAGCITST-DPVLSAL) is mainly comprised of very hydrophobic residues, with a few polar residues interspersed (Figure 8-1, B). The borders of the membrane lipid interface are not known though for purposes of mutational analysis, 26 amino acids were chosen which is larger than required for a typical α-helical transmembrane segment to cross a lipid bilayer.

We compared the amino acid sequence of sod2 with several other related Na^+/H^+ exchanger proteins using the program CLUSTAL Omega (*33*), a multiple sequence alignment tool from EMBL-EBI (*34*). Sod2 did not align well directly with the sequences of human NHE1 or *E. coli* NhaA although isolated regions did show some similarity (not shown). When sod2 was compared with a more closely associated salt tolerance protein SOS1 (*42*) (Figure 8-1, C), there were significant areas of identity and similarity especially in the sequence proposed to be TM IV. In turn, the TM IV region of SOS1 aligned well with TM VI of NHE1 (Figure 8-1, D) permitting a three-way alignment of the TM IV regions of sod2, SOS1 and NHE1. We have recently (*15*) shown that TM VI of NHE1, rather than TM IV, is structurally related to TM IV of NhaA which may account for this finding (see discussion).

Since sod2 is the major salt exporter of *S. pombe* (*19*), initial experiments measured the ability of sod2 TM IV mutants, to rescue salt tolerance in the salt

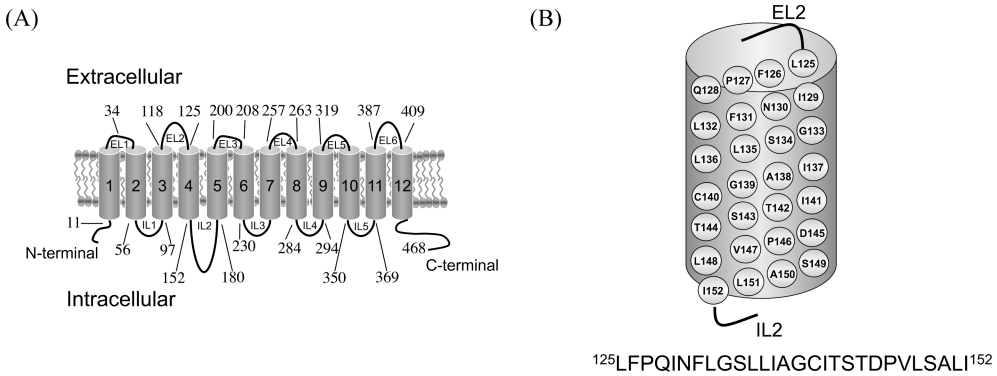

(C)

```
sod2 --------MGWRQLDI---------------DKVHLALIVAGGFITFFCYFSEVFRKKL 36
SOS1 MTTVIDATMAYRFLEEATDSSSSSSSSKLESSPVDAVLFVGMS------LVLGIASRHL 53
NhaA -----------MKHLH---------------RFFSSDASGGIILIIAAILAMIMAN--- 30

sod2 LVGEAVLGSIT----GLIFGPHAAKLV--------DPFSWGDHGDYLTVEICRIVLDVR 83
SOS1 LRGTRVPYTVALLVIGIALGSLEYGAKHNLGKIGHGIRIWNEIDPELL----------- 101
NhaA -SGATSGWYHD----FLETPVQLRVGS--------LE-----INKNMLLWINDALMAVF 71

sod2 VFASAIELPGAYFQHNFR----------SIIVM-----LLPVMAYGWLVTAGFAYALF 126
SOS1 ---LAVFLPALLFESSFSMEVHQIKRCLGQMVLLAVPGVLISTACLGSLVKVTFPY--- 154
NhaA FLLVGLEVKRELMQGSLA----------SLRQA-----AFPVIAAIGGMIVPALLYLA 114
                                                              *
          ----------TMIV----------
sod2 PQINFLGSLLIAGCITSTDPVLSALIVGEGPLAKKTPERI--RSLLIAESGCNDGMAVP 183
SOS1 -EWDWKTSLLLGGLLSATDPVAVVALLKELGAS----KKL--STIIEGESLMNDGTAIV 206
NhaA FNYADPITREGWAIPAATDIAFALGVLALLGSR----VPLALKIFLMALAIIDDLGAII 169
      :     :    .  .:** .::  ::.

sod2 FFYFAIKLLTVKPSRNAGRDWVLLV------VLYECAFGIFFGCVIGYLLSFILKHAQ- 235
SOS1 VFQLFLKM-----AMGQNSDWSSIIKFLLKVALGAVGIGLAFGIASVIWLKFIFNDTVI 260
NhaA IIALFYTN-DLSMASLGVAAVAIAV------LAVLNLCGARRTGVYILVGVVLWTAVL- 220

sod2 KYRLIDAISYYSLPLAIPLLCSGIGTIIGVDDLLM--SFFAGILFNWNDLFSKNIS-AC 291
SOS1 EITLTIAVSYFAYYTAQE--WAGASGVLTVMTLGMFYAAFARTAFKGDS--QKSLHHFW 315
NhaA KS-----------GVHATLAGVIVGFFIPLKE------KHGRS---------PAKR-LE 252

sod2 SVPAFIDQTFSLLFFTYYGTIIPWNNFNW--SVEGLPVWRLIVFSILTLVCRRLPVVFS 348
SOS1 EMVAYIANT---LIFILSGVVIAEGILDSDKIAYQGNSWRFLFLLYVYIQLSRVVVVGV 371
NhaA HVLHPWVAYLILPLFAFANAGVSLQGVTL--DGLTSILPLGIIAGLLIGKPLGISLFCW 309

sod2 VKPLV-----PDIKTWKEALFVGHFGPIGVCAVYMAFLAKLLLSPDEIEKSIYESTTVF 402
SOS1 LYPLLCRFGYGLDWKESIILVWSGLRGAVALALSLSVKQSSGNSHISK---ETGTLFLF 427
NhaA LALRLKLAHLPEGTTYQQIMVVGILCGIGFTMSIFIASLAFGSV----------DPEL 357

sod2 STLNEIIWPIISFVILSSIIVHGFSIH 429
SOS1 FT-------GGIVFLTLIVNGSTTQFV 447
NhaA INWAKLGILVGSISSAVIGYSWLRVRL 388
```

(D)

```
                                  #
sod2TMIV    125 LFPQINFLGSLLIAGCITSTDPVLSALIVGEGPL 158
NHE1TMVI    218 QINNIGLLDNLLFGSIISAVDPVAVLAVFEEIHI 251
                    *.:*..**:.. *::.***    :. *
                                  #
sod2TMIV    125 LFPQINFLGSLLIAGCITSTDPVLSALIVGEGPL 158
Sod2-22pTMV 124 LVPGLNFPASLLMGACITATDPVLAQSVVS-GTF 156
                *.* :** .***:..***:*****:  :*. *.:
                                  #
```

Figure 8-1. Models of sod2. (Continued on page 166.)

Figure 8-1. (Continued from page 165.) (A) Topological model of sod2 based on hydrophobicity analysis (*41*). EL, extracellular loop; IL, intracellular loop. (B) Schematic diagram of amino acids present in TM IV of sod2. (C) Alignment of sod2 with NhaA using SOS1 as an intermediate as described in the "Materials and Methods." Sod2 TM IV and aligned residues in NhaA are labelled with Gonnet PAM 250 amino acid conservation scores between sod2 and NhaA TM IV (*, identical; :, strongly similar; ., weakly similar). The transmembrane segments, from the crystal structure or the homology model of NhaA and sod2 respectively, are highlighted. (D) Sequence alignments of sod2 TM IV with putative analogous transmembrane segment from human NHE1 (TM VI) and Sod2-22p (TM V), coloured and labelled as in (C). The critical threonine residues of sod2, sod2-22p and NhaA are denoted by #.

sensitive sod2::ura4 deletion strain. As both LiCl and NaCl are transported by sod2 (*43*) we examined the ability of mutant proteins to rescue growth in LiCl or NaCl containing medium. Aside from NaCl challenge, LiCl was used for assays in liquid and solid media. LiCl is toxic at lower concentrations than NaCl, avoiding osmotic challenge that might occur with use of high concentrations of NaCl. Figures 8-2 and 8-3 (also Figures 8-S1 and 8-S2) illustrate the effect of mutations of TM IV on the ability to restore salt tolerance in liquid media (summarized in Table 8-S2). Figure 8-2 (and Figure 8-S1) demonstrates that the sod2::ura4 strain is intolerant to LiCl concentrations of 5 and 10 mM. In contrast, *S. pombe* with wild type sod2 protein grows well in LiCl concentration up to 10 mM, with only a slight reduction in growth compared to growth in 0 mM LiCl. Figures 8-4 and 8-5 illustrate complementary experiments in solid media. *S. pombe* containing wild type sod2 was able to grow on solid media containing up to 10 mM LiCl whereas the sod2::ura4 knockout showed reduced growth in 5 mM LiCl and almost no growth in 10 mM LiCl.

A variety of effects were obtained with mutation of TM IV and the mutants were divided into groups according to their characteristics (Table 8-S2). Results are shown in Figures 8-2 through 8-5 and supplementary Figures 8-S1 and 8-S2. Group I mutants showed no effect of the mutation in either liquid or solid media. This included F126A, P127A, Q128A, I129A, F131A, I137A, C140A, I141A, T142A, S143A, L148A and L151A. Group II mutants had very mild effects on growth in either liquid or solid media or both. For example, in some cases they showed good salt tolerance in liquid in the presence of 5 mM LiCl, but slightly reduced growth with 10 mM LiCl. This included N130A, L132A, G133A, S134A, L135A, L136A, G139A, S149A, L151S and I152A. Group III mutants had a very marked effect on

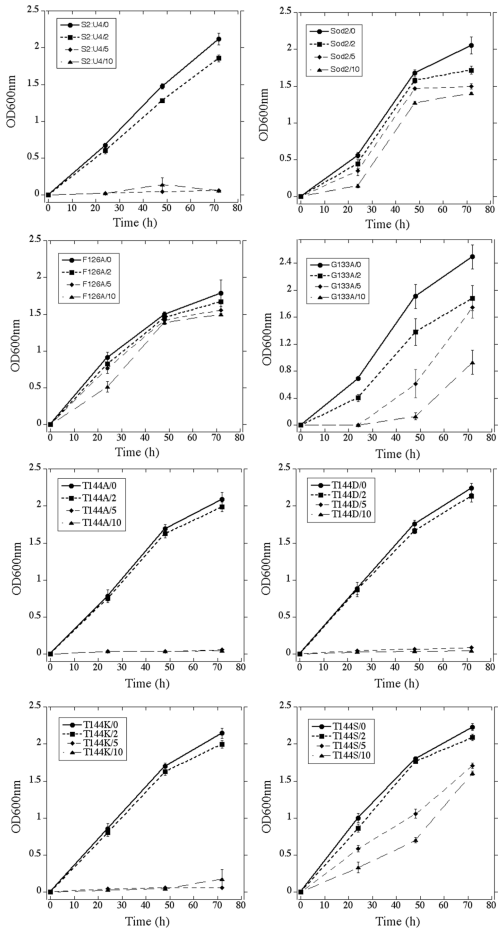

Figure 8-2. Growth of *S. pombe* containing either wild type or TM IV mutant sod2 proteins in liquid media with various concentrations of LiCl. Examples of growth of *S. pombe* containing no sod2 (sod2::ura4), wild type sod2, a mutated sod2 with an intermediate phenotype and a series of T144 mutants are shown. (The growth of all the mutants in LiCl are shown in Figure 8-S1 and summarized in Table 8-S2.) LiCl tolerance of strains was assessed by inoculating 2×10^6 cells into 2.5 mL of medium at 30 °C for up to 72 hours. Growth was assessed by measuring the absorbance of the cell suspensions at 600 nm at the indicated times. Results are the mean ± S.E. of at least three determinations. *S. pombe* were grown in the presence of 0, 2, 5 or 10 mM LiCl. S2:U4 refers to sod2::ura4 (*S. pombe* with the sod2 knockout described earlier (*3*)). Sod2 refers to sod2::ura4 containing the wild type sod2 protein (*19*). In other cases the indicated sod2 TM IV mutant was introduced into S2:U4 with the presence of 0, 2, 5 or 10 mM LiCl as indicated.

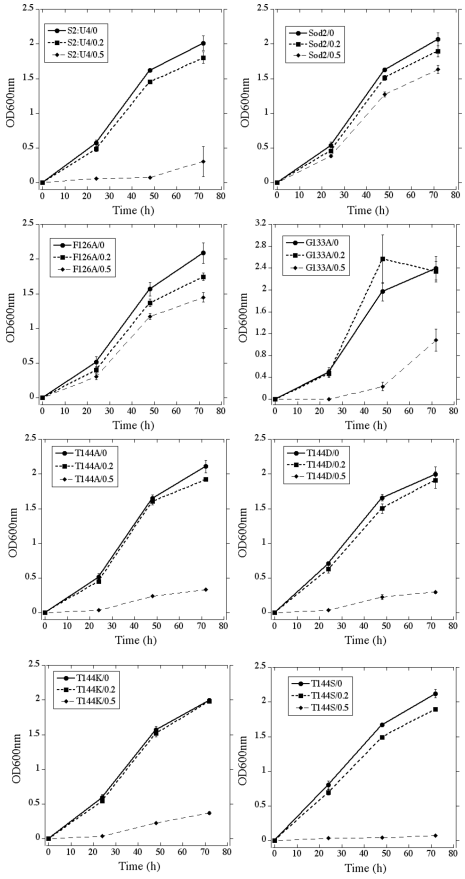

Figure 8-3. Growth of *S. pombe* containing either wild type or TM IV mutant sod2 proteins in liquid media with various concentrations of NaCl as described for Figure 8-2. Examples of growth of *S. pombe* containing no sod2 (sod2::ura4), wild type sod2, a mutated sod2 with an intermediate phenotype and a series of T144 mutants are shown. (All mutants growth in NaCl are shown in Figure 8-S2 and summarized in Table 8-S2.) NaCl was added at concentrations of 0, 0.2 or 0.5 M as indicated. Results are the mean $\pm$ S.E. of at least three determinations.

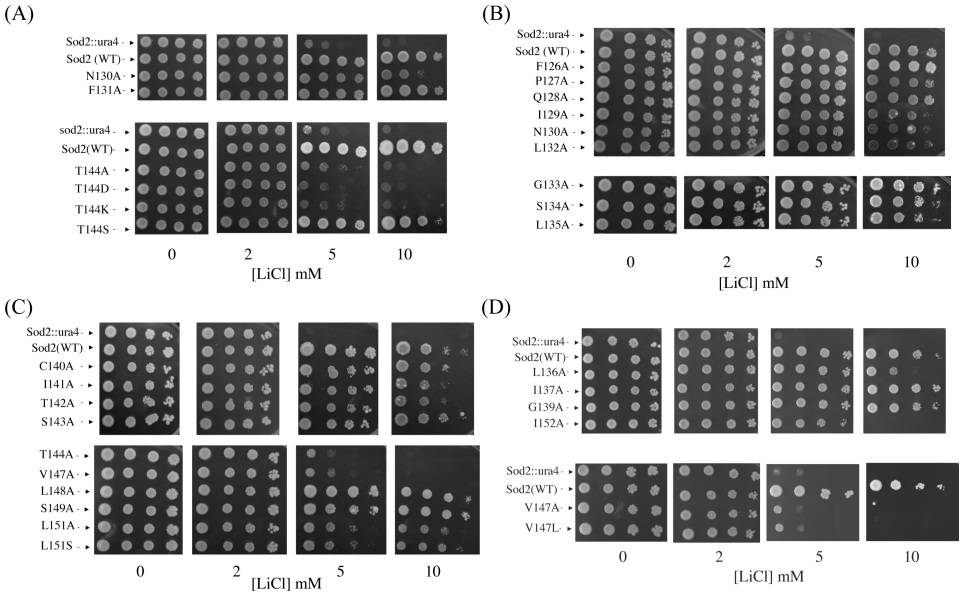

Figure 8-4. Growth of *S. pombe* containing wild type and TM IV mutant sod2 on solid media containing various concentrations of LiCl. Samples of stationary phase cultures of the various yeast strains were taken and were serially diluted 10-fold. These were spotted onto minimal media plates supplemented with LiCl at the concentration indicated. Plates were then incubated for 4–5 days at 30 °C. Sod2(WT) refers to *S. pombe* transformed with pREP-41sod2GFP without any mutations. sod2::ura4 is *S. pombe* with the sod2 knockout described earlier (*43*). Other designations are the sod2::ura4 yeast strain transformed with pREP-41sod2GFP with the indicated point mutation in sod2 (panels A–D). Results are typical of at least 3 experiments.

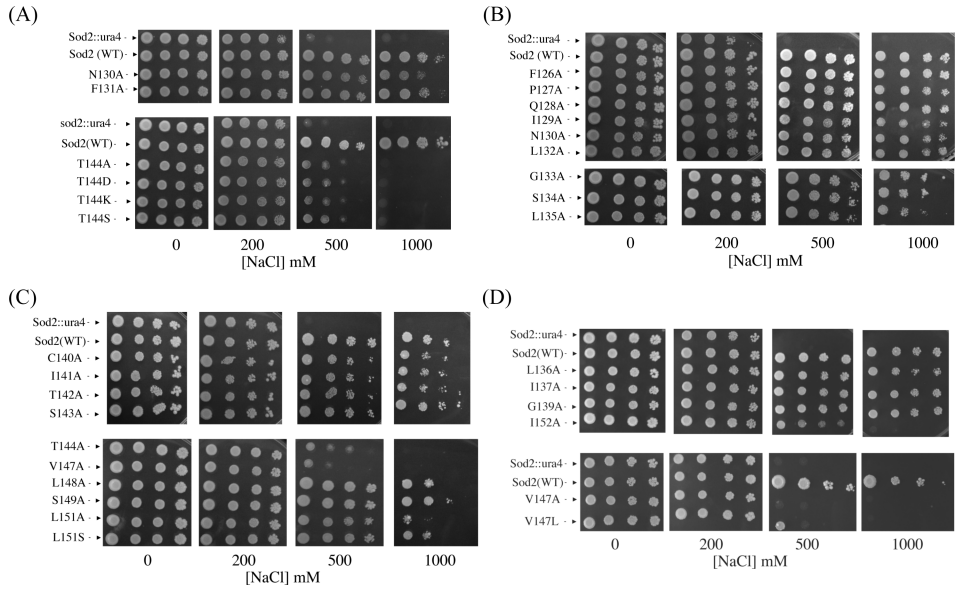

Figure 8-5. Growth of *S. pombe* containing wild type and TM IV mutant sod2 on solid media as described in Figure 8-4 except containing the indicated concentrations of NaCl. Results are typical of at least 3 experiments.

both NaCl and LiCl tolerance in both solid and liquid media. This included T144A, T144D, T144K, V147A and V147L. Group IV and V were categories consisting of one mutant. Group IV consisted of only T144S, which was inactive, or nearly so in NaCl containing media, but functional in LiCl containing media. This mutant was notable since mutation of the same amino acid T144, to either Ala, Asp or Lys created a nearly non-functional protein. Group V was I152A which had an intermediate phenotype, affected partially in both liquid and solid medium, and more so in liquid medium with LiCl.

Western blot analysis was used to determine if all the mutant proteins were expressed. Figure 8-6 demonstrates that the sod2-GFP fusion protein was present as a band of approximately 60 kDa. All mutant proteins were expressed. Ponceau S staining was used to confirm sample transfer after immunoblotting. In some cases there was evidence of immunoreactive degradation products. It was not clear whether this was occurring in vivo or in the process of preparing cell lysates. However, the occurrence of the degradation products was variable from cell lysate to lysate (not shown), possibly indicating that degradation products were produced during sample preparation.

To determine whether the mutant sod2 protein was properly folded we carried out limited digestion with trypsin. This method examines the proteolytic attack on accessible Arg and Lys, and has been used earlier to examine changes in the structure of sod2 (*4*) and of the mammalian Na^+/H^+ exchanger (*44*). We compared the digestion of wild type sod2 with that of the V147A, T144A and T144S mutants (Figure 8-7). We found that the T144A mutant sod2 protein was digested significantly more rapidly than the wild type with the T144S and the V147A showing intermediate patterns of digestion.

Because we found that mutation of T144 and V147 were detrimental to the ability of sod2 to restore growth in salt containing medium, we further examined the subcellular location of the mutant proteins in *S. pombe* by confocal microscopy (Figure 8-8). The H^+-ATPase was used as a plasma membrane marker (Figure 8-8, A). Wild type sod2-GFP had an irregular distribution, partially on the plasma membrane and partially intracellular, similar to what we have noted earlier (*4*, *19*). The H^+-ATPase was primarily located on the plasma membrane with occasional indications of intracellular labelling, possibly due to biosynthesis of the protein. Both T144A and V147A sod2 mutants were distributed in a similar manner as that of the wild type sod2. There was evidence of some co-localization on the plasma membrane, and though this was not complete there were no differences apparent between the

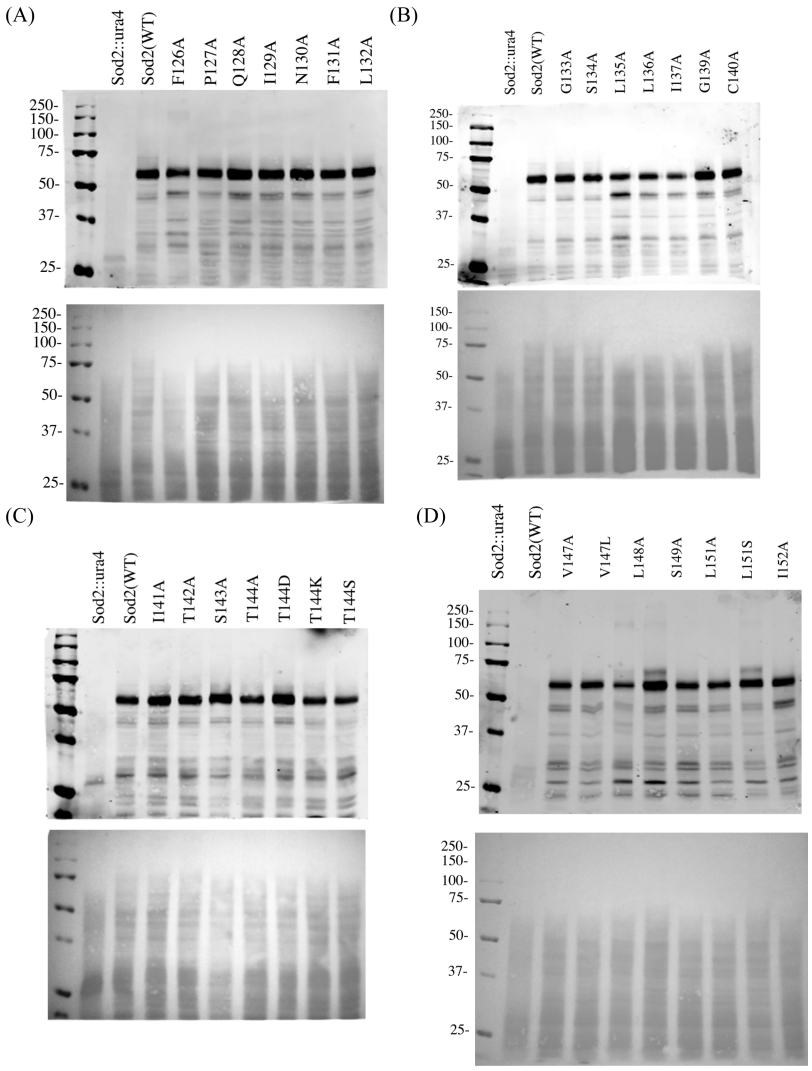

Figure 8-6. Western blot analysis of expression levels of sod2 wild type and mutant containing *S. pombe*. Cell extracts from *S. pombe* strains separated by SDS-PAGE and were blotted with anti-GFP antibody. Molecular weight markers are indicated. A–D, cell extracts of sod2::ura4: untransformed (sod2::ura4); transformed with wild type (WT) sod2 protein; or transformed with sod2 proteins with the mutation indicated. Cell extracts were made as described in the "Experimental procedures." Upper panel, western blot; lower panel, Ponceau S staining of blot prior to immunoreaction.

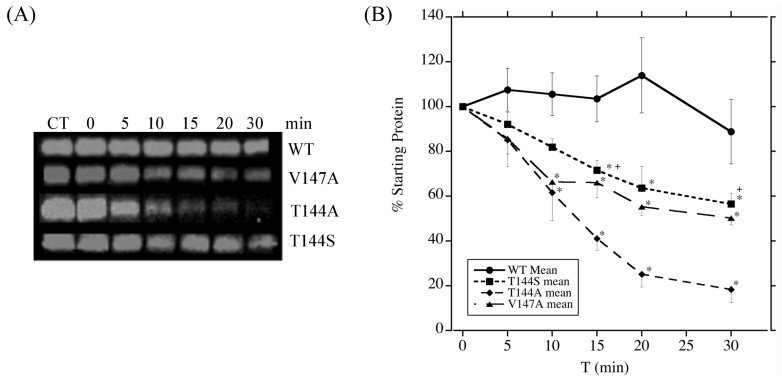

Figure 8-7. Analysis of susceptibility of mutant and wild type sod2 protein to trypsinolysis. Yeast cell membrane fractions were incubated with a 1:200 trypsin:protein ratio for 0–30 min at 30 °C as described in the "Experimental Procedures." Samples were then analyzed by SDS-PAGE and Western blotting using anti-GFP antibody. (A) Western blot of wild type (WT) and sod2 mutant proteins. (B) Summary of quantification of effects of trypsin on percentage of sod2 protein remaining over time. Results are mean ± S.E. of at least 4 experiments. * indicates significantly different from WT at $p < 0.05$. + indicates significantly different from T144A at $p < 0.05$.

wild type sod2 protein and the mutant proteins. We confirmed the observations on the localization of wild type and mutant sod2 using live cell imaging (Figure 8-8, B). All mutants and wild type sod2 had a predominantly plasma membrane localization. Similar to our earlier observations (*4*) the distribution throughout the membrane was not even, with occasional concentration at the apical tips of the membrane.

To gain further insight into the effects of the critical mutations on ion flux in *S. pombe*, we examined the expulsion of intracellular Na^+ and Li^+ as an indication of sod2 activity. It was previously demonstrated (*1*, *45*) that sod2 accounts for most of Na^+ and Li^+ expulsion in *S. pombe* and its deletion or inactivity, results in greatly reduced expulsion of these ions from the cytosol. We examined the decreasing content of these cations after a period of cation loading (*4*). The results are shown in Figure 8-9. After incubation in NaCl containing medium, NaCl content of *S. pombe* expressing wild type sod2 declined relatively rapidly. In contrast, the sod2 knockout and all of the mutants T144A, T144S and V147A, were all greatly impaired in their ability to reduce cellular Na^+ content (Figure 8-9, A). The mutants were also all impaired in their ability to extrude Li^+ (Figure 8-9, B), with the exception of the T144S mutant, which reduced cellular Li^+ content approximately as well as the wild type sod2 protein. The V147A mutant also had a slight tendency towards decreasing cellular Li^+ content.

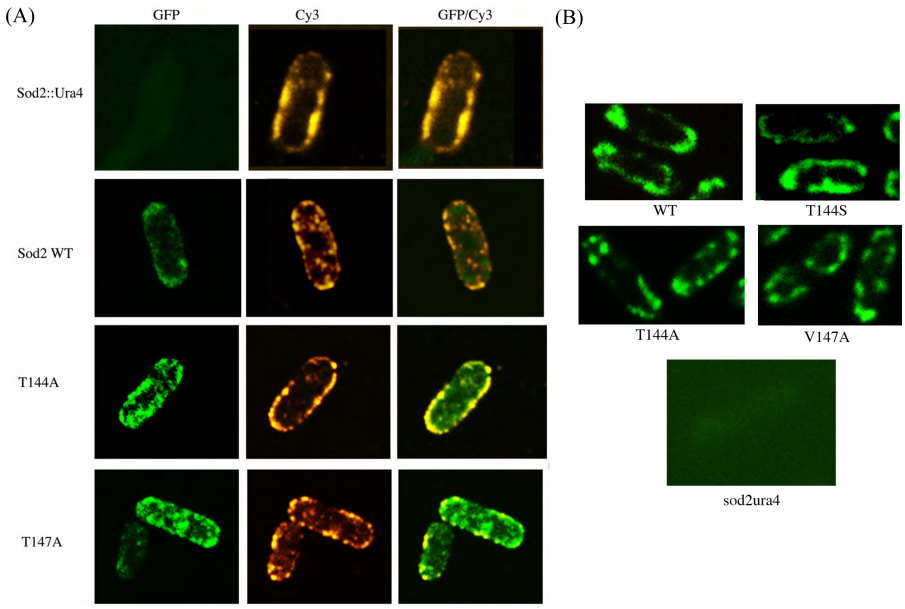

Figure 8-8. Confocal microscopy of *S. pombe* expressing wild type sod2-GFP and sod2-GFP with mutations in TM IV. (A) Exponentially growing cells were harvested treated with Zymolase and washed and mounted on coverslips before imaging. Rows indicate the yeast strain. sod2::ura4 indicates the *S. pombe* knockout strain without the sod2 protein. Sod2 refers to the wild type sod2 protein expressed in *S. pombe*. Rows T144A and T147A indicate sod2 protein with these point mutations. Left column illustrates GFP fluorescence. Centre column Cy3 (red) fluorescence (H^+-ATPase). Right column, illustrates both Cy3 and GFP fluorescence. (B) Exponentially grown cells were harvested and used directly for live cell imaging of GFP fluorescence.

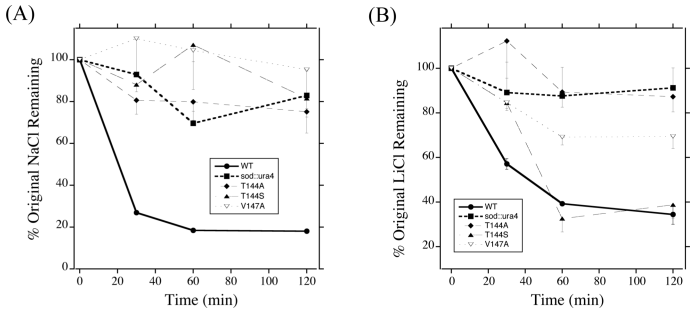

Figure 8-9. Loss of Na^+ or Li^+ content from *S. pombe* containing wild type or mutant sod2 proteins. Cells expressing various indicated sod2 proteins or the sod2::ura4 knockout strain, were incubated in high NaCl (A) or LiCl (B) containing medium for 1 h and resuspended in Na^+ or Li^+ free medium. The Na^+ or Li^+ content was determined by atomic absorption spectrophotometry as described in the "Experimental procedures." Results are the mean ± S.E. of at least 3 experiments. Where not shown S.E. were too small to be displayed.

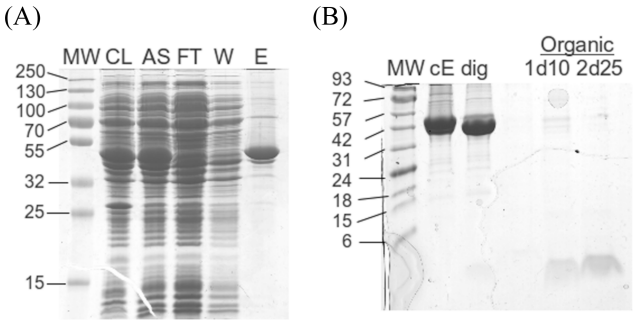

Figure 8-10. SDS-PAGE (12%) analysis of purification of MBP-sod2 fusion protein. (A) Sod2-TM IV fusion protein was produced and purified as described in the "Experimental procedures" and samples from the purification procedure are illustrated. CL, crude bacterial lysate; AS, clarified lysate supernatant after ultracentrifugation; FT, flow through, maltose affinity column unbound fraction; W, maltose affinity column wash fraction; E, maltose affinity column eluted fraction ($\sim$2 mg/mL protein). MW, molecular weight ladder (kDa). (B) Tris-tricine (16%) analysis of TEV cleavage of sod2 fusion protein followed by organic extraction. cE, 10$\times$ concentrated elution fraction; dig, concentrated elution fraction following 3 day cleavage with TEV; Organic, samples of the organic layer following extraction; 1d10, 10 µL of organic layer following one round of extraction; 2d25, 25 µL sample of organic layer following two rounds of extraction; MW, molecular weight ladder (kDa).

To gain molecular insights into how these functionally important residues may be arranged in the structure of sod2 we expressed and purified a peptide representing TM IV (KKKGS-LFPQINFLGSLLIAGCITSTDPVLSALIVG-KKK), containing residues 125–154 of sod2, for NMR experiments. Following purification of a maltose binding protein fusion protein and cleavage with TEV, an organic liquid extraction technique was used to isolate the hydrophobic TM IV peptide from any remaining aqueous contaminants (Figure 8-10). After two rounds of extraction the organic layer contained relatively pure peptide with only trace amounts of contaminants remaining and we proceeded directly with NMR experiments using the sample in organic solvent.

Initially, 1D ^{1}H and then 2D ^{15}N HSQC spectra were used to judge the quality of peptide samples for structure determination while varying the solvent/detergent, pH, and temperature. The peptide was poorly soluble in a $CHCl_3$/MeOH/H_2O mixture, which has been used successfully in previous work for a transmembrane segment of the mammalian Na^+/H^+ exchanger (*16*). It was also poorly soluble in trifluoroethanol/H_2O and although the peptide could be solubilized in dodecylphosphocholine, SDS, or DMSO, these samples only gave moderate quality 2D ^{15}N HSQC spectra (Figure 8-11, A). The peaks were broader and less well resolved than

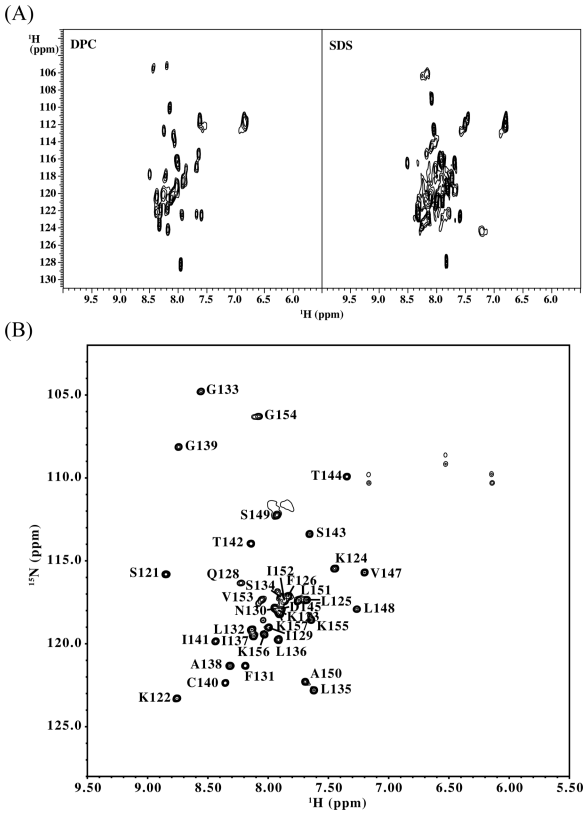

Figure 8-11. 2D ^{15}N HSQC spectra of sod2 TM IV peptide. (A) 2D ^{15}N HSQC spectra of sod2 TM IV peptide in detergent micelles. Samples in detergent micelles were prepared from peptide in organic solvent that was dried under $Ar_{2(g)}$ and reconstituted in 1% DPC or SDS, 10 mM imidazole, 0.25 mM DSS, 95% H_2O, 5% D_2O, pH 6.0. Spectra were acquired at 500 MHz and 30 °C. (B) 2D ^{15}N HSQC of sod2 TM IV in 50% $CDCl_3$/50% isopropanol with assignments indicated. The sample was taken directly from the organic extraction procedure and partially concentrated by slow evaporation under $N_{2(g)}$.

a sample in $CHCl_3$/IPA. The best spectra were obtained in the solvent mixture used for the organic extraction, $CHCl_3$/IPA, and this solvent mixture was used for further NMR analysis. The 1D spectrum showed good dispersion of the backbone amide peaks, however there was an additional broad intensity underneath the amide region which may have been peptide aggregates or impurities. Peaks were well resolved in a 2D ^{15}N HSQC spectrum suggesting that the solvent mixture would be suitable for further experiments (Figure 8-11, B). With the exception of proline residues and the N-terminal glycine, complete backbone resonances and partial side chain resonances assignments were obtained from the 3D NMR spectra. A labelled 2D HSQC spectrum is shown in Figure 8-11, B. A few additional peaks were present in the HSQC that could not be assigned that could result from impurities in the sample or minor conformations from cis-trans isomerization from one or both prolines in the TM IV peptide.

A comparison of the Hα chemical shifts with random coil chemical shifts (*46*) (Figure 8-S3) suggests that there are two alpha-helical regions: residues 128–142 form a longer helix on the N-terminal half of the peptide and residues 147–153 form a shorter helix on the C-terminal half. The residues between the helices, 143–146, have shifts close to random coil values, and are likely dynamic or extended in structure. The termini are also likely unstructured, with Hα shifts close to random coil. The chemical shift data is supported by the $^3J_{\mathrm{HNH}\alpha}$ coupling constants, as the helical regions have coupling constants around 4–6 Hz, consistent with helical structure, and with termini with coupling constants at around 7 Hz, indicating dynamic or unstructured residues. Critical residue T144 has a coupling constant of about 8 Hz, suggesting this region between the two helices is adopting an extended conformation. Values for some residues were not determined due to overlap of peaks in the HN region of the spectrum. Proton-proton distances from NOESY data also support the secondary structure prediction (Figure 8-S4). Hα–HN $(i, i+3)$ and $(i, i+4)$ contacts can be observed within the two helical regions. Further evidence of the extended region between the two helices are shown by the presence of exchange NOE peaks at 4.8 ppm to the residual water in the sample (Figure 8-S5), indicating interactions with water with this region.

A model representing the likely structure that sod2 TM IV could adopt was constructed with Xplor-NIH (*31*) using the $^3J_{\mathrm{HNH}\alpha}$ and the Hα chemical shift data (Figure 8-12). The model structure calculation begins with a simple extended polypeptide upon which the measured NMR restraints are added and energy minimization calculations are performed. This process was followed several times

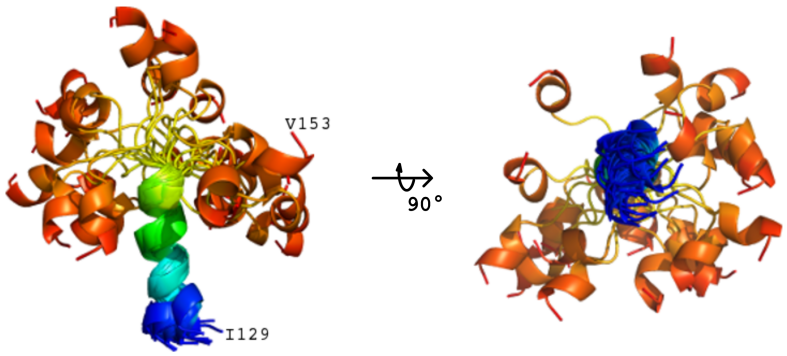

Figure 8-12. Ensemble of 25 models of sod2 TM IV created with Xplor-NIH. (Left) Side view of the ensemble with the structures superimposed along the N-terminal helix. The unstructured, flexible termini are not shown for clarity and the amino and carboxyl ends of the structures are labelled for reference. (Right) View of the same ensemble down the N-terminal helix, showing the flexibility in the position of the C-terminal helix relative to the N-terminal helix.

analyzing violations resulting from conflicts between the data and the model. Residues that had large errors in the calculations, or where the $^{3}J_{\mathrm{HNH}\alpha}$ and chemical shift data conflicted or were ambiguous, were not included in the modelling. The model displays disordered termini, a longer helical stretch of residues 129–142, an extended region from residues 143–147 and a shorter helix from residues 148–153. The model and NMR data has been deposited to the Protein Data Bank (ID: 2M7X) and the Biological Magnetic Resonance Data Bank (Entry: 19216).

To gain insight into the potential role of TM IV in the folded structure of sod2 and to provide evidence that the deduced structure of TM IV was correct, we constructed a homology based model of the entire sod2 protein. The model was based on the crystal structure of *E. coli* NhaA, the only Na^{+}/H^{+} exchanger with a high resolution crystal structure available. As noted above, sod2 did not align directly with NhaA, using the Clustal Omega alignment program (*33*). To overcome this problem we used SOS1 as an alignment template as it aligned with both NhaA and sod2 (Figure 8-1, C). These alignments were then used to construct a sequence comparison between NhaA and sod2. The initial model largely resembled the architecture of NhaA except for one large structural anomaly wherein amino acids 237–255 formed a long loop that traversed parallel through the membrane domain looping around two transmembrane segments. Closer analysis of this feature indicated that several of the residues were in steric conflict and that this structure was invalid. To resolve this we sought to improve our sequence alignment using the TMHMM2 secondary structure prediction algorithm (*35*) to predict the location of α-helical transmembrane

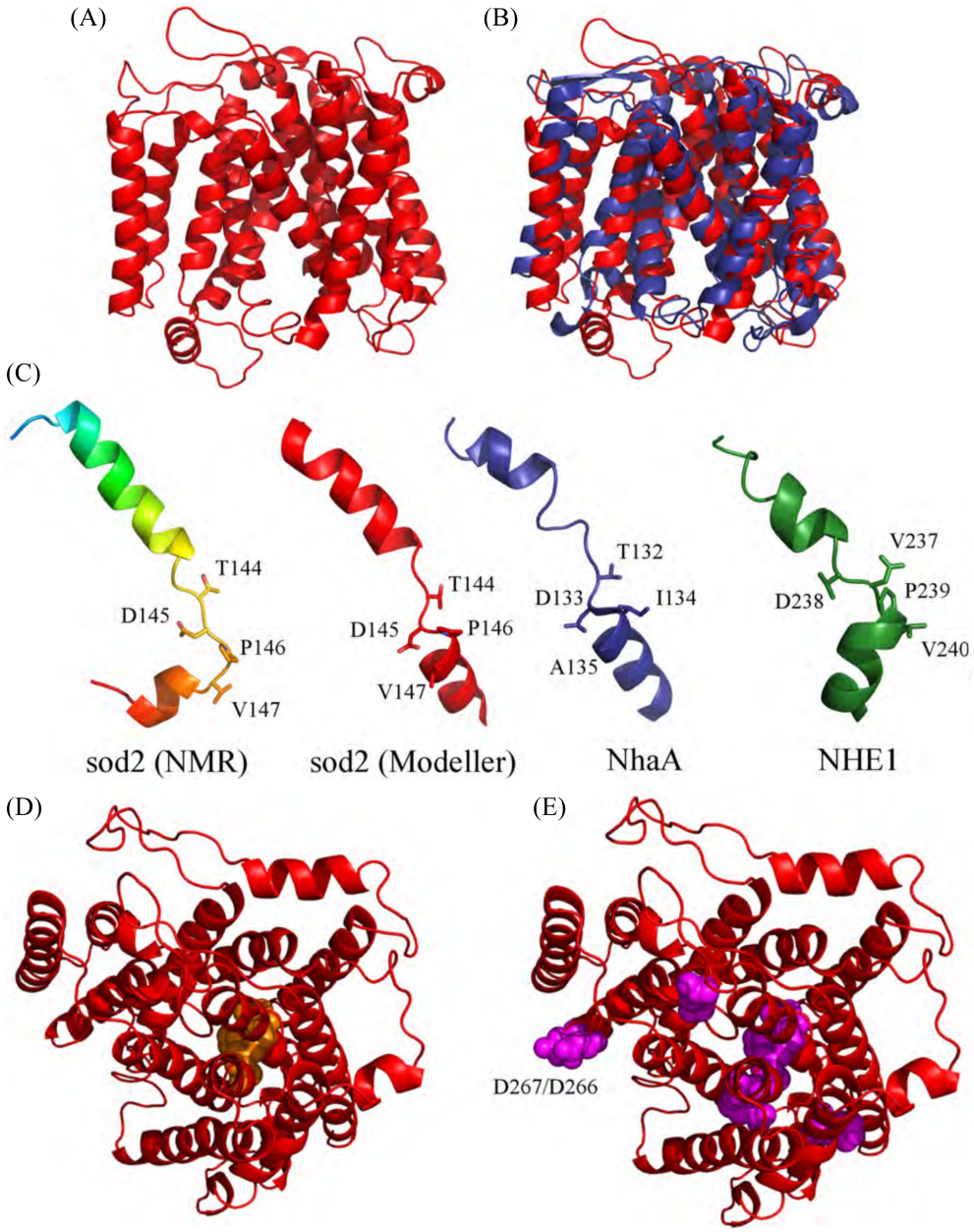

Figure 8-13. Homology model and TM structures compared. (A) Homology model of sod2 membrane domain (residues 12–429) based on the crystal structure of *E. coli* NhaA (PDB:1ZCD) using Modeller software (*32*). (B) Homology model (red) aligned with NhaA (blue). (C) Structures of analogous TM segments of NhaA TM IV (blue) and NHE1 TM VI (green) next to the sod2 TM IV models made with Xplor-NIH (rainbow) and Modeller (red). Key residues have been labelled for each peptide (see discussion). (D) Homology model of sod2 viewed perpendicular to the membrane plane from the extracellular side. The key residues of TM IV (T144–V147) are shown as orange spheres. (E) Reproduction of panel D with all known functional mutations in magenta spheres. D266 and D267 are labelled, showing their distance from the transport pore.

segments in sod2. Significantly, the predicted helical regions aligned approximately with the actual locations of transmembrane segments in NhaA, giving an unbiased indication that our initial alignment was reasonable. The predictions were further corroborated using JPred3 secondary structure prediction algorithm (*36*) which indicated very similar helical regions to TMHMM2. Using these secondary structure predictions the alignment was adjusted so that predicted helices of sod2 lined up with the known helices of NhaA. This alignment replaced the aberrant intramembrane loop at residues 237–255 with a transmembrane alpha-helix that satisfied the steric conflicts. However closer inspection revealed that up to 7 amino acids at the ends of several transmembrane helices dipped back into the membrane. To address this we looked at the predicted length of transmembrane helices in sod2 versus NhaA and noted that many were longer in sod2 than NhaA. Since Modeller does not account for significant differences in transmembrane segment length, short helical restraints were added to the ends of the sod2 transmembrane segments predicted to be longer than the aligned sequence in NhaA. To ensure no undo bias was added by secondary structure prediction the same TMHMM2 and JPred3 algorithms (*35*, *36*) were used to predict helical regions of NhaA. The algorithm predicted helices that aligned nearly perfectly (less than 2 residues different) with the actual location of transmembrane helices in the crystal structure (with the exception of the two short helices, 7 and 8, which were predicted to be one long helix). The resulting model (Figure 8-13, A) no longer appeared to have any structural anomalies and was in good agreement with the NhaA structure (Figure 8-13, B). The validity of the model was confirmed using the protein structure validation software suite (*37*). This evaluation revealed only seven residues with backbone angles outside of the allowable region of the Ramachandran plot. Six of these residues are located in extramembrane loops where the backbone bonds would be flexible enough to adopt a more preferable angle. The seventh residue, V373, is located in the unwound region of transmembrane segment XI. To resolve the significance of this disallowed dihedral angle, sculpting was performed using PyMol (DeLano scientific). Upon relaxation of the region containing V373, an admissible dihedral angle were obtained.

The model was further validated from a bioinformatics standpoint using the ConSurf method (*38*, *39*). Using the ConSurf server (*40*) 91 protein sequences (of $>$ 35% identity and a BLAST score of $>$ 300) were selected and aligned with the sod2 sequence. The server then calculates a Bayesian conservation score (0–9), gives it a corresponding colour and maps it onto the model of sod2 (Figure 8-14). Regions of high sequence conservation (pink to purple) are, as expected, found in the core of

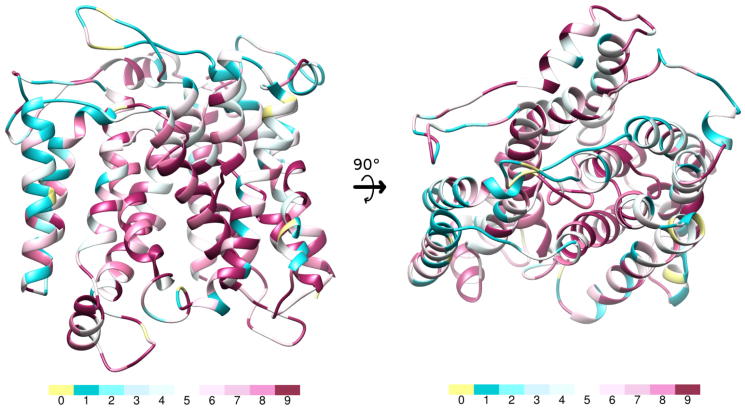

Figure 8-14. ConSurf conservation mapping on sod2 homology model. The ConSurf server was used to create a multiple sequence alignment and calculate the overall conservation score for each residue in sod2. This conservation score (0–9) was mapped onto the homology model of sod2 using a colour scale. Internal regions of the protein important for transport show generally higher levels of conservation and external region of the protein are less well conserved. The key residues in TM IV have either the highest conservation score, 9 (T144, D145, P146) or the second highest, 8 (V147).

the transporter while regions of less conservation (white to blue) are found on the outer surface. Significantly the critical amino acids T144, D145, and P146 all have the highest conservation score of 9 and V147 has a score of 8.

Figure 8-13, C, shows a comparison of the deduced and modelled TM segments of sod2, TM IV and TM IV of NhaA and TM VI of NHE1. All display a characteristic helix–extended region–helix configuration. The NMR structure of TM IV of sod2 is very similar, though not identical, to the structure of sod2 deduced by modelling.

Figure 8-13, D, illustrates the homology model of sod2 viewed perpendicular to the membrane plane from the extracellular side. The key residues of TMIV (T144–V147) are shown as orange spheres and have a central, potentially pore lining location. Figure 8-13, E, illustrates the position of all known functional mutations in the model.

Discussion

Removal of excess salt in plants and yeast is crucial in dealing with excess "toxic" levels of intracellular Na^+. In plants, improvements in salt tolerance has significant agricultural implications for crops. The yeast *Schizosaccharomyces pombe*, is a useful model organism for the study of salt tolerance as the Na^+/H^+

antiporter (sod2) plays the major role in salt removal from the cytosol and its deletion results in a Na^+ and Li^+ sensitive phenotype (*1*). While significant advances have been made on the study of mammalian (*47*) and *E. coli* (*48*) Na^+/H^+ exchangers, there has been much less study on plant and yeast Na^+/H^+ exchangers. Here we present the first systematic examination of a transmembrane segment of this type of transporter by alanine scanning mutagenesis and NMR spectroscopy. Alanine scanning mutagenesis has been used earlier to characterize transmembrane segments of membrane proteins including the NHE1 isoform of the mammalian Na^+/H^+ exchanger (*10*, *49*). The premise is that the small side chain of alanine can substitute for amino acids without disrupting the protein structure, while at the same time altering the nature of the side chain. All the amino acids of TM IV were mutated to alanine, with the exception of A138 and A150 which were already alanine. Also, in earlier studies we had already characterized D145 and P146 (*4*, *17*).

Most of the alanine mutants had either no effect, or mild to intermediate effects on the ability of sod2 to restore salt tolerance in sod2::ura4 *S. pombe* (Table 8-S2, Group I and II mutants). However, effects of mutation of amino acids T144 and V147 were notable and were explored in more detail. Several experiments suggested that the effects we found on these amino acids were on cation coordination either directly or indirectly though a change in conformation of the protein. In support of this hypothesis, the expression level and targeting of these mutant forms of sod2 were normal. Western blot expression (Figure 8-6) of the mutant proteins showed that the level of the mutants was comparable to that of controls. Localization of the T144 and V147 mutants was similar to that of wild type sod2 suggesting that impaired targeting of sod2 was not a cause of failure to restore salt tolerance. However, limited tryptic digestion suggested that there was a change in conformation of the mutant proteins. This was especially noticeable in the T144A protein and was reduced, though not eliminated in the functional T144S protein. These results suggest that a change in conformation of the sod2 protein may be responsible for aberrant transport by sod2. The conservative substitution of T144S, had an intermediate effect on proteolytic sensitivity, suggesting that the hydroxyl side chain restored not only activity, but also a least part of the conformational change.

For T144, mutation to either Ala, Asp or Lys did not restore the ability to confer salt tolerance. However, changing T144 to a serine residue restored the ability to confer resistance to LiCl and to transport LiCl, but not restore NaCl tolerance and transport. The *Zygosaccharomyces rouxii* Na^+/H^+ exchanger is a related member of the yeast plasma membrane Na^+/H^+ antiporters. Amino acids

124–156 of this protein are strikingly similar to amino acids 125–158 of *S. pombe* sod2 with amino acids T141 and T143 of Zrsod2-22p aligning with amino acids T142 and T144 of sod2 respectively (Figure 8-1, D). Previous studies have demonstrated that mutation of T141 and S150 of Zrsod2-22p to Ser and Thr respectively, altered and broadened the cation selectivity of this antiporter and demonstrated that the presence of hydroxyl groups in this region of the protein was critical for cation transport (*50*). Similarly, the nearby residue P145 was also shown to be important in substrate specificity. Amino acid T142 of sod2, which aligns with amino acid T141 of Zrsod2-22p (Figure 8-1, D), was not critical in transport by sod2. Instead, we found that the downstream T144 of sod2 had a role similar to that of T141 of Zrsod2-22p. These results suggest that amino acid T144 functionally, plays a functional role similar to that of T141 of Zrsod2-22p despite the fact that it does not align precisely with amino acid T141 of Zrsod2-22p.

Mutation of T144 to Ala, Lys or Asp severely abrogated activity. However, mutation to serine restored LiCl transport completely, but did not restore NaCl transport (Figure 8-9), suggesting that this hydroxyl might be directly participating in the binding of cations. The ionic radii of Na^+ and Li^+ are 0.95 Å and 0.65 Å respectively (*44*). A simple explanation may be that presentation of the hydroxyl by Ser is such that it can coordinate the smaller Li^+ ion, but not the larger sodium. Alternatively, it is known that hydrogen bond formation between the side chain oxygen atom of a Ser and Thr and the $i-3$ or $i-4$ peptide carbonyl oxygen may induce or stabilize a 3 to 4 degree bend in a helix relative to Ala (*51*). This might cause significant changes in the TM segment that affect cation coordination. Interestingly, T132 of the *E. coli* Na^+/H^+ antiporter NhaA has been shown to participate in cation coordination (*52*) and other Ser or Thr residues have also been shown to be important in cation binding and transport in other membrane transporters (*53–55*). However, experiments on the mammalian NHE1 isoform of the Na^+/H^+ exchanger have shown that not all Ser and Thr residues are important in this regard (*10*, *15*).

As noted above, T144S resulted in the most notable difference in cation selectivity, and was able to restore growth in the presence of LiCl but not NaCl. It also restored the ability of the protein to transport Li^+, but not Na^+, out of the cell. However, mutation of the amino acids L132, G133, S134, L135, L136 and G139 (Group II, Table 8-S2) exhibited phenotypes with slightly depressed growth in both NaCl and LiCl containing media. Although the effect is small, this region is conserved in both human NHE1 and Zrsod2-22p (*50*) (Figure 8-1, D) and it may be

possible that changes in amino acid packing or helix dynamics lead to less efficient transport and therefore reduced resistance. All these amino acids were in a helical region of the protein.

In order to help explain the functional phenomena we expressed and purified sod2 TM IV and analyzed the structure of the protein using NMR. Earlier studies have demonstrated that the amino acid sequence of TM segments of membrane proteins contain most of the required structural information needed to form their native structures (*56*, *57*). For example, Katragadda et al. demonstrated that the structure of individual transmembrane helices of rhodopsin and bacteriorhodopsin corresponded very well to the structures obtained by x-ray crystallography (*58*, *59*). We have also earlier used this approach and successfully produced transmembrane peptides of the mammalian Na^+/H^+ exchanger in *E. coli* or synthetically (*15*, *16*). We therefore produced TM IV of sod2 as a MBP fusion protein. After cleavage free of MBP, we used an organic extraction procedure to purify the TM IV fragment which resulted in a sample of sufficient purity for structure determination by NMR. Hu et al. used a similar protocol and demonstrated that sections of the membrane domain of CorA, M2 and KdpF, are properly folded (*60*).

NMR experiments revealed significant information about the secondary structure of sod2 TM IV. Measuring Hα chemical shift deviations from random coil, we noted that there were contiguous regions of negative deviation which are indicative of helical secondary structure (*61*). Likewise we calculated $^3J_{\mathrm{HNH}\alpha}$ coupling constants from the ratio of the intensities of the diagonal and crosspeaks for each residue in the HNHA spectrum (*27*, *28*). These values are related to the phi-bond dihedral angle. Although the amino terminal portion of the TM IV peptide showed largely alpha-helical character, Hα chemical shift deviations 133 and 139 are closer to random coil values, which could suggest that this N-terminal helix is broken, distorted or dynamic at these positions. Importantly the coupling constants show the same trends as the chemical shift deviations corroborating our secondary structure observations. Although some supporting NOE data was collected the relatively low number of helical distances observed could be a further indication of dynamic behaviour or distortion of the helices. This could simply be a result of the peptide being in organic solvent rather than in a membrane or perhaps it indicates the importance of other transmembrane segments that might stabilize partially unwound helices in the tertiary structure. Additionally, although data for the proline at position 146 could not be observed, it is predicted to be a helix breaker (*62*). This is not unprecedented as the structure of hNHE1 TM IV shows two proline residues that

disrupt the helix and form an extended section (*16*). Most interestingly, all the residues in this segment that have been found to be critical to sod2 function (T144 and V147 in this work, and D145 and P146 shown previously) are found in the extended region or very close to it (Table 8-S2). This is consistent with the results of other structural studies that have shown that discontinuous membrane helices are often involved in substrate coordination, an example being *E. coli* NhaA (*52*). The minor functional effects observed in the flanking helical regions may be connected to the structural dynamics suggested by the NMR data.

Although the data was not sufficient to calculate a precise structure, a model of sod2 TM IV was created using Xplor-NIH (*31*) to better visualize the secondary structure and to provide a basis for comparison to other published structures. We suggest that TM IV of sod2 may be functionally more similar to TM VI of NHE1 than to TM IV of NHE1. This is based on analysis of amino acid alignments, data from experiments that examine the critical amino acids in this region and overall structure of the region. The overall structure of human NHE1 TM VI is similar to that of TM IV of sod2 (Figure 8-13, C). Both contain two helices with an intervening unwound region that is critical in function (*15*). TM IV of human NHE1 has an unwound region, but this is flanked by only one helix (*16*).

Assessment of functional properties of aligned residues also supports the notion that TM IV of sod2 is similar to TM VI of NHE1. Mutation of residues D238 and P239 of human NHE1 results in a non-functional protein. These residues correspond to D145 and P146 in sod2 and we showed earlier that when D145 and P146 of sod2 are mutated that the protein is inactive (*4*, *17*). Similarly, the mutation of V237 of NHE1 to Cys had reduced function in the presence of cysteine-modifying compounds, and this corresponds to T144 of sod2 which is critical to function.

We have earlier also noted that TM VI of NHE1 has more similarities to TM IV of NhaA than TM IV of NHE1 (*15*). Comparison of sod2 TM IV with *E. coli* NhaA TM IV also suggests that although they have different primary structures their secondary structures are similar, both with helix-unwound region-helix configuration (Figure 8-13, C). Interestingly, TM IV of *E. coli* NhaA also contains important residues in this segment as mutation of either T132 or D133 have large effects on the apparent K_m indicating a role in the integrity of the transport mechanism (*6*, *63*). The extended peptide region may help accommodate the charged ion substrate (*52*). Studies on other membrane proteins have confirmed that unwound helices participate in substrate coordination and transport of many membrane proteins aside from Na^+/ H^+ antiporters (*52*, *64*).

In order to assess the effect these mutations might have on the folded structure, and to provide evidence that the deduced structure of sod2 TM IV is valid we constructed a homology model of the membrane domain of sod2. Mounting evidence suggests that a finite number of folds exist for membrane transporters (*65*) and that proteins with quite different primary amino acid sequence can have surprisingly similar structures. For example, the bile acid sodium symporter of *Neisseria meningitides* has a low primary sequence identity to *E. coli* NhaA but the structure is surprisingly similar to that of NhaA (*60*).

With this evidence for justification, we decided to use the functionally related NhaA structure as a template for homology modelling of sod2. After several iterative rounds of modelling, described above, we obtained a model that appears to generally satisfy our NMR data, and the collected biochemical data (Figure 8-13, A). The model is largely free of steric conflicts as demonstrated by 98% of residues falling within the acceptable regions of the Ramachandran plot and remaining residues in flexible regions of the structure (Figure 8-13). Additionally, analysis using the ConSurf method (*38*, *39*) indicates that functionally important regions on the interior of the transporter show the highest levels of conservation (Figure 8-14) including the unwound section of TM IV. This method was also used to validate a model structure of NHE1 (*40*, *66*).

The overall architecture of the model of sod2 indicates the same fold as NhaA (*6*) with helices IV and XI having an unwound, crossed configuration in the membrane (Figure 8-13, B). Functionally critical residues H367 and D241 (*43*), P146 (*4*), and D145 and E173 (*19*) are all situated in or near the putative transport pore (Figure 8-13, E). The exceptions are residues D266 and D267. These residues were found to be critically important for transport activity (*43*) but are not located near the transport site. They are located on a short alpha-helix within a long extracellular loop. A possible explanation is that this long loop may form a "cap-like" structure on the cytoplasmic side of the pore opening. The negative charges could help attract sodium ions for transport. Since this is not a feature found in NhaA it would be unlikely to be predicted by molecular modelling.

Significantly, the critical residues in the model of TM IV T144–P146 are in an extended conformation and face the hypothetical transport pore, in agreement with our deduced NMR structure. This offers further evidence that these residues are involved in ion translocation and supports the NMR structure we obtained (Figure 8-13, C). V147, however, is in a helical conformation and faces towards the outer helices in the homology model. From the homology model, one possible explanation

of the functional defect of V147A is that mutation at this site affects helical packing, likely destabilizing the structure, leading to a functional defect. This is supported by our confocal data that suggests that V147A is targeted the same as the wild type protein and by our trypsinolysis data that shows that V147A is more susceptible to digestion suggesting increased flexibility. Alternatively, Val has a lower propensity to form helices than either Ala or Leu; therefore these mutations may lead to increased helical character perturbing the placement of TM IV in the membrane or decreasing the segment's flexibility preventing proper function (*67*). This is still consistent with the trypsin digestion data as increased helical content may increase overall protein flexibility while decreasing the local flexibility of TM IV. In contrast V147 in the NMR structure is shown to be in an extended conformation. In fact the $^{3}J_{\mathrm{HNH}\alpha}$ coupling constants and chemical shift data for V147 are just past the helical cut-off indicating weak helical character. This suggests that V147 may be more conformationally dynamic than the Ala and Leu mutants and that this flexibility is required for proper function. The fact that V147 is extended in the NMR structure and helical in the homology model (Table 8-S2) further suggests that this position is likely locally flexible and requires the full membrane domain in order to form proper folded helical contacts.

In summary, the secondary structure of the peptide based on NMR data consists of a slightly kinked N-terminal helix at residues 128–142, followed by a flexible extended segment at residues 143–146, and a short C-terminal helix at residues 147–154. This secondary structure is supported by homology modelling of sod2 based on *E. coli* NhaA. The functional data suggest that residues 144–146 appear to have analogous partners in *E. coli* NhaA, human NHE1 and Zrsod2-22p, indicating the importance of this region in transport. Sod2 has a partially unwound helix containing functionally important residues for ion transport consistent with results from human NHE1 and *E. coli* NhaA. This study extends our current molecular understanding of salt tolerance and salt tolerance proteins. Previously we demonstrated that mutation of D145 (*17*) and P146 (*4*) of sod2, resulted in a transport defect that was unable to confer salt tolerance. Our present results demonstrate that the flanking amino acids T144 and V147 are also critical for sod2 structure and function and that TM IV is likely to be directly involved in ion translocation. We have also demonstrated that the hydroxyl of T144 is required for activity and that the conservative Thr to Ser mutation results in the inability to transport Na^{+} while maintaining Li^{+} transport. We suggest that TM IV of sod2 serves a role similar to that of TM IV of *E. coli* NhaA and TM VI of human NHE1.

Acknowledgements

We are grateful for the gift of an anti-H^+-ATPase antibody from Dr. C. Slayman, Yale School of Medicine.

Supplementary Materials

Mutation	Oligonucleotide	Restriction site
F126A	GCATATGCATT**GgcgCC**ACAAATTAACTTTTTAG	NarI
P127A	GCATATGCATTGTT**TgCgCA**AATTAACTTTTTAG	FspI
Q128A	GCATATGCATTGTT**cCCAgc**AATTAACTTTTTAGG	BseYII
I129A	CATATGCATTGTTT**CCtCAg**gcTAACTTTTTAGGATC	Bsu36I
N130A	GTTTCCACAAATTgcCTTTTTA**GGATCc**TTGCTGATCGCAGG	BamHI
F131A	CCACAAATTA**ACgcgT**TAGGATCTTTGC	MluI
L132A	CCACAAATTAACTTT**gccGGc**TCTTTGCTGATCGC	NaeI
G133A	CAAATTAACTTTTTA**Gctagc**TTGCTGATCGCAGG	NheI
S134A	CAAATTAACTTTTTAG**GAgCTc**TGCTGATCGCAGG	SacI
L135A	CTTTTTAGGATC**agcGCT**GATCGCAGGATG	AfeI
L136A	CTTTTTAGGATCTTTGg**cGATCG**CAGGATGTATAAC	PvuI
I137A	GGATCTTTGCTGg**ctGCAG**GATGTATAAC	PstI
G139A	CTTTGCTGATCGCA**GcATGc**ATAACTTCTACTGATC	SphI
C140A	GCTGATCGCA**GGcgcc**ATAACTTCTACTGATC	NarI
I141A	GCTGATCGCAGGA**TGcgcA**ACTTCTACTGATCC	FspI
T142A	CGCAGGATGTATAgC**gTCgAC**TGATCCTGTTC	SalI
S143A	GCAGGATGTATAA**CagCTACTG**ATCCTGTTC	AlwNI
T144A	GGATGTATAACTT**CTgCaG**ATCCTGTTCTATC	PstI
T144D	GGATGTATAACTTCT**gacGATCCTGTc**CTATCAGCATTG	Drd1
T144K	GGATGTATAACTTCTAa**gGATCC**TGTTCTATC	BamH1
T144S	GGATGTATAACTT**CTtCaG**ATCCTGTTCTATC	AlwN1
V147A	GTATAACTTCTAC**gGATCC**TGcTCTATCAGCATTGATTG	BamHI
V147L	GTATAACTTCTAC**gGATCC**TcTTCTATCAGCATTG	BamHI
L148A	CTTCTACTGATCCTGTT**gctagcG**CATTGATTGTAGG	NheI
S149A	CTTCTACTGATCCTGT**gCTAgC**AGCATTGATTGTAG	NheI
L151A	CCTGTTCTATCAGCAg**cgATcG**TAGGAGAAGGAGG	PvuI
L151S	CCTGTTCTATCAGCAT**cgATcG**TAGGAGAAGGAGG	PvuI
I152A	CCTGTTCTATC**AGCgcT**GgcgGTAGGAGAAGGAGGTC	AfeI

Table 8-S1. Oligonucleotides used for site-directed mutagenesis of sod2. Mutated nucleotides are indicated in lowercase letters. Restriction sites that were introduced are in bold. The forward oligonucleotide of the pair used for mutagenesis is shown.

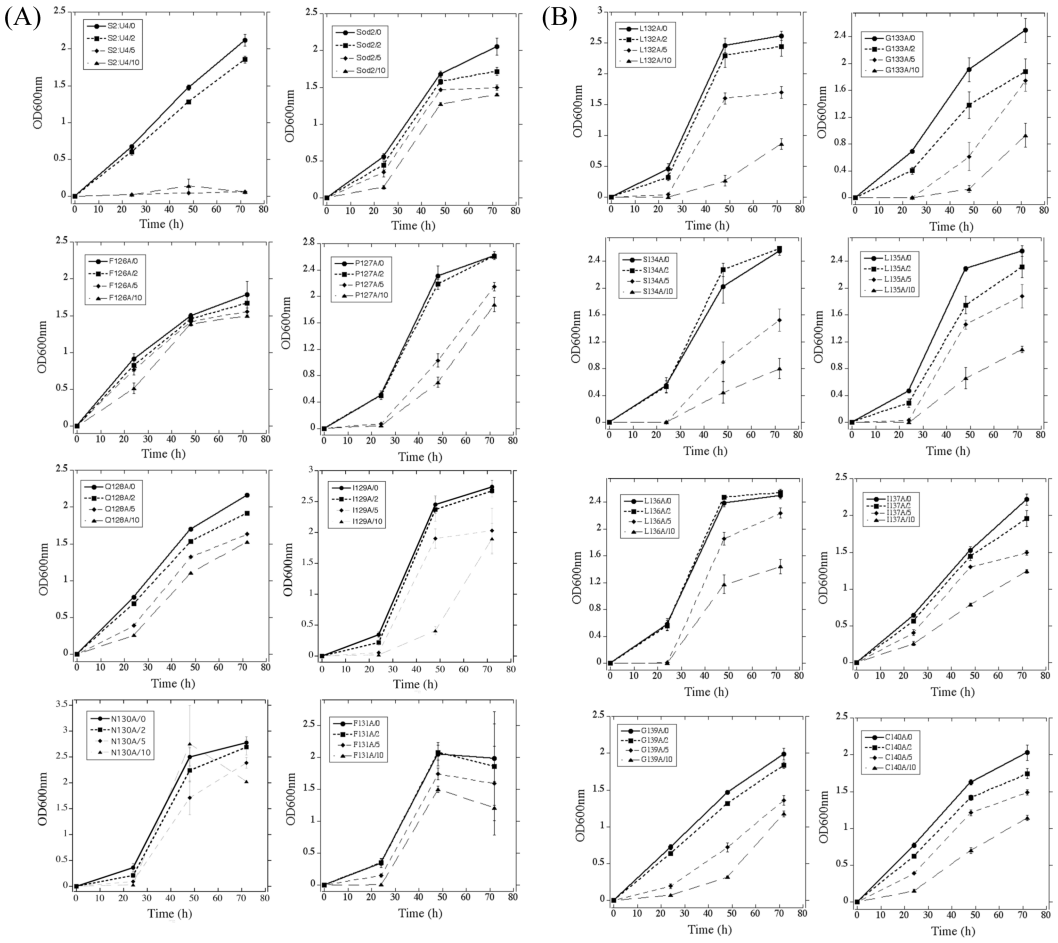

Figure 8-S1. Growth of *S. pombe* containing either wild type or TM IV mutant sod2 proteins in liquid media with various concentrations of LiCl. (Continued on page 191).

Mutation	Liquid LiCl	Liquid NaCl	Solid LiCl	Solid NaCl	Group	Str NMR	Str Model
Sod2 wt	+++	+++	+++	+++	N/A		
F126A	+++	+++	+++	+++	I	D	L
P127A	+++	+++	+++	+++	I	D	L
Q128A	+++	++	+++	+++	I	D	L
I129A	+++	+++	++	+++	I	H	L
N130A	+++	+++	++	+++	II	H	L
F131A	+++	+++	+++	+++	I	H	H
L132A	++	++	++	+++	II	H	H
G133A	++	++	++	++	II	H	H
S134A	++	++	++	++	II	H	H
L135A	++	++	++	++	II	H	H
L136A	+++	+++	++	++	II	H	H
I137A	+++	+++	+++	+++	I	H	H
G139A	+++	+++	++	++	II	H	H
C140A	+++	+++	+++	+++	I	H	H
I141A	+++	+++	+++	+++	I	H	H
T142A	+++	+++	+++	+++	I	H	H
S143A	+++	+++	+++	+++	I	E	E
T144A	-	-	+	+	III	E	E
T144D	-	-	+	+	III	E	E
T144K	-	-	+	+	III	E	E
T144S	+++	-	+++	+	IV	E	E
D145	N/A	N/A	N/A	N/A	N/A	E	E
P146	N/A	N/A	N/A	N/A	N/A	E	H
V147A	-	-	+	+	III	E	H
V147L	-	-	-	-	III	E	H
L148A	+++	+++	+++	+++	I	H	H
S149A	++	+++	+++	+++	II	H	H
L151A	+++	+++	+++	+++	I	H	H
L151S	++	+++	+++	+++	II	H	H
I152A	+	++	++	++	V	H	H

Table 8-S2. Summary of characteristics of sod2 TM IV. Effects of mutation of the amino acids and structural characteristics (Str) of the indicated amino acid in deduced NMR structure and structural model. Growth characteristics are indicated by; +++, growth essentially equivalent to that supported by wild type sod2; ++, growth slightly reduced compared to wild type sod2; +, growth greatly reduced compared to wild type sod2 but still greater than that of sod2 knockout; -, growth essentially equivalent to sod2 knockout yeast. Groupings refer to Group I, no effect of mutation on salt tolerance; II, very mild effect; III, marked effect on NaCl and LiCl tolerance; IV, marked effect on NaCl tolerance only; V, intermediate effect on NaCl and LiCl tolerance. D, disordered; E, extended; H, helix; L, loop.

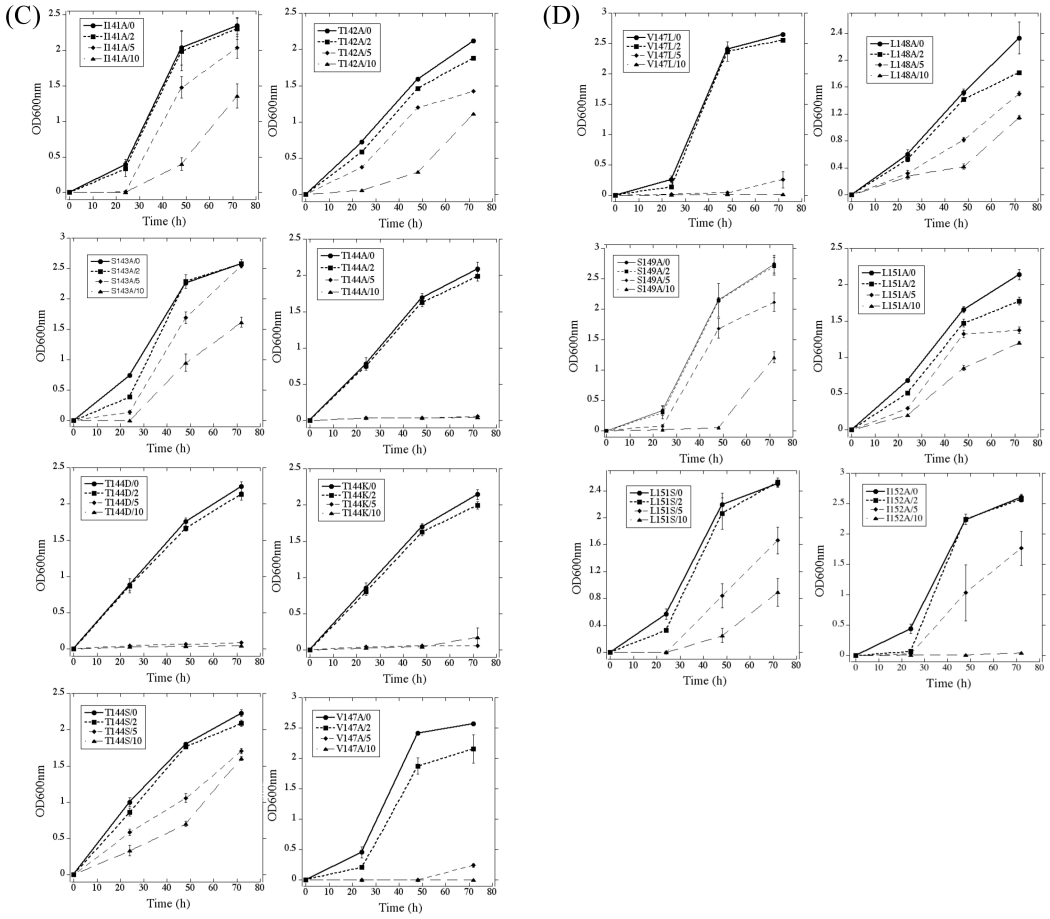

Figure 8-S1. (Continued from page 189). All mutants, sod2 knock out (sod2::ura4), wild type sod2, growth in LiCl are shown. LiCl tolerance of strains was assessed by inoculating 2×10^6 cells into 2.5 mL of medium at 30 °C for up to 72 hours. Growth was assessed by measuring the absorbance of the cell suspensions at 600 nm at the indicated times. Results are the mean ± S.E. of at least three determinations. *S. pombe* were grown in the presence of 0, 2, 5 or 10 mM LiCl. S2:U4 refers to sod2::ura4 (*S. pombe* with the sod2 knockout. Sod2 refers to sod2::ura4 containing the wild type sod2 protein. In other cases the indicated sod2 TM IV mutant was introduced into S2:U4 and grown in the presence of 0, 2, 5 or 10 mM LiCl as indicated.

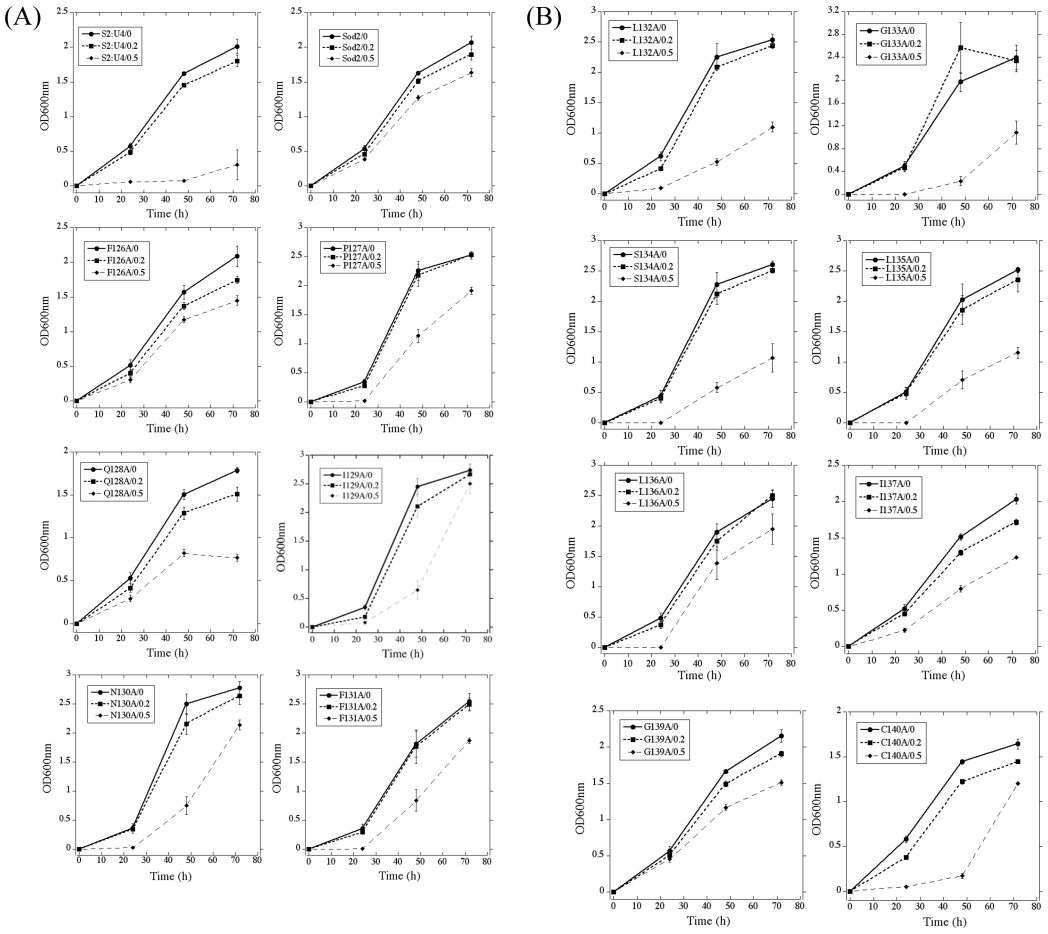

Figure 8-S2. Growth of *S. pombe* containing either wild type or TM IV mutant sod2 proteins in liquid media with various concentrations of NaCl. (Continued on page 193).

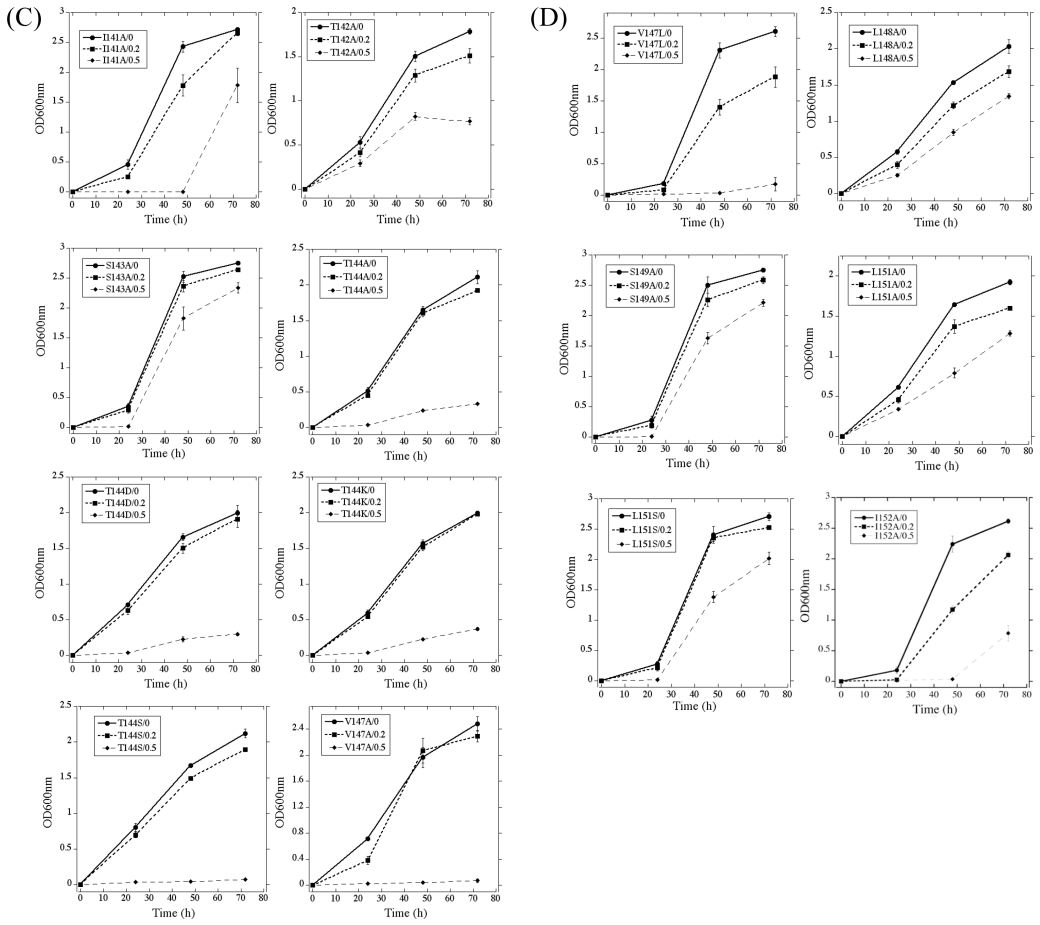

Figure 8-S2. (Continued from page 192). Methods as described for Figure 8-S1. All mutants, sod2 knock out, (sod2::ura4, S2:U4), wild type sod2, growth in NaCl are shown. NaCl was added at concentrations of 0, 0.2 or 0.5 M as indicated. Results are the mean $\pm$ S.E. of at least three determinations.

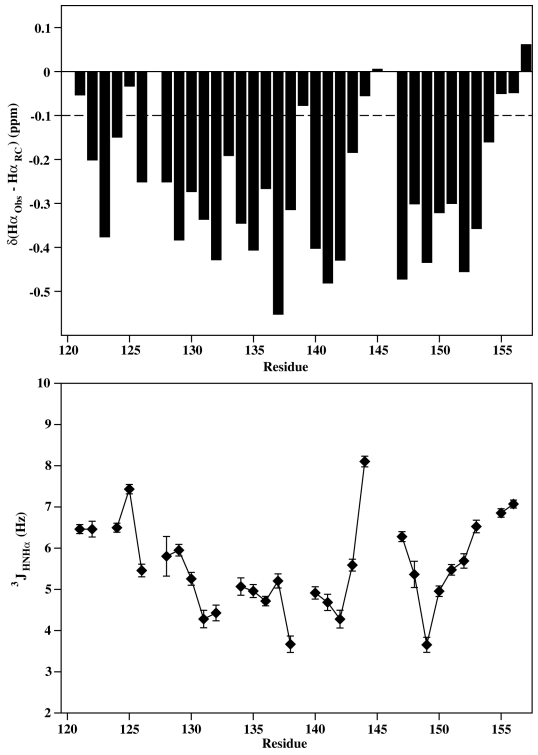

Figure 8-S3. Chemical shift index prediction of sod2 TM IV secondary structure. Contiguous regions with deviations lower than -0.1 ppm (dotted line) from random coil chemical shifts indicate alpha-helical structure. Glycine chemical shifts were averaged if two Hα peaks are resolved. (Bottom) $^3J_{\mathrm{HNH}\alpha}$ coupling constants calculated for the peptide from a 3D HNHA NMR spectrum. Regions approximately < 5 Hz suggest alpha helical structure, and > 8 Hz extended structure. Missing values are glycines or were not calculated due to peak overlap.

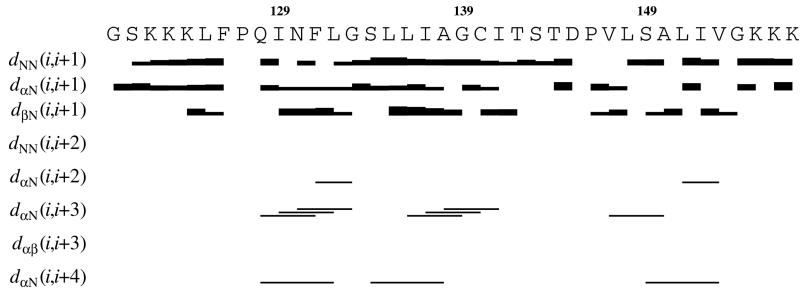

Figure 8-S4. Summary of NOE distances observed in a 3D ^{15}N NOESY-HSQC spectrum of sod2 TM IV. Regions containing $(i, i+3)$ and $(i, i+4)$ contacts suggest helical structure.

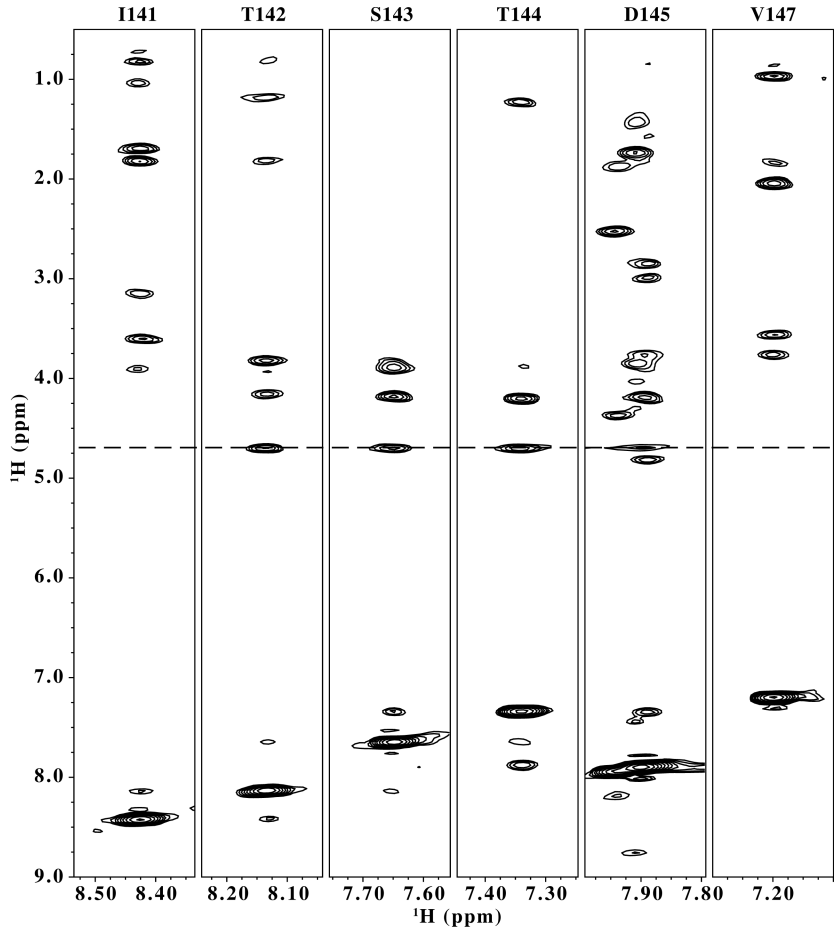

Figure 8-S5. 3D ^{15}N NOESY-HSQC strip plot of the residues in the central extended region of sod2 TM IV showing exchange peaks with water (dotted line).

References

1. Jia, Z. P., McCullough, N., Martel, R., Hemmingsen, S., and Young, P. G. (1992) Gene amplification at a locus encoding a putative Na^+/H^+ antiporter confers sodium and lithium tolerance in fission yeast. *EMBO J. 11*, 1631–1640.
2. Haworth, R. S., Lemire, B. D., Crandall, D., Cragoe, E., Jr, and Fliegel, L. (1991) Characterisation of proton fluxes across the cytoplasmic membrane of the yeast *Saccharomyces cerevisiae*. *Biochim. Biophys. Acta, Bioenerg. 1098*, 79–89.
3. Dibrov, P., Young, P. G., and Fliegel, L. (1998) Functional analysis of amino acid residues essential for activity in the Na^+/H^+ exchanger of fission yeast. *Biochemistry 37*, 8282–8288.
4. Ndayizeye, M., Touret, N., and Fliegel, L. (2009) Proline 146 is critical to the structure, function and targeting of sod2, the Na^+/H^+ exchanger of *Schizosaccharomyces pombe*. *Biochim. Biophys. Acta, Biomembr. 1788*, 983–992.
5. Brett, C. L., Donowitz, M., and Rao, R. (2005) Evolutionary origins of eukaryotic sodium/proton exchangers. *Am. J. Physiol.: Cell Physiol. 288*, C223–C239.
6. Hunte, C., Screpanti, E., Venturi, M., Rimon, A., Padan, E., and Michel, H. (2005) Structure of a Na^+/H^+ antiporter and insights into mechanism of action and regulation by pH. *Nature 435*, 1197–1202.
7. Xiang, M., Feng, M., Muend, S., and Rao, R. (2007) A human Na^+/H^+ antiporter sharing evolutionary origins with bacterial NhaA may be a candidate gene for essential hypertension. *Proc. Natl. Acad. Sci. U.S.A. 104*, 18677–18681.
8. Schushan, M., Xiang, M., Bogomiakov, P., Padan, E., Rao, R., and Ben-Tal, N. (2010) Model-guided mutagenesis drives functional studies of human NHA2, implicated in hypertension. *J. Mol. Biol. 396*, 1181–1196.
9. Slepkov, E. R., Rainey, J. K., Sykes, B. D., and Fliegel, L. (2007) Structural and functional analysis of the Na^+/H^+ exchanger. *Biochem. J. 401*, 623–633.
10. Ding, J., Rainey, J. K., Xu, C., Sykes, B. D., and Fliegel, L. (2006) Structural and functional characterization of transmembrane segment VII of the Na^+/H^+ exchanger isoform 1. *J. Biol. Chem. 281*, 29817–29829.
11. Reddy, T., Ding, J., Li, X., Sykes, B. D., Rainey, J. K., and Fliegel, L. (2008) Structural and functional characterization of transmembrane segment IX of the NHE1 isoform of the Na^+/H^+ exchanger. *J. Biol. Chem. 283*, 22018–22030.
12. Lee, B. L., Li, X., Liu, Y., Sykes, B. D., and Fliegel, L. (2009) Structural and functional analysis of transmembrane XI of the NHE1 isoform of the Na^+/H^+ exchanger. *J. Biol. Chem. 284*, 11546–11556.

13. Lee, B. L., Li, X., Liu, Y., Sykes, B. D., and Fliegel, L. (2009) Structural and functional analysis of extracellular loop 2 of the Na^+/H^+ exchanger. *Biochim. Biophys. Acta, Biomembr. 1788*, 2481–2488.

14. Lee, B. L., Sykes, B. D., and Fliegel, L. (2011) Structural analysis of the Na^+/H^+ exchanger isoform 1 (NHE1) using the divide and conquer approach. *Biochem. Cell Biol. 89*, 189–199.

15. Tzeng, J., Lee, B. L., Sykes, B. D., and Fliegel, L. (2010) Structural and functional analysis of transmembrane segment VI of the NHE1 isoform of the Na^+/H^+ exchanger. *J. Biol. Chem. 285*, 36656–36665.

16. Slepkov, E. R., Rainey, J. K., Li, X., Liu, Y., Cheng, F. J., Lindhout, D. A., Sykes, B. D., and Fliegel, L. (2005) Structural and functional characterization of transmembrane segment IV of the NHE1 isoform of the Na^+/H^+ exchanger. *J. Biol. Chem. 280*, 17863–17872.

17. Wiebe, C. A., Rieder, C., Young, P. G., Dibrov, P., and Fliegel, L. (2003) Functional analysis of amino acids of the Na^+/H^+ exchanger that are important for proton translocation. *Mol. Cell. Biochem. 254*, 117–124.

18. Fliegel, L. (2005) Identification of conserved polar residues important for salt tolerance by the Na^+/H^+ exchanger of *Schizosaccharomyces pombe*. *Mol. Cell. Biochem. 268*, 83–92.

19. Fliegel, L., Wiebe, C., Chua, G., and Young, P. G. (2005) Functional expression and cellular localization of the Na^+/H^+ exchanger Sod2 of the fission yeast *Schizosaccharomyces pombe*. *Can. J. Physiol. Pharmacol. 83*, 565–572.

20. Slepkov, E. R., Chow, S., Lemieux, M. J., and Fliegel, L. (2004) Proline residues in transmembrane segment IV are critical for activity, expression and targeting of the Na^+/H^+ exchanger isoform 1. *Biochem. J. 379*, 31–38.

21. Silva, N. L., Wang, H., Harris, C. V., Singh, D., and Fliegel, L. (1997) Characterization of the Na^+/H^+ exchanger in human choriocarcinoma (BeWo) cells. *Pflugers Arch. 433*, 792–802.

22. Rieder, C. V., and Fliegel, L. (2002) Developmental regulation of Na^+/H^+ exchanger expression in fetal and neonatal mice. *Am. J. Physiol.: Heart Circ. Physiol. 283*, H273–H283.

23. Dibrov, P., Smith, J. J., Young, P. G., and Fliegel, L. (1997) Identification and localization of the sod2 gene product in fission yeast. *FEBS Lett. 405*, 119–124.

24. Douglas, J. L., Trieber, C. A., Afara, M., and Young, H. S. (2005) Rapid, high-yield expression and purification of Ca^{2+}-ATPase regulatory proteins for high-resolution structural studies. *Protein Expr. Purif. 40*, 118–125.

25. Kay, L., Keifer, P., and Saarinen, T. (1992) Pure absorption gradient enhanced heteronuclear single quantum correlation spectroscopy with improved sensitivity. *J. Am. Chem. Soc. 114*, 10663–10665.

26. Zhang, O., Kay, L. E., Olivier, J. P., and Forman-Kay, J. D. (1994) Backbone ^{1}H and ^{15}N resonance assignments of the N-terminal SH3 domain of drk in folded and unfolded states using enhanced-sensitivity pulsed field gradient NMR techniques. *J. Biomol. NMR 4*, 845–858.

27. Vuister, G. W., and Bax, A. (1993) Quantitative *J* correlation: a new approach for measuring homonuclear three-bond J($H^{N}H^{\alpha}$) coupling constants in ^{15}N-enriched proteins. *J. Am. Chem. Soc. 115*, 7772–7777.

28. Grzesiek, S., Kuboniwa, H., Hinck, A. P., and Bax, A. (1995) Multiple-quantum line narrowing for measurement of H^{α}-H^{β} *J* couplings in isotopically enriched proteins. *J. Am. Chem. Soc. 117*, 5312–5315.

29. Delaglio, F., Grzesiek, S., Vuister, G. W., Zhu, G., Pfeifer, J., and Bax, A. (1995) NMRPipe: a multidimensional spectral processing system based on UNIX pipes. *J. Biomol. NMR 6*, 277–293.

30. Johnson, B. A. (2004) Using NMRView to visualize and analyze the NMR spectra of macromolecules. *Methods Mol. Biol. 278*, 313–352.

31. Schwieters, C. D., Kuszewski, J. J., Tjandra, N., and Clore, G. M. (2003) The Xplor-NIH NMR molecular structure determination package. *J. Magn. Reson. 160*, 65–73.

32. Eswar, N., Webb, B., Marti-Renom, M. A., Madhusudhan, M. S., Eramian, D., Shen, M.-Y., Pieper, U., and Sali, A. (2006) Comparative protein structure modeling using Modeller. *Curr. Protoc. Bioinform. 15*, 5.6.1—5.6.30.

33. Sievers, F., Wilm, A., Dineen, D., Gibson, T. J., Karplus, K., Li, W., Lopez, R., McWilliam, H., Remmert, M., Söding, J., Thompson, J. D., and Higgins, D. G. (2011) Fast, scalable generation of high-quality protein multiple sequence alignments using Clustal Omega. *Mol. Syst. Biol. 7*, 539.

34. Goujon, M., McWilliam, H., Li, W., Valentin, F., Squizzato, S., Paern, J., and Lopez, R. (2010) A new bioinformatics analysis tools framework at EMBL-EBI. *Nucleic Acids Res. 38*, W695–W699.

35. Krogh, A., Larsson, B., von Heijne, G., and Sonnhammer, E. L. (2001) Predicting transmembrane protein topology with a hidden Markov model: application to complete genomes. *J. Mol. Biol. 305*, 567–580.

36. Cole, C., Barber, J. D., and Barton, G. J. (2008) The Jpred 3 secondary structure prediction server. *Nucleic Acids Res. 36*, W197–W201.

37. Bhattacharya, A., Tejero, R., and Montelione, G. T. (2007) Evaluating protein structures determined by structural genomics consortia. *Proteins 66*, 778–795.

38. Landau, M., Mayrose, I., Rosenberg, Y., Glaser, F., Martz, E., Pupko, T., and Ben-Tal, N. (2005) ConSurf 2005: the projection of evolutionary conservation scores of residues on protein structures. *Nucleic Acids Res. 33*, W299–W302.

39. Glaser, F., Pupko, T., Paz, I., Bell, R. E., Bechor-Shental, D., Martz, E., and Ben-Tal, N. (2003) ConSurf: identification of functional regions in proteins by surface-mapping of phylogenetic information. *Bioinformatics 19*, 163–164.

40. Ashkenazy, H., Erez, E., Martz, E., Pupko, T., and Ben-Tal, N. (2010) ConSurf 2010: calculating evolutionary conservation in sequence and structure of proteins and nucleic acids. *Nucleic Acids Res. 38*, W529–W533.

41. Wiebe, C. A., Dibattista, E. R., and Fliegel, L. (2001) Functional role of polar amino acid residues in Na^+/H^+ exchangers. *Biochem. J. 357*, 1–10.

42. Shi, H., Ishitani, M., Kim, C., and Zhu, J. K. (2000) The *Arabidopsis thaliana* salt tolerance gene SOS1 encodes a putative Na^+/H^+ antiporter. *Proc. Natl. Acad. Sci. U.S.A. 97*, 6896–6901.

43. Dibrov, P., Young, P. G., and Fliegel, L. (1998) Physiological consequences of expression of the Na^+/H^+ antiporter sod2 in *Escherichia coli*. *Mol. Cell. Biochem. 183*, 125–132.

44. Murtazina, R., Booth, B. J., Bullis, B. L., Singh, D. N., and Fliegel, L. (2001) Functional analysis of polar amino-acid residues in membrane associated regions of the NHE1 isoform of the mammalian Na^+/H^+ exchanger. *Eur. J. Biochem. 268*, 4674–4685.

45. Dibrov, P., and Fliegel, L. (1998) Comparative molecular analysis of Na^+/H^+ exchangers: a unified model for Na^+/H^+ antiport? *FEBS Lett. 424*, 1–5.

46. Wishart, D. S., Bigam, C. G., Holm, A., Hodges, R. S., and Sykes, B. D. (1995) ^1H, ^{13}C and ^{15}N random coil NMR chemical shifts of the common amino acids. I. Investigations of nearest-neighbor effects. *J. Biomol. NMR 5*, 67–81.

47. Kemp, G., Young, H., and Fliegel, L. (2008) Structure and function of the human Na^+/H^+ exchanger isoform 1. *Channels 2*, 329–336.

48. Padan, E. (2008) The enlightening encounter between structure and function in the NhaA Na^+/H^+ antiporter. *Trends Biochem. Sci. 33*, 435–443.

49. Fleming, K. G., and Engelman, D. M. (2001) Specificity in transmembrane helix-helix interactions can define a hierarchy of stability for sequence variants. *Proc. Natl. Acad. Sci. U.S.A. 98*, 14340–14344.

50. Kinclova-Zimmermannova, O., Zavrel, M., and Sychrova, H. (2006) Importance of the seryl and threonyl residues of the fifth transmembrane domain to the substrate specificity of yeast plasma membrane Na^+/H^+ antiporters. *Mol. Membr. Biol. 23*, 349–361.

51. Ballesteros, J. A., Deupi, X., Olivella, M., Haaksma, E. E., and Pardo, L. (2000) Serine and threonine residues bend α-helices in the $\chi_1 = g^-$ conformation. *Biophys. J. 79*, 2754–2760.

52. Padan, E., Kozachkov, L., Herz, K., and Rimon, A. (2009) NhaA crystal structure: functional-structural insights. *J. Exp. Biol. 212*, 1593–1603.

53. Díez-Sampedro, A., Wright, E. M., and Hirayama, B. A. (2001) Residue 457 controls sugar binding and transport in the Na^+/glucose cotransporter. *J. Biol. Chem. 276*, 49188–49194.

54. Kamiya, T., and Maeshima, M. (2004) Residues in internal repeats of the rice cation/H^+ exchanger are involved in the transport and selection of cations. *J. Biol. Chem. 279*, 812–819.

55. Li, H., and Pajor, A. M. (2003) Serines 260 and 288 are involved in sulfate transport by hNaSi-1. *J. Biol. Chem. 278*, 37204–37212.

56. Cunningham, F., and Deber, C. M. (2007) Optimizing synthesis and expression of transmembrane peptides and proteins. *Methods 41*, 370–380.

57. Hunt, J. F., Earnest, T. N., Bousché, O., Kalghatgi, K., Reilly, K., Horváth, C., Rothschild, K. J., and Engelman, D. M. (1997) A biophysical study of integral membrane protein folding. *Biochemistry 36*, 15156–15176.

58. Katragadda, M., Alderfer, J. L., and Yeagle, P. L. (2001) Assembly of a polytopic membrane protein structure from the solution structures of overlapping peptide fragments of bacteriorhodopsin. *Biophys. J. 81*, 1029–1036.

59. Katragadda, M., Chopra, A., Bennett, M., Alderfer, J. L., Yeagle, P. L., and Albert, A. D. (2001) Structures of the transmembrane helices of the G-protein coupled receptor, rhodopsin. *J. Pept. Res. 58*, 79–89.

60. Hu, N.-J., Iwata, S., Cameron, A. D., and Drew, D. (2011) Crystal structure of a bacterial homologue of the bile acid sodium symporter ASBT. *Nature 478*, 408–411.

61. Wishart, D. S., Sykes, B. D., and Richards, F. M. (1991) Relationship between nuclear magnetic resonance chemical shift and protein secondary structure. *J. Mol. Biol. 222*, 311–333.

62. Cordes, F. S., Bright, J. N., and Sansom, M. S. P. (2002) Proline-induced distortions of transmembrane helices. *J. Mol. Biol. 323*, 951–960.

63. Galili, L., Rothman, A., Kozachkov, L., Rimon, A., and Padan, E. (2002) Trans membrane domain IV is involved in ion transport activity and pH regulation of the NhaA-Na^+/H^+ antiporter of *Escherichia coli*. *Biochemistry 41*, 609–617.

64. Screpanti, E., and Hunte, C. (2007) Discontinuous membrane helices in transport proteins and their correlation with function. *J. Struct. Biol. 159*, 261–267.

65. Oberai, A., Ihm, Y., Kim, S., and Bowie, J. U. (2006) A limited universe of membrane protein families and folds. *Protein Sci. 15*, 1723–1734.

66. Landau, M., Herz, K., Padan, E., and Ben-Tal, N. (2007) Model structure of the Na^+/H^+ exchanger 1 (NHE1): functional and clinical implications. *J. Biol. Chem. 282*, 37854–37863.

67. Pace, C. N., and Scholtz, J. M. (1998) A helix propensity scale based on experimental studies of peptides and proteins. *Biophys. J. 75*, 422–427.

Chapter 9

NMR structural analysis of transmembrane pair VI and VII of the NHE1 isoform of the Na^+/H^+ exchanger

BLL performed the NMR experiments and structure calculations, and Claudia Alves performed the protein expression and purification. The introduction was written by BLL, CA, and Larry Fliegel. The peptide purification methods were written by CA. The NMR methods and results were written by BLL.

Summary

The mammalian Na^+/H^+ exchanger isoform 1 (NHE1) is a ubiquitously expressed plasma membrane pH regulatory protein. It removes a single intracellular H^+ in exchange for one extracellular Na^+. The catalytic membrane domain is comprised of 500 N-terminal amino acids and is predicted to contain 12 transmembrane (TM) segments. While the crystal structure of the *E. coli* Na^+/H^+ exchanger NhaA has been deduced, large multi pass eukaryotic membrane proteins continue to be refractory to expression, purification and crystallization. As such, we have adopted a "divide and conquer" approach to investigating the structure and function of NHE1. We have previously determined the structures for several single-TM segments of NHE1 using NMR. To gain further insight into the structure and function of NHE1, we have expressed and determined the structure of a two-TM segment of NHE1, TM VI–VII. The TM segment is expressed as a fusion protein with maltose binding protein, which has allowed us to produce the milligram amounts necessary for structural studies. We use high-resolution solution-state NMR spectroscopy to determine the structure of TM VI–VII in dodecylphosphocholine micelles. The structure of TM VI is similar to previous studies, and contains a central extended segment while TM

VII adopts a straight helix. The final structure is similar to TM 4–5 of *E. coli* NhaA and may suggest a similar structure between the two proteins.

Introduction

The N-terminal 500 amino acids of mammalian NHE1 protein consist of 12 transmembrane (TM) segments that comprise the catalytic component of the protein. Two general models of the topology of NHE1 exist. One model is based on cysteine accessibility studies (*1*) while the second is based on computational comparison with the crystal structure of the *E. coli* Na^+/H^+ exchanger NhaA (*2*). The two models are compared in Kemp et al. (*3*)). The models vary from one another after amino acid 315, however prior to this region the models are essentially identical although the later model predicts that the first two transmembrane segments are non-essential for ion transport. Amino acids 226–275 are predicted to form two transmembrane segments in both models.

Expression and purification of entire membrane domains of eukaryotic proteins has proven to be a problematic goal. However, studies have demonstrated that the amino acid sequence of TM segments of membrane proteins possess much of the required structural information needed to form their higher order structures (*4–6*) We have therefore earlier examined and expressed single TM segments of NHE1 including TM VI and TM VII. For TM VI our studies showed that it is a pore lining TM segment that has a helical region, followed by an unwound region followed by another unwound region (*7*, *8*). Our studies of TM VII demonstrated that it was predominantly α-helical and that it was critical to NHE1 function and contains pore lining residues (*9*, *10*).

While much of the required structural information has been demonstrated to be contained within the primary amino acid sequence of TM segments, interactions between TM segments can obviously not be studied with single TM segments. Additionally, Hunt et al. (*5*) have suggested that in some cases, external constraints between helices can affect the conformation of TM segments. For this reason in this study we examined a pair of TM segments, TM VI–VII, that are linked together by a short intracellular loop. We developed an expression system to express and purify the pair of TM segments and have determined the structure of this TM pair in DPC micelles using NMR.

Materials and methods

Materials

Amylose affinity resin was from New England Biolabs (Pickering, ON, Canada). Lipofectamine™ 2000 reagent was from Invitrogen (Carlsbad, CA, USA) and PWO DNA polymerase was from Roche Applied Science (Roche Molecular Biochemicals, Mannheim, Germany). Sulpho-NHS-SS-Biotin was from Pierce Chemical Company (Rockford, IL, USA).

Expression and purification of the NHE1 C-terminus

To produce TM VI–VII of human NHE1 we expressed it as a fusion protein with maltose binding protein (MBP) in *E. coli*. We used a modified version of a system described earlier (*11*). Synthetic DNA coding for amino acids 226–274 of TM VI–VII was purchased from GenScript (GGATCCAAAAAAAAAGATAACTTATTATTCGGTTCTATTATTTCTGCTGTTGATCCAGTTGCTGTTTTAGCTGTTTTCGAAGAAATTCACATTAACGAATTATTACACATTTTAGTTTTCGGTGAATCTTTATTAAACGATGCTGTTACTGTTGTTTTATATAAAAAAAAATGAGAATTC). The BamHI-EcoRI sites of the pUC57-TMVI-VII plasmid were used to insert the sequence into the vector pMPLB (*11*) after removal of the insert in the vector with BamHI and EcoRI. This created an inducible plasmid expressing maltose binding protein fused to TM VI–VII and with a cleavable TEV site separating the maltose binding protein and TM VI–VII (pMBPVI-VII). The DNA sequence was codon optimized for expression in *E. coli*. Poly-lysine sequences were added to both ends of the two-TM sequence to aid in solubility of the peptide as described earlier (*7*). After cleavage of the fusion protein with TEV protease this would result in a peptide of the sequence GSKKKDNLLFGSIISAVDPVAVLAVFEEIHINELLHILVFGESLLNDAVTVVLYKKK, with the N-terminal additional GS residues remaining from the TEV cleavage site.

The plasmid pMBPVI-VII was transformed into several *E. coli* strains including XL1 blue, DH5α, BL21 Star (DE-3)pLysS, Topp 10, and Topp 11. After trials with different strains and temperatures (not shown), XL1 blue was chosen for expression. Bacterial culture and protein expression was performed at 37 °C with induction at an OD_{600} of about 1.0 and with 0.2 mM IPTG for 20 hours. The cells were harvested at 4 °C by centrifugation at $6000 \times g$ for 30 min. Pellets from 1 L cultures were resuspended in 50 mL Amylose Buffer (20 mM Tris-HCl, 200 mM

NaCl, 1mM EDTA, pH 7.4), divided in two parts and stored at -80 °C. Preliminary experiments produced unlabelled protein. Later experiments produced ^{15}N isotopically labelled peptide for more detailed characterization of the structure. For these experiments cells were prepared essentially as described earlier (*12*). *E. coli* were grown in a minimal medium containing 87 mM NaH_2PO_4, 34 mM K_2HPO_4, 4 mM $MgSO_4$, 1.8 µM $FeSO_4$, 55.5 mM glucose, pH 7.3. The medium was supplemented with 1 g $(^{15}NH_4)_2SO_4$. Minimal medium was inoculated with 40 mL of pre-culture and the culture was grown in a 5 L fermenter (BIOSTAT B from B. Braun Biotech International) at 37 °C, 500 rpm, pH 7.0 up to an OD_{600} of 0.8–1.0. Protein expression was induced with 0.2 mM IPTG and the balance of procedures were as described above for unlabelled protein.

The cell pellet solution was thawed and cells were lysed using an EmulsiFlex homogenizer at 15000–20000 psi. Homogenization was repeated six times at 4 °C. The lysate suspension was centrifuged at $50000 \times g$ for 30 min at 4 °C and the supernatant was collected and stored on ice. 30 mL aliquots of the supernatant were applied to a column with amylose resin in Amylose buffer. The column was washed with 4 column volumes of of Amylose buffer and elution was with with 40 mM maltose in 2.5 column volumes of Amylose buffer. Samples of the lysate and eluted fractions were examined by SDS-PAGE.

MBP-TMVI-VII cleavage and peptide isolation

The eluted fractions were concentrated to 5 mg/mL using an Amicon-15 Ultra 30000 MWCO filter at 4300 rpm at 4 °C. Proteolysis of the fusion protein was achieved by incubating the fusion protein with 10 U/mg amount of TEV protease at 21 °C overnight. This tended to cause the TM VI–VII peptide to come out of solution so the sample containing the MBP protein and TM VI–VII peptide was centrifuged at $100000 \times g$ for 45 min at 4 °C and the supernatant containing mostly maltose binding protein was discarded. The pellet was suspended in 20 mL/100mg digested protein with re-suspension buffer 1 (50 mM phosphate pH 8.0 (Na_2HPO_4/NaH_2PO_4) plus 1 M guanidine-HCl), using a glass homogenizer, and incubated for 30 min at room temperature. This sample was centrifuged at $10000 \times g$ for 20 min at 4 °C. The pellet which was rich in TM VI–VII peptide, was dissolved in 5 mL/100mg digested protein with re-suspension buffer 2 (50 mM phosphate pH 7.2 (Na_2HPO_4) plus 7 M guanidine-HCl). This sample was centrifuged $10{,}000 \times g$ for 10 min at 4 °C and the supernatant was collected. 50 µL samples were saved in each step to be analyzed in 16% Tricine gels containing 6 M urea (*13*).

The supernatant of TM VI–VII in 7 M guanidine-HCl was purified using the facilities from Institute for Biomolecular Design at University of Alberta. It was applied onto a preparative reverse-phase Zorbax 300SB-C8 column (9.4 × 250 mm, 5 μm particle size, Agilent Technologies). Buffer A consisted of 0.1% trifluoroacetic acid in water and buffer B was 0.1% trifluoroacetic acid in acetonitrile. The column was equilibrated with buffer A at a flow rate of 2.0 mL/min. The peptide was injected and a linear gradient from 20 to 80% buffer B was run for 135 min. The fractions were collected every minute and analyzed using a narrow bore reversed phase HPLC column (Supelco Discovery C18 column, 5 μm, 2.1 × 125 mm). Buffers A and B were used and the gradient was from 20 to 98% buffer B over 35 min. Fractions were analyzed by MALDI-TOF mass spectrometry. TM VI–VII containing fractions were pooled and lyophilized.

NMR spectroscopy

NMR sample preparation and structure calculation were performed as described in Chapter 2. ^{15}N-isotopic labelling of the peptide also allowed us to investigate the dynamics of the peptide in DPC micelles. T_1 and T_2 NMR relaxation measurements were acquired on a 600 MHz NMR spectrometer. 2D ^{15}N HSQC spectra were acquired using the gNhsqc pulse sequence in VnmrJ with an initial 4 s delay and relaxation times of 0.1, 0.3, 0.5, 0.7, 0.9, 1.1, 1.3 s for T_1 measurements and 0.01, 0.03, 0.05, 0.07, 0.09, 0.11, 0.13 s for T_2 measurements. Spectra were processed in NMRPipe and assigned in NMRViewJ. T_1 and T_2 values were obtained by fitting peak intensities to an exponential decay curve within NMRViewJ.

Results and discussion

Initial characterization of purified TM VI–VII peptide in DPC micelles utilized the 1D ^{1}H NMR spectra of non-isotopically labelled peptide samples. NMR spectra with well resolved and reasonably narrow amide peaks were obtained under the conditions used in our previous NMR studies on single transmembrane helices of NHE1. Increasing the temperature to 40 °C did not appear to improve the spectral quality, and increasing pH to 6 decreased the quality slightly. Therefore spectra were obtained at 30 °C and pH 5 for structure determination. ^{15}N isotopically labelled peptide showed good resolution and dispersion in 2D ^{1}H-^{15}N HSQC NMR spectra, and allowed for additional 3D NMR experiments for assignment and structure calculation as well as ^{15}N relaxation measurements. The amide proton region of

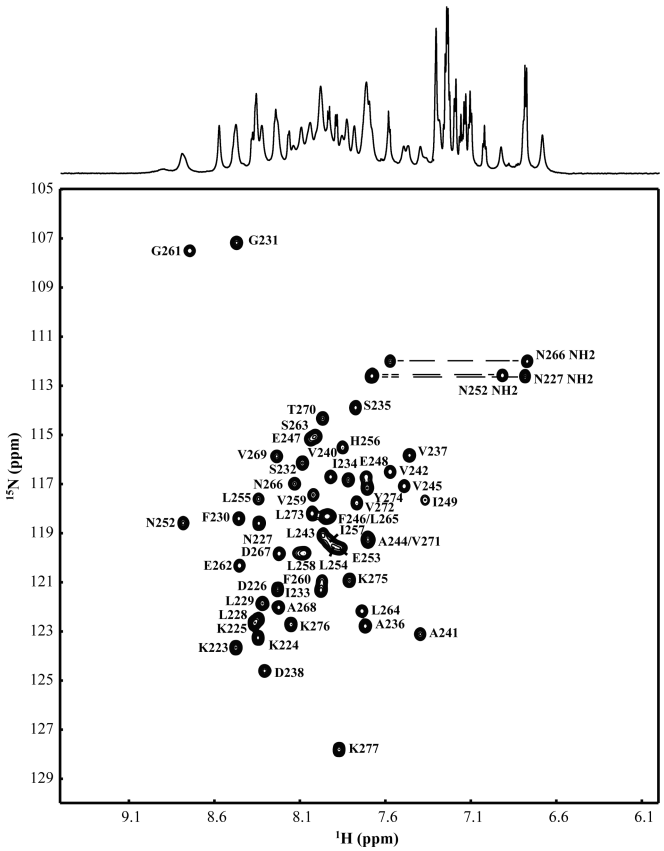

Figure 9-1. NMR spectra of TM VI–VII in DPC micelles. (Top) Amide/aromatic region of the 1D ^{1}H NMR spectrum of unlabelled TM VI–VII peptide, showing amide, amine and aromatic peaks. (Bottom) Corresponding region from a 2D ^{1}H-^{15}N HSQC spectrum of ^{15}N-labelled TM VI–VII showing only amide peaks, with peak assignments shown.

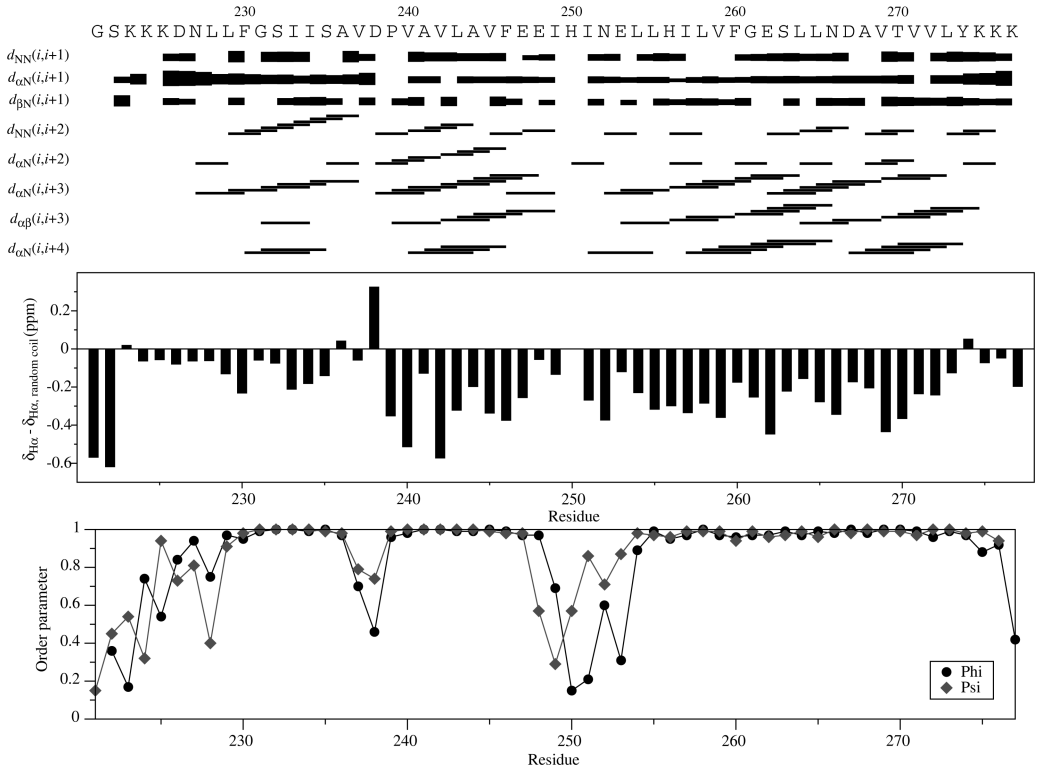

Figure 9-2. Summary of NMR structural data for TM VI–VII in DPC micelles. (Top) Summary of short/medium range residue distances obtained from the 2D and 3D NOESY NMR spectra. Lines/bars represent observed distances between residues. Continuous $d_{\alpha N}(i,i+3)$ and $d_{\alpha N}(i,i+4)$ contacts are indicative of helical structure. Adopted from CYANA (*15*) output. (Center) Chemical shift index prediction of secondary structure (*16*). Contiguous regions of negative deviation of the peptide Hα chemical shifts from random coil chemical shifts suggest helical structure. (Bottom) Dihedral angle order parameters for the final TM VI–VII structural ensemble. Values of 1 represent regions with identical dihedral angles across the structures, while values of 0 represent a random distribution of angles.

the 1D ^{1}H NMR spectrum and the assigned 2D ^{1}H-^{15}N HSQC NMR spectrum are shown in Figure 9-1.

The peptide was assigned using standard methods (*14*) using homonuclear 2D ^{1}H-^{1}H TOCSY, NOESY and DQF-COSY NMR spectra. The chemical shifts of some residues were similar those of the previously assigned individual TM VI (*7*) and TM VII (*9*) peptides, which aided the assignment process. The amide cross-peaks in the 2D ^{1}H-^{15}N HSQC NMR spectrum were assigned using 3D ^{1}H-^{15}N TOCSY and NOESY HSQC NMR spectra, which also provided structural restraints.

The distance restraints obtaining using the 2D and 3D NOESY spectra with mixing times of 150–200 ms were used to generate structural models of the peptide.

Unique NOE restraints	
Intraresidue	452
Sequential	392
Medium range ($i+2$ to $i+4$)	389
Long range ($\geq i+5$)	31
Ambiguous	484
Dihedral angle restraints	
Phi	35
Psi	35
Restraint violations	
NOE (>0.5Å)	5
Dihedral (>5.0°)	2
Ramachandran plot statistics	
Favoured regions	58.2%
Additionally allowed regions	30.5%
Generously allowed regions	8.6%
Disallowed regions	2.7%

Table 9-1. Structure calculation statistics for TM VI–VII in DPC micelles for the final top 25 out of 50 lowest energy structures.

A further 2D homonuclear NOESY with a longer mixing time of 400 ms in D_2O was used to help look for methyl and aromatic side chain contacts. The helical restraints observed are summarized in Figure 9-2. The $d_{\alpha N}(i,i+3)$ and $d_{\alpha N}(i,i+4)$ contacts and negative deviations of Hα chemical shifts from random coil chemical shifts (*16*) suggest that the regions of the helices are in agreement with the previous published individual helix structures. NOE distance restraints were calibrated based on peak intensity rather than volume due to peak overlap, and the iterative procedure to relax the restraints was used for the same reason. Dihedral angle restraints were based on chemical shift index predictions and preliminary structure calculations that did not use dihedral restraints. Helical regions were restrained to $\phi = -60 \pm 30^\circ$ and $\psi = -40 \pm 40^\circ$. Statistics from final 25 out of 50 structures are shown in Table 9-1.

The secondary structure of the final 25 structures agree with the NMR distance and dihedral restraints. The dihedral angle order parameters (lower panel of Figure 9-2) show that TM VI contains two structurally conserved regions corresponding to two short α-helices spanning residues 229–236 in the N-terminus (TM VIn) and 239–247 in the C-terminus (TM VIc). Among the 25 ensemble members, the two short helices do not have a fixed orientation with respect to each other, but adopt angles of around 0°–90°. TM VII contains one long helical region between residues 255–274. While this helix can be superimposed along its entire length, superimposition over a shorter portion of TM VII reveals some slight differences in the curvature of the TM segment among the ensemble members.

The final 25 structures of TM VI–VII show that the two helical regions are similar to the previously published structures of the corresponding individual TM

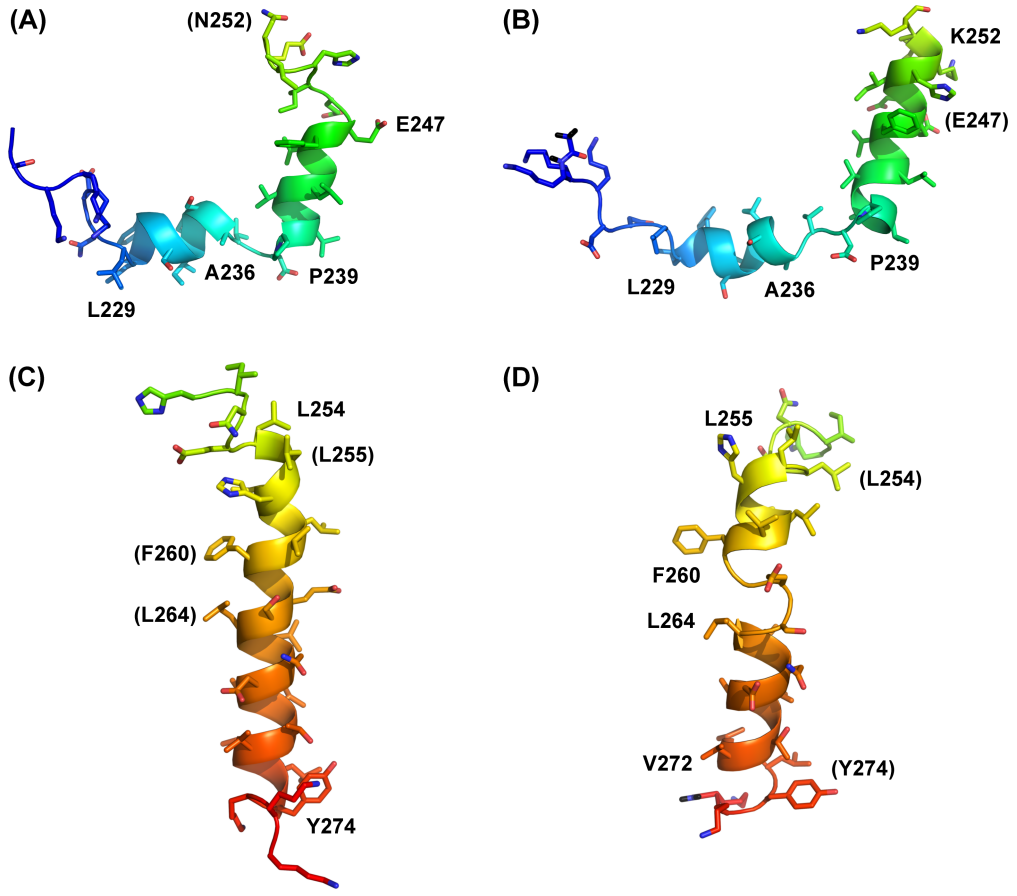

Figure 9-3. Comparisons of the TM segments of TM VI–VII with previously published structures. Comparisons of TM VI (221–250) (A) and TM VII (250–277) (C) from the structure of TM VI–VII in this study with the individual TM VI (B) and TM VII (D) structures from previous studies (*7*, *9*). The residues at the ends of the α-helices are labelled. Residues in parentheses are the helix termini of the opposing single or two-TM structure.

segments. (Figure 9-3). The overall structure and helix orientations of TM VI are mostly similar in the single-TM peptide and the TM VI–VII peptide in this study. However, in comparison to the previously published individual TM structures, TM VIc is shorter in TM VI–VII, while in the single-TM peptide, it extends further to include H250 and 2 of the 3 lysine tags (numbered as 251–253). These lysine tags are not present in the TM VI–VII peptide, which only contains the native loop residues. There is a larger difference in the structure of TM VII in the single-TM study and TM VI-VII in this study. The helical boundaries of TM VII are similar, spanning residues 254–274 in TM VI–VII compared to residues 255–272 in TM VII. The slight difference at the C-terminal end of TM VII could be due to one additional C-terminal lysine residue present in the TM VI–VII peptide that is not present in the single-TM peptide. The single TM structure of TM VII revealed a kink at residues 260–263 in the middle of the TM that allowed the two halves of TM VII to adopt either a straight or hairpin conformation. TM VII in TM VI–VII, however, forms a straight helix and does not appear to be kinked.

T_1 and T_2 relaxation measurements provide a measure of the motional properties of the peptide and are consistent with the secondary structure (Figure 9-4). The ratio of T_1/T_2 is proportional to the local rate of motion in the molecule, with lower ratios corresponding to more mobile regions and higher ratios to less mobile regions. The low T_1/T_2 ratio at the termini suggest that the termini (221–228 and 274–277) are quite mobile. Values increase up to a plateau which correspond to the location of the structured helical regions. TM VIn has a lower T_1/T_2 ratio than TM VIc, suggesting the N-terminal helix is more mobile than the C-terminal helix. Interestingly, the TM VIc has a similar T_1/T_2 ratio compared to TM VII, suggesting they are tumbling at about the same rate, even though TM VIc is about half the size of TM VII. This could suggest that there is interaction between TM VI and TM VII. The connecting loop between TM VI and TM VII may be undergoing slow conformational exchange on μs to ms timescales which could explain the decrease in T_2 and increase in T_1/T_2 ratio at residues 248–249 as well as the disappearance of residues 250–251 in the 2D HSQC spectrum . This is also reflected in the structure, where this region has lower backbone dihedral order parameters compared to the helices. This suggests that the loop does not have a fixed structure, however interaction between TM VI and TM VII could be partially restricting the conformation of the loop. Reddy et al. published relaxation data at three spectrometer frequencies for TM VII that was ^{15}N labelled at 6 specific residues (*17*). A comparison of the data obtained by Reddy et al. and in this study are shown in Figure 9-S1. Values

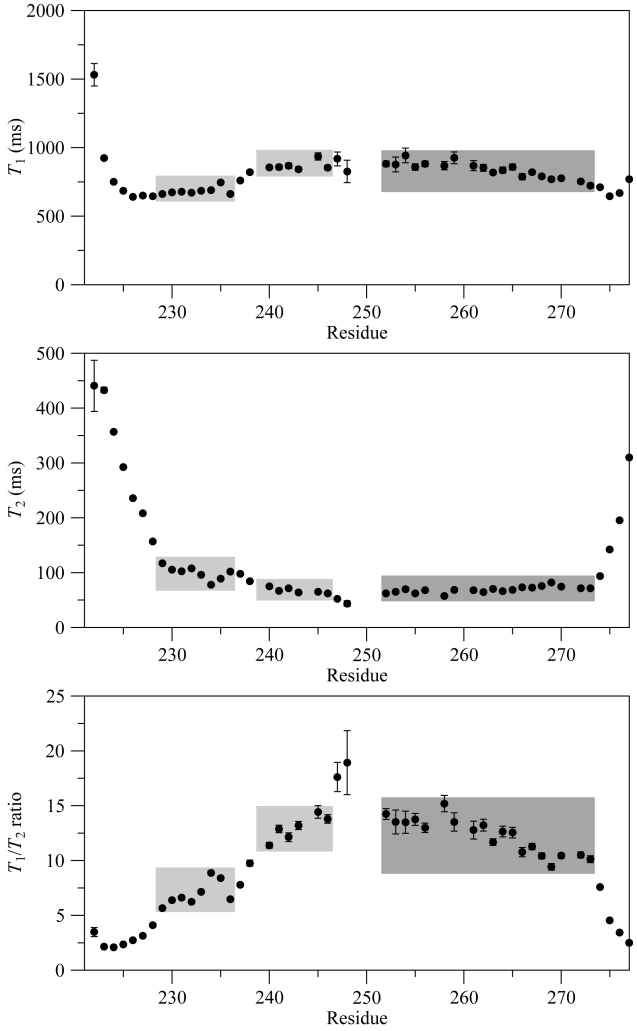

Figure 9-4. NMR ^{15}N T_1 and T_2 relaxation times and T_1/T_2 ratios for TM VI–VII in DPC micelles. Plateau regions represent the helical regions as determined by NOE and chemical shift NMR data. Helical regions of TM VI are coloured light grey, and TM VII a dark grey.

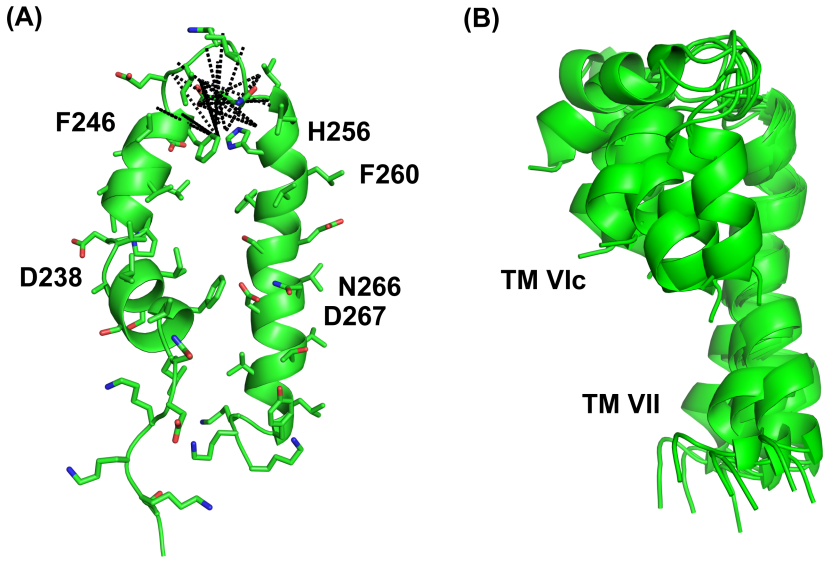

Figure 9-5. The structure of TM VI–VII in DPC micelles. (A) A representative structure of TM VI–VII showing TM–TM interaction, with the observed long range NOE restraints used in the structure calculation shown as dotted lines. (B) Superimposition of the 10 members of the structural ensemble of TM VI–VII that contain TM–TM interactions as defined by PROMOTIF. The structures are superimposed over the backbone Cα atoms of residues 254–264 of TM VI–VII. Residues 220–237 of TM VI are not shown for clarity.

for T_2 at 600 MHz are slightly higher in the individual TM VII likely reflecting the smaller size of the single TM peptide compared to TM VI-VII. T_1 values appear to be similar and perhaps slightly lower for TM VII in TM VI–VII at the C-terminus. T_1/T_2 ratios are larger for TM VII in TM VI–VII on the N-terminus but similar at the C-terminus. Overall the comparison is consistent with the higher molecular weight of TM VI–VII and less mobility at the N-terminus of TM VII in the two TM peptide due to the presence of TM VI.

The calculated structures show a weak interaction between TM VI and TM VII. Based on PROMOTIF (*18*) structural analysis, TM VIn does not interact at all with TM VII, which would also be consistent with the relaxation results. 10 out of the 25 final structures show an interaction between the TM VIc and TM VII according to PROMOTIF. A representative structure is shown in Figure 9-5, A, with the identified long range restraints shown. Long range restraints occur mainly between residues close to, or within, the interhelical loop. Many contacts originate from F246 and H256 to other residues in the vicinity. NOE contacts between the lower half of the TM VIc and TM VII could not be observed, suggesting that this region TM VIc interacts very weakly or not at all with TM VII. As a result of this, the

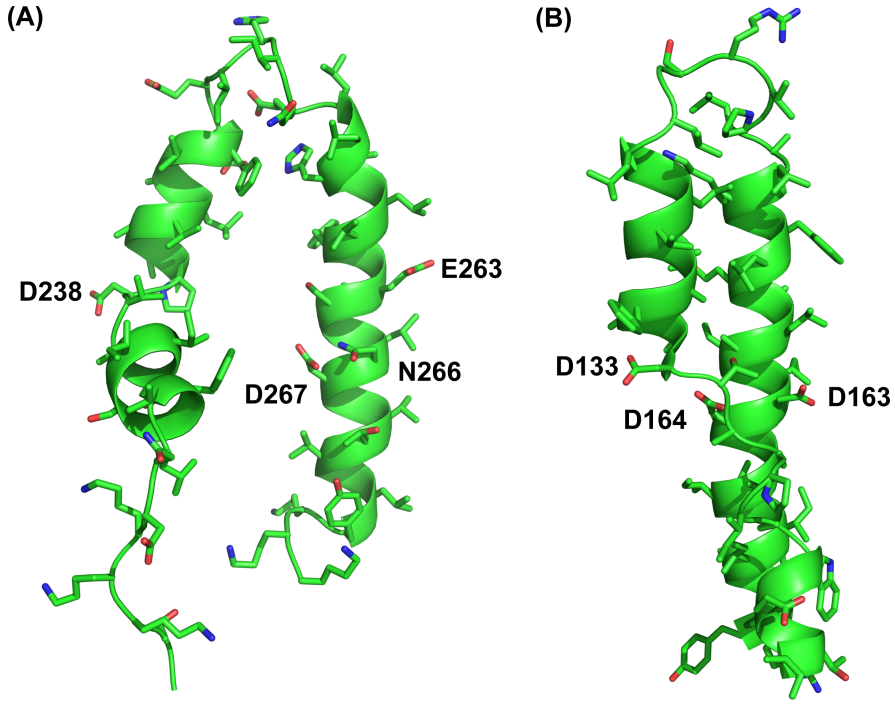

Figure 9-6. Comparison of a representative NMR structure of TM VI–VII with TM 4–5 of NhaA. Functionally important residues are labelled.

TM VIc does not always lie along TM VII in the structural ensemble, but sometimes orients perpendicularly to TM VII. The conformational flexibility prevents defining a precise interface between TM VI and VII. However, in the 10 structures above, the interactions between the helices are primarily between F246 on TM VI and H254 on TM VII. These residues are part of the helical regions of their respective TMs, and likely other residues on the same face of both helices could participate in the interaction, even though no NOE contacts could be observed. An ensemble of structures showing the potential TM–TM interactions is shown in Figure 9-5, B.

Landau et al. (*2*) suggest that the TM VI–VII region examined in this paper are equivalent to TM 4–5 in NhaA, based on homology modelling and evolutionary conservation analyses. TM 4 of NhaA contains two short helices separated by an extended region and contains a conserved aspartate (D133) at the start of the C-terminal helix. TM 5 of NhaA is a straight helix containing two conserved and functionally important aspartate residues (D163–D164) involved in ion binding and transport (*19*, *20*). In a three dimensional model of NHE1 by Landau et al. (*2*) based on the NhaA structure, TM VI–VII of NHE1 shows the same features as TM 4–5 of NhaA. The model has TM VI positioned such that the extended region is placed near the side chains of TM VII, N266-D267, where this cluster of charged

and polar residues would be predicted to play a role in the ion binding and transport mechanism. N266–D267 are proposed to be homologous to D163–D164 in NhaA. They further orient TM VI and TM VII such that on the cytoplasmic halves of TM VI and TM VII, including residues P239, V242–L243, F246 on TM VI and L255–H256, V259–260, S263 on TM VII, as well as N266–D267 form a face on which the helices interact. The extracellular ends of the helices do not interact as strongly in the model or in NhaA. NMR studies on TM VI–VII show that this region in NHE1 has a similar structure to TM 4–5 in NhaA. TM VI has the same discontinuous structure and TM VII is a straight helix. TM VI does not lie completely along TM VII as it does in the Landau model. Interactions between the N-terminal and extended region of TM VI and TM VII are missing. Due to the lack of restraints along TM VI and TM VII, the extended region comes close to the acidic residues of TM VII only in a few structures. The interface closer to the loop, however is similar. It includes the residues predicted to interact in the Landau model, particularly the aromatic residues. A comparison of the NMR structure of TM VI–VII and TM 4–5 of NhaA is shown in Figure 9-6. The weaker interaction of TM VI and TM VII compared to those predicted in the Landau model likely suggest that additional interactions in the full protein may be important in maintaining the structure of TM VI–VII, by anchoring the free ends of the peptide and providing additional packing constraints to encourage the proper interaction of the helices. Nevertheless, the partial interaction of the two helices in the NMR structure suggest that the weak interactions in TM VI–VII and the structure of the connecting loop play a partial role in defining the structure and folding of this region. The crystal structure of NhaA, off which the Landau model is based, is an "acid-locked" inactive state (*21*). Conformational changes occur in NhaA on activation and during transport which include changes in the conformation of TM 6 (*19*, *22*). Thus it may also be important that the interaction between TM 6 and 7 not be strong to allow for these conformational changes as well.

In conclusion, we have successfully expressed and solved the structure of a two-transmembrane segment of the Na^+/H^+ exchanger, NHE1. The structure of TM VI–VII in DPC micelles consists of two helices separated by an extended region in TM VI, and a straight helix in TM VII. A resemblance of NHE1 TM VI–VII to TM 4–5 of NhaA may suggest that these two regions share the same structure and function in the full protein. Further experiments using mutagenesis will help to confirm the conclusions made by NMR in this study. This study may also hold promise for solving the structures of larger transmembrane segments as well as the complete structure of NHE1.

Supplementary Materials

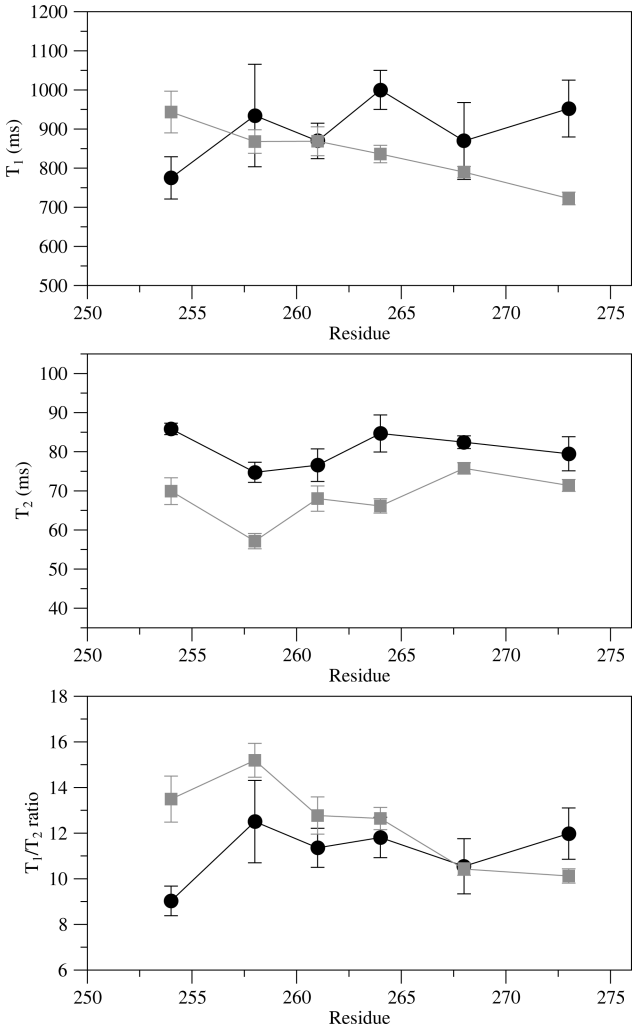

Figure 9-S1. Comparison of ^{15}N relaxation data for TM VII from TM VI–VII (this study, grey squares) and from the isolated TM VII (black circles) from Reddy et al. (*17*), at a 600 MHz spectrometer frequency, showing T_1, T_2 and T_1/T_2.

References

1. Wakabayashi, S., Pang, T., Su, X., and Shigekawa, M. (2000) A novel topology model of the human Na^+/H^+ exchanger isoform 1. *J. Biol. Chem. 275*, 7942–7949.
2. Landau, M., Herz, K., Padan, E., and Ben-Tal, N. (2007) Model structure of the Na^+/H^+ exchanger 1 (NHE1): functional and clinical implications. *J. Biol. Chem. 282*, 37854–37863.
3. Kemp, G., Young, H., and Fliegel, L. (2008) Structure and function of the human Na^+/H^+ exchanger isoform 1. *Channels 2*, 329–336.
4. Cunningham, F., and Deber, C. M. (2007) Optimizing synthesis and expression of transmembrane peptides and proteins. *Methods 41*, 370–380.
5. Hunt, J. F., Earnest, T. N., Bousché, O., Kalghatgi, K., Reilly, K., Horváth, C., Rothschild, K. J., and Engelman, D. M. (1997) A biophysical study of integral membrane protein folding. *Biochemistry 36*, 15156–15176.
6. Katragadda, M., Chopra, A., Bennett, M., Alderfer, J. L., Yeagle, P. L., and Albert, A. D. (2001) Structures of the transmembrane helices of the G-protein coupled receptor, rhodopsin. *J. Pept. Res. 58*, 79–89.
7. Tzeng, J., Lee, B. L., Sykes, B. D., and Fliegel, L. (2010) Structural and functional analysis of transmembrane segment VI of the NHE1 isoform of the Na^+/H^+ exchanger. *J. Biol. Chem. 285*, 36656–36665.
8. Tzeng, J., Lee, B. L., Sykes, B. D., and Fliegel, L. (2011) Structural and functional analysis of critical amino acids in TMVI of the NHE1 isoform of the Na^+/H^+ exchanger. *Biochim. Biophys. Acta, Biomembr. 1808*, 2327–2335.
9. Ding, J., Rainey, J. K., Xu, C., Sykes, B. D., and Fliegel, L. (2006) Structural and functional characterization of transmembrane segment VII of the Na^+/H^+ exchanger isoform 1. *J. Biol. Chem. 281*, 29817–29829.
10. Ding, J., Ng, R. W. P., and Fliegel, L. (2007) Functional characterization of the transmembrane segment VII of the NHE1 isoform of the Na^+/H^+ exchanger. *Can. J. Physiol. Pharmacol. 85*, 319–325.
11. Douglas, J. L., Trieber, C. A., Afara, M., and Young, H. S. (2005) Rapid, high-yield expression and purification of Ca^{2+}-ATPase regulatory proteins for high-resolution structural studies. *Protein Expr. Purif. 40*, 118–125.
12. Slepkov, E. R., Rainey, J. K., Li, X., Liu, Y., Cheng, F. J., Lindhout, D. A., Sykes, B. D., and Fliegel, L. (2005) Structural and functional characterization of transmembrane segment IV of the NHE1 isoform of the Na^+/H^+ exchanger. *J. Biol. Chem. 280*, 17863–17872.
13. Schägger, H. (2006) Tricine-SDS-PAGE. *Nat. Protoc. 1*, 16–22.
14. Wüthrich, K. (1986) *NMR of Proteins and Nucleic Acids*, John Wiely & Sons, New York, NY.

15. Güntert, P. (2004) Automated NMR structure calculation with CYANA. *Methods Mol. Biol. 278*, 353–378.

16. Wishart, D. S., Sykes, B. D., and Richards, F. M. (1992) The chemical shift index: a fast and simple method for the assignment of protein secondary structure through NMR spectroscopy. *Biochemistry 31*, 1647–1651.

17. Reddy, T., Li, X., Fliegel, L., Sykes, B. D., and Rainey, J. K. (2010) Correlating structure, dynamics, and function in transmembrane segment VII of the Na^+/H^+ exchanger isoform 1. *Biochim. Biophys. Acta, Biomembr. 1798*, 94–104.

18. Hutchinson, E. G., and Thornton, J. M. (1996) PROMOTIF—a program to identify and analyze structural motifs in proteins. *Protein Sci. 5*, 212–220.

19. Arkin, I. T., Xu, H., Jensen, M. Ø., Arbely, E., Bennett, E. R., Bowers, K. J., Chow, E., Dror, R. O., Eastwood, M. P., Flitman-Tene, R., Gregersen, B. A., Klepeis, J. L., Kolossváry, I., Shan, Y., and Shaw, D. E. (2007) Mechanism of Na^+/H^+ antiporting. *Science 317*, 799–803.

20. Rimon, A., Kozachkov-Magrisso, L., and Padan, E. (2012) The unwound portion dividing helix IV of NhaA undergoes a conformational change at physiological pH and lines the cation passage. *Biochemistry 51*, 9560–9569.

21. Hunte, C., Screpanti, E., Venturi, M., Rimon, A., Padan, E., and Michel, H. (2005) Structure of a Na^+/H^+ antiporter and insights into mechanism of action and regulation by pH. *Nature 435*, 1197–1202.

22. Appel, M., Hizlan, D., Vinothkumar, K. R., Ziegler, C., and Kühlbrandt, W. (2009) Conformations of NhaA, the Na^+/H^+ exchanger from *Escherichia coli*, in the pH-activated and ion-translocating states. *J. Mol. Biol. 386*, 351–365.

Chapter 10

Preliminary NMR studies of three-transmembrane fragments of NHE1 and full-length *E. coli* NhaA

Grant Kemp performed TM V–VII peptide expression and purification, Arghya Basu and Yongsheng Liu performed NhaA expression and purification, and BLL performed the NMR experiments.

Summary

The Na^+/H^+ exchanger isoform 1 (NHE1) is an integral membrane protein responsible for regulating intracellular pH. It is predicted to contain 12 transmembrane (TM) helices based on cysteine scanning accessibility studies. To gain further insight into the structure and function of NHE1, we have adopted a "divide and conquer approach." We have previously examined individual TM helices of NHE1, using NMR to determine the structure of individual helices, and detailed mutagenesis studies to examine their function. More recently, we have solved the structure of a two transmembrane region of NHE1, containing TMs VI–VII. In this chapter, we describe preliminary results on experiments with larger, three-TM regions, containing TM V–VII and TM X–XII. We successfully expressed and obtained good quality NMR spectra of the TM V-VII peptide. We further obtain 1D ^{13}C solid state NMR spectra of *E. coli* NhaA in lipid bilayers. These experiments may allow us further study the TM–TM interactions between the helices of NHE1 as well as provide a starting point to studying the full length NHE1 using solid-state NMR.

Introduction

We have previously been successful in using combined NMR and biochemical techniques to characterize the structure and function of individual transmembrane (TM) helices of NHE1. 5 TM helices, TM IV, VI, VII, IX, and XI, as well as two extracellular loops, EL2 and EL4 have been studied in this manner (*1–7*). The TM helices were not simple alpha-helices, but rather were found to contain unusual structural features in the NMR structures such as kinks and extended regions. Furthermore, these regions correlated well with residues that were functionally important in the full protein. TM IV contained regions of beta-turn, extended and helical character. TM VI and XI contain extended regions in the center of the TM helices surrounded on either side by more canonical helical segments. TM IV contained a short helical segment and a short region of overlapping beta-turns. TM VII and IX contain kinks in the center of the helices. These regions all contain functionally important residues; mutation of these residues often strongly reduced the activity of NHE1 in vitro.

While we can obtain detailed structural information about single TM helices in this manner, we would also like to know about the interactions and relative positions of the TM helices within NHE1. Interactions between transmembrane helices are important for the proper folding and incorporation of membrane proteins into the lipid bilayer, which can also affect the function of the protein. In cells, the insertion of the TM helices is regulated by the Sec translocation machinery (*8*), and the helices were generally found to enter the translocon sequentially and were displaced into the bilayer environment as the next helix entered (*9*). However, additional TM–TM interactions may be need to stabilize certain TM helices in the bilayer. In aquaporin, the first two TMs returned to the translocon to interact with the third TM as it exited the translocon (*9*). Marginally hydrophobic TM helices were found to require the presence of the flanking loop regions or adjacent TM helices to properly insert (*10*).

To examine the TM–TM interactions in NHE1, we previously studied a two TM segment corresponding to the TM VI and TM VII regions (residues 227–270) of the protein (Chapter 9). TM VI–VII is suggested to represent TM 4–5 of NHE1 by Landau et al. (*11*). TM 4 and 5 of NhaA contain three negatively charged aspartate residues in the center of the TM helices: D133, D164, and D165. These three aspartates are believed to be directly involved in the ion binding and transport mechanism of NhaA (*12*, *13*). The Landau model suggests that these residues would

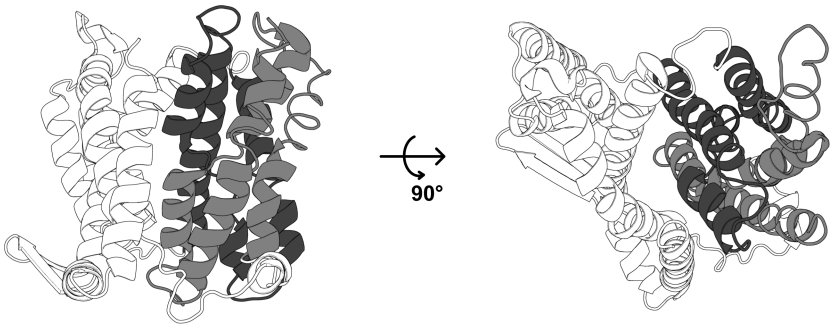

Figure 10-1. Crystal structure of NhaA highlighting the three-TM regions. TM 3–5 (residues 94–175) and TM 10–12 (residues 293–384) are shaded in dark grey and light grey, respectively. The cytoplasmic side of the exchanger is at the top and the periplasmic side on the bottom for the left-side cartoon.

be homologous to D240, N263, and D264 in NHE1, residues which we have shown to be important for NHE1 function. The structure of this critical region can help us understand the details of the transport mechanism of NHE1. Due to the larger size of this peptide compared to the single transmembrane segments, the peptide was produced biosynthetically. The peptides were produced as fusion proteins to maltose binding protein (MBP), to improve solubility, stability and handling of the peptides during expression and purification (*14*). The NMR structure of the TM regions in TM VI–VII are nearly identical to the individually determined TM VI and TM VII structures. The two TM regions appear to be only weakly interacting around the proximity of the connecting loop, but not interacting along the remainder of the length of the regions. Nevertheless, the structure was similar to TM 4–5 of NhaA.

In NhaA, TM 4 and 5 interact along their lengths in the crystal structure, unlike the NMR structure of TM VI–VII in DPC micelles. TM 4 and 5 also interact with TM 3 in NhaA to form a three-helix bundle. TM 3–5 in turn interact with TM 10–12 forming a structure with a two-fold symmetry (*15*). Figure 10-1 shows the structure of NhaA and the critical TM 3–5 and TM 10–12 bundles. This 6-helix motif is also present in the structures of the *Methanococcus jannaschii* Na^+/H^+ exchanger NhaP1 (*16*) and the bile acid/sodium symporter ASBT (*17*). TM 3 in NhaA is proposed to be homologous to TM V in NHE1 (*11*). Therefore, it may be possible that TM V in NHE1 is important in the proper folding of TMs V–VII. The additional helix and its interactions may help to restrain the ends of the TM VI and/or TM VII in the NMR structure of TM VI–VII where the two ends do not interact. Similarly, TM X and XII in NHE1 may be important in maintaining the structure of the TM X–XII segment.

For this reason we decided to investigate the structures of the regions TM V–VII and TM X–XII of NHE1. As with TM VI–VII, these peptides were produced as MBP fusion proteins as described previously (Chapter 8). We were successful in expressing the TM V–VII segment which also gave promising preliminary NMR spectra. Additional NMR spectral acquisition is underway which may allow us to determine the structure of this three-TM segment of NHE1.

In addition to examining the structures of large segments of NHE1, we also describe NMR experiments on full length *E. coli* NhaA. NhaA can form both 2D (*18*) and 3D crystals (*19*) which has allowed for a structure to be solved to 3.45 Å using x-ray diffraction (*15*). NhaA can be overexpressed in milligram amounts in *E. coli* (*19*), and since it is expressed in defined minimal media (*20*), can potentially be ^{15}N- and/or ^{13}C-isotopically labelled for NMR studies without significant modification of the expression protocols. NMR studies of NhaA could provide information about the dynamics or inhibitor binding of the protein at atomic resolution, building upon the static picture provided by x-ray crystallography or the lower resolution information from biochemical experiments and 2D crystallography. NhaA can also be used as a model Na^+/H^+ exchanger with which we can develop the methodologies needed to eventually study full-length NHE1 using NMR. NHE1 can be overexpressed in *Saccharomyces cerevisiae* (*21*), where further optimization of the expression could allow for sufficient protein for NMR studies of NHE1.

The large size of NhaA, combined with the additional size from the solubilizing detergent micelles would make solution-state NMR difficult. While large membrane protein structures have been determined by solution-state NMR (*22*, *23*), they require multiple samples with different labelling schemes, high levels of deuteration, and expensive site-specific labelling schemes. A recent structure of the 37 kDa CXCR1 GPCR protein using magic-angle spinning (MAS) solid-state NMR techniques and uniform ^{15}N- and ^{13}C-labelling suggests that solid-state NMR may be a promising method for determining membrane protein structures (*24*). In MAS NMR, the sample is physically spun rapidly, which cancels out the factors that cause broad lines in non-spinning solid-state NMR and in solution-state NMR of large proteins, and results in the sharp lines of "solution-state-like" spectra. MAS NMR would also allow for the study of membrane proteins in lipid vesicles, a more native-like environment than the detergents used for solution-state NMR or x-ray crystallography. Therefore, in this chapter, we also present our preliminary work on performing MAS solid-state NMR studies of NhaA in liposomes.

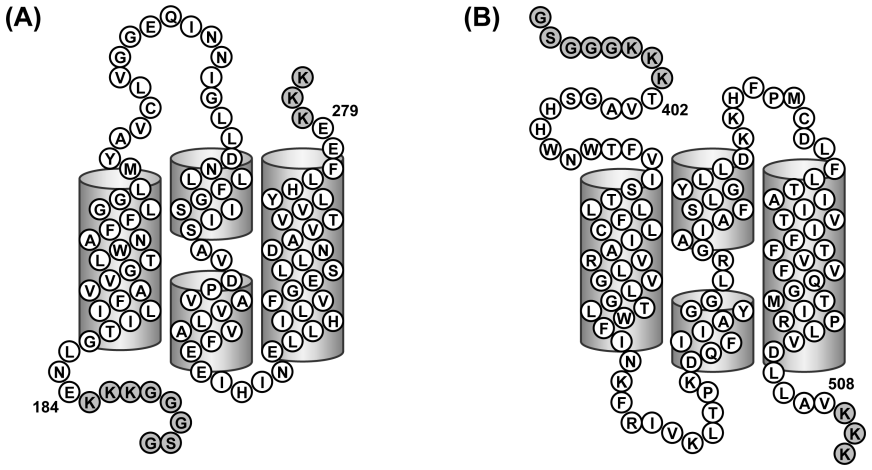

Figure 10-2. Sequences and predicted topologies for TM V–VII and TM X–XII of NHE1. TM V–VII (residues 184–279) (A) and TM X–XII (residues 402–508) (B) were expressed as maltose binding protein fusions with a glycine spacer, an TEV cleavage site (which leaves the N-terminal G and S residues on the peptide), and three lysines on the N- and C- termini of the peptide. Native NHE1 residues are shown in white, and added residues are shown in grey. Topology predictions are based on the Landau et al. model (*11*) however the boundaries of the helices only vary by a few residues for these regions compared to the Wakabayashi et al. model (*25*).

Methods

TM V–VII and TM X–XII were overexpressed and purified as described for sod2 TM IV (Chapter 8), however an additional HPLC purification step was performed after organic extraction. The sequences and predicted topologies for these two regions are shown in Figure 10-2. HPLC purification resulted in peptide dissolved in isopropanol (IPA)/water which could be exchanged by evaporation or lyophilization of the solvent. NMR sample preparation and spectral acquisition were performed as described in Chapter 2. Samples in detergent were produced by dissolving the detergent in the IPA/water mixture, followed by dilution, lyophilization, and reconstitution in water/buffer. NMR spectra acquired included 1D ^{1}H NMR spectra for preliminarily examination of unlabelled peptides and 2D ^{1}H-^{15}N HSQC spectra for ^{15}N-labelled peptides. 3D NOESY and TOCSY-HSQC spectra were also obtained for TM VI–VII in SDS micelles. Spectra were obtained at 30 °C and at spectrometer frequencies of 500 or 600 MHz.

NhaA expression and purification was performed as described (*20*). The *E. coli* strain expressing His-tagged NhaA was a gift from Dr. Etana Padan. Briefly, NhaA expressing cells were grown in minimal media containing 7.5 mM $(NH_4)_2SO_4$

as the sole nitrogen source and 0.5% glycerol as the sole carbon source. ^{13}C labelled NhaA was produced by replacing the 0.5% glycerol with 0.25% [U-^{13}C]-glycerol. Cultures were grown in standard flasks rather than a fermenter as described in the protocol. The bacteria were lysed using ultrasonication, and the bacterial membranes containing NhaA were isolated using centrifugation. The membranes were solubilized in a DDM-containing buffer and His-tagged NhaA was purified using a nickel affinity column. The purified NhaA was then dialyzed against pH 4 buffer and further purified by gel filtration chromatography. The purified protein was stored at 4 °C.

NhaA liposome samples were also prepared as described (*20*). Purified NhaA was concentrated using centrifugal concentration (Millipore Amicon concentrators, 30 kDa cutoff). 12.5 mg *E. coli* polar lipids (Avanti) were solubilized in ∼12.5 mg DDM. Concentrated NhaA was added to the lipid/detergent solution and incubated on ice for 30 min. Detergent removal and liposome reconstitution was performed by adding activated Biobeads to the solution and incubating overnight at 4 °C. An additional volume of Biobeads was then added and the sample incubated at room temperature for 1 h. Liposomes were pelleted by ultracentrifugation at $100000 \times g$ at 4 °C for 1 h. The resulting lipid pellet was then transferred to a thin walled MAS NMR rotor by centrifugation in a swinging bucket rotor. MAS NMR was performed at room temperature and at a spinning speed of 9 kHz. 1D direct ^{13}C-NMR spectra (using the pulse sequence onepul.c in VnmrJ (Agilent Inc.)) and 1D tangent-ramped cross-polarization ^{13}C-NMR (tancpx.c) spectra were acquired for the sample.

Results

TM V–VII and TM X–XII

The two three-TM peptides were designed based on the Landau et al. model (*11*) of NHE1. The regions correspond to TM 3–5 and 10–12 in the Landau et al. model, and also cover TM V–VII and X–XII in the Wakabayashi et al. model (*25*), representing residues 184–279 and 402–508 of NHE1. While the numbering of the helices are different in the two models, the sequences and predicted boundaries of the helices are nearly the same, only varying by a few residues on the ends of the helices. Lysines were added to the termini as in previous studies (*2–4*) to aid in the solubility and purification of the peptides. A TEV cleavage site on the N-terminus was included to separate MBP from the TM peptide. Glycine spacers

between the TEV cleavage site and the remainder of the protein aided in the efficient cleavage of the TM segments from MBP. The sequences of the peptides are shown in Figure 10-2.

Initial characterization of the peptides utilized the peptide directly obtained from the organic extraction step, similar to TM IV of sod2 (Chapter 8). A 1D ^{1}H NMR spectrum of TM V–VII in chloroform/methanol/water showed reasonable resolution and dispersion of peaks in the amide and aromatic region. Attempts to reconstitute the peptide in detergent micelles generally resulted in broader, less defined peaks in the amide/aromatic region of the spectra. ^{15}N labelling allowed us to use 2D ^{1}H-^{15}N HSQC spectra for screening of samples. The additional spectral dimension allowed us to examine the quality of the samples in a clearer way than the 1D spectra. The quality of the samples can be determined through the dispersion and linewidth of the peaks, which represent the amide H–N pairs in the sample. Non-deuterated solvents and detergents can also now be used; signals from these components will not be visible in the HSQC spectra. The same trend was seen in ^{15}N-labelled samples as the unlabelled samples: peptide dissolved in solvent resulted in narrow peaks and peptide dissolved in detergents resulted in broader peaks. Various solvent combinations and proportions were tested, including chloroform/isopropanol/water, chloroform/trifluoroethanol, and pure isopropanol. Detergents tested included DPC, SDS, LPPC, and LDAO. In some cases, salt concentration, and temperature were also varied, although without significant effect. Due to the somewhat poorer quality of the initial X–XII 1D ^{1}H spectra compared to TM V–VII, we decided to focus on the optimization of the TM V–VII peptide expression and sample preparation for NMR spectroscopy.

The 1D ^{1}H NMR spectra contained additional non-peptide, non-detergent peaks that were likely a contaminant from the organic extraction procedure. Therefore, an additional HPLC purification step was performed. HPLC purification provided peptide solubilized in isopropanol/water. This vastly improved the purity of the samples, as the unidentifiable peaks were no longer present in the 1D NMR spectra. The additional purification step may have also improved the quality of the TM V–VII peptide. The peptide could be incorporated into detergent micelles by addition of detergent to the purified peptide in isopropanol/water, followed by dilution with water and lyophilization of the sample. The samples were then redissolved in 95% H_2O, 5% D_2O, 0.25 mM DSS, and 1–10 mM imidazole for NMR. 2D HSQC spectra of ^{15}N-labelled TM V–VII in solvent and detergents are shown in Figure 10-3. Low concentration samples (< 0.5 mM) containing TM V–VII in

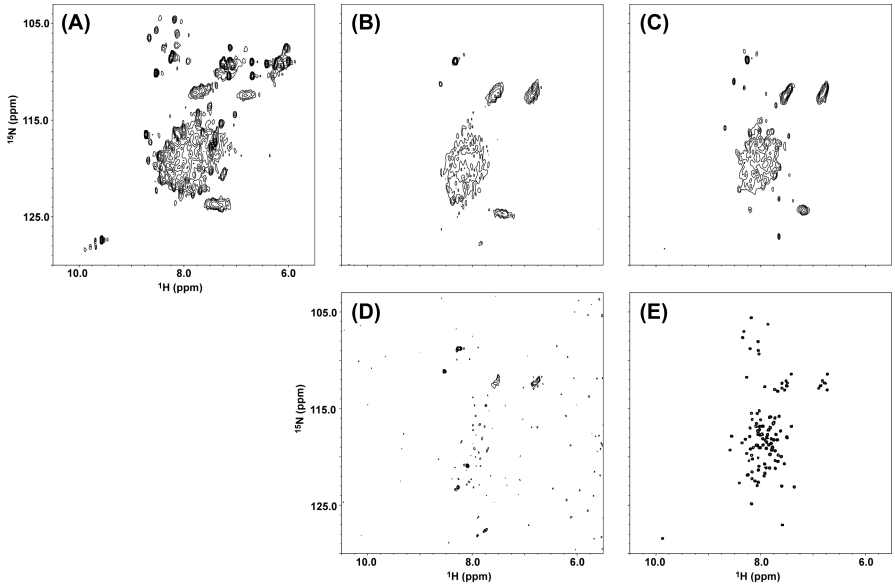

Figure 10-3. 2D ^{1}H-^{15}N HSQC spectra of TM V–VII in different membrane mimetic conditions. (A) Spectrum of TM V–VII in chloroform/isopropanol/water directly from the organic extraction step (see Methods). (B–E) Spectra of TM V–VII in DPC (B,D) and SDS (C,E), without (B,C) and with (D,E) HPLC purification. The spectra from peptide that did not undergo HPLC (A–C) were obtained on a 500 MHz spectrometer, while spectra of HPLC-purified peptide (D–E) were obtained on a 600 MHz spectrometer. A spectrum of HPLC purified peptide in organic solvent was not obtained due to artifacts arising from the intense isopropanol signal.

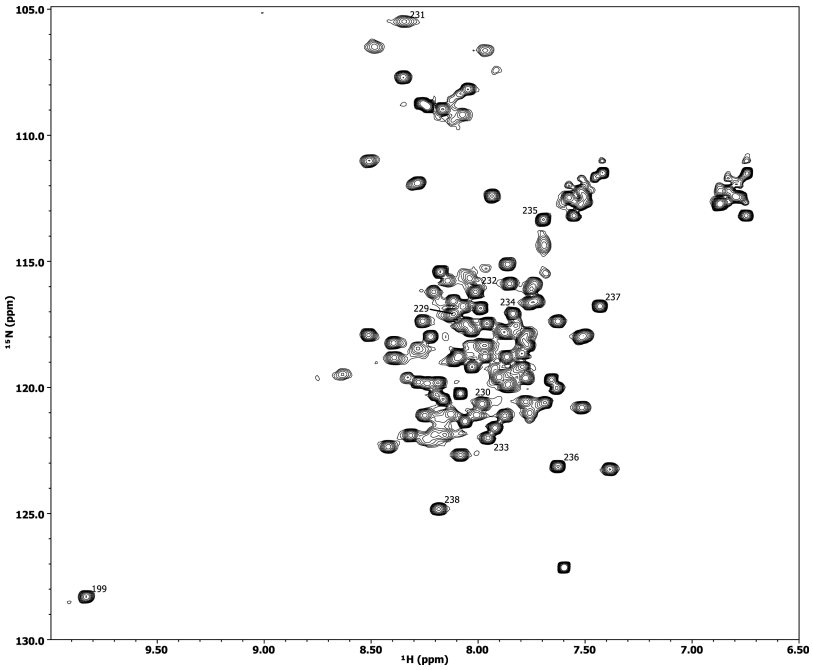

Figure 10-4. 2D ^{1}H-^{15}N HSQC spectrum of TM V–VII in SDS micelles. The indole HN of F199 and a fragment of TM VI has been assigned and is labelled.

DPC did not provide good HSQC spectra, however, surprisingly, samples in SDS provided excellent spectra containing ∼90% of the total number of expected peaks (Figure 10-4). The narrow peaks and the use of a strong detergent such as SDS may have suggested an unfolded peptide. However, CD spectroscopy suggested that the peptide was predominantly helical (not shown), and therefore may still be folded even in high SDS concentrations.

More concentrated samples (∼0.5–1 mM) of ^{15}N-labelled TM V–VII were used to obtain 2D ^{1}H-^{15}N HSQC, 2D ^{15}N-filtered ^{1}H-^{1}H NOESY and 3D NOESY-HSQC spectra. The HSQC spectrum (Figure 10-4) contains approximately the same number of peaks as the low concentration sample, however the peaks are broader, with more variation in the heights/linewidths of the peaks, and some peak positions have shifted. The differences could reflect peptide and/or detergent concentration-dependent differences in the sample. HN–HN peaks are clearly visible in the 2D NOESY spectrum, suggesting that helical structure is present. The lower concentration of peptide in the previous samples likely prevented the easy identification of HN–HN contacts, which were near the noise level in those samples. The NOESY-HSQC spectrum also appear to contain HN–Hα crosspeaks downfield of the water signal. This may be the downfield shifted Asp Hα also observed in TM VI (*4*) and TM VI–VII (Chapter 9).

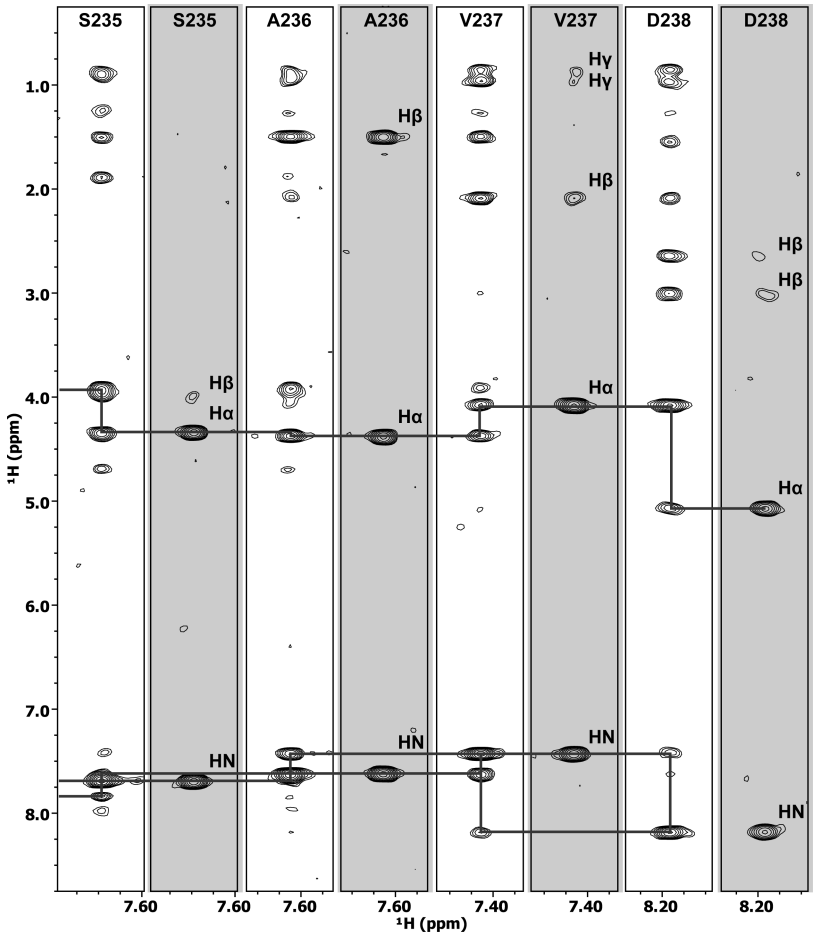

Figure 10-5. Strip plot for assignment of TM V–VII. The strips show regions from the 1H-1H 2D planes of the 3D NOESY-HSQC (white strips) and 3D TOCSY-HSQC (shaded strips). The residues are labelled on top and identifiable TOCSY peaks are labelled on the TOCSY strips to the side of the peaks. Sequential HN–HN and Hα–HN connectivities used in assignment are shown as lines connecting the relevant NOESY peaks in the strips.

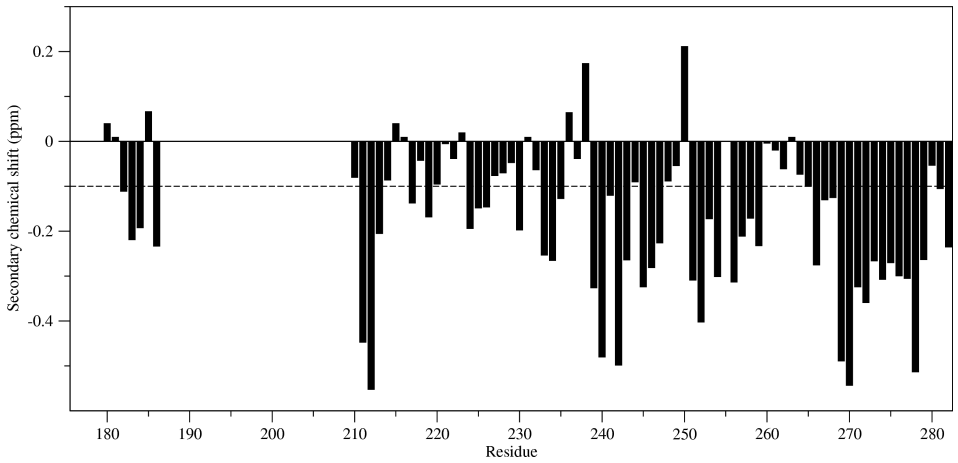

Figure 10-6. Predicted secondary structure of TM V–VII using Hα chemical shifts. TM V (residues 187–209), L255, and the N-terminus could not be assigned and are not shown. The difference between observed Hα chemical shifts and random coil chemical shifts (*26*) is related to secondary structure (*27*). Contiguous regions < -0.1 ppm are indicative of helical conformation, while regions > 0.1 ppm are indicative of extended conformation.

The excellent quality of the spectra of TM V–VII in SDS micelles should allow us to assign a large portion the peptide. An example of the assignment process using the 3D TOCSY and NOESY spectra is shown in Figure 10-5 for the extended region of TM VI (residues 235–238). We were able to assign the majority of TM VI and TM VII backbone resonances for the peptide except for L255. A prediction of the secondary structure of the peptide using Hα chemical shifts is shown in Figure 10-6. The trends in secondary chemical shift in TM VI (residues 227–249) are similar to the individual peptide (Chapter 6) and the 2-TM peptide (Chapter 9), indicating the secondary structure is also similar to the previously determined structures. TM VII (residues 251–273) appears to be mostly helical except for a small region (260–264) in the center of the helix. This corresponds to the kink seen in the isolated TM VII peptide structure (*2*), although the kink is not seen in the 2-TM peptide (Chapter 9). However, neither of the two previous peptides contain such a trend in chemical shifts. Additional NOE distance restraints may help confirm or deny the presence of a kink in this 3-TM peptide. TM V (residues 191–221) could not be assigned, as the peaks appear to become broad and low in intensity over this region. Aggregation or conformational heterogeneity of TM V is the likey cause. These missing peaks may be observable with further optimization of the ^{15}N-labelled samples or possibly with alternative isotopic labelling schemes that include ^{2}H- and/or ^{13}C-labelling. ^{13}C-labelling will also allow us to assign the side chain proton and carbon resonances

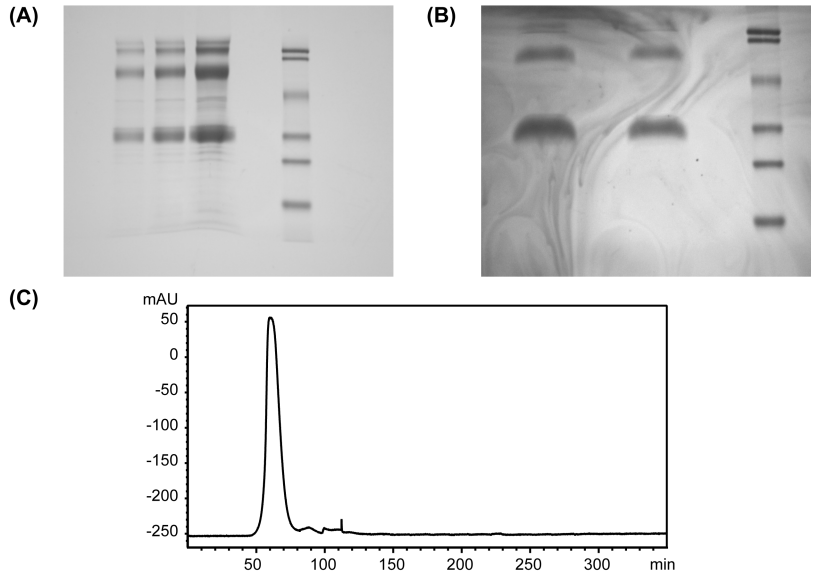

Figure 10-7. Purification of NhaA. SDS-PAGE gels of NhaA overexpression in *E. coli* after (A) purification on a nickel-affinity column and (B) after gel filtration. (C) Elution profile from gel filtration. Molecular weight standards in the rightmost lanes, and varying volumes of NhaA loaded in each lane.

such that we can search for interresdiue side chain contacts that would define the tertiary structure of the TM V–VII peptide in SDS micelles.

NhaA

NhaA expression followed the protocol of Venturi et al. (*20*). The yields of protein obtained were similar to the protocol, and appeared quite pure after gel filtration (Figure 10-7). The protein also appeared to be reasonably stable at 4 °C for a period of months. Some samples precipitated over time; it is possible that the detergent concentration or protein purity of those samples were less than ideal. For NMR spectroscopy, the protein was labelled with uniformly ^{13}C-labelled glycerol. We found that reducing the glycerol concentration from 0.5 to 0.25% for isotopic labelling did not have a significant effect on the yield of protein, while reducing costs. A longer incubation time of the protein with the nickel-affinity resin also increased the yield of recovered protein. The elution profile of the protein during the final purification step by size exclusion chromatography showed only a single peak, suggesting the protein was relatively pure and homogeneous at this point.

The protein was reconstituted in liposomes for NMR studies following the protocol in Venturi et al. (*20*). For NMR, 12.5 mg lipid and 3–4 mg NhaA were solubilized in DDM and the detergent removed using Biobeads to form proteolipo-

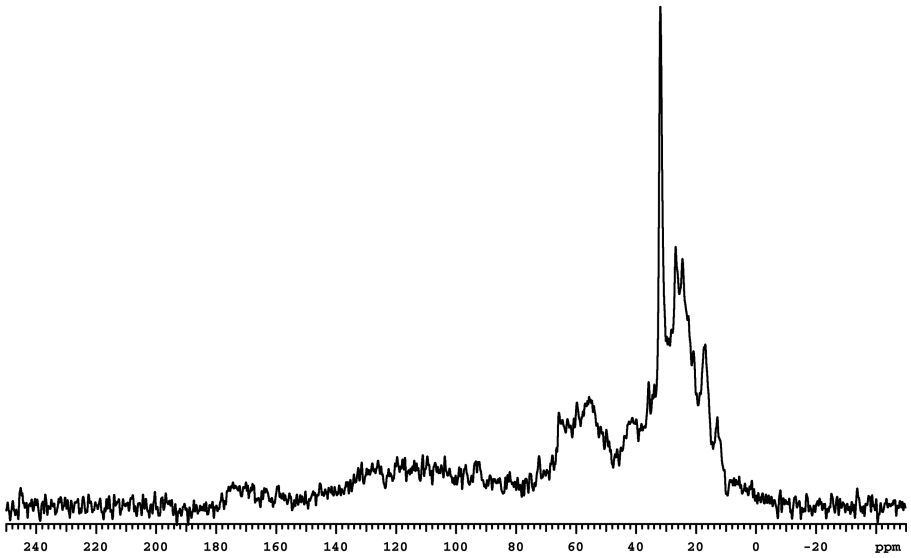

Figure 10-8. 1D ^{13}C MAS NMR spectrum of NhaA in liposomes.

somes. *E. coli* lipids were used as per the protocol, for a native lipid environment. Dimyrystolphosphatidylcholine (DMPC) is a commonly used synthetic lipid for model membranes. In our hands, attempts to form DMPC liposomes using Biobeads was not very successful. Reconstitution in DMPC resulted in large aggregates or large multilamellar vesicles that could be pelleted at low centrifugation speeds. In comparison, reconstituted liposomes using the *E. coli* lipid formed a milky solution that was only pelleted at high speeds. Reconstituted proteoliposomes can be spun down in an ultracentrifuge, resulting in a pellet with a gel like consistency. This pellet can then be transferred to a MAS rotor for NMR spectroscopy. Centrifugation of the sample into the rotor was the most efficient method, using a swinging-bucket rotor to ensure level packing of the lipid in the rotor. A swinging bucket rotor allowed for more level packing of lipid into the rotor.

NMR experiments were performed at 9 kHz spinning speeds. 1D spectra showed reasonable signal strength at the aliphatic carbon region, including the presence of natural abundance lipid peaks (Figure 10-8). The intensity of the carbonyl and aromatic peaks were low, possibly due to lower than expected concentrations of protein or conformational exchange. A large number of scans were needed for each 1D spectrum, making it impractical to continue with further 2D experiments due to the time that would be needed. The concentration of the protein was estimated to be about 1/8 of the total possible yield using the Bio-Rad DC Protein Assay. Losses during reconstitution, and particularly during the transfer and removal of the sample

to and from the rotor, and protein aggregation or degradation over time could account for some of the losses.

Discussion

Preliminary experiments on 3-TM segments of NHE1 suggest that they may be suitable for solution state NMR experiments and structure determination. In particular, TM V–VII gave promising spectra both in organic solvents and in SDS. Initial attempts at spectral acquisition with TM X–XII were not successful. Despite the reputation of SDS as a denaturant, SDS may still be suitable membrane mimetic for membrane proteins (*28*) and has been used to study TM–TM interactions (*29*). Renthal (*30*) suggests that SDS could bind to membrane proteins, possibly inserting between the TM helices, without large changes in structure. SDS may then still allow us to observe TM–TM interactions between the helices. While the NMR spectra in organic solvent mixtures were also promising, the more homogeneous environment offered by organic solvents may be a poorer mimic of the membrane compared to SDS. Thus SDS or other detergents may allow for a more "native" representation of the 3-TM segments in membranes compared to organic solvents. Further sample optimization, including temperature, pH, or salt, and screening a wider variety of detergents may find other suitable conditions for NMR other than SDS and organic solvents. The excellent quality of the spectra of TM V–VII in SDS may allow us to determine the structure of TM V–VII in SDS micelles, and may also suggest that similar quality spectra might be obtained for TM X–XII.

We obtained preliminary solid-state NMR spectra on full-length NhaA. NhaA has been successfully crystallized both as 3D crystals in detergents (*15*) and 2D crystals in membranes (*18*). Therefore it would also likely be a good candidate for NMR studies, which requires pure and conformationally homogeneous samples to obtain good quality NMR spectra. We were able to see the aliphatic region of the spectrum, however the aromatic and carbonyl signals were much weaker than expected. The sample was prepared at pH 7–8. NhaA is active at this pH (*15*). Performing the experiment at a lower pH, where NhaA is inactive, and where it was successfully crystallized (*15*, *19*), could improve the quality of the NMR spectra. Lower temperatures have also been shown to improve the spectral quality, by decreasing motion and increasing cross polarization efficiency (*31*). Such modifications may allow us to obtain higher quality spectra suitable for multidimensional solid-state NMR.

References

1. Slepkov, E. R., Rainey, J. K., Li, X., Liu, Y., Cheng, F. J., Lindhout, D. A., Sykes, B. D., and Fliegel, L. (2005) Structural and functional characterization of transmembrane segment IV of the NHE1 isoform of the Na^+/H^+ exchanger. *J. Biol. Chem. 280*, 17863–17872.
2. Ding, J., Rainey, J. K., Xu, C., Sykes, B. D., and Fliegel, L. (2006) Structural and functional characterization of transmembrane segment VII of the Na^+/H^+ exchanger isoform 1. *J. Biol. Chem. 281*, 29817–29829.
3. Reddy, T., Ding, J., Li, X., Sykes, B. D., Rainey, J. K., and Fliegel, L. (2008) Structural and functional characterization of transmembrane segment IX of the NHE1 isoform of the Na^+/H^+ exchanger. *J. Biol. Chem. 283*, 22018–22030.
4. Tzeng, J., Lee, B. L., Sykes, B. D., and Fliegel, L. (2010) Structural and functional analysis of transmembrane segment VI of the NHE1 isoform of the Na^+/H^+ exchanger. *J. Biol. Chem. 285*, 36656–36665.
5. Lee, B. L., Li, X., Liu, Y., Sykes, B. D., and Fliegel, L. (2009) Structural and functional analysis of extracellular loop 2 of the Na^+/H^+ exchanger. *Biochim. Biophys. Acta, Biomembr. 1788*, 2481–2488.
6. Lee, B. L., Li, X., Liu, Y., Sykes, B. D., and Fliegel, L. (2009) Structural and functional analysis of transmembrane XI of the NHE1 isoform of the Na^+/H^+ exchanger. *J. Biol. Chem. 284*, 11546–11556.
7. Lee, B. L., Liu, Y., Li, X., Sykes, B. D., and Fliegel, L. (2012) Structural and functional analysis of extracellular loop 4 of the Nhe1 isoform of the Na^+/H^+ exchanger. *Biochim. Biophys. Acta, Biomembr. 1818*, 2783–2790.
8. White, S. H., and von Heijne, G. (2008) How translocons select transmembrane helices. *Annu. Rev. Biophys. 37*, 23–42.
9. Sadlish, H., Pitonzo, D., Johnson, A. E., and Skach, W. R. (2005) Sequential triage of transmembrane segments by Sec61α during biogenesis of a native multispanning membrane protein. *Nat. Struct. Mol. Biol. 12*, 870–878.
10. Hedin, L. E., Ojemalm, K., Bernsel, A., Hennerdal, A., Illergård, K., Enquist, K., Kauko, A., Cristobal, S., von Heijne, G., Lerch-Bader, M., Nilsson, I., and Elofsson, A. (2010) Membrane insertion of marginally hydrophobic transmembrane helices depends on sequence context. *J. Mol. Biol. 396*, 221–229.
11. Landau, M., Herz, K., Padan, E., and Ben-Tal, N. (2007) Model structure of the Na^+/H^+ exchanger 1 (NHE1): functional and clinical implications. *J. Biol. Chem. 282*, 37854–37863.
12. Maes, M., Rimon, A., Kozachkov-Magrisso, L., Friedler, A., and Padan, E. (2012) Revealing the ligand binding site of NhaA Na^+/H^+ antiporter and its pH dependence. *J. Biol. Chem. 287*, 38150–38157.

13. Arkin, I. T., Xu, H., Jensen, M. Ø., Arbely, E., Bennett, E. R., Bowers, K. J., Chow, E., Dror, R. O., Eastwood, M. P., Flitman-Tene, R., Gregersen, B. A., Klepeis, J. L., Kolossváry, I., Shan, Y., and Shaw, D. E. (2007) Mechanism of Na^+/H^+ antiporting. *Science 317*, 799–803.

14. Douglas, J. L., Trieber, C. A., Afara, M., and Young, H. S. (2005) Rapid, high-yield expression and purification of Ca^{2+}-ATPase regulatory proteins for high-resolution structural studies. *Protein Expr. Purif. 40*, 118–125.

15. Hunte, C., Screpanti, E., Venturi, M., Rimon, A., Padan, E., and Michel, H. (2005) Structure of a Na^+/H^+ antiporter and insights into mechanism of action and regulation by pH. *Nature 435*, 1197–1202.

16. Goswami, P., Paulino, C., Hizlan, D., Vonck, J., Yildiz, O., and Kühlbrandt, W. (2011) Structure of the archaeal Na^+/H^+ antiporter NhaP1 and functional role of transmembrane helix 1. *EMBO J. 30*, 439–449.

17. Hu, N.-J., Iwata, S., Cameron, A. D., and Drew, D. (2011) Crystal structure of a bacterial homologue of the bile acid sodium symporter ASBT. *Nature 478*, 408–411.

18. Williams, K. A., Geldmacher-Kaufer, U., Padan, E., Schuldiner, S., and Kühlbrandt, W. (1999) Projection structure of NhaA, a secondary transporter from *Escherichia coli*, at 4.0 Å resolution. *EMBO J. 18*, 3558–3563.

19. Screpanti, E., Padan, E., Rimon, A., Michel, H., and Hunte, C. (2006) Crucial steps in the structure determination of the Na^+/H^+ antiporter NhaA in its native conformation. *J. Mol. Biol. 362*, 192–202.

20. Venturi, M., and Padan, E. (2003) Purification of NhaA Na^+/H^+ antiporter of *Escherichia coli* for 3D and 2D crystallization, in *Membrane Protein Purification and Crystallization* (Hunte, C., Jagow, G. V., and Schägger, H., Eds.) 2nd ed., pp 179–190, Academic Press, San Diego, CA.

21. Moncoq, K., Kemp, G., Li, X., Fliegel, L., and Young, H. S. (2008) Dimeric structure of human Na^+/H^+ exchanger isoform 1 overproduced in *Saccharomyces cerevisiae*. *J. Biol. Chem. 283*, 4145–4154.

22. Reckel, S., Gottstein, D., Stehle, J., Löhr, F., Verhoefen, M.-K., Takeda, M., Silvers, R., Kainosho, M., Glaubitz, C., Wachtveitl, J., Bernhard, F., Schwalbe, H., Güntert, P., and Dötsch, V. (2011) Solution NMR structure of proteorhodopsin. *Angew. Chem., Int. Ed. 50*, 11942–11946.

23. Gautier, A., Mott, H. R., Bostock, M. J., Kirkpatrick, J. P., and Nietlispach, D. (2010) Structure determination of the seven-helix transmembrane receptor sensory rhodopsin II by solution NMR spectroscopy. *Nat. Struct. Mol. Biol. 17*, 768–774.

24. Park, S. H., Das, B. B., Casagrande, F., Tian, Y., Nothnagel, H. J., Chu, M., Kiefer, H., Maier, K., De Angelis, A. A., Marassi, F. M., and Opella, S. J. (2012) Structure of the chemokine receptor CXCR1 in phospholipid bilayers. *Nature 491*, 779–783.

25. Wakabayashi, S., Pang, T., Su, X., and Shigekawa, M. (2000) A novel topology model of the human Na^+/H^+ exchanger isoform 1. *J. Biol. Chem. 275*, 7942–7949.

26. Wishart, D. S., Bigam, C. G., Holm, A., Hodges, R. S., and Sykes, B. D. (1995) ^1H, ^{13}C and ^{15}N random coil NMR chemical shifts of the common amino acids. I. Investigations of nearest-neighbor effects. *J. Biomol. NMR 5*, 67–81.

27. Wishart, D. S., Sykes, B. D., and Richards, F. M. (1991) Relationship between nuclear magnetic resonance chemical shift and protein secondary structure. *J. Mol. Biol. 222*, 311–333.

28. Tulumello, D. V., and Deber, C. M. (2009) SDS micelles as a membrane-mimetic environment for transmembrane segments. *Biochemistry 48*, 12096–12103.

29. Bordag, N., and Keller, S. (2010) α-helical transmembrane peptides: a "divide and conquer" approach to membrane proteins. *Chem. Phys. Lipids 163*, 1–26.

30. Renthal, R. (2006) An unfolding story of helical transmembrane proteins. *Biochemistry 45*, 14559–14566.

31. Frericks, H. L., Zhou, D. H., Yap, L. L., Gennis, R. B., and Rienstra, C. M. (2006) Magic-angle spinning solid-state NMR of a 144 kDa membrane protein complex: *E. coli* cytochrome bo_3 oxidase. *J. Biomol. NMR 36*, 55–71.

Chapter 11

Conclusions

While the human Na^+/H^+ exchanger NHE1 isoform was first isolated in the late 1980's, many of the studies of the protein initially focused on the function and regulation of NHE1 (*1*, *2*). The structure and mechanism of NHE1, however, was not as well studied. Only the cysteine and histidine residues of NHE1 had been thoroughly studied (*3*, *4*). Some mutations, primarily located around the fourth predicted TM segment, had been also discovered that were involved in inhibitor binding (*5*, *6*). A detailed investigation into the topology of NHE1 was performed by Wakabayashi et al. (*7*), who suggested that NHE1 contained 12 TM helices on the basis of cysteine scanning mutagenesis experiments. The topology model of Wakabayashi et al. provided experimental evidence for the location of important residues in the protein which were targeted in newer studies (*8–10*).

Collaboration between the Fliegel and Sykes labs provided the first detailed structural information on NHE1. Cysteine-scanning mutagenesis of NHE1 TM IV was combined with NMR structure determination of a TM IV peptide to give insight into this important TM region (*11*). The NMR structure provided structural information which could be used for interpreting the functional results obtained through mutagenesis. Similar studies on TM VII (*12*) and TM XI (*13*) followed. Around this time, the crystal structure of *Escherichia coli* NhaA, a bacterial homologue to NHE1, provided the first structure of a Na^+/H^+ exchanger (*14*), and which has since been used to develop an understanding of the mechanism and regulation of NhaA and Na^+/H^+ exchange (*15*). A homology model by Landau et al. (*16*) of NHE1 based on the structure of NhaA provided a modified topology which conflicted with some of the results of Wakabayashi et al. (*7*).

To gain further insight into the structure and function of NHE1, we initially investigated additional critical regions of the exchanger, using NMR spectroscopy

to determine the structures of the regions in membrane mimetics, and concurrent mutagenesis experiments to investigate the functions of these regions and lend support to the NMR structures.

We started by examining the structure and function of a peptide representing the second extracellular loop (EL 2) between TMs III and IV (Chapter 3). The NMR spectra of EL 2 revealed multiple conformations due to cis–trans isomerization about the two prolines. One of the species, the cis-Pro-trans-Pro isomer, appeared to adopt a beta-turn. Another extracellular loop that we examined later, EL 4, between TMs VII and VIII, was much longer in sequence and did not appear to have any structure (Chapter 4). There was a strong correlation between the structure of EL 2 and the functional results. The two functionally important residues, P154 and F155, could help maintain the structure of the peptide in solution. Mutations of these residues may alter the structure of EL 2 and the organization of the TM helices, thereby altering NHE1 activity. The relationship between the structure and function of EL 4, however, is not as clear. EL 4 neither formed structure natively in aqueous solution nor adopted any structure in solvents such as TFE and DMSO. On the other hand, the functional data suggests that it is unlikely to be a passive, flexible loop, simply linking the two TM helices together. EL 4 is important, as nearly all of the mutations that were made in EL 4 affected NHE1 activity, and it must be partially structured or buried, as suggested by the differential sensitivity of residues in EL 4 to extracellularly-applied MTSET.

Next, we examined the structure and function of transmembrane segment XI (TM XI) (Chapter 5). This was an interesting TM segment as early hydropathy-based predictions of NHE1 topology did not identify this region as a TM segment (*17*). Experiments by Wakabayashi et al. (*7*, *18*) confirmed that TM XI was transmembrane in nature. The critical nature of the numerous glycine residues and a charged arginine residue, some which had been studied earlier (*18*), and the structural and functional importance of TM 11 in NhaA (*14*), suggested that a detailed structural and functional characterization of this segment would be insightful. We indeed found that TM XI of NHE1 resembles TM 11 of NhaA, containing a short extended region containing glycine and arginine in the center of an otherwise alpha-helical TM segment. The structure resembled the TM IV NMR structure (*11*), and TM 4 and 11 of NhaA. This structure could also explain the functional results. Mutation of the glycine residues could affect the flexibility or TM packing interactions in the protein, while R458 may be important in balancing the electrostatic charges and helix dipoles within the core of NHE1, similar to the function of the charged residues in NhaA (*14*, *19*).

In comparison to TM XI, only one study examining the residues of TM VI had been performed previously (*8*) that did not suggest that TM VI was particularly important. However, modelling by Landau et al. (*16*) suggested that this segment was equivalent to TM 4 of NhaA, which is central to the mechanism of the *E. coli* exchanger (*14*). Of the TM segments of NHE1 that had not yet been examined, TM VI stood out as a poorly characterized, but potentially important and pore-lining TM segment, therefore we set out to characterize the structure and function of TM VI (Chapters 6 and 7). Cysteine-scanning and site-directed mutagenesis studies showed that this region is important to the function of NHE1. TM VI showed a helix-extended-helix structure, similar to TM XI. The structure of TM VI is similar to NhaA TM 4, lending support to the model of Landau et al. and the structural similarity between NHE1 and NhaA. D238 and P239, at one end of the extended region, may be important in maintaining the structure and function of TM VI. Disruptive mutations to cysteine could disrupt the structure of this region, inhibiting NHE1 function, while the mutations by Murtazina et al. (*8*) of D238N and P239A could maintain the structure and function of this region. In NhaA, D133 is suggested to be central to the ion binding and transport activity in the protein which may suggest D238 in NHE1 plays a similar role. Paramagnetic relaxation experiments using NMR may suggest that the extended region of TM VI is not only solvent-exposed, but that it may be binding the Mn^{2+} ions used in the experiments. This could suggest a micelle surface localization, but, more intriguingly, could also suggest a pore-forming, trans-micelle topology, with Mn^{2+} bound in the center.

Due to the similarity between the structures of NHE1 TM VI and TM XI to NhaA TM 4 and TM 11, in Chapter 7 we also attempted to make a model of the NMR structures of the two TMs of NHE1 interacting in the same manner as in NhaA and the model by Landau et al., who also propose a similarity between these pairs of helices. Overall, the model is similar to NhaA and the Landau 3D model of NHE1, with some differences that may be due to the 90° bend in the TM VI NMR structure. The model lends support to the alignment of TM VI of NHE1 onto TM 4 of NhaA and TM XI of NHE1 onto TM 11 of NhaA.

The structure of sod2 TM IV (Chapter 8) also contains a helix-extended-helix structure and a highly conserved Asp residue at the start of the C-terminal helix, much like NHE1 TM VI and NhaA TM 4. Combined with the results of Brett et al. (*20*), which shows that the NHE family members have similar hydropathy profiles, it seems increasingly likely that all of the Na^+/H^+ exchangers have the same membrane-domain fold containing two crossed, discontinuous helices that are

central to the transport mechanism. A recent structure of an unrelated transporter, ASBT (*21*), shows that this fold is not unique to Na^+/H^+ exchangers, but may be used in other transporters as well.

Our results from the investigation of single TM helices may help us to distinguish between the two topology models proposed by Wakabayashi et al. (*7*) and Landau et al. (*16*). The two topology models are described in Chapter 1 along with a comparison of the previously studied TM IV, VII and IX helices to NhaA in a one-to-one manner and to the assignments made by Landau et al. The properties of TM VII seem most similar to TM 5 of NhaA rather than TM 7, but how the other helices relate to NhaA was unclear. Our studies of TM VI and TM XI suggest that they are equivalent to TM 4 and TM 11 of NhaA, with similar structures and functions, and that TM IV may represent TM 2 rather than TM 4 of NhaA as previously predicted (*22*), therefore suggesting that the topology proposed by Landau et al. is more accurate.

TM 4 and TM 11 are part of the two three-TM bundles in NhaA forming an inverted-repeat motif, and consist of TM 3–5 and 10–12 related by a two fold symmetry. Therefore, TM V–VII and X–XII most likely form the equivalent bundles in NHE1. The inverted-repeats in NhaA can also include the two TMs preceding the three-TM bundles, forming groups of 5 TMs, TM 1–5 and TM 8–12. The structures of NhaP1 (*23*) and ASBT (*21*) also show the same inverted-repeat motif. Similarity of NHE1 to NhaA would suggest that TM III–VII of NHE1 form the first repeat equivalent to TM 1–6 in NhaA, with TM IV equivalent to TM 2. The biochemical data on TM IV and the modelling by Landau et al. (Chapter 1) also suggest this similarity. The second repeat would contain TM X–XII plus the two previous helices, and would correspond to TM 8–12 of NhaA. The sequence of these two helices would depend on which topology model is correct: whether residues $\sim$315–410 contain two TMs and an IM segment as in the Wakabayashi model, or four TMs as in the Landau model. The current evidence for TM IX (Chapter 1) cannot distinguish between the two possibilities, and additional studies would be needed to confirm the topology of this region. The structure of NhaP1 and models of sod2 (Chapter 8) and Nha2 (*24*) suggest the latter possibility, with two short TM helices corresponding to TM 7–8 of NhaA, while the smaller ASBT structure (*21*), which lacks the short helices, could suggest the former. The remaining helices, TM I–II, are likely not part of the "core" fold and mechanism of NHE1 as they are poorly conserved (*16*, *20*), but are clearly present as two additional TMs at the N-terminal end of the protein.

Overall, the model by Landau et al. likely is an accurate representation of

NHE1 TMs III–XII, corresponding to TM 1–12 of NhaA, with two additional TM helices, TM I–II, at the N-terminus. The correct topology and number of TMs around residues 315–410 is still unclear, resulting in a total of either 12 or 14 helices for NHE1. Investigation of this disputed region with further NMR and biochemical studies could allow us to distinguish between these possibilities.

Cysteine scanning mutagenesis combined with MTSES/MTSET accessibility studies have allowed us to further define the pore of NHE1. MTSES/MTSET accessibility alone would provide information on the extracellular, solvent-exposed residues of NHE1, without any knowledge of the importance of these residues to the function of protein. The inhibition of activity upon MTSES/MTSET reaction shows that the introduced cysteine residues are near the transport pathway in NHE1, where the compounds can sterically or electrostatically inhibit ion transport.

In our studies, we have found that the extracellular halves of both TM VI and TM XI contain residues that react with MTSET and inhibit the activity of the protein. This suggests that TM VI and TM XI are both part of the extracellular ion translocation pathway. EL 4 and TM IV also contain extracellularly accessible pore lining residues. These regions together likely form the extracellular pore of NHE1. Studies have found that TM 2, 4, and 8 on NhaA are accessible to extracellularly applied MTSET (*25–27*). This agrees with the results in NHE1 where the equivalent TMs IV, VI, and IX also react with MTSET.

Residues in the centres of the TM helices were also found to be accessible. These residues are on the extended segments of TM VI and TM XI and would support the roles of these regions in ion binding or conformational changes. This would be consistent with the charged residues in the center of NhaA that are solvent accessible (*19*, *28*) and ion binding (*29*) and include the extended segments of TM 4 and 11 of that protein. Exposed backbone groups in the structurally similar ASBT are involved in the binding of one of the two sodium ions in the protein (*21*). Thus is seems likely that the extended segments of TM VI and XI along with their charged residues, D238 and R458, are located at the center of the mechanism of NHE1.

We also found residues on intracellular helix of TM VI that were reactive with extracellularly applied MTSET. This result is also seen in TM VII (*12*) and two loops, IL 2 and IL 4 (*7*), which contained extracellularly accessible intracellular residues. MTSET is positively charged and impermeable to the membrane, so the reactivity of these regions would be due to the ability of MTSET to travel through the pore of NHE1. Therefore these regions are likely part of the intracellular half of the pore of NHE1. This would agree with the crystal structure of NhaA where TM 2, 4,

5, and 9 form the cytoplasmic pore (*14*). The other region that may be intracellularly located, but extracellularly accessible, contains residues ∼360–380 which form an extracellular loop in the Wakabayashi model, but form the intracellular part of TM 9 of the Landau model. While the correct orientation of this region is still unclear, it is interesting to note that these accessible residues are located near IL 2 and IL 4 in the Landau 3D model, which could suggest this entire region is somehow accessible from the extracellular side. Curiously, in contrast to this region in NHE1, Tzubery et al. found that TM 9 of NhaA is inaccessible from the periplasmic side (*30*).

The remaining TM helix that has been studied, TM IX, was also found to have pore-lining residues. However, the two different topologies for this TM result in different interpretations of the positioning of these residues. The Wakabayashi model results in an extracellular and membrane-central positioning of these residues, while the Landau model would result in intra- and extracellular locations for the same residues.

Our studies on single TM regions of NHE1 have provided novel insight into the structures of those TM helices and their function. Single TMs, however, do not tell us about how those TMs are arranged in the plane of the membrane. The NMR structures also flexible around the kinks and extended regions in the NMR structures, while they would not be so flexible when interacting with the other TM helices in the full protein. To gain insight into the TM-TM interactions and the 3D TM organization of NHE1, we started producing and examining larger 2–3 TM segments of NHE1.

Some of these multi-TM segments were favourable for expression and NMR spectroscopy while others were not. We first attempted to obtain spectra of a synthetic peptide containing TM III–IV, to determine the structures of these two peptides and the intervening loop (EL 2). However, we were not able to obtain NMR spectra that were suitable for structure determination. While there is a very short loop connecting the two TMs, it is possible that we were unable to obtain suitable spectra due to a lack of interactions between the helices. In the Landau model, these two helices correspond to TM 1–2 of NhaA which do not interact with each other. We next attempted to express TM VI–VII using MBP fusions (Chapter 9). TM VI–VII could be expressed and purified in the milligram amounts needed for NMR spectroscopy while another related peptide, TM VI–VIII, could not be expressed in sufficient amounts. The presence or absence of interactions between the TMs may have played a role in whether the segments could be successfully expressed. TM VI–VII interact in the NMR structure, and the equivalent TM 4–5 in NhaA also interact. TM VIII,

however, corresponds to TM 6 of NhaA, which is connected to the previous TMs by a long loop and does not interact with TM 4–5. The two three-TM regions that we expressed, TM V–VII and X–XII (Chapter 10) correspond to TM 3–5 and 10–12 of NhaA, respectively. The peptides may interact and form stable bundles similar to the structures in NhaA, allowing for their successful expression and purification. We found that these regions both could be expressed in milligram amounts, and we focused on TM V–VII for NMR analysis. The quality of the NMR spectra of TM VI–VII and TM V–VII were comparable to the individual TM segments of TM VI and TM VII, indicative of homogeneous and folded structures, which may also suggest interactions between the TM helices. Our experience seems to suggest that segments that contain TM-TM interactions perform better in protein expression and NMR analysis. They could, perhaps, provide a stable, compact domain that is less prone to degradation or aggregation, more amenable to purification, and provide well resolved NMR spectra.

We found that the structure of TM VI–VII looks very similar to the structures of the individual TM VI and TM VII in DPC micelles determined previously (*12*, *31*), although the structure of TM VI–VII is missing the kink seen in the single-TM structure. The structure is also similar to the structure of TM 4–5 of NhaA (Chapter 9). While there is an interaction between the two TMs in the NMR structure, it only appears to occur near the connecting loop (IL 3). The helix termini that are distal to the loop do not interact. It may be that the lack of interaction is important, in allowing for the conformational changes required of the exchanger, or it could be that TM V, which we predict to be part of one of the three TM bundles of NHE1 and which would interact with TM VI–VII, is required to fix the orientation of the TM VI–VII termini. We were able to successfully express, obtain excellent 2D and 3D ^{15}N-filtered NMR spectra of TM V–VII in SDS micelles, and assign most of the backbone, which may allow us to obtain the secondary structure and TM-TM interactions of this peptide and confirm the three-TM bundle structure predicted for this region (Chapter 10). Additional NMR experiments using ^{13}C-labelling or paramagnetic relaxation may be needed to help us to determine the 3D structure of this segment. The combination of current and future single TM and loop structures, along with TM interactions obtained from multiple TM segments such as TM VI–VII and V–VII or biochemical cross-linking experiments could allow us to build a three-dimensional model of NHE1.

The “divide and conquer” method for membrane proteins is based on simple physical principles describing how peptides fold and interact with membranes and

suggests that TM helices can fold and be studied on an individual level. Bordag et al. (*32*) review the principles and the results of membrane protein structure and TM interaction that have been investigated, and list a large number of papers in which TM segments have been investigated using this method. We have found in our studies of NHE1 that various factors need to be considered in the experimental design, the production of the peptides, sample preparation, and the interpretation of the data.

The design of the sequence of the peptide used in the structural investigation could affect its outcome. Many of the TM helices investigated in NHE1 were based on the Wakabayashi model, and focused on the TM region only. Longer peptides, containing residues from both the Wakabayashi and Landau models may allow us to better compare the two models. TM IX (*33*), for example, could be extended more on the N-terminus, to cover the N-terminal half of TM 7 in the Landau model. Terminal residues should also be considered. The ends of the TM helices may be more clearly defined if more of the loop residues, which could cap the TM helices, were included. The terminal lysines, while they help with the solubility and purification of the peptide, might affect its final structure. The TM VI NMR structure provides an example of this, where residues 247–250 and the three C-terminal lysines adopted a helical structure in the single-TM peptide, while the helix ended at residue 247 in the TM VI–VII peptide, which contained only native loop residues.

Most of the single TM NHE1 peptides were chemically synthesized, which provided a reasonable amount of pure, if unlabelled peptide. Their small size means that the NMR spectra are simple enough that these unlabelled peptides are often sufficient for structure determination. Some NHE1 peptides were produced in bacteria, however. TM IV was produced using GB1 (*11*), while sod2 TM 4 and the multi-TM peptides were produced using MBP. We initially attempted to produce TM XI using GB1, however the expression was poor. The size and complexity of the multi-TM peptides meant that they required bacterial expression for isotopic labelling. Not all of the multi-TM peptides could be expressed. However, as described above, we found that interacting TM regions appeared to be easier to express and study using NMR.

In general, we have had good success with using DPC as a membrane mimetic for determining the structures of NHE1 segments. The DPC choline headgroup makes it a good mimic of natural eukaryotic membranes, where phosphatidylcholine is the major component. In some cases, suitable NMR spectra could not be obtained in DPC, and other detergents or organic solvents were necessary. In sod2 TM 4

and NHE1 TM IV, organic solvent systems were used, while for TM V–VII, SDS was used. While there may be some concern about the more disruptive nature of these mimetics, SDS (*34*) and organic solvents (*35–37*) appear to be able to support secondary structure formation in a similar manner to DPC.

Overall, in our studies with single TM helices, the structures agree with the functional results, the available 3D models, and show some consistent structural features in the case of TM VI, TM VII–VII and sod2 TM 4. This suggests that the divide and conquer approach, when good quality peptides and NMR data can be obtained, is excellent for single TMs. In most cases, the TM peptides of NHE1 were able to adopt structures independently. TM IV appear to be an exception so far, as it contained very little helical structure, despite being predicted by hydropathy, Wakabayashi et al. (*7*), and Landau et al. (*38*) to be a TM helix.

The success of the divide and conquer approach is less clear for studies on multiple TM helices. Only a weak interaction was observed in TM VI–VII, which could suggest additional helices are necessary for the proper folding of this region (possibly TM V–VII). The extended region of TM VI and exposed helix termini are unlikely to insert spontaneously into the membrane, and might require the assistance of other, more hydrophobic regions, to overcome the barrier to insertion of TM VI (*39*). Alternatively, the detergent/solvent systems used may inhibit the formation of tertiary structure. The mechanisms that stabilize the secondary structures could serve to destabilize tertiary TM-TM interactions (*35–37*, *40*). Recent studies have also shown that the interactions between TM helices during folding are complicated and involve multiple interactions or rearrangements after insertion (*41*, *42*). The reconstitution of NhaA activity from its fragments (*43*) and the expression and reconstitution of GPCR fragments (*44*, *45*), nevertheless suggest that some fragments can stably insert and interact with membranes or membrane mimetics and the structures of these larger NHE1 fragments can still provide insight into the structure of the protein.

The divide and conquer approach can provide detailed secondary structure and interhelical structural information, however the results should be interpreted with caution. We have used complementary biochemical studies to help support our structures and assist in determining the structure-function relationship of the single TM segments under study. Therefore, mutagenesis experiments based on the multi-TM regions and their NMR structures would provide support that the structures are relevant in the full protein.

We also obtained preliminary ^{13}C spectra of full length *E. coli* NhaA using

magic angle spinning solid-state NMR spectroscopy (Chapter 10). Solid-state NMR can allow us to examine NhaA in lipid membranes, a more native environment than detergent micelles. While the divide and conquer methodology allows us to gain insight into individual or small numbers of TM helices in NHE1, solid-state NMR could allow us to study entire protein. Solid-state NMR has been developing rapidly, allowing for the assignment of the spectra of large proteins, and the study of their structures, dynamics, conformational changes, and drug binding (*46*). NhaA provides an excellent model protein for initial NMR investigations as established protocols for its expression, characterization, structural investigation already exist. We were only able to get a moderate quality 1D ^{13}C NMR spectrum of NhaA, however further optimization could allow us to perform structural studies of NhaA. Overexpression and single particle EM microscopy of NHE1 (*47*) suggested that NHE1 might also be suitable for structural studies, and the techniques developed here could allow us to examine the structure and function of the full length NHE1 protein.

References

1. Fliegel, L., Murtazina, R., Dibrov, P., Harris, C., Moor, A., and Fernandez-Rachubinski, F. A. (1998) Regulation and characterization of the Na^+/H^+ exchanger. *Biochem. Cell Biol. 76*, 735–741.
2. Wakabayashi, S., Ikeda, T., Iwamoto, T., Pouysségur, J., and Shigekawa, M. (1997) Calmodulin-binding autoinhibitory domain controls "pH-sensing" in the Na^+/H^+ exchanger NHE1 through sequence-specific interaction. *Biochemistry 36*, 12854–12861.
3. Wang, H., Singh, D., and Fliegel, L. (1998) Functional role of cysteine residues in the Na^+/H^+ exchanger effects of mutation of cysteine residues on targeting and activity of the Na^+/H^+ exchanger. *Arch. Biochem. Biophys. 358*, 116–124.
4. Wang, D., Balkovetz, D. F., and Warnock, D. G. (1995) Mutational analysis of transmembrane histidines in the amiloride-sensitive Na^+/H^+ exchanger. *Am. J. Physiol. 269*, C392–C402.
5. Counillon, L., Franchi, A., and Pouysségur, J. (1993) A point mutation of the Na^+/H^+ exchanger gene (NHE1) and amplification of the mutated allele confer amiloride resistance upon chronic acidosis. *Proc. Natl. Acad. Sci. U.S.A. 90*, 4508–4512.
6. Counillon, L., Noël, J., Reithmeier, R. A., and Pouysségur, J. (1997) Random mutagenesis reveals a novel site involved in inhibitor interaction within the fourth transmembrane segment of the Na^+/H^+ exchanger-1. *Biochemistry 36*, 2951–2959.
7. Wakabayashi, S., Pang, T., Su, X., and Shigekawa, M. (2000) A novel topology model of the human Na^+/H^+ exchanger isoform 1. *J. Biol. Chem. 275*, 7942–7949.
8. Murtazina, R., Booth, B. J., Bullis, B. L., Singh, D. N., and Fliegel, L. (2001) Functional analysis of polar amino-acid residues in membrane associated regions of the NHE1 isoform of the mammalian Na^+/H^+ exchanger. *Eur. J. Biochem. 268*, 4674–4685.
9. Slepkov, E. R., Chow, S., Lemieux, M. J., and Fliegel, L. (2004) Proline residues in transmembrane segment IV are critical for activity, expression and targeting of the Na^+/H^+ exchanger isoform 1. *Biochem. J. 379*, 31–38.
10. Hisamitsu, T., Yamada, K., Nakamura, T. Y., and Wakabayashi, S. (2007) Functional importance of charged residues within the putative intracellular loops in pH regulation by Na^+/H^+ exchanger NHE1. *FEBS J. 274*, 4326–4335.
11. Slepkov, E. R., Rainey, J. K., Li, X., Liu, Y., Cheng, F. J., Lindhout, D. A., Sykes, B. D., and Fliegel, L. (2005) Structural and functional characterization of transmembrane segment IV of the NHE1 isoform of the Na^+/H^+ exchanger. *J. Biol. Chem. 280*, 17863–17872.

12. Ding, J., Ng, R. W. P., and Fliegel, L. (2007) Functional characterization of the transmembrane segment VII of the NHE1 isoform of the Na^+/H^+ exchanger. *Can. J. Physiol. Pharmacol. 85*, 319–325.

13. Reddy, T., Ding, J., Li, X., Sykes, B. D., Rainey, J. K., and Fliegel, L. (2008) Structural and functional characterization of transmembrane segment IX of the NHE1 isoform of the Na^+/H^+ exchanger. *J. Biol. Chem. 283*, 22018–22030.

14. Hunte, C., Screpanti, E., Venturi, M., Rimon, A., Padan, E., and Michel, H. (2005) Structure of a Na^+/H^+ antiporter and insights into mechanism of action and regulation by pH. *Nature 435*, 1197–1202.

15. Padan, E. (2008) The enlightening encounter between structure and function in the NhaA Na^+/H^+ antiporter. *Trends Biochem. Sci. 33*, 435–443.

16. Landau, M., Herz, K., Padan, E., and Ben-Tal, N. (2007) Model structure of the Na^+/H^+ exchanger 1 (NHE1): functional and clinical implications. *J. Biol. Chem. 282*, 37854–37863.

17. Sardet, C., Franchi, A., and Pouysségur, J. (1989) Molecular cloning, primary structure, and expression of the human growth factor-activatable Na^+/H^+ antiporter. *Cell 56*, 271–280.

18. Wakabayashi, S., Hisamitsu, T., Pang, T., and Shigekawa, M. (2003) Mutations of Arg^{440} and Gly^{455}/Gly^{456} oppositely change pH sensing of Na^+/H^+ exchanger 1. *J. Biol. Chem. 278*, 11828–11835.

19. Arkin, I. T., Xu, H., Jensen, M. Ø., Arbely, E., Bennett, E. R., Bowers, K. J., Chow, E., Dror, R. O., Eastwood, M. P., Flitman-Tene, R., Gregersen, B. A., Klepeis, J. L., Kolossváry, I., Shan, Y., and Shaw, D. E. (2007) Mechanism of Na^+/H^+ antiporting. *Science 317*, 799–803.

20. Brett, C. L., Donowitz, M., and Rao, R. (2005) Evolutionary origins of eukaryotic sodium/proton exchangers. *Am. J. Physiol.: Cell Physiol. 288*, C223–C239.

21. Hu, N.-J., Iwata, S., Cameron, A. D., and Drew, D. (2011) Crystal structure of a bacterial homologue of the bile acid sodium symporter ASBT. *Nature 478*, 408–411.

22. Slepkov, E. R., Rainey, J. K., Sykes, B. D., and Fliegel, L. (2007) Structural and functional analysis of the Na^+/H^+ exchanger. *Biochem. J. 401*, 623–633.

23. Goswami, P., Paulino, C., Hizlan, D., Vonck, J., Yildiz, O., and Kühlbrandt, W. (2011) Structure of the archaeal Na^+/H^+ antiporter NhaP1 and functional role of transmembrane helix 1. *EMBO J. 30*, 439–449.

24. Schushan, M., Xiang, M., Bogomiakov, P., Padan, E., Rao, R., and Ben-Tal, N. (2010) Model-guided mutagenesis drives functional studies of human NHA2, implicated in hypertension. *J. Mol. Biol. 396*, 1181–1196.

25. Herz, K., Rimon, A., Olkhova, E., Kozachkov, L., and Padan, E. (2010) Transmembrane segment II of NhaA Na^+/H^+ antiporter lines the cation passage, and Asp65 is critical for pH activation of the antiporter. *J. Biol. Chem. 285*, 2211–2220.

26. Diab, M., Rimon, A., Tzubery, T., and Padan, E. (2011) Helix VIII of NhaA Na^+/H^+ antiporter participates in the periplasmic cation passage and pH regulation of the antiporter. *J. Mol. Biol. 413*, 604–614.

27. Rimon, A., Kozachkov-Magrisso, L., and Padan, E. (2012) The unwound portion dividing helix IV of NhaA undergoes a conformational change at physiological pH and lines the cation passage. *Biochemistry 51*, 9560–9569.

28. Olkhova, E., Padan, E., and Michel, H. (2007) The influence of protonation states on the dynamics of the NhaA antiporter from *Escherichia coli*. *Biophys. J. 92*, 3784–3791.

29. Maes, M., Rimon, A., Kozachkov-Magrisso, L., Friedler, A., and Padan, E. (2012) Revealing the ligand binding site of NhaA Na^+/H^+ antiporter and its pH dependence. *J. Biol. Chem. 287*, 38150–38157.

30. Tzubery, T., Rimon, A., and Padan, E. (2008) Structure-based functional study reveals multiple roles of transmembrane segment IX and loop VIII-IX in NhaA Na^+/H^+ antiporter of *Escherichia coli* at physiological pH. *J. Biol. Chem. 283*, 15975–15987.

31. Tzeng, J., Lee, B. L., Sykes, B. D., and Fliegel, L. (2010) Structural and functional analysis of transmembrane segment VI of the NHE1 isoform of the Na^+/H^+ exchanger. *J. Biol. Chem. 285*, 36656–36665.

32. Bordag, N., and Keller, S. (2010) α-helical transmembrane peptides: a "divide and conquer" approach to membrane proteins. *Chem. Phys. Lipids 163*, 1–26.

33. Reddy, T., Li, X., Fliegel, L., Sykes, B. D., and Rainey, J. K. (2010) Correlating structure, dynamics, and function in transmembrane segment VII of the Na^+/H^+ exchanger isoform 1. *Biochim. Biophys. Acta, Biomembr. 1798*, 94–104.

34. Tulumello, D. V., and Deber, C. M. (2009) SDS micelles as a membrane-mimetic environment for transmembrane segments. *Biochemistry 48*, 12096–12103.

35. Duarte, A. M. S., van Mierlo, C. P. M., and Hemminga, M. A. (2008) Molecular dynamics study of the solvation of an alpha-helical transmembrane peptide by DMSO. *J. Phys. Chem. B 112*, 8664–8671.

36. Roccatano, D., Colombo, G., Fioroni, M., and Mark, A. E. (2002) Mechanism by which 2,2,2-trifluoroethanol/water mixtures stabilize secondary-structure formation in peptides: a molecular dynamics study. *Proc. Natl. Acad. Sci. U.S.A. 99*, 12179–12184.

37. Mottamal, M., Shen, S., Guembe, C., and Krilov, G. (2007) Solvation of transmembrane proteins by isotropic membrane mimetics: a molecular dynamics study. *J. Phys. Chem. B 111*, 11285–11296.

38. Landau, M., Mayrose, I., Rosenberg, Y., Glaser, F., Martz, E., Pupko, T., and Ben-Tal, N. (2005) ConSurf 2005: the projection of evolutionary conservation scores of residues on protein structures. *Nucleic Acids Res. 33*, W299–W302.

39. Hedin, L. E., Ojemalm, K., Bernsel, A., Hennerdal, A., Illergård, K., Enquist, K., Kauko, A., Cristobal, S., von Heijne, G., Lerch-Bader, M., Nilsson, I., and Elofsson, A. (2010) Membrane insertion of marginally hydrophobic transmembrane helices depends on sequence context. *J. Mol. Biol. 396*, 221–229.

40. Renthal, R. (2006) An unfolding story of helical transmembrane proteins. *Biochemistry 45*, 14559–14566.

41. Sadlish, H., Pitonzo, D., Johnson, A. E., and Skach, W. R. (2005) Sequential triage of transmembrane segments by Sec61α during biogenesis of a native multispanning membrane protein. *Nat. Struct. Mol. Biol. 12*, 870–878.

42. Kauko, A., Hedin, L. E., Thebaud, E., Cristobal, S., Elofsson, A., and von Heijne, G. (2010) Repositioning of transmembrane α-helices during membrane protein folding. *J. Mol. Biol. 397*, 190–201.

43. Karasawa, A., Mitsui, K., Matsushita, M., and Kanazawa, H. (2007) Functional assembly of the Na^+/H^+ antiporter of *Helicobacter pylori* from partial fragments in vivo. *Biochemistry 46*, 14272–14283.

44. Caroccia, K. E., Estephan, R., Cohen, L. S., Arshava, B., Hauser, M., Zerbe, O., Becker, J. M., and Naider, F. (2011) Expression and biophysical analysis of a triple-transmembrane domain-containing fragment from a yeast G protein-coupled receptor. *Biopolymers 96*, 757–771.

45. Potetinova, Z., Tantry, S., Cohen, L. S., Caroccia, K. E., Arshava, B., Becker, J. M., and Naider, F. (2012) Large multiple transmembrane domain fragments of a G protein-coupled receptor: biosynthesis, purification, and biophysical studies. *Biopolymers 98*, 485–500.

46. Opella, S. J. (2013) Structure determination of membrane proteins by nuclear magnetic resonance spectroscopy. *Annu. Rev. Anal. Chem.* In press.

47. Moncoq, K., Kemp, G., Li, X., Fliegel, L., and Young, H. S. (2008) Dimeric structure of human Na^+/H^+ exchanger isoform 1 overproduced in *Saccharomyces cerevisiae*. *J. Biol. Chem. 283*, 4145–4154.

Appendix A

^{19}F NMR investigation of the binding of calcium sensitizers to cardiac troponin C

BLL performed the expression, purification, and labelling of TnC with the assistance of David Corson and Melissa Crane, and performed the NMR with the assistance of Ian Robertson and Brian Sykes.

Introduction

Troponin is a heterotrimeric complex consisting of troponin C (TnC), troponin I (TnI), and troponin T (TnC) responsible for the calcium-dependent regulation of muscle contraction (*3*, *4*). A crystal structure of the troponin complex is shown in Figure A-1. TnT anchors the other two proteins to tropomyosin. The C-terminal "inhibitory region" of TnI interacts with actin, maintaining the troponin-tropomyosin complex in a conformation that blocks myosin binding sites in actin, preventing muscle contraction. Troponin C contains two structurally similar domains. The C-terminal domain constitutively binds two Ca^{2+} ions and residues 34–71 of TnI, and acts as an anchor for the protein. The N-terminal domain binds one Ca^{2+} upon the stimulated influx of Ca^{2+} into the cell. This allows it to bind to the "switch" region of TnI (residues 147–163), removing the TnI inhibitory region interacting with actin. This results in conformational changes in the troponin-tropmyosin complex, exposing regions of the actin filament that allows for myosin binding and muscle contraction.

Troponin C is a critical protein in the regulation of muscle contraction, and presents a promising target for drugs seeking to regulate muscle contraction in diseased hearts. We investigate the binding of three fluorine-containing compounds to human cardiac TnC (TnC), whose structures are shown in Figure A-2. Trifluoperazine (TFP) acts as a Ca^{2+}-sensitizer, increasing the affinity of TnC to calcium (*3*).

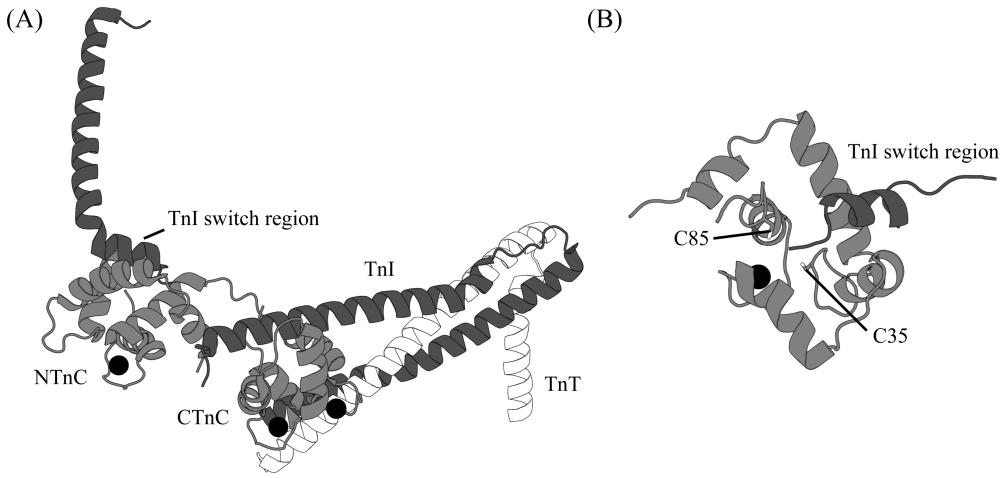

Figure A-1. Structures of cardiac TnC and the troponin complex. (A) Crystal structure of human cardiac troponin complex (PDB: 1J1E) determined by Takeda et al. (*1*). Troponin T (TnT), troponin I (TnI), and the N- (NTnC) and C-terminal (CTnC) are shown. Ca^{2+} ions are shown as spheres. The "switch region" region of TnI, which binds to NTnC is also labelled. (B) NMR structure (PDB: 1MXL) determined by Li et al. (*2*) of the cardiac N-terminal domain of TnC (NTnC) binding to a peptide representing the switch region of TnI (residues 147–163). The two cysteines in the molecule, C35 and C85, are shown as sticks.

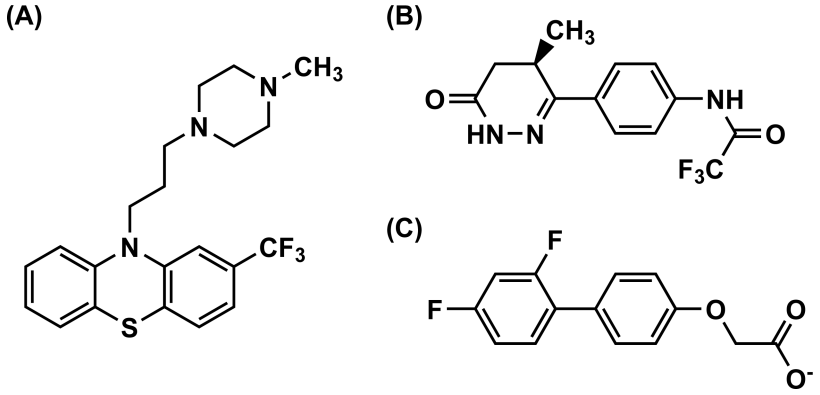

Figure A-2. Structures of TnC-interacting compounds. (A) Trifluoperazine (TFP). (B) Fluorinated derivative of levosimendan (OR1896-CF_3). (C) 2′,4′-difluoro-(1,1′-biphenyl)-4-yloxy acetic acid (DFBP-O).

However, it also inhibits the binding of TnI to TnC. The remaining two compounds are analogs of the Ca^{2+}-sensitizer levosimendan. One compound is a fluorinated derivative of a metabolite of levosimendan, OR1896-CF_3 (*5*). The second compound, DFBP-O, is structurally similar to levosimendan, and may act as a Ca^{2+}-sensitizer, while being more stable in solution (*6*).

Human cardiac TnC contains two cysteine residues on its N-terminal domain (NTnC). The two cysteines are shown in Figure A-1, B. C85 points into the hydrophobic pocket of NTnC where TnI binds in a Ca^{2+}-sensitive manner. C35 is located on the opposite side of the domain, exposed to solvent. The unique chemistry of cysteine sulfhydryl groups can be used to attach numerous functional groups to the cysteine side chain. We attach two CF_3-containing groups to the cysteines in TnC to monitor on the conformational changes and and binding of fluorinated compounds using ^{19}F 1D NMR spectroscopy.

^{19}F NMR spectroscopy offers advantages over NMR using other nuclei. Along with ^{1}H and ^{31}P, ^{19}F is present in 100% natural abundance so it does not require expensive isotopic enrichment. It is also absent from biological systems, so there is no interfering background signal. It has high sensitivity (83% of ^{1}H) and a large chemical shift range, allowing for the detection and resolution of signals. Many drugs also contain fluorine, making ^{19}F NMR an ideal method for examining drug-protein interactions.

Methods

Expression and purification of wild-type troponin C

Human, wild-type, full-length cardiac TnC was expressed and purified as described previously (*7*). BL21(DE3)pLysS *E. coli* were transformed with a pET3a plasmid containing TnC (*7*) via heat shock (ice, 30 min; 42 °C water bath, 90 s; ice, 2 min) and grown overnight on agar plates (7.5 g agar/500 mL media) made with 2 × TY media (5 g/L NaCl, 16 g/L tryptone, 10 g/L yeast extract, 50 µg/mL ampicillin and 25 µg/mL chloramphenicol). Frozen bacterial stocks were made by growing the transformed bacteria in 20 mL 2 × TY media for 4 hours at 37 °C. 10 mL glycerol was added and aliquots were frozen in liquid nitrogen and stored at −80 °C for later use. Four flasks, each containing 250 mL media, were each inoculated with 10 mL of an overnight starter culture, and incubated at 37 °C until an OD_{600} of 0.5–1.0 was reached. 30 mg/250 mL IPTG was added to the culture to

induce expression and incubated for a further 3 h. Cells were pelleted at $5000 \times g$, 4 °C, 15 min and stored at −20 °C. Cells were lysed with three passages through a French press after resuspension in 25 mL of 50 mM Tris-HCl, pH 8, 100 µL of protease inhibitor cocktail, 5 µL/25 mL of 0.1 M PMSF, 1 µL/mL of 10 mg/mL DNAse stock, and 0.25g/100mL $MgSO_4$. Cellular debris was pelleted at $35000 \times g$, 30 min, 4 °C. The supernatant was loaded onto a DEAE column and washed with 50 mM Tris, 0.1 M NaCl, 2 mM $MgCl_2$, 0.01% NaN_3, pH 8, and eluted with a 0.1–0.55 M NaCl gradient overnight. Fractions containing TnC were collected and loaded overnight onto a phenylsepharose column with 50 mM tris, 50 mM NaCl, 5 mM $CaCl_2$, 1 mM $MgCl_2$, 0.01% NaN_3, 1 mM DTT, pH 7.5, then eluted using 50 mM tris, 1 mM EDTA, 1 mM DTT, 0.01% NaN_3, pH 7.5. Purified protein was run on a G25 sephadex column equilibrated with 10 mM NH_4HCO_3, lyophilized, and stored at 4 °C.

Fluorine labelling of troponin C

Lyophilized TnC was reduced and calcium removed by dissolving the protein in 25 mM NH_4HCO_3, 5 mM DTT and 0.2 M EDTA pH 8.5, and passing it through a G25 column equilibrated with 25 mM NH_4HCO_3. For labelling, the reduced protein was dissolved in 0.1 M K_3PO_4, 0.1 M KCl, 21 mM EGTA, pH 9 at a volume of 4 mL per 5 mg protein. 5 mM DTT and 20 µL $BrCH_2COCF_3$ was added per 5 mL solution and incubated for 30 min at room temperature with gentle agitation. The solution was concentrated with a 3K Macrosep spin column (VWR), then 0.2 M EDTA and 25 mM NH_4HCO_3 were added and the solution was run again through a G25 column, lyophilized, and stored at 4 °C.

NMR spectroscopy

NMR samples contained 0.5 mM fluorinated TnC, 8 mM $CaCl_2$, 0.1 mM KCl, 10 mM imidazole, 0.25 mM DSS, 5% D_2O, 0.5 mM sodium trifluoroacetate (TFA), pH 7. Samples totalling 200–250 µL were transferred to a 3 mm NMR tube for ^{19}F NMR on a 600 MHz spectrometer. Samples were titrated with DMSO-d_6 stock solutions of TFP, OR1896-CF_3, or DFBP-O. A sample containing equimolar concentrations of fluorinated TnC, TnI(128–163), and TnI(34–71) was also titrated with TFP. TnI peptides were purchased from GI Biochem (Shanghai) Ltd. ^{19}F NMR spectra were acquired at 30 °C or 10 °C, with an acquisition time of 3 s, a relaxation delay of 2 s, and 512 scans per spectrum. TFA was referenced to 0 ppm.

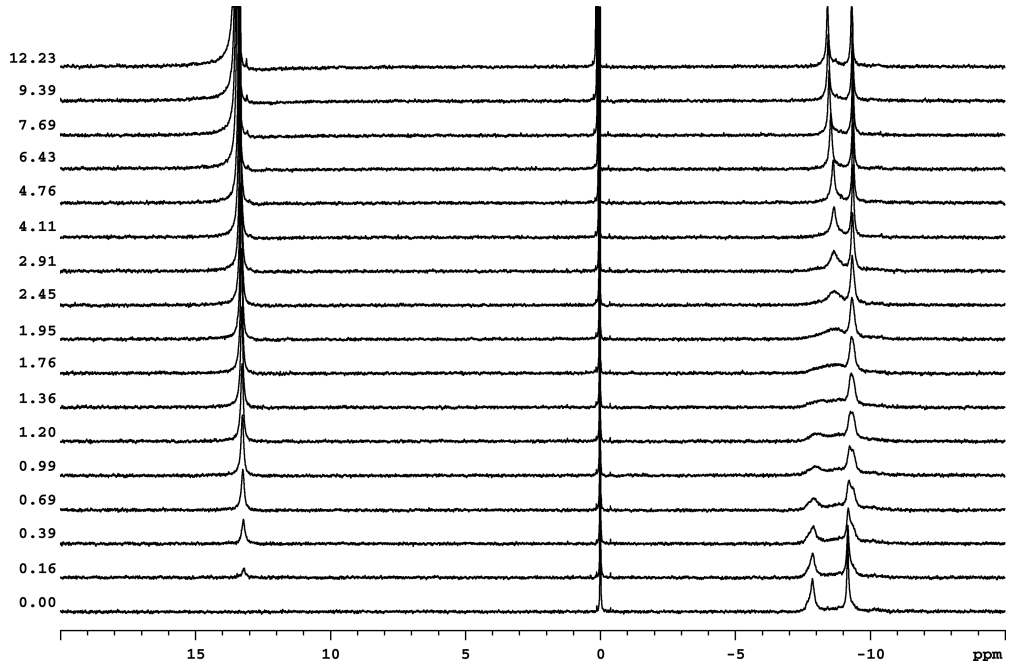

Figure A-3. Titration of TFP into Ca^{2+}-saturated TnC. A series of 1D ^{19}F NMR spectra are shown for the titration of a stock solution of TFP in DMSO-d_6 into a sample of Ca^{2+}-saturated TnC at pH 7. Peaks between -7 to -10 ppm come from the fluorinated TnC. The peak at $\sim$13 ppm shows the increasing concentration of TFP. The initial spectrum is referenced to a TFA standard at 0 ppm. Numbers on the left side show the ratio of the concentration of drug:protein obtained by integration of the drug and protein peaks.

Results

SDS-PAGE gel electrophoresis and mass spectrometry verified the purity of the TnC preparation and mass spectrometry verified the fluorination of the two cysteines on TnC. 1D ^{19}F NMR spectra of fluorinated TnC showed a strong peak from the TFA internal standard and two peaks from the two CF_3-labelled cysteines in the protein. The two peaks showed different widths. The broader, upfield peak at about 8.2 ppm is tentatively assigned to C85, which sits in the vicinity of the hydrophobic pocket of the N-terminal, regulatory domain. The asymmetric shape of the peak suggests both a broader and sharper component to the peak, possibly representing an equilibrium between multiple conformations of the CF_3-labelled side chain. The sharper, downfield peak at about 9.2 ppm is thought to be the surface-exposed C35 opposite the hydrophobic pocket.

Titration of fluorinated TnC with TFP is shown in Figure A-3. Binding of TFP to TnC results in slow to intermediate chemical exchange for the two peaks.

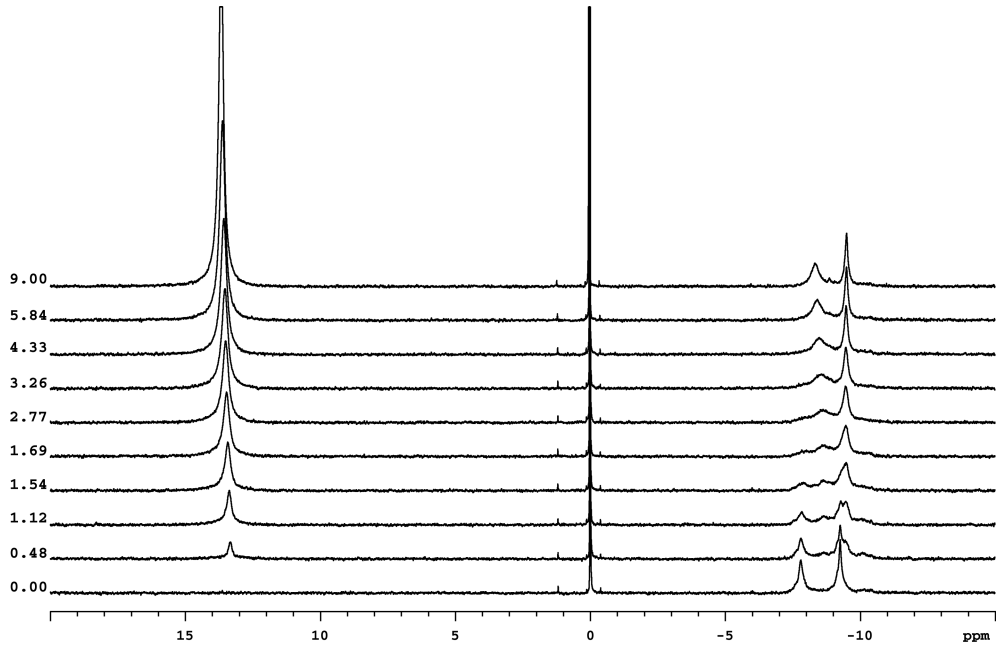

Figure A-4. Titration of TFP into Ca^{2+}-saturated TnC at 10 °C.

As the TFP concentration is increased, the two peaks undergo line broadening and chemical shift changes, while a second set of peak increase in intensity. Reducing the temperature to 10 °C slows down the rate of chemical exchange for both residues (Figure A-4).

Figure A-5 shows that the TFA peak undergoes a slight downfield shift over the course of the titration that is also observed in the other titrations described below. A similar shift is also present for the TFP peak. Changes in the sample conditions, either pH or DMSO concentration, are likely responsible for the shifts.

The titration of OR1896-CF_3 into TnC did appear to affect the spectrum of TnC (Figure A-6). Furthermore, the compound appeared to be forming precipitate while the relative concentrations of OR1896-CF_3 (with a fluorine chemical shift of $\sim$0.1 ppm) and protein stopped increasing partway through the titration, indicating that the compound was poorly soluble. DFBP-O behaved similarly to OR1896-CF_3. The chemical shifts of the two fluorines on DFBP-O occur at about -37 ppm and -39 ppm in H_2O (*5*), however the spectra were acquired with a spectral width of -22 to 22 ppm, resulting in the aliasing of the peaks to the observed 7 ppm and 5 ppm positions, respectively. The titration of the DFBP-O into TnC resulted in a broadening and shifting of the C85 peak (Figure A-7), however, like OR1896-CF_3, the concentration of the DFBP-O stops increasing, indicating it may also be poorly soluble.

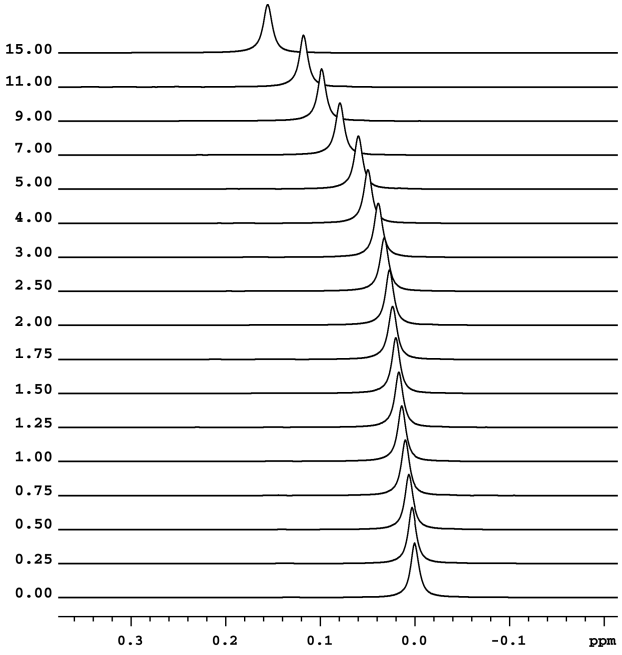

Figure A-5. Chemical shift changes of TFA during the titration of TFP into TnC. Expansion of the TFA region from Figure A-3.

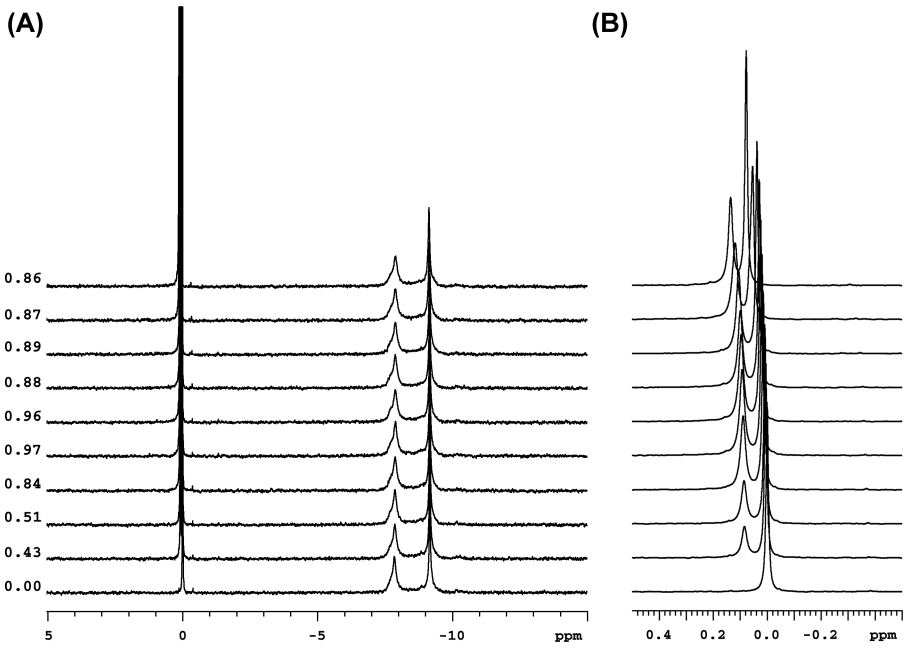

Figure A-6. Titration of OR1896-CF_3 into TnC. (A) Full spectrum. (B) Expansion of spectra showing the TFA (0 ppm) and OR1896-CF_3 (0.1 ppm) peaks, displayed at $1/4\times$ scale relative to (A).

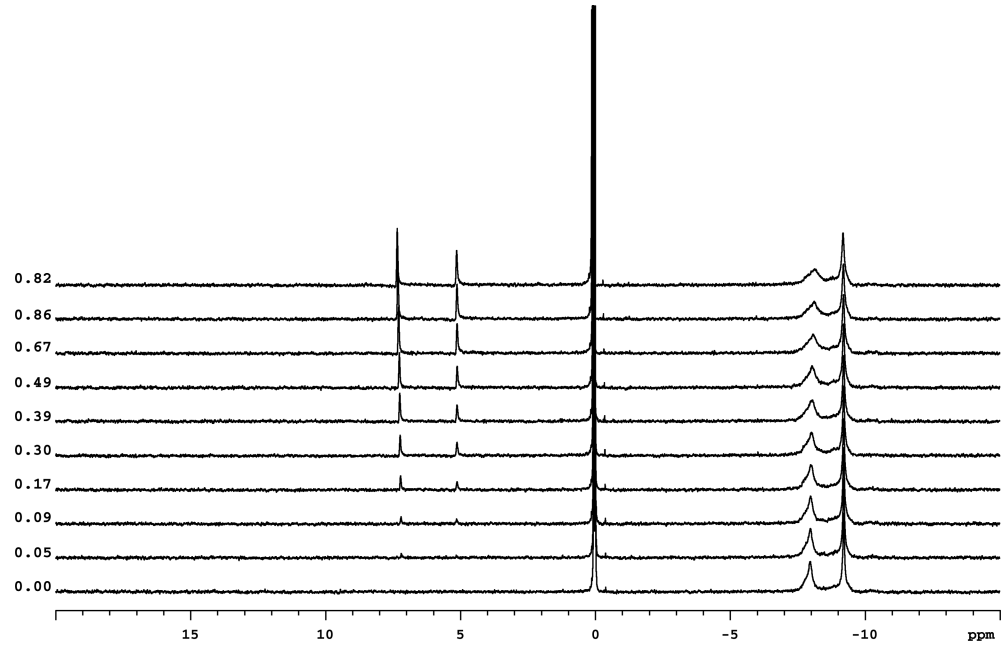

Figure A-7. Titration of DFBP-O into TnC.

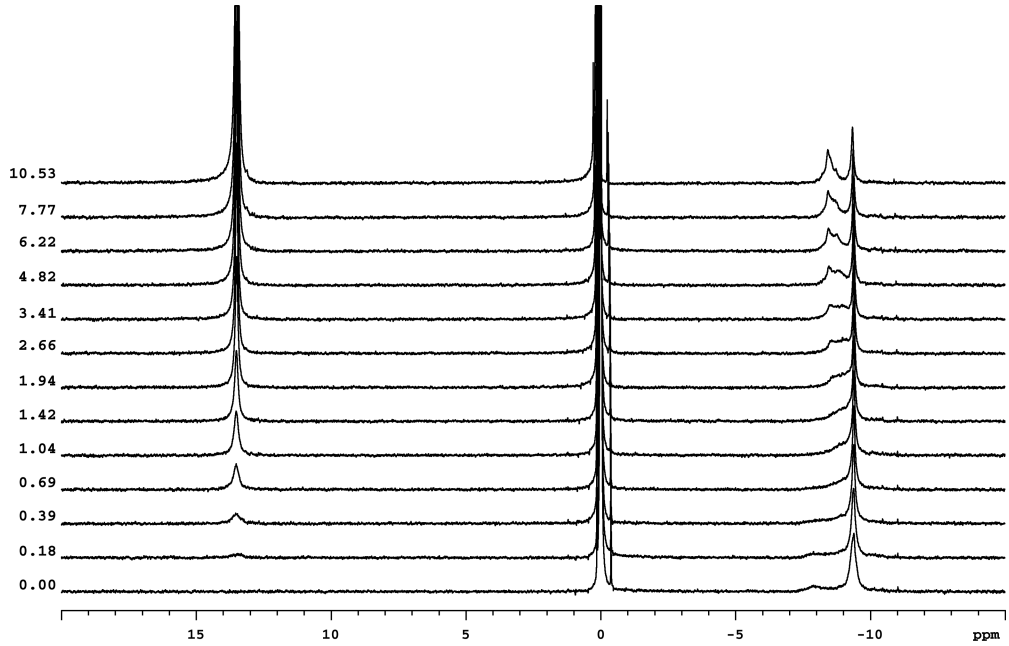

Figure A-8. Titration of TFP into TnC·TnI(34–71)·TnI(128–163).

The spectrum of TnC with the TnC-binding regions of TnI shows a very broad peak at C85, and a moderately sharp peak at C35 (Figure A-8). Titration of TFP results in a narrowing of the C35 peak. C85 first becomes more broad, then increases in intensity into least two broad peaks that begin to resolve into a single, sharper peak.

In conclusion, we attempted to ^{19}F NMR to monitor the binding of fluorine-containing drugs to fluorine-labelled TnC. Of the three drugs that were investigated, only TFP was sufficiently soluble for NMR studies. The spectra of fluorine labelled TnC showed multiple conformations for the two labelled cysteines. Titration with TFP resulted in spectra slow to intermediate exchange phenomena, indicating moderately tight binding of TFP to TnC, however, due to the multiple conformations and overlap of the peaks, it is difficult to quantify the results. The larger changes to C85 compared to C35 suggest that TFP binding affects the conformation of TnC in the vicinity of the hydrophobic pocket of the regulatory domain.

References

1. Takeda, S., Yamashita, A., Maeda, K., and Maéda, Y. (2003) Structure of the core domain of human cardiac troponin in the Ca^{2+}-saturated form. *Nature 424*, 35–41.
2. Li, M. X., Spyracopoulos, L., and Sykes, B. D. (1999) Binding of cardiac troponin-$I_{147–163}$ induces a structural opening in human cardiac troponin-C. *Biochemistry 38*, 8289–8298.
3. Li, M. X., Robertson, I. M., and Sykes, B. D. (2008) Interaction of cardiac troponin with cardiotonic drugs: a structural perspective. *Biochem. Biophys. Res. Commun. 369*, 88–99.
4. Kass, D. A., and Solaro, R. J. (2006) Mechanisms and use of calcium-sensitizing agents in the failing heart. *Circulation 113*, 305–315.
5. Robertson, I. M. (2011) NMR investigation into the therapeutic potential of troponin. Ph.D. Thesis, University of Alberta, Canada.
6. Robertson, I. M., Sun, Y.-B., Li, M. X., and Sykes, B. D. (2010) A structural and functional perspective into the mechanism of Ca^{2+}-sensitizers that target the cardiac troponin complex. *J. Mol. Cell. Cardiol. 49*, 1031–1041.
7. Li, M. X., Saude, E. J., Wang, X., Pearlstone, J. R., Smillie, L. B., and Sykes, B. D. (2002) Kinetic studies of calcium and cardiac troponin I peptide binding to human cardiac troponin C using NMR spectroscopy. *Eur. Biophys. J. 31*, 245–256.

Appendix B

The carboxyl-terminal segment of apolipoprotein A-V undergoes a lipid-induced conformational change

A version of this chapter has been published as:

- Kasuen Mauldin,[1,2] Brian L. Lee,[3] Marta Oleszczuk,[3] Brian D. Sykes,[3] and Robert O. Ryan.[1,2] (2010) The carboxyl-terminal segment of apolipoprotein A-V undergoes a lipid-induced conformational change. *Biochemistry 49*, 4821–4826.

KM performed protein expression and characterization. BLL and MO performed the NMR experiments. BLL performed the NMR analysis. The manuscript was written by KM and BLL and edited by ROR and BDS.

Abstract

Apolipoprotein (apo) A-V is a 343-residue, multidomain protein that plays an important role in regulation of plasma triglyceride homeostasis. Primary sequence analysis revealed a unique tetraproline sequence (P293–P296) near the carboxyl terminus of the protein. A peptide corresponding to the 48-residue segment beyond the tetraproline motif was generated from a recombinant apoA-V precursor wherein P295 was replaced by Met. Cyanogen bromide cleavage of the precursor protein, followed by negative affinity chromatography, yielded a purified peptide.

[1]Center for Prevention of Obesity, Cardiovascular Disease and Diabetes, Children's Hospital Oakland Research Institute, 5700 Martin Luther King Jr. Way, Oakland, California 94609
[2]Department of Nutritional Sciences and Toxicology, University of California, Berkeley, California 94720
[3]Department of Biochemistry, School of Molecular and Systems Medicine, 347 Medical Science Building, University of Alberta, Edmonton, Alberta, Canada T6G 2H7

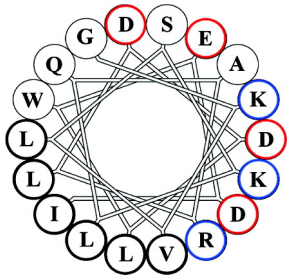

Figure B-1. Helical wheel projection of residues G311–I328 of apoA-V.

Nondenaturing polyacrylamide gel electrophoresis verified that apoA-V(296–343) solubilizes phospholipid vesicles, forming a relatively heterogeneous population of reconstituted high-density lipoprotein with Stokes' diameters > 17 nm. At the same time, apoA-V(296–343) failed to bind a spherical lipoprotein substrate in vitro. Far-UV circular dichroism spectroscopy revealed the peptide is unstructured in buffer yet adopts significant α-helical secondary structure in the presence of the lipid mimetic solvent trifluoroethanol (TFE; 50% v/v). Heteronuclear multidemensional NMR spectroscopy experiments were conducted with uniformly ^{15}N- and ^{15}N/^{13}C-labelled peptide in 50% TFE. Peptide backbone assignment and secondary structure prediction using TALOS+ reveal the peptide adopts α-helix secondary structure from residues 309 to 334. In TFE, apoA-V(296–343) adopts an extended amphipathic α-helix, consistent with a role in lipoprotein binding as a component of full-length apoA-V.

Introduction

Apolipoprotein (apo) A-V was discovered in 2001 in a comparative genomics study (*1*) and as an mRNA upregulated during rat liver regeneration (*2*). Subsequent research has shown that apoA-V serves as a potent modulator of plasma triacylglycerol (TG) homeostasis. Mature apoA-V is a nonglycosylated protein comprised of 343 amino acids. An interesting feature of apoA-V is the presence of four consecutive Pro near the carboxyl (C) terminus (P293–P296). Indeed, this sequence element in apoA-V is conserved across species including human, rat, mouse, olive baboon, cow, wild boar, and dog but not frog or chicken. Whereas the 47-residue segment C-terminal to the tetraproline sequence in human apoA-V was postulated to comprise an independent structural domain, guanidine hydrochloride denaturation studies showed this segment comprises part of a larger C-terminal domain (*3*). A recombinant C-terminal truncated apoA-V, missing the region beyond residue 292,

displayed defective lipid binding activity compared to full-length apoA-V. Furthermore, in the absence of a C-terminal domain, the N-terminal domain of apoA-V (residues 1–146) loses its capacity to bind larger lipoprotein substrates, such as very low density lipoprotein (*4*). When taken together with observations that naturally occurring C-terminal truncated apoA-V mutants in humans are associated with severe hypertriglyceridemia (HTG) (*5*, *6*), it is conceivable that residues 296–343 of apoA-V are required for proper functioning of this protein. In the present study, we have designed a protocol for expression and purification of recombinant of apoA-V(296–343). Structure-function analyses reveal unique lipid-binding properties of this peptide while heteronuclear multidimensional NMR studies provide evidence that, although apoA-V(296–343) is unstructured in buffer alone, it adopts α-helix secondary structure in a lipid mimetic environment.

Experimental procedures

Preparation of apoA-V(296–343)

Site-directed mutagenesis was performed with the QuikChange II XL site-directed mutagenesis kit (Strategene) on an N-terminal His tag-containing human apoA-V construct encoding residues 148–343. Primers were designed to mutate the sole naturally occurring Met at position 253 (numbering corresponds to sequence position in mature, full-length apoA-V) to Ile and P295 to Met. Introduction of the desired mutations was verified by DNA sequencing. The variant apoA-V(148–343) was cloned into pET20b+ vector, and unlabelled, uniformly ^{15}N-labelled, or double ^{15}N/^{13}C-labelled variant apoA-V(148–343) were expressed in *Escherichia coli* BL21 cells cultured in NCZYM (unlabelled protein) or M9 minimal media (isotopically labelled protein) and purified as described previously for full-length recombinant apoA-V (*7*). Purified variant apoA-V(148–343) was then solubilized in 80% formic acid at a concentration of 5 mg/mL. CNBr was added at a CNBr:Met ratio > 100 and incubated under N_2 atmosphere for 24 h in the dark. The reaction was quenched by addition of $>$ 10-fold excess deionized water and the sample lyophilized to remove residual CNBr. The freeze-dried product was resuspended and subjected to affinity chromatography on a Hi-Trap Ni^{2+} chelation column. Since only the unreacted variant apoA-V(148–343) substrate and the N-terminal CNBr cleavage product, apoA-V(148–295), possess a His tag, apoA-V(296–343) elutes in the unbound fraction free of contamination.

Analytical procedures

Protein concentration in samples was determined with the bicinchoninic acid assay (Pierce) using bovine serum albumin as standard. SDS-PAGE was performed on 4–12% acrylamide slab gels using the NuPAGE MES buffer system (Invitrogen) at a constant 200 V for 35 min. Gels were stained with Gel Code Blue (Pierce). Mass spectrometry was performed on an Applied Biosystems Voyager System 6322. The matrix used was R-cyano-4-hydroxycinnamic acid, and the matrix and sample were dissolved in 1:1 water:acetonitrile (0.1% TFA) and drop cast.

Preparation of apoA-V(296–343) reconstituted high-density lipoprotein (rHDL)

Bilayer vesicles of dimyristoylphosphatidylcholine (DMPC) were prepared as described (*7*) and incubated in the presence of apoA-V(296–343) at a DMPC:peptide weight ratio of 3:1. Following bath sonication at 24 °C, the complexes generated were characterized by nondenaturing gradient polyacrylamide gel electrophoresis as described by Nichols et al. (*8*).

Low-density lipoprotein (LDL) binding assay

Human LDL (Intracel) was incubated for 90 min at 37 °C in the presence or absence of *Bacillus cereus* phospholipase C (PL-C) (0.6 unit/ 50 μg of LDL protein). Where indicated, apoA-V(296–343) or recombinant human apoA-I (*9*) was included in the reaction mixture (50 μg/50 μg of LDL protein). Incubations were conducted in 50 mM Tris-HCl, pH 7.5, 150 mM NaCl, and 2 mM $CaCl_2$ in a total sample volume of 200 μL. Sample turbidity was measured at 340 nm on a Spectramax 340 microtiter plate reader (Sunnyvale, CA) (*10*).

Far-UV circular dichroism (CD) spectroscopy

Far-UV CD spectroscopy measurements were performed on an AVIV410 spectrometer. Scans were obtained between 195 and 245 nm in 10 mM sodium phosphate, pH 7.4, using a protein concentration of 0.5 mg/mL.

Nuclear magnetic resonance (NMR) spectroscopy

NMR experiments were performed on 1.5 mM samples of uniformly ^{15}N- or $^{15}N/^{13}C$-labelled apoA-V(296–343) in 500 μL of NMR buffer (90% H_2O/10% D_2O containing 90 mM KCl, 9 mM imidazole, and 0.5 mM 2,2-dimethyl-2-silapentane-5-sulfonate (DSS-d_6) as an internal chemical shift reference) without and with

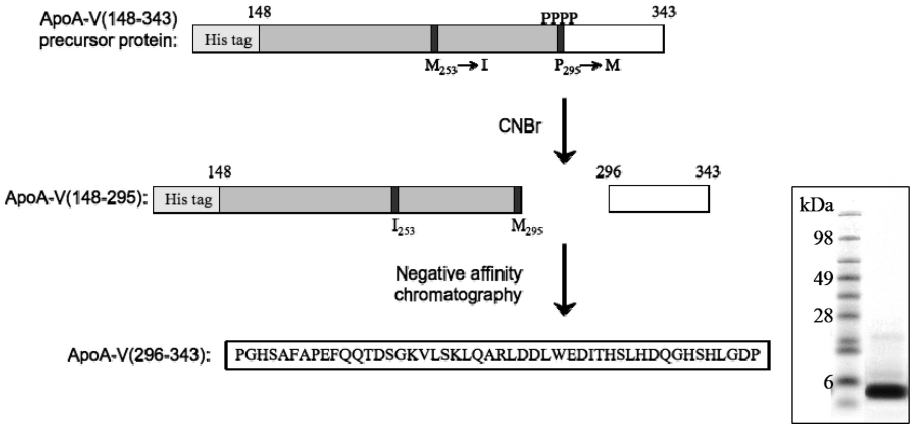

Figure B-2. Flow chart of the apoA-V(296–343) production method and SDS-PAGE of peptide purity.

50% trifluoroethanol (TFE-d_3). NMR experiments were carried out at 25 °C on Varian INOVA 500, 600, and 800 MHz NMR spectrometers. Data were processed using NMRPipe (*11*) and analyzed with NMRView (*12*). Sequential assignment of the backbone atoms of apoA-V(296–343) was obtained using 2D ^{1}H-^{15}N-HSQC, 3D ^{15}N-edited NOESY (75 ms mix), HNHA, HNCACB, and CBCA(CO)NNH experiments. 2D ^{13}C-HSQC, 3D H(CCO)NH, C(CO)NNH, and ^{13}C-edited NOESY (100 ms mix) experiments provided side-chain assignments. Secondary structure predictions were obtained using the program TALOS+ (*13*).

Results

Isolation of purified apoA-V(296–343) peptide

Due to the size of the peptide under investigation (48 amino acids) and a desire to generate isotopically enriched apoA-V(296–343), a protocol was established to generate recombinant peptide from a larger, apoA-V(148–343) precursor. Site-directed mutagenesis was performed to replace the sole Met in this fragment with Ile, while a second mutagenesis introduced Met in place of P295. As predicted, CNBr cleavage of the resulting variant apoA-V(148–343) yielded two major fragments. Negative affinity chromatography was performed to isolate the peptide from unreacted precursor protein and the apoA-V(148–295) CNBr reaction product (Figure B-2). One litre of culture media yielded ∼2 mg of high-purity peptide.

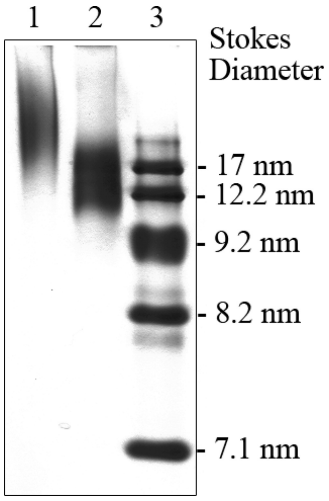

Figure B-3. Native PAGE of apoA-V(296–343)·DMPC complexes. ApoA-V(296–343)·DMPC complexes were prepared as described under Experimental Procedures and applied to a 4–20% acrylamide gradient gel. Following electrophoresis the gel was stained with Gel Code Blue. Lane 1, apoA-V(296–343)·DMPC complexes (5 μg of protein); lane 2, full-length apoA-V·DMPC complexes (5 μg of protein); lane 3, molecular size standards.

apoA-V(296–343) reconstituted high-density lipoproteins

Incubation of apoA-V(296–343) with bilayer vesicles of DMPC induced rapid clearing of solution turbidity, indicative of rHDL formation. Native PAGE analysis revealed a relatively heterogeneous population of particles with a Stokes' diameter $>$ 17 nm (Figure B-3). The rHDL generated in this reaction are larger in size than discoidal particles formed with full-length apoA-V.

apoA-V(296–343) lipoprotein binding properties

When isolated human LDL is incubated with PL-C, conversion of phosphatidylcholine to diacylglycerol induces lipoprotein particle instability, aggregation, and sample turbidity development (Figure B-4). In control incubations lacking PL-C, no change in LDL sample turbidity was observed. When conducted in the presence of apoA-I, LDL was protected from PL-C induced aggregation and turbidity development as a result of apoA-I association with the modified particle surface (*10*). By contrast, corresponding incubations with apoA-V(296–343) failed to protect LDL from PL-C-induced sample turbidity development.

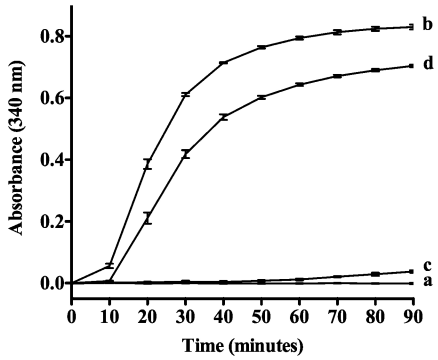

Figure B-4. Effect of apoA-V(296–343) and apoA-I on PL-C-induced aggregation of human LDL. Human LDL (50 µg of protein) was incubated at 37 °C in the absence (curve a) or presence (curve b) of PL-C (0.6 unit). Other incubations contained LDL, PL-C, and 50 µg of apoA-V(296–343) peptide (curve d) or 50 µg of apoA-I (curve c). Sample absorbance at 340 nm was measured as a function of time. The values reported are the mean ± standard deviation ($n = 3$).

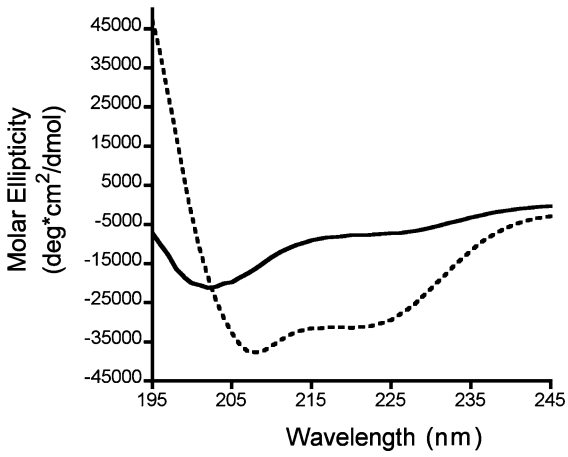

Figure B-5. Far-UV CD of 0.5 mg/mL apoA-V(296–343) in 10 mM sodium phosphate, pH 7.4 (solid line), and in 50% TFE (dashed line).

Far-UV CD spectroscopy

Far-UV CD spectroscopy analysis indicates apoA-V(296–343) is largely unstructured in buffer (Figure B-5). In the presence of the lipid mimetic cosolvent, TFE (50% v/v), however, major minima at 208 and 222 nm are present, indicative of α-helix secondary structure. The far-UV CD spectrum of apoA-V(296–343)·DMPC complexes is similar to that of apoA-V(296–343) in TFE (data not shown).

NMR of ^{15}N-labelled apoA-V(296–343)

When bacteria used to express the variant apoA-V(148–343) were cultured in M9 minimal media containing ^{15}N as the sole nitrogen source, uniformly ^{15}N-labelled apoA-V(296–343) was generated. Mass spectrometry analysis of the sample yielded a value of 5388 Da, in good agreement with the expected theoretical calculated mass for a fully ^{15}N-enriched peptide (5387.7 Da). NMR spectra were collected in buffer, the detergent dodecylphosphocholine (DPC), and the lipid mimetic cosolvent TFE. Comparison revealed the spectra were best resolved in TFE. Thus, assignment and structure calculation were performed under this condition. Two dimensional ^{15}N-^{1}H correlation spectroscopy of ^{15}N-labelled apoA-V(296–343) in NMR buffer gave rise to a spectrum that showed poor resonance dispersion, consistent with a general lack of secondary structure under these conditions (Figure B-6, a). By contrast, spectra recorded in 50% NMR buffer/50% TFE displayed significantly increased chemical shift dispersion, consistent with adoption of secondary structure (Figure B-6, b). Given the prospect of assigning these resonances and ultimate structure determination, a second apoA-V(296–343) peptide, enriched in both ^{15}N and ^{13}C, was generated. Using a panel of heteronuclear multidimensional NMR experiments, the backbone and sidechain atoms of apoA-V were assigned. As seen in Figure B-6, b, all resonances, except for G297, H298, S338, and H339, which were not visible in the ^{15}N-^{1}H HSQC, have been assigned. The C$'$, Cα, Cβ, Hα, HN, and N backbone atom chemical shifts in proteins are sensitive to the secondary structure confirmation in proteins (*14*). The TALOS+ program (*13*) was used to compare the experimental chemical shifts to a database of protein structures and associated chemical shifts to predict the secondary structure using a chemical shift index (CSI). Positive CSI values show probable β-sheet occurrence while negative values indicate helical conformation. Prediction of the secondary structure using TALOS+ indicated peptide residues 309–334 adopt α-helix under these experimental conditions (Figure B-7).

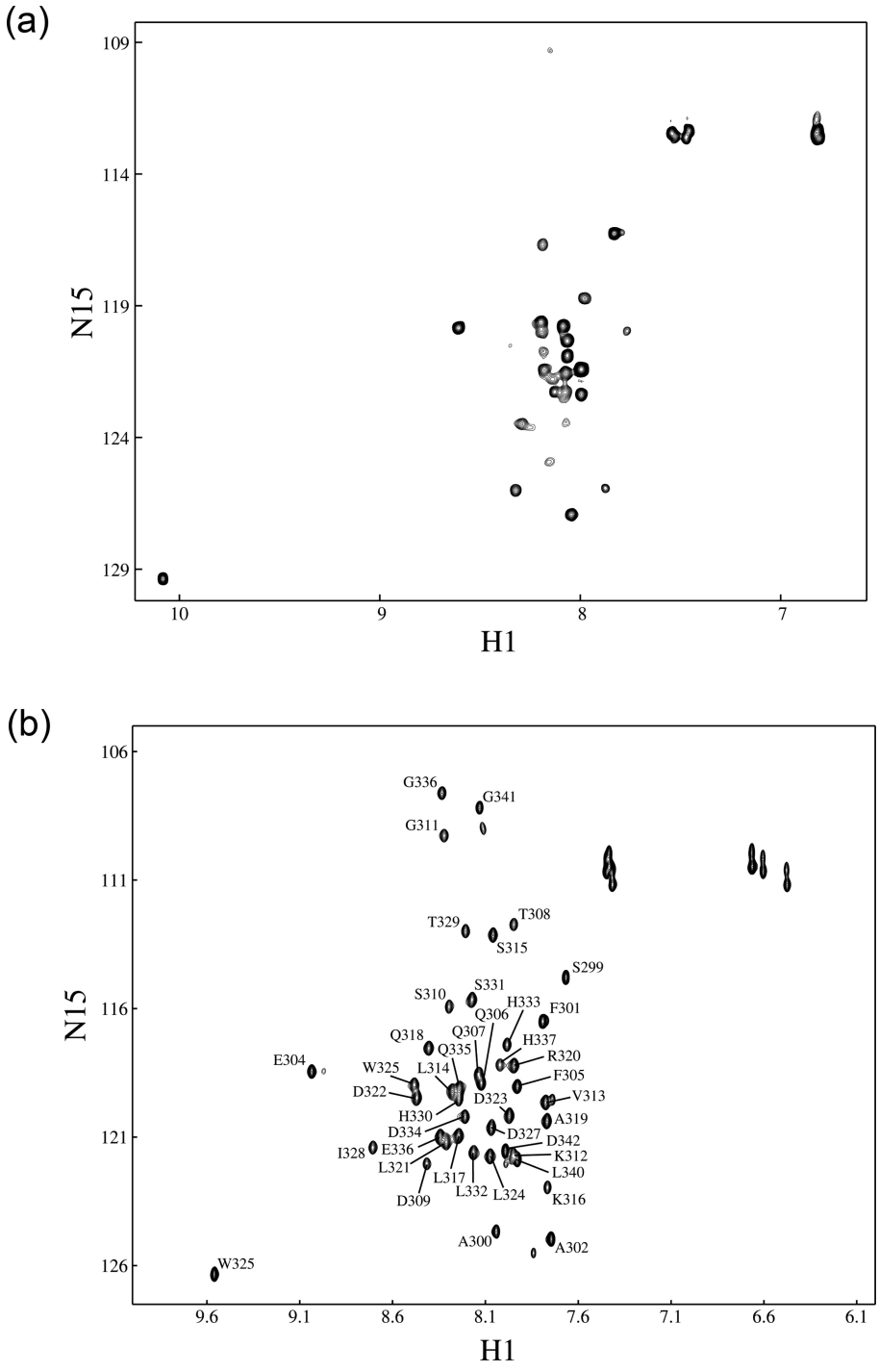

Figure B-6. (a) 2D ^{1}H-^{15}NHSQC of ^{15}N-labelled apoA-V(296–343) in NMR buffer acquired at 500 MHz. (b) 2D ^{1}H-^{15}NHSQC of ^{15}N-labelled apoA-V(296–343) in 50% NMR buffer/50% TFE acquired at 800 MHz. Peak assignments are indicated.

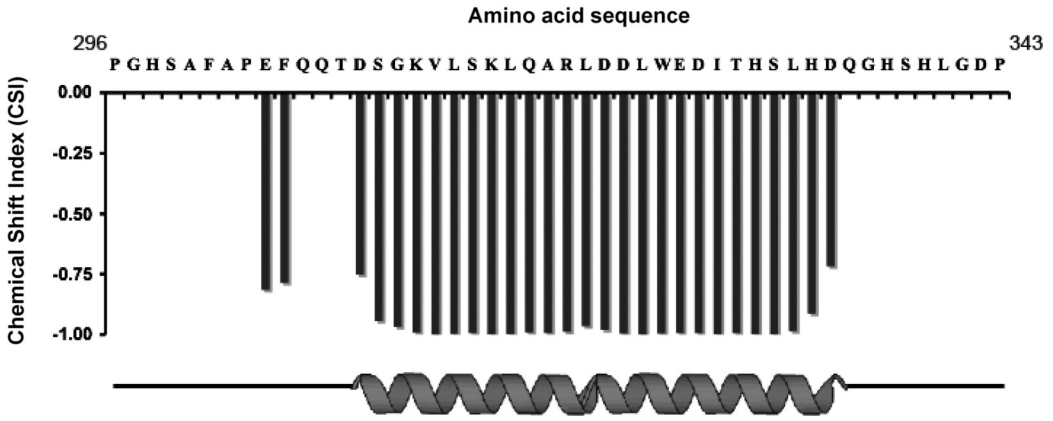

Figure B-7. Secondary structure prediction using the TALOS+ program. Residues G297,H298, S338, and H339 could not be assigned and are not predicted.

Discussion

The mechanism whereby apoA-V influences plasma TG homeostasis has been the subject of intensive investigation (*15*, *16*). Studies have revealed that this protein associates with plasma lipoproteins and possesses the capacity to bind cell surface molecules including heparan sulfate proteoglycans (HSPG), members of the LDL receptor family, and glycosylphosphatidylinositol high-density lipoprotein binding protein 1 (*16*). Considering evidence from genetically engineered mouse models and population studies investigating correlations between common single nucleotide polymorphisms in APOAV and elevated plasma TG, better understanding of apoA-V structure and function relations may lead to new strategies to treat HTG. The fact that apoA-V concentration in plasma is extremely low ($\sim$100 ng/mL) suggests it possesses potent biological activity (*17*).

Limited proteolysis and denaturation studies reveal apoA-V is comprised of two independently folded structural domains (*18*). The N-terminal domain, comprising residues 1–146, adopts a helix bundle molecular architecture in the absence of lipid (*18*). The C-terminal domain, comprising residues 147–343, is less well understood but is known to contain a sequence element (residues 186–227) that is rich in positively charged amino acids and lacks negatively charged residues. It has been postulated that this region of the protein is responsible for apoA-V interactions with cell surface proteins and HSPG (*19–21*).

In lipid binding studies, while the peptide corresponding to apoA-V(296–343) displays high phospholipid vesicle solubilization activity and undergoes a 16 nm blue shift in wavelength of maximum tryptophan fluorescence emission (arising from the single Trp at sequence position 325) in the presence of phospholipid (*3*),

it fails to associate with the surface of a spherical lipoprotein substrate. This result illustrates important differences between lipoprotein binding and vesicle solubilization activity. The ability of apolipoproteins to bind PL-C-treated LDL is dependent on creation of binding sites, via PL-C-mediated conversion of phosphatidylcholine to diacylglycerol, whereas interaction with phospholipid bilayer vesicles proceeds optimally at the phospholipid gel to liquid-crystal phase transition temperature (*22*). It appears that the lack of secondary structure in buffer precludes recognition/binding to the surface of a lipoprotein yet its intrinsic capacity to associate with lipid is retained in the phospholipid vesicle solubilization assay, perhaps owing to the induction of secondary structure as part of the solubilization reaction.

A concept that has emerged from structural studies conducted to date is that the C-terminal segment beyond the four consecutive Pro may be responsible for initiation of apoA-V lipid binding activity. This interpretation is consistent with the lipid binding properties of other apolipoproteins, such as apoE and apoA-I (*23*), and is supported by data showing that removal of this C-terminal region results in an impaired ability of apoA-V to bind lipid (*3*). It may be postulated that initiation of lipid binding is mediated by hydrophobic interactions between nonpolar residues in the C-terminal peptide and the hydrophobic lipid surface and/or ionic interactions between charged residues and phospholipid headgroups. In both types of interactions, the C-terminal peptide may be envisioned to mediate initial recognition of the lipoprotein particle, followed by stable binding of the entire protein.

The experiments described in this study indicate that in order to initiate lipid binding, apoA-V(296–343) may need to exist within the context of the intact protein. Far-UV CD and NMR spectroscopy experiments show that apoA-V(296–343) is unstructured in buffer alone. In the case of other apolipoproteins, adoption of a more loosely folded structure correlates with enhanced lipid binding activity (*24*). It is conceivable the C-terminal region of apoA-V initiates lipid binding and that this process induces stable secondary structure formation in this segment of the protein. In this case, it seems plausible that lipid binding elicits a subsequent conformational change in the N-terminal helix bundle that results in opening of the bundle and exposure of its hydrophobic interior to potential lipid interaction sites. A consequence of this may also include exposure of the positively charged sequence motif (residues 186–227) that underlies the biological effects of apoA-V.

In an effort to test hypotheses related to this model, we sought to characterize the structural properties of the C-terminal peptide. In order to study the peptide in isolation, methods were developed to produce recombinant peptide. Using this

system, efficient stable isotope enrichment of the peptide was readily achieved. A panel of heteronuclear multidimensional NMR experiments was employed to assign the apoA-V(296–343) spectrum and define its structure in a lipid mimetic environment. Results obtained suggest apoA-V(296–343) undergoes a lipid-induced conformational change, transitioning from an unstructured or molten globule-like state in the lipid-free environment to α-helix in a lipid mimetic environment. NMR analysis reveals the region between residues 309–334 adopts a α-helix secondary structure under these conditions. These data confirm the prediction from the Coils program (*25*) that the region between Gly311 and Leu332 in apoA-V(296–343) adopts α-helical secondary structure. Edmundson helical wheel projection (*26*) of G311–I328 reveals this region forms an amphipathic α-helix with clearly demarcated polar and nonpolar faces (Figure B-1). Primary sequence analysis reveals almost all of the hydrophobic and charged residues within apoA-V(296–343) reside within this α-helix segment. Thus, it may be considered that, in the presence of lipid, the extreme carboxyl terminus of apoA-V adopts an amphipathic α-helix. This induction of structure supports the concept that the C-terminal region of apoA-V may serve as a lipid sensor that functions in initiation of full-length apoA-V lipid binding activity and subsequent structure conformation changes in the entire protein, as seen with apoE and apoA-I (*23*). The known ability of apoA-V to transfer between high-density lipoprotein and very low density lipoprotein suggests the present findings are physiologically relevant (*4*, *27*).

Since our data show apoA-V C-terminal peptide can adopt structure, it must be considered that, when present in the context of the intact protein, the C-terminal region possesses a more defined structure. Indeed, an important question arising from this study relates to whether the C-terminal peptide structure determined here resembles that of the peptide when present in the context of the intact protein. To determine this, expressed protein ligation represents a potential strategy to generate a segmentally isotope-labelled full-length apoA-V wherein only residues 296–343 are enriched with stable isotope (*28*). Such an approach would allow detailed analysis of the solution properties and lipid binding induced conformational changes in this region of the protein within the context of the intact apoA-V protein.

Acknowledgments

The authors thank Dr. Clayton Mauldin of the University of California, Berkeley, for assistance with mass spectrometry analysis and Dr. Susan Marqusee of the University of California, Berkeley, for access to the circular dichroism spectrophotometer.

References

1. Pennacchio, L. A., Olivier, M., Hubacek, J. A., Cohen, J. C., Cox, D. R., Fruchart, J. C., Krauss, R. M., and Rubin, E. M. (2001) An apolipoprotein influencing triglycerides in humans and mice revealed by comparative sequencing. *Science 294*, 169–173.
2. van der Vliet, H. N., Sammels, M. G., Leegwater, A. C., Levels, J. H., Reitsma, P. H., Boers, W., and Chamuleau, R. A. (2001) Apolipoprotein A-V: a novel apolipoprotein associated with an early phase of liver regeneration. *J. Biol. Chem. 276*, 44512–44520.
3. Beckstead, J. A., Wong, K., Gupta, V., Wan, C.-P. L., Cook, V. R., Weinberg, R. B., Weers, P. M. M., and Ryan, R. O. (2007) The C terminus of apolipoprotein A-V modulates lipid-binding activity. *J. Biol. Chem. 282*, 15484–15489.
4. Wong-Mauldin, K., Raussens, V., Forte, T. M., and Ryan, R. O. (2009) Apolipoprotein A-V N-terminal domain lipid interaction properties *in vitro* explain the hypertriglyceridemic phenotype associated with natural truncation mutants. *J. Biol. Chem. 284*, 33369–33376.
5. Marçais, C., Verges, B., Charrière, S., Pruneta, V., Merlin, M., Billon, S., Perrot, L., Drai, J., Sassolas, A., Pennacchio, L. A., Fruchart-Najib, J., Fruchart, J.-C., Durlach, V., and Moulin, P. (2005) Apoa5 Q139X truncation predisposes to late-onset hyperchylomicronemia due to lipoprotein lipase impairment. *J. Clin. Invest. 115*, 2862–2869.
6. Priore Oliva, C., Pisciotta, L., Li Volti, G., Sambataro, M. P., Cantafora, A., Bellocchio, A., Catapano, A., Tarugi, P., Bertolini, S., and Calandra, S. (2005) Inherited apolipoprotein A-V deficiency in severe hypertriglyceridemia. *Arterioscler., Thromb., Vasc. Biol. 25*, 411–417.
7. Beckstead, J. A., Oda, M. N., Martin, D. D. O., Forte, T. M., Bielicki, J. K., Berger, T., Luty, R., Kay, C. M., and Ryan, R. O. (2003) Structure-function studies of human apolipoprotein A-V: a regulator of plasma lipid homeostasis. *Biochemistry 42*, 9416–9423.
8. Nichols, A. V., Krauss, R. M., and Musliner, T. A. (1986) Nondenaturing polyacrylamide gradient gel electrophoresis. *Methods Enzymol. 128*, 417–431.
9. Ryan, R. O., Forte, T. M., and Oda, M. N. (2003) Optimized bacterial expression of human apolipoprotein A-I. *Protein Expr. Purif. 27*, 98–103.
10. Liu, H., Scraba, D. G., and Ryan, R. O. (1993) Prevention of phospholipase-C induced aggregation of low density lipoprotein by amphipathic apolipoproteins. *FEBS Lett. 316*, 27–33.
11. Delaglio, F., Grzesiek, S., Vuister, G. W., Zhu, G., Pfeifer, J., and Bax, A. (1995) NMRPipe: a multidimensional spectral processing system based on UNIX pipes. *J. Biomol. NMR 6*, 277–293.

12. Johnson, B. A. (2004) Using NMRView to visualize and analyze the NMR spectra of macromolecules. *Methods Mol. Biol. 278*, 313–352.

13. Shen, Y., Delaglio, F., Cornilescu, G., and Bax, A. (2009) TALOS+: a hybrid method for predicting protein backbone torsion angles from NMR chemical shifts. *J. Biomol. NMR 44*, 213–223.

14. Wishart, D. S., Sykes, B. D., and Richards, F. M. (1991) Relationship between nuclear magnetic resonance chemical shift and protein secondary structure. *J. Mol. Biol. 222*, 311–333.

15. Wong, K., and Ryan, R. O. (2007) Characterization of apolipoprotein A-V structure and mode of plasma triacylglycerol regulation. *Curr. Opin. Lipidol. 18*, 319–324.

16. Forte, T. M., Shu, X., and Ryan, R. O. (2009) The ins (cell) and outs (plasma) of apolipoprotein A-V. *J. Lipid Res. 50 Suppl*, S150–S155.

17. O'Brien, P. J., Alborn, W. E., Sloan, J. H., Ulmer, M., Boodhoo, A., Knierman, M. D., Schultze, A. E., and Konrad, R. J. (2005) The novel apolipoprotein A5 is present in human serum, is associated with VLDL, HDL, and chylomicrons, and circulates at very low concentrations compared with other apolipoproteins. *Clin. Chem. 51*, 351–359.

18. Wong, K., Beckstead, J. A., Lee, D., Weers, P. M. M., Guigard, E., Kay, C. M., and Ryan, R. O. (2008) The N-terminus of apolipoprotein A-V adopts a helix bundle molecular architecture. *Biochemistry 47*, 8768–8774.

19. Lookene, A., Beckstead, J. A., Nilsson, S., Olivecrona, G., and Ryan, R. O. (2005) Apolipoprotein A-V-heparin interactions: implications for plasma lipoprotein metabolism. *J. Biol. Chem. 280*, 25383–25387.

20. Merkel, M., Loeffler, B., Kluger, M., Fabig, N., Geppert, G., Pennacchio, L. A., Laatsch, A., and Heeren, J. (2005) Apolipoprotein AV accelerates plasma hydrolysis of triglyceride-rich lipoproteins by interaction with proteoglycan-bound lipoprotein lipase. *J. Biol. Chem. 280*, 21553–21560.

21. Nilsson, S. K., Lookene, A., Beckstead, J. A., Gliemann, J., Ryan, R. O., and Olivecrona, G. (2007) Apolipoprotein A-V interaction with members of the low density lipoprotein receptor gene family. *Biochemistry 46*, 3896–3904.

22. Narayanaswami, V., Wang, J., Kay, C. M., Scraba, D. G., and Ryan, R. O. (1996) Disulfide bond engineering to monitor conformational opening of apolipophorin III during lipid binding. *J. Biol. Chem. 271*, 26855–26862.

23. Saito, H., Lund-Katz, S., and Phillips, M. C. (2004) Contributions of domain structure and lipid interaction to the functionality of exchangeable human apolipoproteins. *Prog. Lipid Res. 43*, 350–380.

24. Soulages, J. L., and Bendavid, O. J. (1998) The lipid binding activity of the exchangeable apolipoprotein apolipophorin-III correlates with the formation of a partially folded conformation. *Biochemistry 37*, 10203–10210.

25. Lupas, A., Van Dyke, M., and Stock, J. (1991) Predicting coiled coils from protein sequences. *Science 252*, 1162–1164.

26. Schiffer, M., and Edmundson, A. B. (1967) Use of helical wheels to represent the structures of proteins and to identify segments with helical potential. *Biophys. J. 7*, 121–135.

27. Nelbach, L., Shu, X., Konrad, R. J., Ryan, R. O., and Forte, T. M. (2008) Effect of apolipoprotein A-V on plasma triglyceride, lipoprotein size, and composition in genetically engineered mice. *J. Lipid Res. 49*, 572–580.

28. Hauser, P. S., Raussens, V., Yamamoto, T., Abdullahi, G. E., Weers, P. M. M., Sykes, B. D., and Ryan, R. O. (2009) Semisynthesis and segmental isotope labeling of the apoE3 N-terminal domain using expressed protein ligation. *J. Lipid Res. 50*, 1548–1555.

Appendix C

NMR analysis of a myristoylated fragment of the huntingtin protein

This formed part of a collaborative investigation with Dr. Luc Berthiaume and Dr. Dale Martin from the Department of Cell Biology, University of Alberta.

Introduction

Huntington's disease is a neurodegenerative disorder that causes impaired motor function, cognitive decline, and psychiatric disorders (*1*). 5–10 people out of 100,000 develop the disease, which eventually result in dementia and death. The gene responsible for the disease encodes for the protein huntingtin (Htt) and contains a CAG repeat sequence that encodes for a polyglutamine-repeat sequence near the N-terminus of the protein. The disease affects individuals with mutant forms of the protein containing 36 or more of these repeats. The mutant form of the protein appears to be more prone to aggregation and forms intracellular aggregates in neurons. The function of the Htt protein and the mechanism by which the polygutamine-tract results in cellular dysfunction is not clear.

Ravikumar et al. (*2*) found that the intracellular aggregates may have a protective effect in cells by the stimulation of autophagy for the removal of the misfolded proteins. The Htt aggregates sequester and inhibit the activity of the kinase mTOR. This allows for the activation of other proteins involved in the formation of autophagosomes.

Htt has also been found to be cleaved by caspases (*3*). The polyglutamine-containing fragment of Htt is implicated in its neurodegenerative effects. Htt is cleaved C-terminal to residue 552 by caspases 2 and 3 and also at residue 586 by caspase 6. The newly made N-terminus released by cleavage at residue 552 contains a conserved motif G-X-X-X-(S/T/C) that allows for the addition of a

myristoyl group to newly exposed N-terminal glycine (*4*, *5*). Myristoylation can regulate protein-membrane and protein-protein interactions (*4*). Specifically, the myristoylated Htt fragment of residues 553–586 appears to induce the formation of autophagosome-like vesicles when expressed in HeLa cells (*6*). To investigate the molecular details of the induction of vesicles by this myristoylated peptide, we used NMR spectroscopy to examine the structure of the peptide in the membrane mimetic dodecylphosphocholine (DPC).

Methods

Synthetic peptide representing a myristoylated fragment of the huntingtin protein (sequence GTQASSPISDSSQTTTEGPDSAVTPSDSSEIVLD, N-terminal myristoylate, C-terminal NH_2) was purchased from Biomatik (ON, Canada).

Aqueous NMR samples contained 5% D_2O, 0.25 mM DSS, 10 mM imidazole, and 100 mM KCl. Samples in perdeuterated DPC micelles were the same as the aqueous samples, with the addition of a 1:75 molar ratio of peptide:detergent. NMR spectra were acquired at a temperature of 10 °C, and a pH of 5.5. 1D ^{1}H NMR spectra and 2D ^{1}H-^{1}H DQF-COSY, TOCSY, and NOESY spectra were acquired on a 600 MHz spectrometer for sequential assignment and secondary structure analysis.

Results

Investigation of the peptide at low concentration and at 30 °C revealed good quality NMR spectra that were suitable for structure determination. Sample of the peptide at 2 mM concentrations showed broad lines, suggesting that the peptide undergoes aggregation at millimolar concentrations. Dilution of the peptide resulted in sharper lines and less aggregation (Figure C-1). Millimolar concentrations of the peptide in DPC detergent micelles remained sharp, however, and were suitable for further studies using NMR spectroscopy. Slight broadening of the peptide peaks were observed at lower DPC:peptide ratios, suggesting weak aggregation in DPC (not shown). Some change in the amide peak dispersion upon DPC addition suggested that the peptide interacted with the micelles and possibly adopt secondary structure (Figure C-2).

The sample temperature was reduced to 10 °C to attempt to encourage structure formation in the peptide, and the pH reduced from 6.5 to 5.5 to decrease the water–backbone amide exchange rate and increase the intensity of the amide peaks. 2D COSY, TOCSY and NOESY spectra were acquired for sequential assignment and

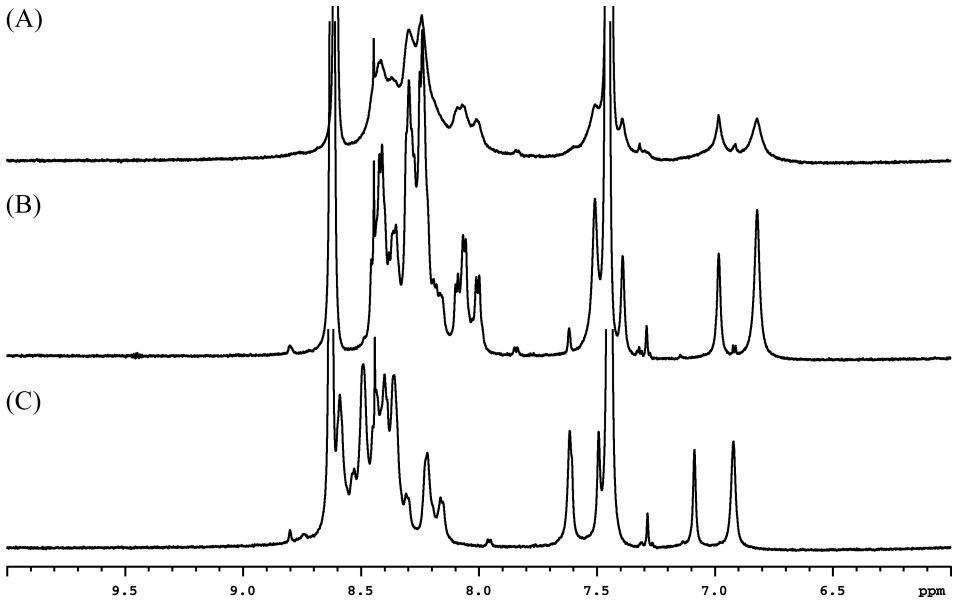

Figure C-1. Concentration-dependent aggregation of the HTT peptide in aqueous solution. The amide region of the 1D ^{1}H NMR spectra are shown for the peptide at concentrations of (A) 2 mM, (B) 1 mM (diluted from sample (A)), and (C) 1 mM at 30 °C, pH 6.

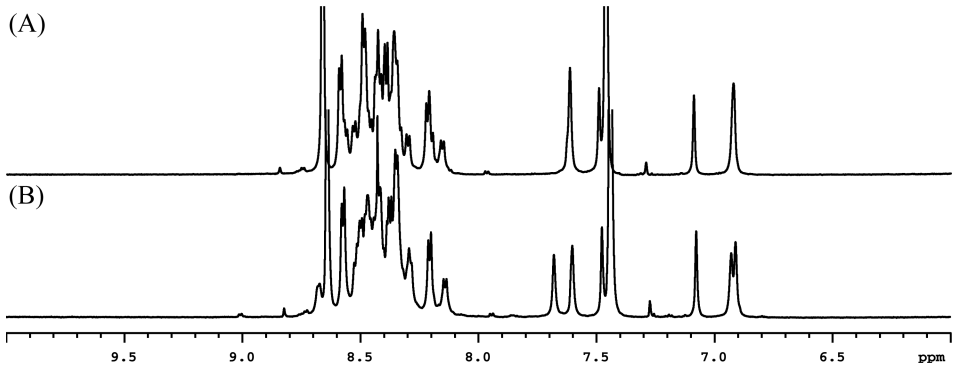

Figure C-2. Changes in the NMR spectrum of HTT upon DPC addition. The amide/aromatic region of the NMR spectrum is shown. (A) 1 mM peptide in buffer, 10 °C, pH 5.3. (B) Addition of 75 mM DPC to the sample in (A).

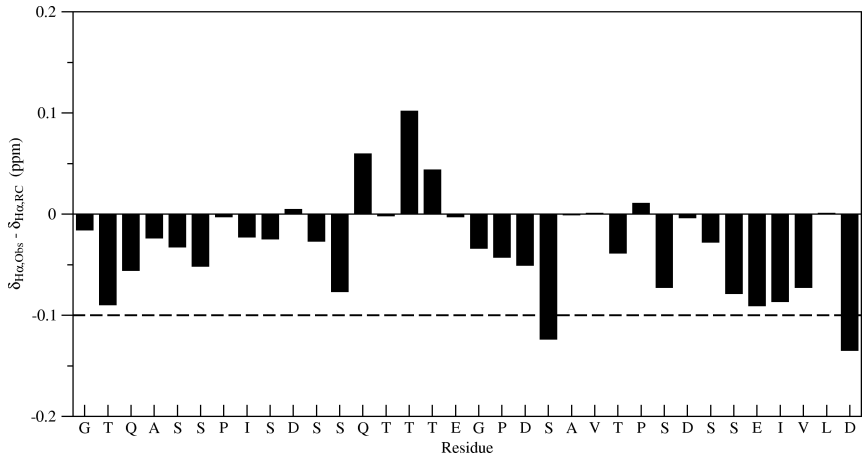

Figure C-3. Secondary structure of the HTT peptide based on Hα chemical shifts. The peptide Hα chemical shifts were compared to random coil chemical shifts in water (*7*). Contiguous regions with negative deviations below -0.1 ppm (dotted line) suggest alpha-helical structure, while regions with positive deviations above 0.1 ppm suggest beta-sheet structure.

structural analysis using standard methods (*8*). Assignment of the peptide provided Hα chemical shifts which can be used to determine the secondary structure of the peptide (*9*). A comparison of the chemical shifts of the peptide in DPC with respect to random coil chemical shifts in water (*7*) showed that the peptide was primarily unstructured (Figure C-3).

Discussion

NMR analysis of the myristoylated cleavage product of Htt protein suggests that it is largely unstructured in solution, and that it could interact with membranes, as suggested by its interactions with DPC micelles. In solution, the peptide aggregated at millimolar concentrations, possibly by forming micelle-like structures (*10*). There may be some evidence of weak aggregation in DPC micelles as there was some slight broadening of the peptide peaks at lower DPC:peptide ratios. The peptide also formed higher-order aggregates, perhaps trimers or tetramers, in SDS-PAGE gels (Martin, D., personal communication), suggesting that this aggregation may be important in the function of the peptide, however there is no clear evidence of aggregation of the peptide in DPC micelles. The peptide, in localizing to membranes, could also serve to recruit other proteins involved in vesicle formation and autophagy.

References

1. Landles, C., and Bates, G. P. (2004) Huntingtin and the molecular pathogenesis of Huntington's disease. *EMBO Rep. 5*, 958–963.
2. Ravikumar, B., Vacher, C., Berger, Z., Davies, J. E., Luo, S., Oroz, L. G., Scaravilli, F., Easton, D. F., Duden, R., O'Kane, C. J., and Rubinsztein, D. C. (2004) Inhibition of mTOR induces autophagy and reduces toxicity of polyglutamine expansions in fly and mouse models of Huntington disease. *Nat. Genet. 36*, 585–595.
3. Wellington, C. L., Ellerby, L. M., Gutekunst, C.-A., Rogers, D., Warby, S., Graham, R. K., Loubser, O., van Raamsdonk, J., Singaraja, R., Yang, Y.-Z., Gafni, J., Bredesen, D., Hersch, S. M., Leavitt, B. R., Roy, S., Nicholson, D. W., and Hayden, M. R. (2002) Caspase cleavage of mutant huntingtin precedes neurodegeneration in Huntington's disease. *J. Neurosci. 22*, 7862–7872.
4. Martin, D. D. O., Beauchamp, E., and Berthiaume, L. G. (2011) Post-translational myristoylation: fat matters in cellular life and death. *Biochimie 93*, 18–31.
5. Martin, D. D. O., Ahpin, C. Y., Heit, R. J., Perinpanayagam, M. A., Yap, M. C., Veldhoen, R. A., Goping, I. S., and Berthiaume, L. G. (2012) Tandem reporter assay for myristoylated proteins post-translationally (TRAMPP) identifies novel substrates for post-translational myristoylation: PKCε, a case study. *FASEB J. 26*, 13–28.
6. Martin, D. D. O. (2011) Post-translational myristoylation during cell death. Ph.D. Thesis, University of Alberta, Canada.
7. Wishart, D. S., Bigam, C. G., Holm, A., Hodges, R. S., and Sykes, B. D. (1995) ^{1}H, ^{13}C and ^{15}N random coil NMR chemical shifts of the common amino acids. I. Investigations of nearest-neighbor effects. *J. Biomol. NMR 5*, 67–81.
8. Wüthrich, K. (1986) *NMR of Proteins and Nucleic Acids*, John Wiely & Sons, New York, NY.
9. Wishart, D. S., Sykes, B. D., and Richards, F. M. (1991) Relationship between nuclear magnetic resonance chemical shift and protein secondary structure. *J. Mol. Biol. 222*, 311–333.
10. Sankaram, M. B. (1994) Membrane interaction of small N-myristoylated peptides: implications for membrane anchoring and protein-protein association. *Biophys. J. 67*, 105–112.

Appendix D

NMR analysis of the PINK1 putative transmembrane domain

This chapter forms part of an investigation into a protein being studied by Dr. Joanne Lemieux and Melissa Morrison in the Department of Biochemistry, University of Alberta.

Introduction

PTEN-induced kinase 1 (PINK1) is a 581 amino acid protein implicated in an autosomal recessive form of Parkinson's disease (*1–3*). Mitochondrial dysfunction has been implicated in Parkinson's disease. PINK1 contains an N-terminal mitochondrial targeting sequence, a putative transmembrane domain, a serine/threonine kinase domain, and a C-terminal regulatory domain. PINK1 normally targets to the mitochondrial inner membrane via the TIM/TOM translocation complex, followed by cleavage of the N-terminal and transmembrane domains by an intramembrane protease PARL, releasing the kinase domain into the intramembrane space where it is eventually degraded. Mitochondrial damage leading to a loss of polarization of the inner membrane inhibits the normal trafficking of PINK1, which instead accumulates on the outer membrane where it is then able to phosphorylate outer membrane and cytosolic proteins. In particular, PINK1 activity may recruit the E3 ubiquitin ligase Parkin to the mitochondria, which targets the mitochondria for autosomal degredation. Mutations in PINK1 could affect its processing or activity and lead to the accumulation of defective mitochondria.

Presenilin-associated rhomboid-like protein (PARL), a mitochondrial membrane protease, has been suggested to cleave PINK1 near the transmembrane domain during normal processing of the protein (*4*). Rhomboid proteases are transmembrane proteins containing six or seven transmembrane helices (*5*). They cleave within or

near transmembrane helices using a serine protease-like mechanism. The active site contains a catalytic serine and histidine dyad, in comparison to the catalytic triad found in other serine proteases. The active site is found buried in the membrane domain, such that the substrate must either enter via a "lateral gate" in the membrane, or through the unfolding and solvent exposure of the cleavage site. To gain insight into the structure of the putative transmembrane domain and its interactions with PARL, we examined the secondary structure of the PINK1 TM domain using NMR spectroscopy.

Methods

Synthetic peptide representing the PINK1 putative transmembrane region (sequence AGPCGRAVFLAFGLGLGLIEE) was purchased from Biomatik (ON, Canada). The purity and identity of the peptide was confirmed using HPLC, mass spectrometry, and through sequential assignment of the peptide using NMR.

The peptide was dissolved in either DMSO-d_6 or 50% TFE-d_3/50% H_2O. Dissolution of the peptide in TFE/H_2O followed the procedures of Caroccia et al. TFE was added to the peptide and sonicated in a water bath for 15 min. H_2O containing 0.1% TFA was slowly added to the peptide/TFE suspension with vortexing, and the mixture sonicated for an additional 15 min. PINK1 samples in perdeuterated DPC or SDS contained 0.5 mM PINK1, 38 mM detergent, 5% D_2O, 0.25 mM DSS, 1 mM imidazole and 2 mM DTT, with the sample pH adjusted to 6. The samples of PINK1 dissolved in DMSO or TFE contained 2 mM peptide. The total volume of the samples were between 500–600 µL.

NMR spectra were acquired on a 600 MHz spectrometer at 30 °C. The lock frequency was centred on the DMSO or TFE deuterium peak and NMR spectra were referenced to the residual DMSO or TFE ^{1}H signal at 2.50 ppm or 3.88 ppm, respectively. Detergent-containing samples in aqueous solution were locked onto the HDO signal and referenced to DSS. 1D ^{1}H NMR spectra were used to judge sample quality and 2D ^{1}H-^{1}H DQF-COSY, TOCSY (60 s mixing time), and NOESY (150–200 ms mixing times) spectra were acquired for the samples in DMSO and TFE for spectral assignment and structural studies. The assignment of the NMR spectra followed standard procedures (*6*).

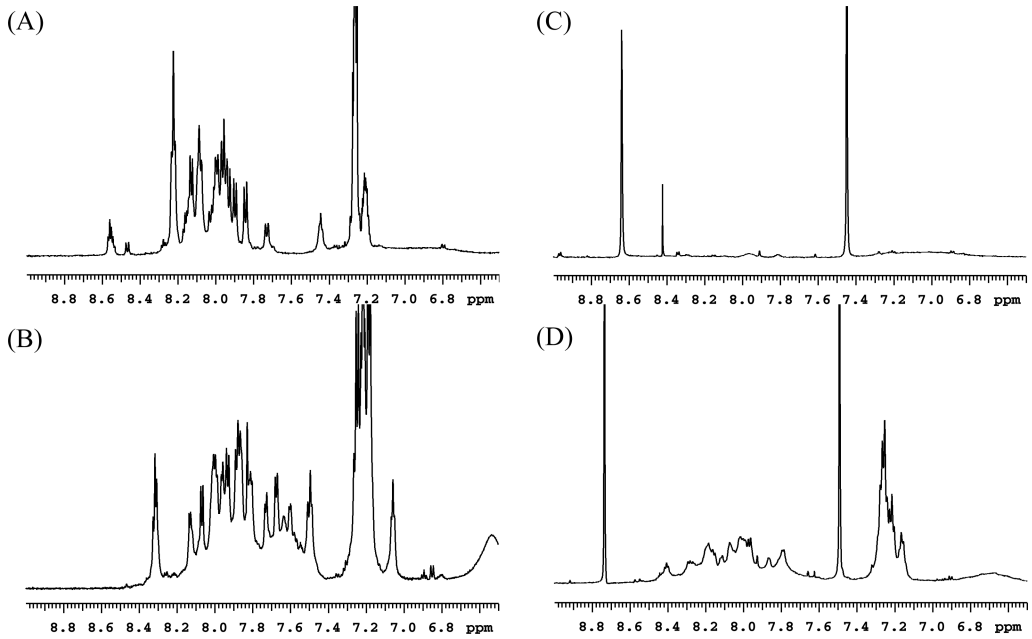

Figure D-1. 1D NMR spectra of PINK1 in membrane mimetics. The amide/aromatic region of the corresponding 1D spectra are shown. 2 mM PINK1 in (A) DMSO and (B) 50% TFE/50% H_2O. 0.5 mM PINK1 in 75 mM of (C) DPC and (D) SDS.

Results

Attempts to express and purify a peptide representing the PINK1 putative transmembrane region using the MBP fusion protein system (*7*) were only partially successful. Samples of the peptide may have been poorly soluble or contained contaminants that resulted in poor 1D ^{1}H NMR spectra. Chemically synthesized peptide was purchased, and provided good spectra in DMSO and TFE/H_2O. The micellar detergents DPC and SDS were also tested. The peptide did not appear to be soluble in DPC, while only moderate quality spectra were obtained for SDS-solubilized PINK1. 1D ^{1}H NMR spectra of PINK1 in DMSO, TFE, DPC and SDS are shown in Figure D-1.

1D ^{1}H NMR spectra of DMSO-solubilized PINK1 peptide presented narrow lines and moderate dispersion of peaks in the amide region ($\sim$7–9 ppm) of the spectra. Broad peaks at 12–13 ppm could be observed, corresponding to the three carboxyl groups (two Glu and the C-terminus) in the peptide. 2D NOESY NMR spectra showed numerous $d_{\mathrm{NN}}(i,i+1)$ contacts. Sequential assignment revealed that two conformations of the peptide were present, a result of the cis–trans isomerization of the peptide bond preceding the proline in the sequence. The trans-Pro conformer peaks were strong in intensity and were easily assigned. Based on integration of

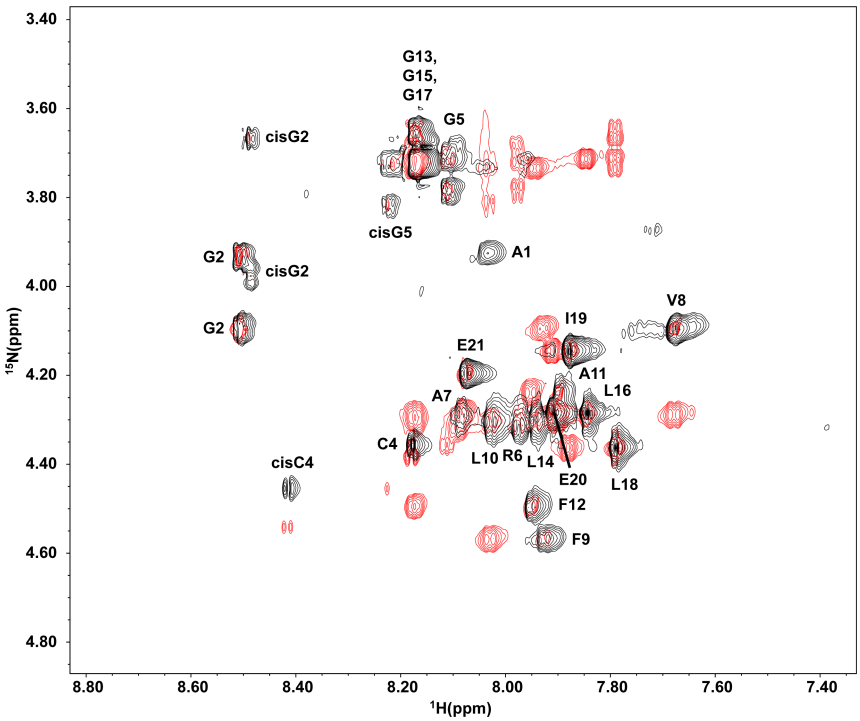

Figure D-2. Sequential assignment of PINK1 peptide in DMSO. 2D ^{1}H-^{1}H TOCSY (black) and NOESY (red) spectra are overlaid, and the HN-Hα "fingerprint" region is shown. TOCSY crosspeaks are labelled with their corresponding residues. cis indicates resonances from the cis-Pro conformer.

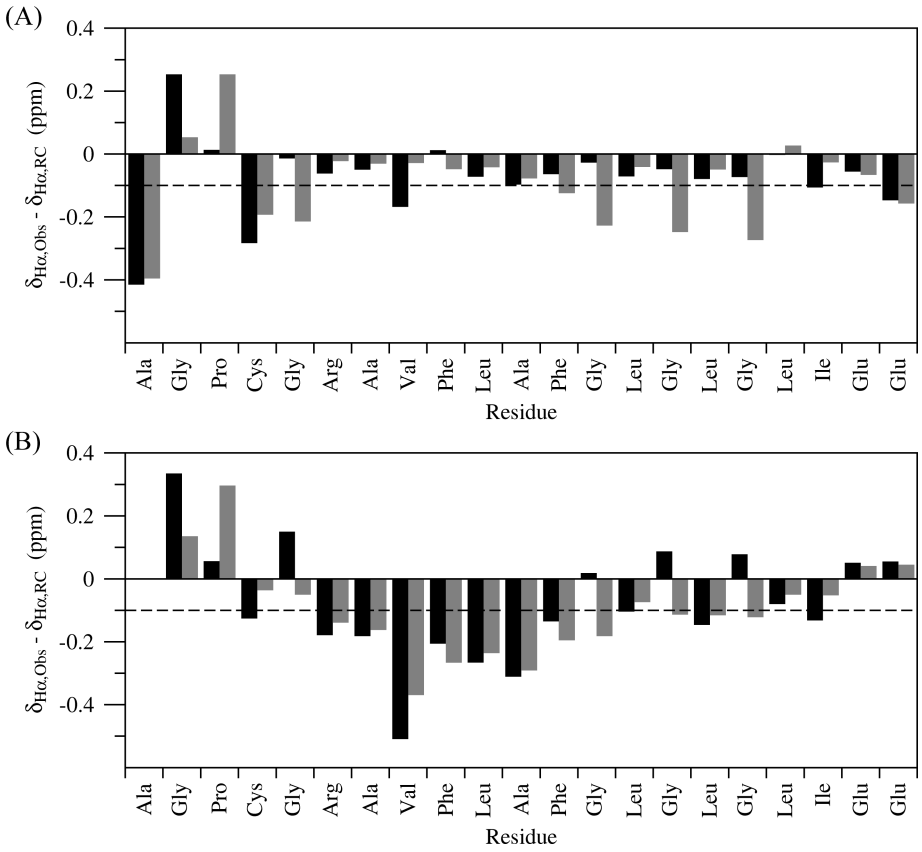

Figure D-3. Secondary structure of PINK1 based on chemical shifts. The chemical shifts of the PINK1 Hα protons are compared to random coil Hα chemical shifts in water (black) (*8*) and in DMSO (grey) (*9*, *10*). Differences in Hα chemical shifts between PINK1 and random coil larger than -0.1 ppm are indicative of a helical conformation.

the peaks in the 2D spectra, the cis-Pro conformer was estimated to consist of approximately 25% of the population of the sample. The cis-Pro conformer could not be fully assigned due to the low intensity of the peaks and overlap with the trans conformer peaks for residues that were distant in sequence from the proline. The fingerprint region of the TOCSY and NOESY 2D ^{1}H-^{1}H NMR spectra are shown in Figure D-2 with the intraresidue crosspeaks labelled.

Comparison of the chemical shifts of the peptide versus random coil chemical shifts in water (*8*), and DMSO (*9*, *10*) were used to estimate the secondary structure content of the peptide (Figure D-3). No contiguous regions exceeding -0.1 ppm or $+0.1$ ppm were observed, suggesting that the peptide did not contain significant alpha-helix or beta-sheet structure, and was primarily random coil. The relative intensities of the NOE peaks were also indicative of a random coil structure. The NOESY spectrum contains cross-peaks that correlate two ^{1}H atoms in the peptide

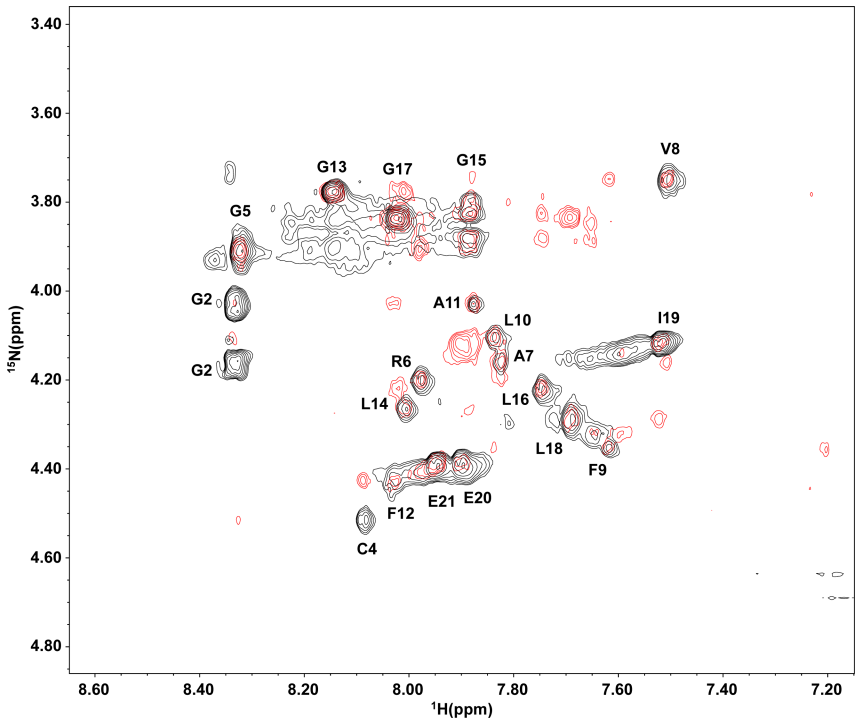

Figure D-4. Sequential assignment of PINK1 peptide in 50% TFE.

that are close in space. The intensity (I) of peaks in an NOESY spectrum are related to the distance (r) between the two correlated protons such that $I \propto 1/r^6$. Weak $d_{\alpha N}(i,i)$ and strong $d_{N\alpha}(i,i+1)$ NOE peaks coupled with weak $d_{NN}(i,i+1)$ peaks indicated an extended or unstructured peptide.

To see if the peptide could adopt helical structure, we attempted to determine the secondary structure of the peptide in a TFE/H_2O mixture, which can stabilize alpha-helical structure (*11*). 1D ^{1}H NMR spectra showed better dispersion in the amide region (Figure D-1, B), however there appeared to be some broader peaks underneath the amide peaks. It is unknown if these peaks represent the cis conformer of the peptide or are some impurity in the sample.

2D NOESY spectra of the peptide in TFE/H_2O showed better dispersion of the d_{NN} peaks, and better dispersion of the peaks in the HN-Hα "fingerprint" region (Figure D-4). Chemical shift analysis using both DMSO and H_2O chemical shifts showed that the termini were likely to be in an extended conformation, as suggested by the positive secondary chemical shifts, while G5–F11 showed a strong negative deviation in chemical shifts, suggesting a short helical structure to this region. The GL-repeat region between residues 13–18 may be weakly helical based on the smaller chemical shift deviation of the Hα chemical shifts. The NOESY

spectra also suggest that the peptide is more structured in TFE/H_2O. The d_{NN} and $d_{N\alpha}$ crosspeaks are slightly more intense than the $d_{\alpha N}$ peaks between residues 7–18 which contain the short helical region and the GL repeats. The opposite is true for the termini, which would suggest they are extended.

Based on the NMR results, the PINK1 transmembrane domain in DMSO is unstructured, which may suggest that this region does not inherently form an alpha-helical structure. In 50% TFE, the peptide appears to form a short helix at the N-terminal half over residues 5–11. The C-terminal half of the peptide may be weakly helical. This suggests that the peptide could potentially function as a transmembrane helix, however it may require structure inducing solvents or, in cells, a membrane environment to properly fold.

References

1. Mills, R. D., Sim, C. H., Mok, S. S., Mulhern, T. D., Culvenor, J. G., and Cheng, H.-C. (2008) Biochemical aspects of the neuroprotective mechanism of PTEN-induced kinase-1 (PINK1). *J. Neurochem. 105*, 18–33.
2. McCoy, M. K., and Cookson, M. R. (2012) Mitochondrial quality control and dynamics in Parkinson's disease. *Antioxid. Redox Signal. 16*, 869–882.
3. Trempe, J.-F., and Fon, E. A. (2013) Structure and function of parkin, PINK1, and DJ-1, the three musketeers of neuroprotection. *Front. Neurodegener. 4*, 38.
4. Jin, S. M., Lazarou, M., Wang, C., Kane, L. A., Narendra, D. P., and Youle, R. J. (2010) Mitochondrial membrane potential regulates PINK1 import and proteolytic destabilization by PARL. *J. Cell Biol. 191*, 933–942.
5. Ha, Y. (2009) Structure and mechanism of intramembrane protease. *Semin. Cell Dev. Biol. 20*, 240–250.
6. Wüthrich, K. (1986) *NMR of Proteins and Nucleic Acids*, John Wiely & Sons, New York, NY.
7. Douglas, J. L., Trieber, C. A., Afara, M., and Young, H. S. (2005) Rapid, high-yield expression and purification of Ca^{2+}-ATPase regulatory proteins for high-resolution structural studies. *Protein Expr. Purif. 40*, 118–125.
8. Wishart, D. S., Bigam, C. G., Holm, A., Hodges, R. S., and Sykes, B. D. (1995) ^{1}H, ^{13}C and ^{15}N random coil NMR chemical shifts of the common amino acids. I. Investigations of nearest-neighbor effects. *J. Biomol. NMR 5*, 67–81.
9. Bundi, A., Grathwohl, C., Hochmann, J., Keller, R. M., Wagner, G., and Wüthrich, K. (1975) Proton NMR of the protected tetrapeptides TFA-Gly-Gly-L-X-L-Ala-OCH_3, where X stands for one of the 20 common amino acids. *J. Magn. Reson. 18*, 191–198.
10. Tremblay, M.-L., Banks, A. W., and Rainey, J. K. (2010) The predictive accuracy of secondary chemical shifts is more affected by protein secondary structure than solvent environment. *J. Biomol. NMR 46*, 257–270.
11. Buck, M. (1998) Trifluoroethanol and colleagues: cosolvents come of age. Recent studies with peptides and proteins. *Q. Rev. Biophys. 31*, 297–355.